UNCLASSIFIED

AD 295 917

Reproduced
by the

ARMED SERVICES TECHNICAL INFORMATION AGENCY
ARLINGTON HALL STATION
ARLINGTON 12, VIRGINIA

UNCLASSIFIED

Best
Available
Copy

NOTICE: When government or other drawings, specifications or other data are used for any purpose other than in connection with a definitely related government procurement operation, the U. S. Government thereby incurs no responsibility, nor any obligation whatsoever; and the fact that the Government may have formulated, furnished, or in any way supplied the said drawings, specifications, or other data is not to be regarded by implication or otherwise as in any manner licensing the holder or any other person or corporation, or conveying any rights or permission to manufacture, use or sell any patented invention that may in any way be related thereto.

63-2-3

ASD-TDR-62-877

295917

CATALOGED BY ASTIA

ADVANCED SOLAR THERMIONIC POWER SYSTEMS

TECHNICAL DOCUMENTARY REPORT NO. ASD-TDR-62-877

December 1962

Directorate of Aeromechanics
Aeronautical Systems Division
Air Force Systems Command
Wright-Patterson Air Force Base, Ohio

Project No. 8173, Task No. 817305

ASTIA

(Prepared under Contract No. AF 33(616)-7411
by the Thompson Ramo Wooldridge Inc.,
Cleveland, Ohio)

NOTICES

When Government drawings, specifications, or other data are used for any purpose other than in connection with a definitely related Government procurement operation, the United States Government thereby incurs no responsibility nor any obligation whatsoever; and the fact that the Government may have formulated, furnished, or in any way supplied the said drawings, specifications, or other data, is not to be regarded by implication or otherwise as in any manner licensing the holder or any other person or corporation, or conveying any rights or permission to manufacture, use, or sell any patented invention that may in any way be related thereto.

Qualified requesters may obtain copies of this report from the Armed Services Technical Information Agency, (ASTIA), Arlington Hall Station, Arlington 12, Virginia.

This report has been released to the Office of Technical Services, U.S. Department of Commerce, Washington 25, D.C., in stock quantities for sale to the general public.

Copies of this report should not be returned to the Aeronautical Systems Division unless return is required by security considerations, contractual obligations, or notice on a specific document.

16-41886, 200, 1-28-63

FOREWORD

This report was initiated by the Flight Accessories Laboratory, Aeronautical Systems Division, Wright-Patterson Air Force Base, Ohio. The research and development work upon which this report is based was accomplished by the New Product Research Department, Tapco Division, Thompson Ramo Wooldridge Inc., and its subcontractor, the Thermo Electron Engineering Corporation, Cambridge, Massachusetts,under Air Force Contract AF 33(616)-7411, Item No. VII, Project No. 8173, Task 817305-4, "Design Study for Advanced Solar Thermionic Power Systems." The report covers all work performed during the period from June, 1960 to August 1962.

Captain Eugene F. Redden and Mr. A. E. Wallis monitored the project for the Flight Accessories Laboratory of the Aeronautical Systems Division.

The Thompson Ramo Wooldridge Inc. engineering report number is ER-5038.

ABSTRACT

This report contains a state-of-the-art survey of all components required for advanced solar thermionic power systems in the 1-10 KW range suitable for application in aerospace vehicles. The results of the survey and development program were used in a comprehensive parametric study to determine design criteria applicable to these systems. The development program included evaluation of thermionic converters of the vacuum and vapor type. The details of the design, fabrication, performance tests, and evaluation of the thermionic converters and generators built during the program are presented.

The importance of the proper selection of solar receiver configuration, as well as the requirement for high precision solar concentrators, is treated extensively. Consideration is also given to the requirements of the orientation subsystem, energy storage subsystem and the many control requirements necessary to adequately orient the solar concentrator arrays, store energy for the shade portion of the orbital cycle and properly condition the electrical power required by the vehicle load.

The Appendix presents a detailed design, performance, and test specification for a 1.5 KW, 28 volts solar thermionic power system. This design is based on all the knowledge accumulated in this program.

PUBLICATION REVIEW

The publication of this report does not constitute approval by the Air Force of the findings or conclusions contained herein. It is published for the exchange and stimulation of ideas.

TABLE OF CONTENTS

LIST OF ILLUSTRATIONS

LIST OF ILLUSTRATIONS CONT'D

LIST OF ILLUSTRATIONS CONT'D

LIST OF ILLUSTRATIONS CONT'D

APPENDIX

LIST OF TABLES

1.0 INTRODUCTION

The primary objective of the Air Force program described in this report was to establish design criteria for advanced solar thermionic power systems in the 1-10 KW range suitable for application in aerospace vehicles.

The program to accomplish this objective included a state-of-the-art survey of all system components as well as a comprehensive research, design, development, test and evaluation program directed toward advancing the art for thermionic converter and generators.

The major system component study was carried out by the TAPCO Division of Thompson Ramo Wooldridge Inc. and included thermionic generators, solar concentrators, orientation subsystems, energy storage subsystems and control subsystems. The research, design, development, fabrication and electrical characteristic studies of thermionic converters were performed by the Thermo Electron Engineering Corporation under a subcontract. The thermionic generator performance tests and evaluations were conducted by Thompson Ramo Wooldridge.

Results of these study and development efforts were then used to establish the governing factors, design limitations and feasibility of solar thermionic power systems over the power range of interest.

The design of a solar thermionic power system with a continuous power output rating of 1500 watts at 28 volts was completed. A detailed performance and test specification for this 1.5 KW system was also established. This design is based on the state-of-the-art of components as established during the program.

Manuscript released by the authors (August 1962) for publication as an ASD Technical Document Report.

2.0 SUMMARY

At the time work on this program was begun, it was generally believed that both the close spaced vacuum and cesium vapor type thermionic converters held great promise for application in solar thermionic power systems. A comparative evaluation of both types based on intensive research and development efforts during early phases of the program showed a marked superiority in the cesium type converters. Efforts to develop the cesium converter had resulted in the attainment of nearly 500 hours of operation at watt densities of over 10 watts/cm^2 with calculated efficiencies of over 15% in experimental models. The vacuum close spaced units had been made to operate for only 20 hours at power densities of 0.4 watts/cm^2 at calculated efficiencies of 4.0%. This marked difference in performance, coupled with several still-unsolved structural problems associated with the close spaced converters, resulted in a recommendation to discontinue work on vacuum type converters. It was subsequently decided that two promising cesium vapor type thermionic generators would be evaluated during the remainder of the program.

The first generator utilized two cylindrical geometry converters connected in series. Each converter was designed to produce 200 watts at 1 volt with 15% overall efficiency as the design objective. Converter #1 produced 160 watts at approximately .8 volts with a 10.6% efficiency. Converter #2 produced 200 watts at .8 volts with a 13.6% overall efficiency. Both converters were successfully operated in series with a combined output of 310 watts at 1.5 volts and an overall efficiency of 9.6%, as determined by the ratio of total electrical output to total electrical power input.

The second generator configuration is called the cubical cavity generator because of the arrangement of five flat emitter faces to form a cubical cavity absorber. The sixth face of the cube served to admit flux from a solar concentrator. Two generators of this configuration were designed, but only the second design rated at 125 watts was completed and performance tested. This generator was tested in the laboratory for over 72 hours and produced 122 watts at 3.7 volts with a 7.6% overall efficiency. An evaluation of the performance of each generator configuration is treated in the body of this report.

In addition to the development and evaluation program carried out on the thermionic generators, the state-of-the-art in all other major component areas

was subject to close examination. Components such as solar concentrators, orientation subsystems, energy storage systems, electrical controls and structural concepts were all carefully studied to determine what hardware and configurations might be applicable to a prototype thermionic power system at this time.

Because of the temperatures associated with the efficient operation of thermionic generators,only precision, rigid type solar concentrators in conjunction with highly efficient cavity type solar receivers are suitable for solar thermionic power systems. Solar concentrator requirements and fabrication techniques perfected at this time indicate that only nickel electroformed concentrators are acceptable for a systems application. The state-of-the-art as it exists today limits the size of such concentrators to 5 feet in diameter,with reflectivities on the order of 89% being the best attainable. Development in the area of lightweight precision aluminum concentrators has shown much promise and may eventually replace the nickel concentrators at half the weight penalty, but to date such concentrators have not met the optical requirements for thermionic systems.

It was immediately recognized that one of the major control areas associated with a thermionic power system is that of sun acquisition and tracking. For the studies conducted in this program, it was assumed that inertial or course pulse jet control would be used to sun-orient the vehicle within $\pm$ 5 degrees to help minimize fuel requirements and control complexity. Subsequent evaluation of generator and concentrator performance indicated an orientation of $\pm$ 6 minutes or better was actually required for the thermionic system. Also, because such a system was to be made of many module assemblies with attendant alignment problems because of the many hinge joints and structural members involved, some method of providing a fine orientation control for each module is required. A relatively simple mechanism called a heliotropic mount was evaluated to determine its ability to fulfill this need.

The heliotropic mount,which consists of a series of bimetallic sensor-actuator elements,detects the improper location of the concentrator focal spot on the generator face due to uneven heating of the bimetal sensors. This uneven heating results in a corrective force in the bimetal elements which repositions

the concentrator to restore proper alignment. The feasibility of the heliotropic orientation mechanism has been demonstrated by Thompson Ramo Wooldridge under a corporate-sponsored program. The further demonstration of its practical application with a thermionic module remains to be accomplished.

Studies of the various techniques for energy storage, such as inertial, thermal and electro-chemical, indicate that only the latter is presently suitable for high-temperature thermionic system applications. While work is being carried on to perfect the use of several thermal storage materials, these are far from achieving state-of-the-art recognition. Among the many electro-chemical storage systems, only two seem practical for a long-term orbital application. These two are nickel-cadmium and silver-cadmium storage batteries. The silver-cadmium batteries, however, enjoy a considerable weight-to-power advantage over nickel-cadmium and require far less limiting of the depth of discharge to obtain high cycle life.

Other areas, such as structures and deployment concepts, electrical systems controls, thermal controls, and orientation and start-up controls, are covered in detail in body of this and other reports. The state-of-the-art in these areas appears to be sufficiently advanced to meet the requirements of the thermionic power system.

The results of all studies and developments were incorporated in a parametric design study and tempered with practical considerations and limitation in present day state-of-the-art hardware. As a result of all knowledge gained in the program, it has been established that the practical ranges for solar thermionic systems for orbital applications would seem to be for power ranges of from 200 watts to 3000 watts. This limitation is dictated by practical structural considerations.

The Appendix of this report presents a detailed design, performance and test specification for a 1.5 KW, 28 volt continuous power system. The design presented has a specific weight of 440 lb/KW. As thermionic converter and generator efficiencies increase and solar concentrator weight decreases, marked improvements in specific weight can be expected.

3.0 SOLAR THERMIONIC SYSTEM COMPONENTS

3.1 Thermionic Generators

Work on the hardware portion of the program was initiated during June of 1960 with the objective of establishing design criteria for future solar thermionic power systems. The program included design studies, theoretical and experimental studies of electrical characteristics; and prototype design, development, fabrication and test. This work was to be performed concurrently for both the vacuum and vapor types of thermionic converters and was to be followed by an evaluation of the relative merits of each. The design goals for the prototype vacuum generator were 250 watts output at 28 volts, and an overall 10% efficiency. The vapor type generator had design goals of 250 watts output at 28 volts, with a 15% efficiency. Other design objectives were the achievement of 100 thermal cycles and 100 hours of full-load operation. Theoretical and experimental studies of the electrical characteristics of both types of converters were performed. A 15 watt vapor converter was operated for 500 hours and achieved power densities of up to 6 watts/cm^2. The vacuum converter test units did not fare as well. Based upon the prototype design, a test module of 2.5 watts output, which could be mass-produced and assembled into a generator, had been planned. The test converters which were built fell well short of this objective.

The prototype design for the vapor generator required two cylindrical converters, each producing 200 watts. These converters were to be series connected, and the output was to be delivered to a DC-DC converter capable of stepping up the voltage to 28 volts.

Under test, one converter produced approximately 200 watts at an efficiency of 13.6%, while the other produced 160 watts at an efficiency of 10.6%. These efficiencies were based on measured values of power output and power input.

Following the difficulties encountered in achieving the required power output from the vacuum modules, development work was continued until March 1961. At this point, an evaluation was conducted and a recommendation made that work on the vacuum type generator be discontinued. Two major factors influenced this decision. First, the performance of the vacuum converter had not lived up to previous expectations of performance, and the fabrication of a modular unit to be used in assembling a 250 watt generator was considerably more complicated than had been expected. Therefore, it was concluded that a vacuum type generator would be so complicated and expensive as to be impractical. In

addition, progress in the vapor converter area had been very rapid and it had become obvious that a generator using the vapor principle would be greatly superior to one using the vacuum approach.

It was also recommended that the vacuum approach be dropped in favor of developing a cubical cavity cesium generator. This recommendation was accepted and development of such a generator was initiated. The prototype generator was completed in May 1962. It consisted of five cesium filled converters connected in series and mounted on a cavity block. The emitters were heated by a two-stage electron bombardment heater. This generator was designed so that it could also be solar tested subsequent to laboratory testing. Initial electrical tests have shown an output of 90 watts at 5 volts, and 122 watts at 3.7 volts. In the course of limited solar testing with a 5 foot concentrator, the generator was able to produce nearly 20 watts with a solar constant of only 75 watts per square foot.

Generator Concepts

Since the objective of the entire program was to establish design criteria for future solar thermionic power systems, the design goals for the prototype units were chosen with reference to the requirements of a solar powered conversion system for satellite operation. Thus, an output voltage of 28 volts was chosen. This is the normal voltage required for aerospace auxiliary power devices. The generator was designed for use with a solar concentrator. The heat rejection system was to be exclusively dependent upon radiation; the system was required to operate only in vacuum, and a design criteria was to be minimum weight per unit of power output; since any satellite would be expected to pass in and out of the earth's shadow, system warmup with a minimum number of auxiliary operations, and the ability to withstand thermal cycling were also given consideration. The power level of 250 watts and the efficiency objectives of 10% for vacuum generators and 15% for vapor filled generators were thought to be reasonable values which could be expected by the end of the program.

Vacuum Type Generators

At the time that the program was initiated, the vacuum converter type of generator appeared to promise more rapid development toward the goal of practical hardware. Among the expected advantages were: relatively simple structure, no corrosion problem, rapid startup due to lack of dependence upon bringing a gas-

filled envelope to temperature, attractiveness of simple modular construction, ease of replacement of defective modules, the possibility of low-cost mass production, and lower emitter temperature than cesium converters.

The major obstacles in the development of the vacuum close spaced converter were: (1) the choice of a suitable emitter material, (2) the attainment of close interelectrode space ($\leq$ 10μ) to reduce the effect of space charge, and (3) the achievement of a collector work function of 1.8 volts or less to ensure reasonable output powers, efficiencies, and converter life.

The evaluation of emitter materials showed the impregnated tungsten emitter to be the most logical one for use in close-spaced converters; further, the shim spacer assembly technique was proven successful; however the fundamental problem of achieving a low work function collector with long life remains to be solved. Another major problem requiring solution is the satisfactory development of techniques for producing vacuum diodes reliably and easily in the quantities required for the assembly of high-power devices. The state-of-the-art in vacuum converters is summarized in Table 3.1.

While efforts in the development of the cesium vapor thermionic converters had resulted in converters that operated for over 500 hours at power densities in excess of 10 watts per square centimeter with adjusted efficiencies of over 15%, vacuum close-spaced converters had operated for only 20 hours at power densities of 0.4 watts per square centimeter and adjusted efficiencies of 4.0%.

It was therefore recommended that the program be redirected to exclude further work on vacuum close-spaced converters for solar thermionic application and to direct all efforts toward increasing the performance and life of the vapor converter.

Cesium Type Generator with Cylindrical Geometry

Development of a cesium filled thermionic converter was at a much earlier stage than the vacuum development at the time the program was initiated. Such problems as cesium corrosion, ceramic-to-metal seals, cesium reservoir control and structural complications had yet to be solved. However, the potential for achieving higher power density with respect to both volume and weight and a higher conversion efficiency indicated that the problems were worth attacking. Therefore, it was decided that one phase of the program should be an attempt

Table 3.1 Evaluation Summary Chart for Close-Spaced Vacuum Thermionic Converters

	Work Function	Life	Spacing	Radiator Compatibness	Efficiency (Thermal)	Reliability: Chemical	Reliability: Mechanical	Economy	Best of Group	Remarks (Chief Limitations)
Emitter										
Oxide Coated	Poor (1.8-1.9 ev)	Fair (2000 hrs)	Poor			Poor	Poor	Poor		Tends to flake. Easily poisoned.
Impregnated Tungsten	Good	Good (15,000 hrs)	Fair		Good	Fair	Good	Fair	✱	Special care required to prevent poisoning.
Thoriated Tungsten	Good	Fair	Good		Poor	Poor	Good	Poor		Easily poisoned. Min temp 1800°K.
Carburized Thoriated Tungsten	Good	Good (30,000 hrs)	Poor		Poor	Fair	Poor	Poor		Coarse structure. Prone to flaking.
Spacer										
Sapphire Rod		Fair	Good		Fair	Good	Poor	Fair		High preloading induces creep.
Insulated Wire		Good	Good		Good	Good	Fair	Fair		Low transverse strength.
Shim		Good	Good		Fair	Good	Good	Good	✱	
Collector										
Barium Impregnated Tungsten	Good	Poor (10 hrs)	Poor	Good		Good				Poor machinability.
Nickel	Good	Poor	Good	Good		Good				Low work function for short periods.
Molybdenum	Good	Poor	Good	Good		Good				Low work function for short periods.
Copper Oxide	Good	Poor	Good	Poor		Poor				High vapor pressure at 550°C.
Molybdenum Oxide	Good	Over 200 hrs	Good	Fair		Fair			✱	Maximum temperature 575°C.

to develop a generator based upon a high-powered cylindrical vapor-filled converter.

Cubical Cavity Generator

When it became apparent that a vacuum generator was impractical, the cubical cavity generator was substituted. Such a generator is at a disadvantage when compared to the cylindrical configuration since it is made up of five separate converters which must be mounted in a supporting block with the thermionic converter emitters forming a cavity absorber. Since there are flux leakage paths in the cavity between the emitters some heat flows through the cavity without any portion being converted to electrical output. In addition, the configuration of a converter for mounting in a cubical cavity is such that the converter itself has greater heat losses than a converter of cylindrical configuration.

The cubical cavity, however, has one very significant advantage which may, under certain circumstances, allow it to exhibit superior characteristics to those of the cylindrical converter. Each of the five converters mounted on the cavity block is capable of producing approximately the same value of 1 volt at its terminals as the cylindrical converter. Since the five converters of the cavity are connected in series, the generator will deliver its power at 5 volts.

3.1.1 Theoretical Study of Cesium Vapor Thermionic Converters

Cesium converters are capable of various modes of operation. Although it is not possible to identify the precise conditions under which a certain mode of operation merges into another, these modes of operation are easily characterized. The factor that is probably most important in characterizing the possible modes of operation is the average number of collisions undergone by the electrons during their travel from the emitter to the collector. Thus, the modes of operation may be grouped into two broad categories: "collision free" modes and "plasma" modes. In the collision free modes, the electrons leaving the emitter seldom undergo substantial collisions before reaching the collector; such a condition is achieved, of course, by using relatively low cesium vapor pressures and small interelectrode spacings. In the plasma modes, the interelectrode spacing is relatively large, the cesium vapor pressure is relatively high, and most emitted electrons collide several times with cesium atoms and ions before reaching the collector.

The plasma mode of operation was chosen to achieve the design goals of the contract. In the plasma mode of operation, the high vapor pressure of the cesium results in copious ionization of the cesium atoms striking the emitter. The resulting buildup of cesium ions in front of the emitter creates a sheath potential at the emitter, as illustrated in Figure 3.1.1. This potential distribution has the effect of accelerating the emitted electrons and thus imparts to them a considerable velocity which is later randomized because of multiple collisions with the atoms and ions in the interelectrode space. To satisfy plasma boundary conditions, a second sheath potential, which is also shown in Figure 3.1.1, is created at the collector.

Figure 3.1.1 defines nomenclature pertaining to the operation of the cesium plasma converter: ϕ_E and ϕ_C are the emitter and collector work functions, respectively; V_E and V_C are the corresponding sheath potentials; and V is the output voltage, which is

$$V = (\phi_E - \phi_C) - (V_E + IR_{Cs} + IR_L - V_C), \tag{1}$$

where IR_{Cs} is the voltage drop across the cesium plasma and IR_L is the voltage drop in the optimized emitter lead.

If we let T_e denote the temperature of the electron phase in the plasma, the corresponding randomized current I_e will be given by

$$I_e = v_e q_e = N_e C_e / 2\sqrt{\pi} \quad \text{amp/cm} \tag{2}$$

where

$C_e = \sqrt{2kT_e/m_e}$, v_e = electron production rate, electrons/cm^2/sec,

q_e = electron charge, N_e = electron density in the plasma,

m_e = electron mass.

Equation (2) is of little use because the electron density N_e cannot be predicted with sufficient accuracy. It is possible, however, to eliminate the randomized current as a variable by writing the following simultaneous equations for the net current:

$$I = I_s - I_e \exp\left(-\frac{V_E}{kT_e}\right), \tag{3}$$

MOTIVE DIAGRAM FOR CESIUM PLASMA CONVERTER

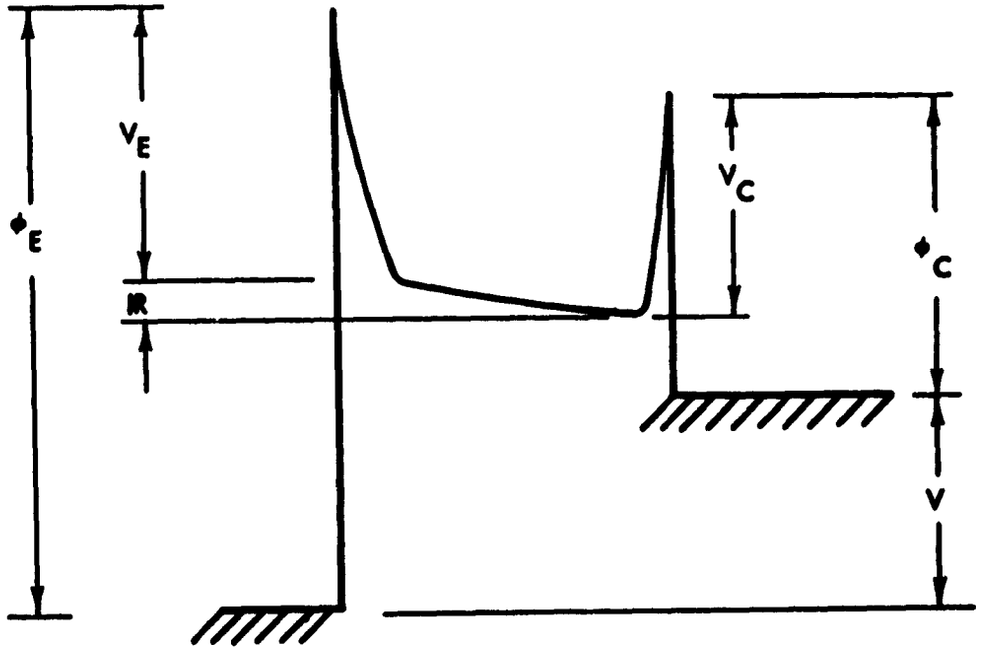

Fig. 3.1.1

$$I = I_e \exp\left(-\frac{V_C}{kT_e}\right) - I_p. \qquad (4)$$

The first of these equations states that the emitted electrons are all accelerated into the plasma by the emitter sheath and hence contribute the amount I_s to the net current. The net current is not I_s because some of the electrons in the plasma have sufficient kinetic energy to overcome the emitter sheath, and become captured by the emitting surface. This reduction in current is expressed by the last term in Equation (3). Equation (4) expresses the net current in terms of the sheath potential at the collector. The net current is that fraction of the randomized current I_e which reaches the collector, reduced by the ion randomized current I_p which is transformed (at the collector by electron capture) into a neutral atom "current."

Equations (3) and (4) may be combined with Equation (1) to yield:

$$\frac{V}{kT_e} - \frac{\phi_E - \phi_C - IR_{Cs} - IR_L}{kt_e} = \ln \frac{I_s - I}{I_p + I} \qquad (5)$$

and, if the IR drop is neglected,

$$\frac{dV}{d\{\ln (I_s - I)/(I_p + I)\}} = kT_e \qquad (6)$$

If the sheath potential V_E is not much greater than kT_E, Equation (3) shows that I and I_e are of the same order of magnitude. Therefore, provided that the current I has sufficient magnitude (e.g., greater than 20% of I_s), $I \gg I_p$. Equation (6) thus becomes

$$\frac{dV}{d\{\ln (I_s - I)/I\}} = kT_e \qquad (7)$$

Equation (7) is of great interest. It states that if the emitter temperature is maintained constant (so as to make I_s constant), the resulting plot of V vs $\ln [(I_s - I)/I]$ should have the slope kT_e.

To calculate the IR drop appearing in Equations (1) and (5), we can assume the plasma to be completely ionized. The electrical conductivity is given by

$$\sigma = \frac{19,141}{\ln (p - 1)} \left(\frac{kT_e}{q_e} \right)^{3/2} \text{ mho/m}, \qquad (8)$$

where

$$p = 12\pi n\lambda_D^3, \quad n\lambda_D^2 = 3.134 \times 10^4 T_e \text{ meter}^{-1},$$

q_e = electron charge, k = Boltzmann's constant,

n = density of the electrons.

Predicted Performance of the Cesium Plasma Converter

From Equation (5) it is possible to construct curves showing output and efficiency for the converter if we choose certain parameters of operation and estimate the electron temperature in the cesium plasma.

The parameters chosen are:

emitter temperature = 2000°K,
cesium condensation temperature = 600°K
collector temperature = 900°K,
spacing = 0.010 in.

From the Langmuir and Taylor data for cesium coverage on tungsten, we can determine the following:

emitter work function = 3.05 volts,
emitter saturation current = 10 amp/cm^2,
collector work function = 1.81 volts.

Early data obtained at Thermo Electron Engineering Corporation indicated a range in electron temperature of from 5000°K to 10,000°K. Curves have been calculated for the extremes of this range.

The diameter and length of the emitter lead have been optimized for maximum efficiency. This is necessary since a lead with too large a diameter will cause a large heat loss by conduction, and a lead with too small a diameter will cause a large I^2R loss. The I^2R in the cesium is neglected in these calculations because they are generally quite small.

The current voltage characteristics of the cesium plasma converter are presented in Figure 3.1.2. The ideal efficiency, based only on electron cooling heat loss, emitter-to-collector radiation heat loss, cesium conduction heat loss, and optimized lead conduction loss, is plotted against voltage in Figure 3.1.3.

Subsequent tests of thermionic devices show a reasonable agreement with the theory except that it appears electron temperatures are frequently below 5000°K and the internal impedance characteristics of the converters are much higher than would be indicated by the calculations. In the course of the theoretical study, it became evident that more data would be necessary to pinpoint the exact operating conditions of cesium plasma converters. An experimental program was formulated to study electrical output (current and power versus voltage) and efficiency as functions of the important variable parameters, namely, the emitter, collector, and cesium condensation temperatures, and also to study the transient changes in output associated with sudden changes in applied load.

3.1.2 Design and Construction of the Cesium Plasma Test Converter

The final design of the cesium plasma test converter was completed early in October 1960. The converter cross-section is shown in Figure 3.1.4. In the final design, a metal ceramic insulator with a large inside diameter was used to permit recessing of the tantalum emitter into the emitter casing. This shortened the copper collector and made the entire converter more compact. Cylindrical radiators were machined as integral parts of the emitter casing and the collector. Two long copper tubes were connected to the collector half of the casing. A copper block, grooved to accept insulated heater wire around it, was brazed near the end of one tube. This block is the cesium reservoir. Its temperature can be controlled to the desired cesium condensation temperature by passing current through the heater wire. The cesium capsule is within the copper tube below the cesium reservoir. A copper plug is brazed into the bottom end of the copper tube. The second copper tube is the evacuation tube, which is connected to a vacuum system capable of maintaining pressures of the order of 10^{-6} mm mercury.

CURRENT VERSUS VOLTAGE CURVES FOR CESIUM CONVERTER OPERATION

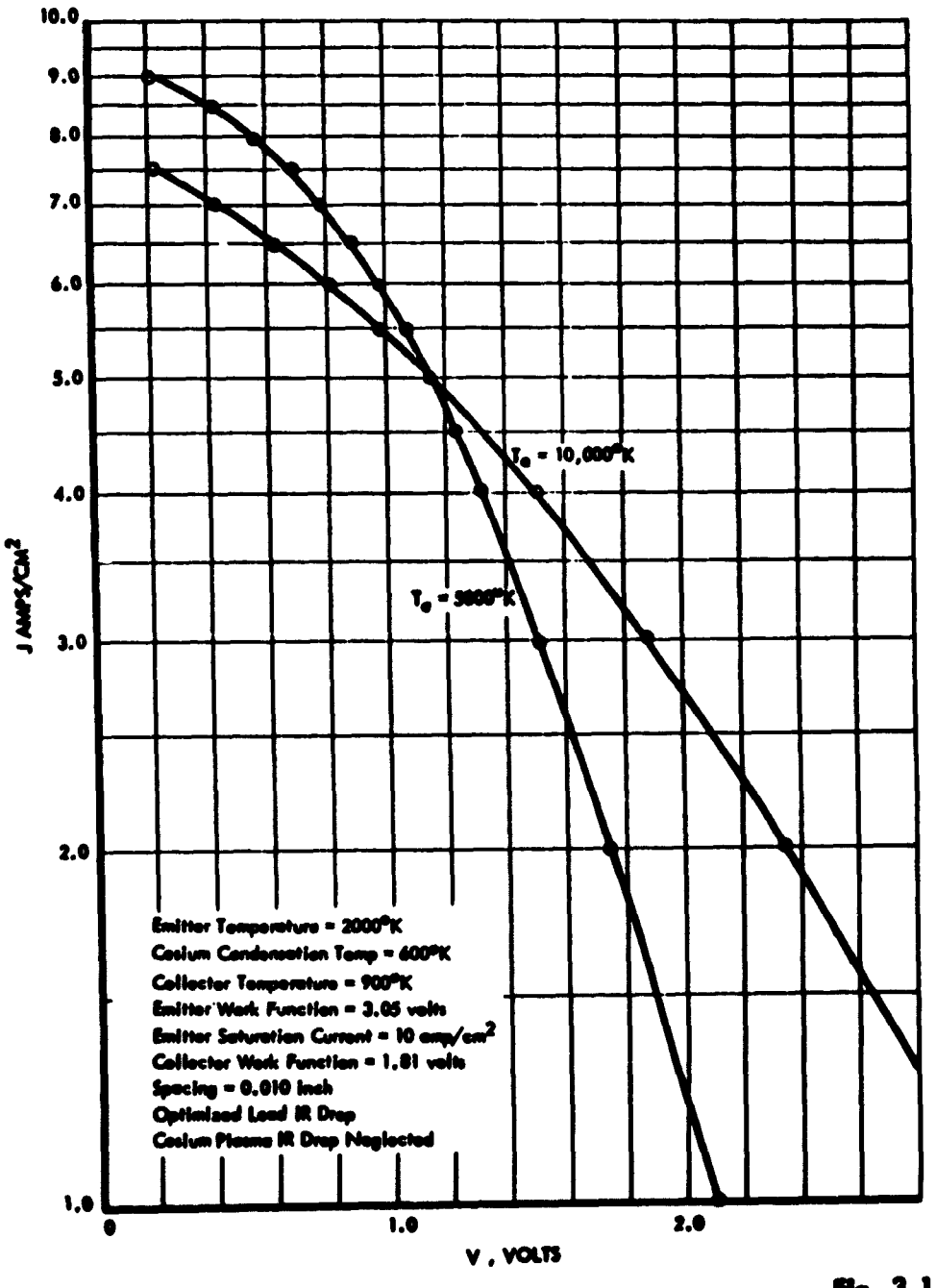

Fig. 3.1.2

IDEAL EFFICIENCY VERSUS VOLTAGE FOR CESIUM CONVERTER OPERATION

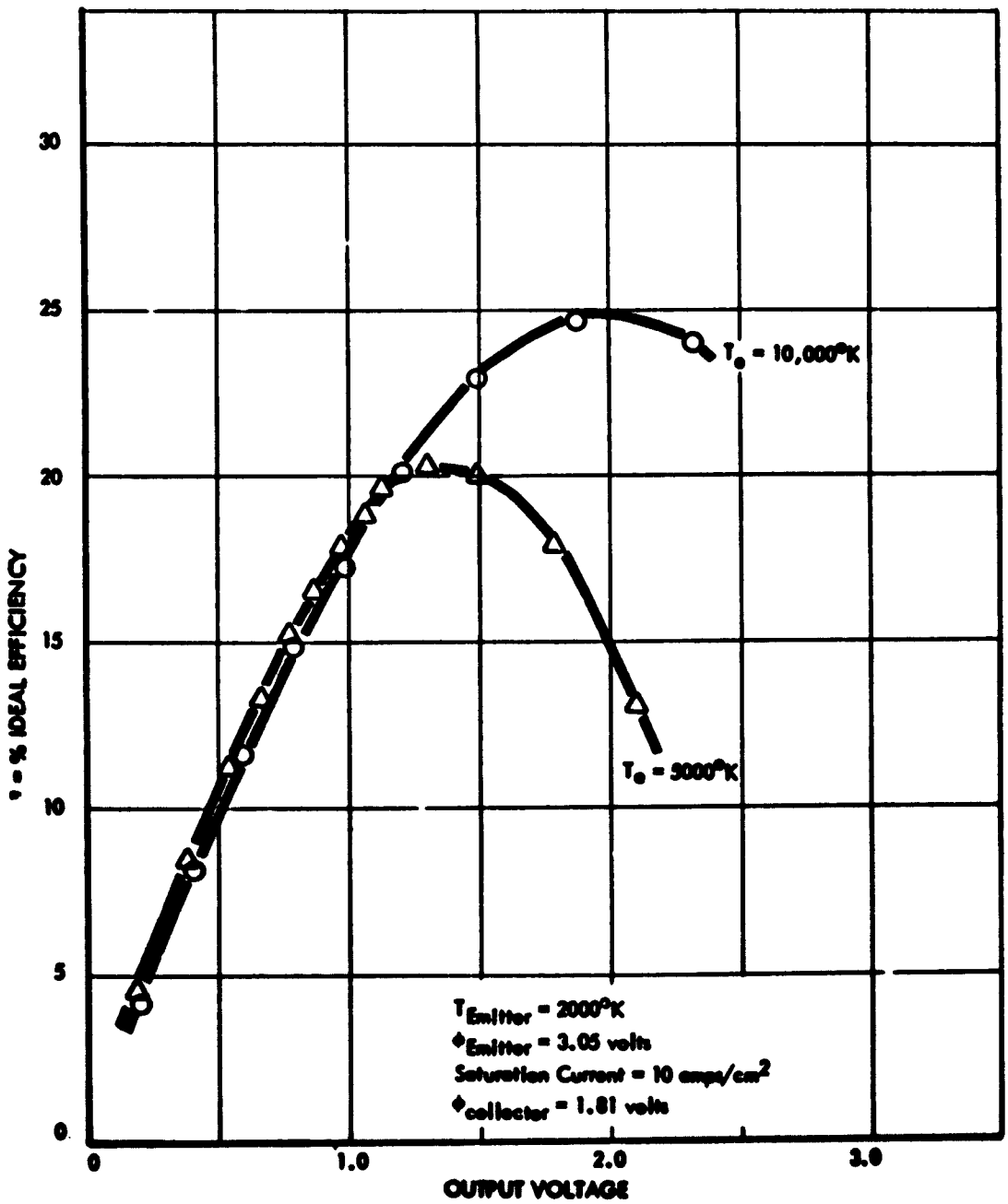

Fig. 3.1.3

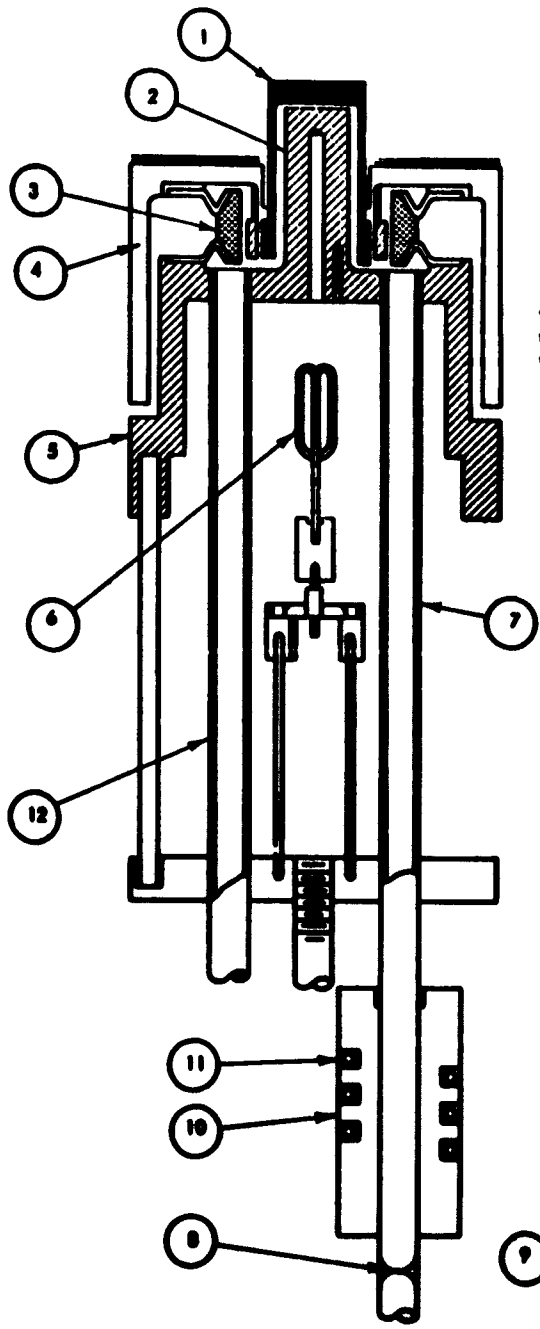

1. Emitter
2. Collector
3. Housing insulating seal
4. Emitter radiator
5. Collector radiator
6. Collector heater
7. Cesium tube
8. Cesium tubulation crimp-off
9. Cesium capsule
10. Cesium reservoir
11. Cesium reservoir heater
12. Evacuation tube

Fig. 3.1.4

The collector heater is a tungsten filament through which alternating current is passed. Part of the heat radiated by this filament is absorbed by the collector, thus increasing the collector temperature. The ends of the filament are brazed onto molybdenum cylinders, which in turn are brazed onto ceramic metal leadthroughs. The two leadthroughs are brazed to a mounting plate.

The electron heating filament is mounted just above the emitter. It is identical to the collector heater as far as support structure is concerned. The tungsten filament is S-shaped, with the plane of the S parallel to the surface of the emitter.

The brazes used were chosen on the basis of mechanical strength, ductility, wettability, vacuum-tightness, melting point, and vapor pressure. Since little data on the corrosive effects of cesium on these brazes was available, and a life of only about 50 hours was necessary, no effort was made to test the brazes in a cesium atmosphere before constructing the converter.

The completed converter was outgassed, evacuated, and crimped off. The cesium capsule was crushed, and the cesium tube heated to drive the cesium into the test converter. Then, the cesium tube was crimped and severed just below the cesium reservoir to eliminate the crushed glass capsule.

The unit was then mounted on its leadthrough ring by connecting alumina tubing between the unit and a mounting plate and connecting threaded stainless steel rods between the mounting plate and the leadthrough ring. The thermocouples and leads were attached to leads from the leadthrough ring, and the top plate (carrying the electron-heating apparatus) was put into place. A view of the entire test assembly is given in Figure 3.1.5. External leads, meters, power supplies, and associated test equipment are not shown.

Preliminary Evaluation

When the test setup was completed and the vacuum surrounding the converter was satisfactory, the cesium converter was ready for test. The emitter was slowly heated to about 2000°K. It was left at this temperature for about one hour, by the end of which time the emitter casing and collector casing had reached equilibrium temperatures. These equilibrium temperatures, obtained with no heat applied to the collector or cesium reservoir, were 850°K on the collector, about 820°K on the collector casing, 870°K on the emitter casing, and 900°K on

ELECTRICAL CHARACTERISTICS STUDY TEST CONVERTER

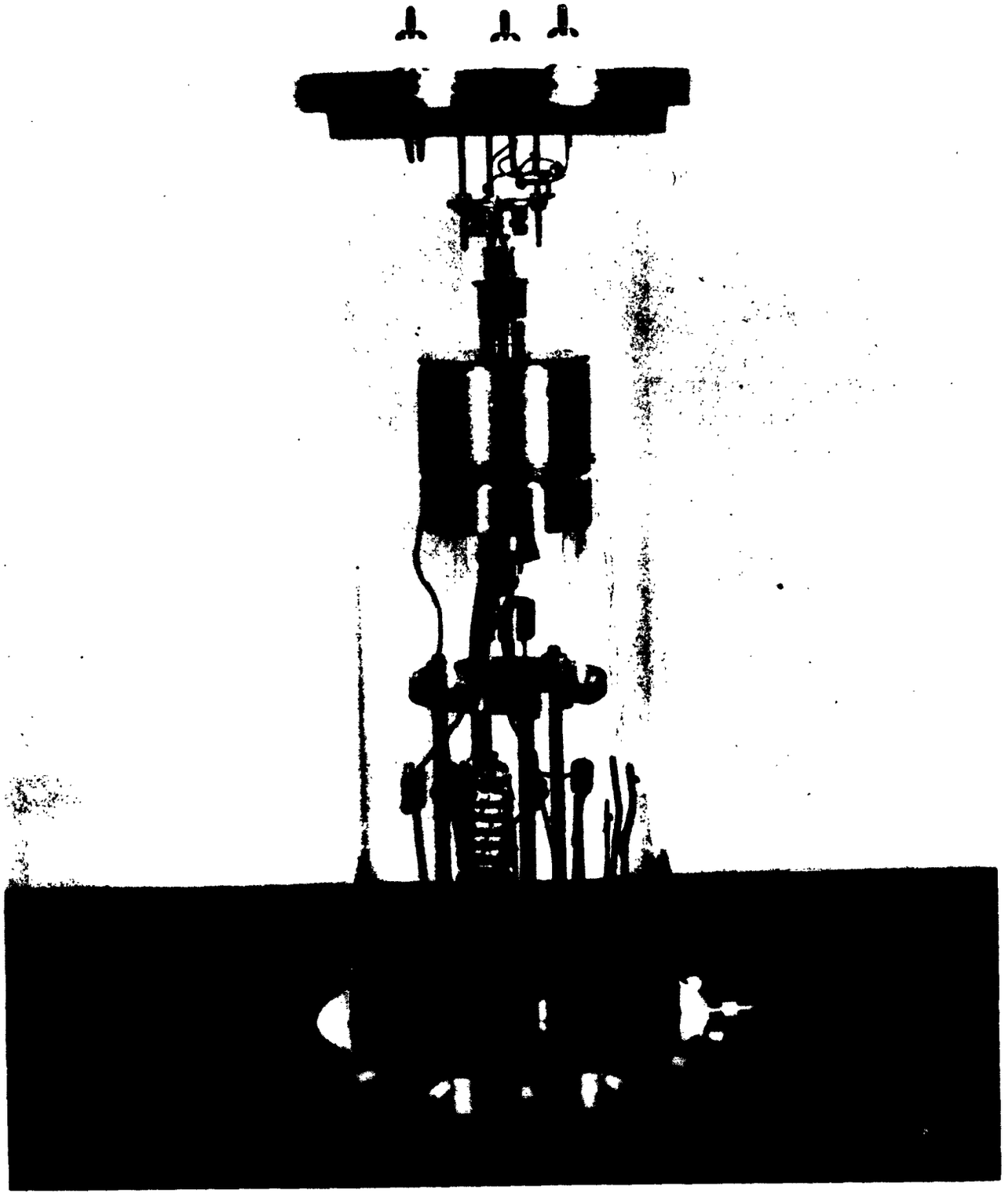

Fig. 3.1.5

the cesium reservoir. The temperatures measured were very close to the predicted (design) temperatures for no collector or cesium-reservoir heating and an emitter temperature of 2000°K. It was found that a constant emitter temperature was fairly easy to maintain for the length of time necessary to take current-voltage and other necessary data. The emitter temperature was found to be controllable from the lowest to the highest values desired.

The collector heater was used to obtain high collector temperatures, and was found to be very satisfactory and easily regulated. The cesium reservoir heater was capable of producing cesium condensation temperatures of over 700°K, the highest temperature of interest. It was quite simple to regulate and came to a constant equilibrium temperature in a very few minutes. A constant cesium condensation temperature is a necessity while making tests, and was readily obtained in this unit. The maximum deviation (fluctuation) occurring during all tests was 2°C. Pyrometer temperature measurements appeared to be fairly easy to obtain, provided that the side of the emitter next to the top edge was read (to avoid the effect of reflections from the electron-heating filament) and that the temperature correction for tantalum was used. Deposits occurred on the glass wall of the vacuum envelope, making accurate measurement of the emitter temperature difficult. The tantalum emitter appeared to become yellowish, and perhaps changed substantially in emissivity. Taking the above into consideration, it appears that the emitter temperature as read by an optical pyrometer was within 100°C of the true emitter temperature. However, during each current-vs-voltage test, it was possible to maintain the emitter temperature constant within 10°C.

Test Results

The test results are summarized in Figures 3.1.6 through 3.1.9.

The results were very encouraging in that high power outputs were obtained and the effects of emitter, collector and cesium reservoir temperatures and inter-electrode spacing were easily observed. In retrospect, it is now obvious that the very high values of current and power density were misleading. Subsequent testing of other units, using more sophisticated techniques, has indicated that areas other than the calculated emitter area were probably contributing to the measured value of power output in the test vehicle under consideration. Therefore, while the shape of the curves and the relative trends of the curves with

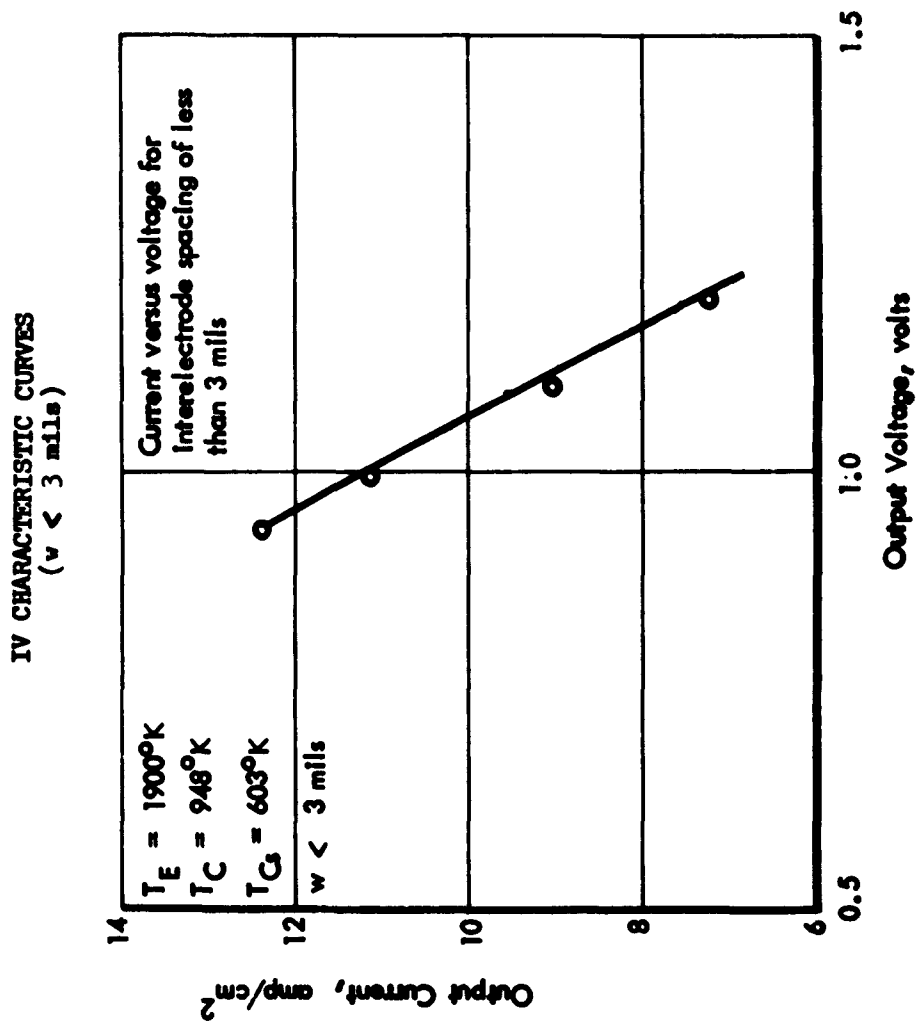
IV CHARACTERISTIC CURVES
(w < 3 mils)
Current versus voltage for interelectrode spacing of less than 3 mils
T_E = 1900°K
T_C = 948°K
T_{Cs} = 603°K
w < 3 mils
Output Current, amp/cm²
14
12
10
8
6
0.5
1.0
1.5
Output Voltage, volts

Fig. 3.1.6

IV CHARACTERISTIC CURVES
(w = 3 mils)

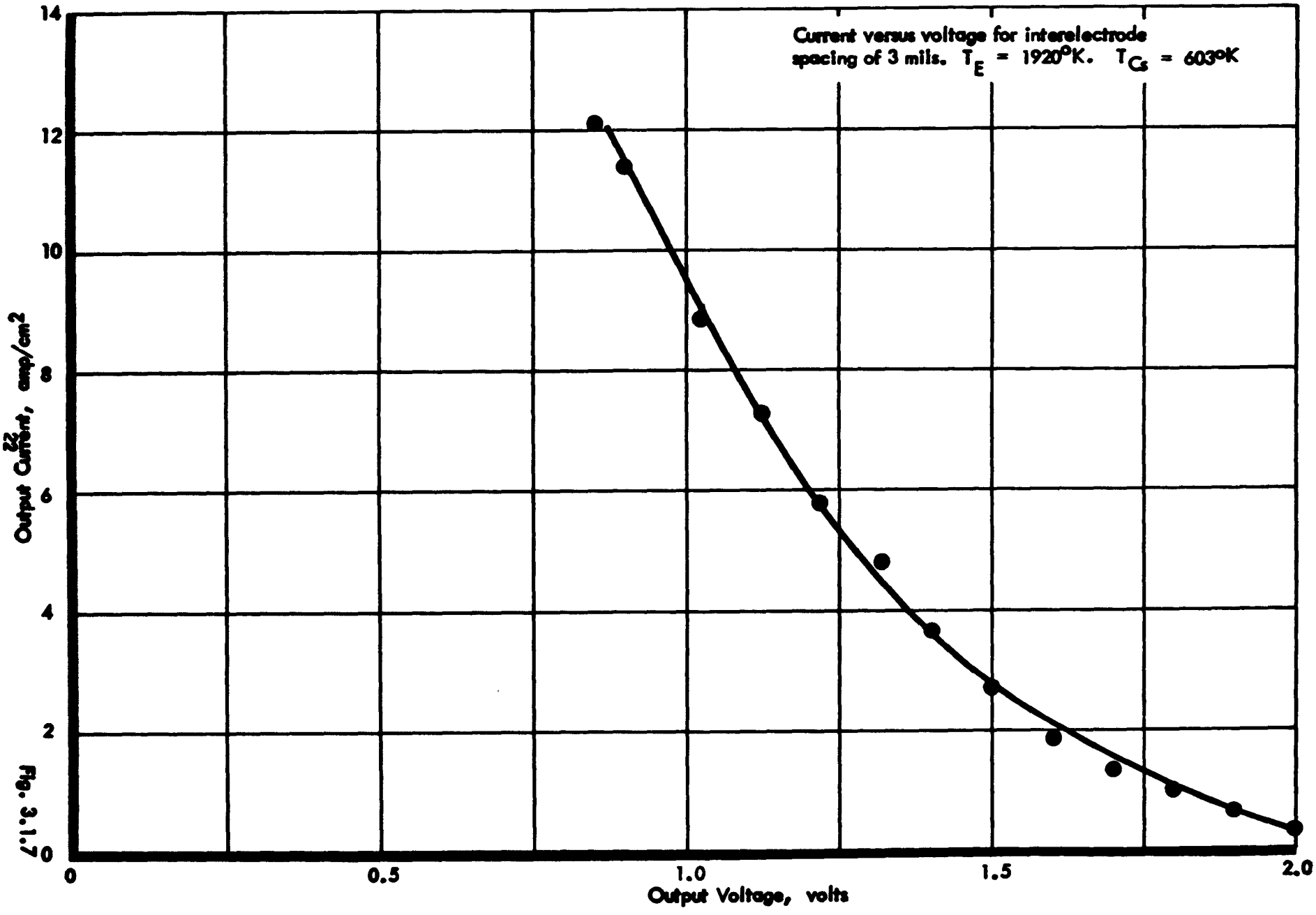

Fig. 3.1.7

IV CHARACTERISTIC CURVES
(T_E = 2000°K)

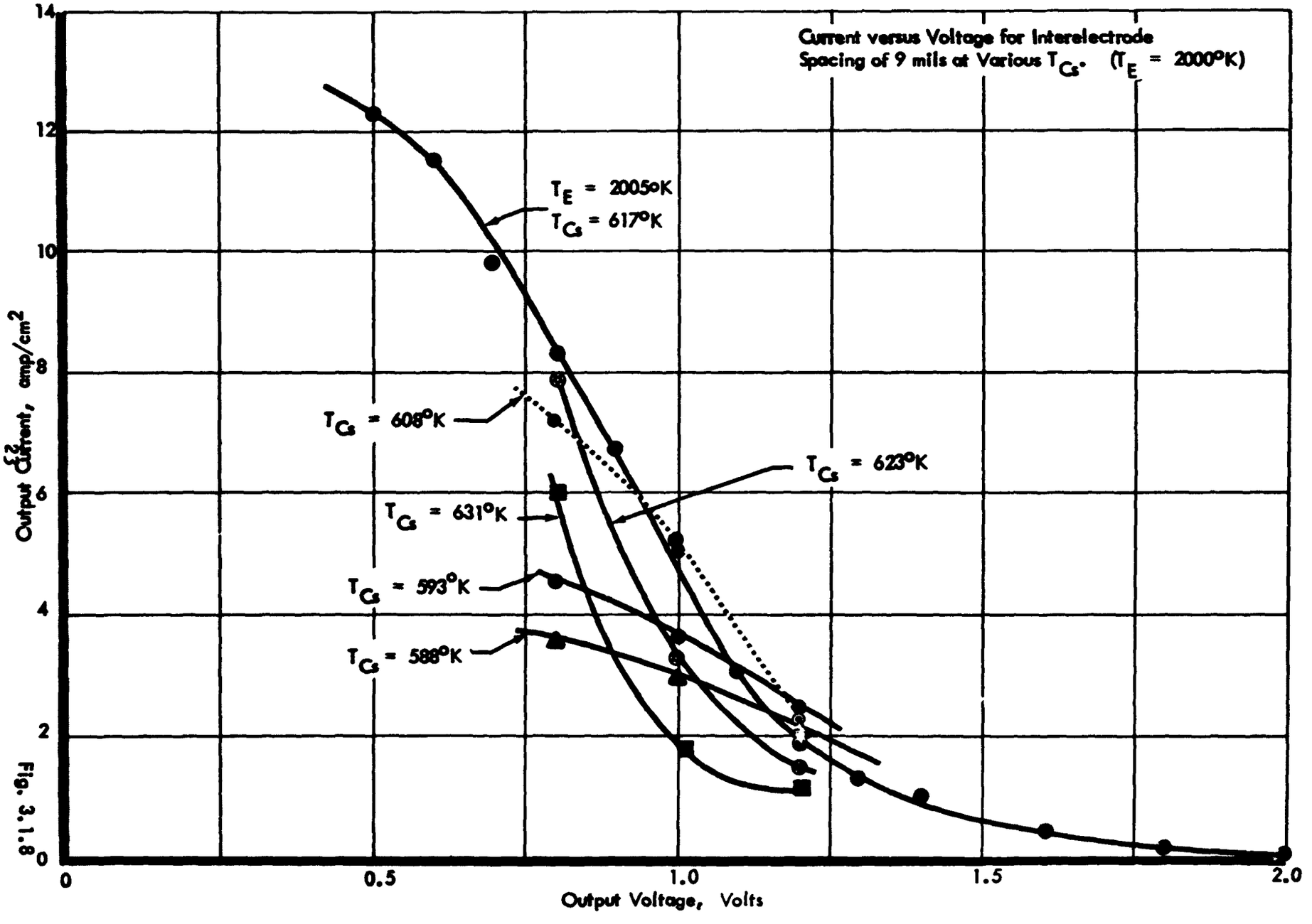

Fig. 3.1.8

IV CHARACTERISTIC CURVES
(T_E = 2095°K)

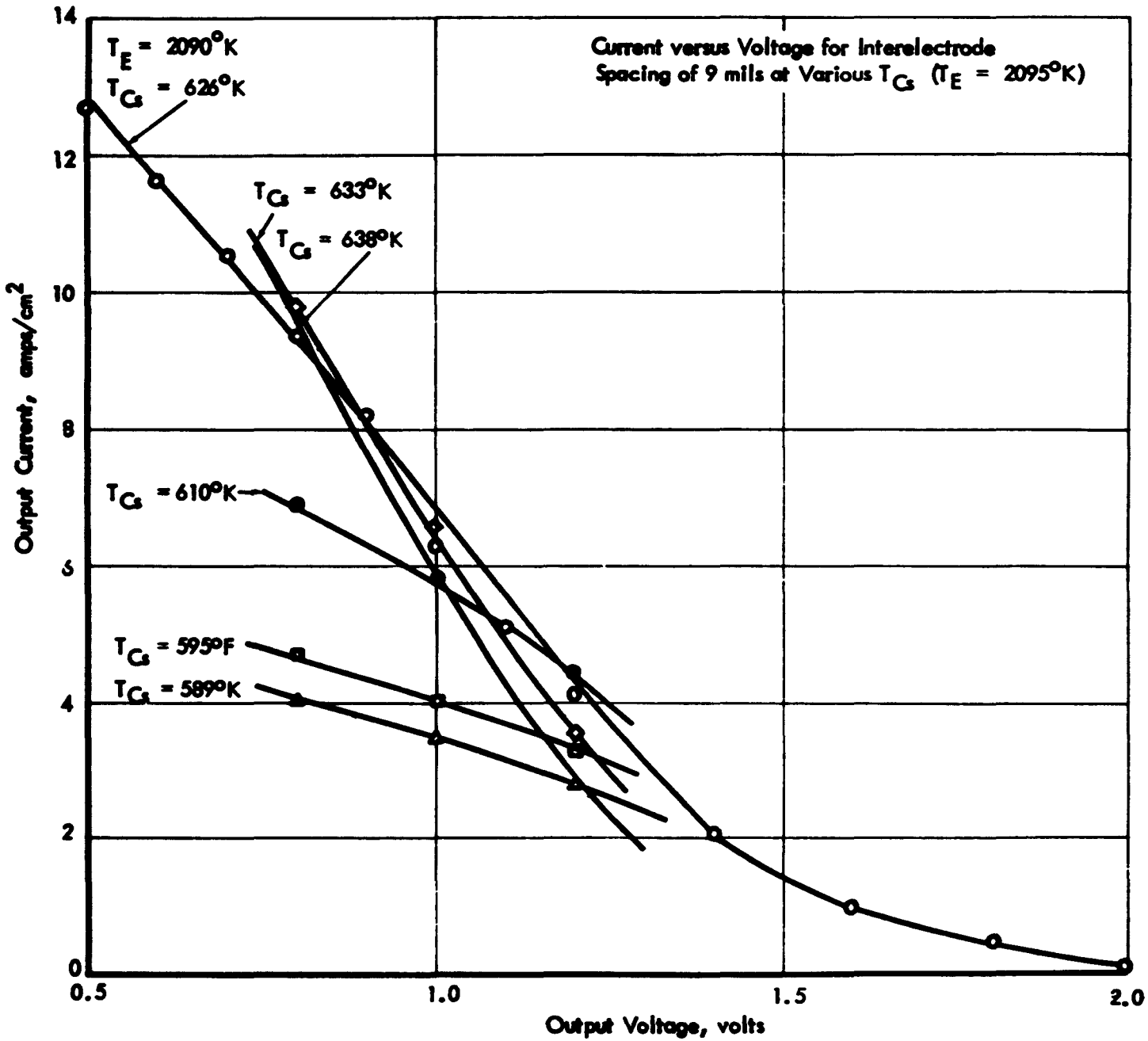

Fig. 3.1.9

respect to emitter, collector and cesium reservoir temperatures and inter-electrode spacing are significant and useful, the magnitude of the values of power density and current density must be discarded in favor of more recent experimental results. At the time that these experiments were performed, however, the results provided a much-needed framework for guidance in converter design.

3.1.3 Thermionic Generator Tests and Evaluation

Introduction

Two thermionic generators have been built under this program. The objective of the program is to obtain data on the performance of two promising state-of-the-art thermionic generators which can be utilized in the development of a prototype generator for incorporation in advanced thermionic power systems in the 1-10 KW range for aerospace applications. The first generator assembly consisted of two 200-watt cylindrical geometry converters connected in series with a DC-DC converter to raise the output voltage from 2 to 28 volts DC. A complete description of the two-converter generator and the test program carried out on this cylindrical configuration is presented in Part I of the Performance Test Report, Item IV under contract No. AF 33(616)-7411. The second generator assembly, called the cubical cavity thermionic generator, was subsequently tested and the pertinent data was presented in Part II of the Performance Test Report.

This second generator configuration consists of five thermionic converters of identical design mounted in a cubical block. The converters are shaped so the emitters form a small cubical cavity absorber within the generator assembly. This configuration differs from the cylindrical geometry converters in that a higher output voltage can be obtained from a single assembly of converters that form the solar cavity absorber for a single solar concentrator. The cavity is efficient in utilizing solar energy, and the converter design is felt to be far more reliable from the structural standpoint.

200-Watt Cylindrical Generators

Systematic tests have been carried out on the two 200-watt thermionic converters. A complete set of characteristic performance curves has been obtained for both converters under a variety of operating conditions. Sufficient data have been obtained to permit a complete optimization of all pertinent parameters for this converter configuration. The characteristic data is intentionally related to input power to fulfill the need under this program for an evaluation of converter performance associated with a constant power input from a solar concentrator. The presentation is extended,however,

to relate overall performance to emitter temperature to permit a comparison with data generated by other investigators and to simplify the analysis of converter performance.

Each of the converters was found to function well during all tests. Units #1 and #2 were shown to possess an overall efficiency of 10.6 and 13.6% respectively as determined by the ratio of electrical output to total electrical input. Unfortunately, some performance degradation was observed in Unit #2 in the course of the testing. A decline of about 1.5% was observed in Unit #2. Unit #1 on the other hand had experienced an improvement of about the same magnitude during the first few test runs,thereby raising its efficiency from 9% to nearly 10.6% under optimum conditions. The reasons for these changes are not known for certain, nor is a complete explanation available for the difference in performance between units #1 and #2. The most logical explanation that can be made at this time is that impurities and outgassing cause the difference noted in these units. However careful examination of the disassembled converter #2, which failed during the test series and was subsequently rebuilt, showed no sign of contamination or breakdown of the electrode materials.

As experience was gained in the operation of the converters it was found possible to extend the operational and data range. At first some concern was felt over the possibility of overheating the emitters, and overstressing the seal assembly in the higher voltage or open circuit region of testing. Fortunately, as the test proceeded it was found possible to make what are felt to be fairly accurate readings of temperature in the emitter cavity despite complications of geometry and electron bombardment heating. Because of this it was then possible to observe temperature changes which resulted from load variations and assure that no damage would result from the practice of testing over the entire voltage scale of the converter. This extension of the test region,coupled with the pyrometric temperature measurements,subsequently permitted the generation of complete parametric type performance data.

Following the completion of individual tests the two converters were connected in series and operated as a generator. The combined output of the converters in series was found to be about 320 watts under optimum conditions,but the

overall output with the DC-DC converter as part of the generator assembly was only 149 watts due to the relatively low efficiency of the electronic circuitry. The mismatch between the thermionic generator which produced maximum power output at 1.5 volts with the two converters in series, and the DC-DC converter which was designed for maximum performance at 2 volts reduced overall efficiency to about 5%.

Of particular importance in the series testing was the observation of a passive mode of operation in the converters. In this mode it was noted that a converter in series can actually be made to operate as a simple forward-conducting diode or even as a power consuming element in the circuit. This mode of operation is induced by improper maintenance of cesium coverage on the emitter.

An attempt to analyze converter performance data was also made using current theory. Here some discrepancies were noted. The principal source of difficulty seems to stem from the fact that in the high current regions the thermionic converters act like purely resistive devices. From this it is suggested that the mechanism of operation is not adequately understood, and that methods used to calculate plasma impedance are not adequate. It is concluded that more data will be required from converters of different configurations and of different materials to more clearly define the high pressure plasma mode of operation.

Test Equipment and Procedures

The basic vacuum test stand is shown in Figure 3.1.10. This photograph shows a single converter mounted on the right half of a 4 inch dual vacuum system. Also shown are the low impedance water-cooled load bank on the front of the stand, the main bombardment power supply, piggy back filament heater, thermocouple potentiometer, vacuum control panel and assorted meters for measuring converter characteristics and power outputs. Also shown are several of the blowers used to cool the pyrex vacuum envelope and the nitrogen reservoirs and supply tank. Not shown is the pyrometric equipment used to obtain temperature measurements in the emitter cavity.

DUAL VACUUM TEST STAND

Fig. 3.1.10

200 Watt Converter Assembly

The converter configuration used in this test program is shown in the half section view in Figure 3.1.11. This design utilizes an emitter which is compatible with solar powering. The cylindrical cavity emitter configuration is an efficient absorber of radiant energy. It can be seen that by removing the electron gun assembly and modifying the thin support section between the emitter and emitter radiator this assembly could be made to accept concentrated solar energy.

The following general specifications and dimensions apply to this configuration:

Emitter material	- tantalum
Collector material	- copper
Electron gun	- molybdenum
Filaments	- tungsten
Insulator assembly	- high density alumina
Emitter diameter	- 1.06 inches
Emitter length	- 1.45 inches
Electrode spacing	- 0.006 inches
Emitter area	- 31 cm^2
Emitter design temp.	- 2000°K
Collector design temp.	- 915°K

The performance characteristics under constant input power conditions are shown in Figures 3.1.12 and 3.1.13 for near optimum conditions for Unit #1. Figure 3.1.14 shows a comparable optimized curve for Unit #2 showing an overall efficiency of 13.6% at over 200 watts output. The operation of the converters under non-optimum conditions with a constant input power can be summarized as in Figure 3.1.15 shown for Unit #2 with a variety of cesium temperatures.

The tests carried out were directed towards developing optimization curves of cesium temperature, collector temperature, and load voltage as a function of emitter temperature, as shown in Figures 3.1.16, 3.1.17, and 3.1.18.

SECTION DRAWING OF 200-WATT CONVERTER

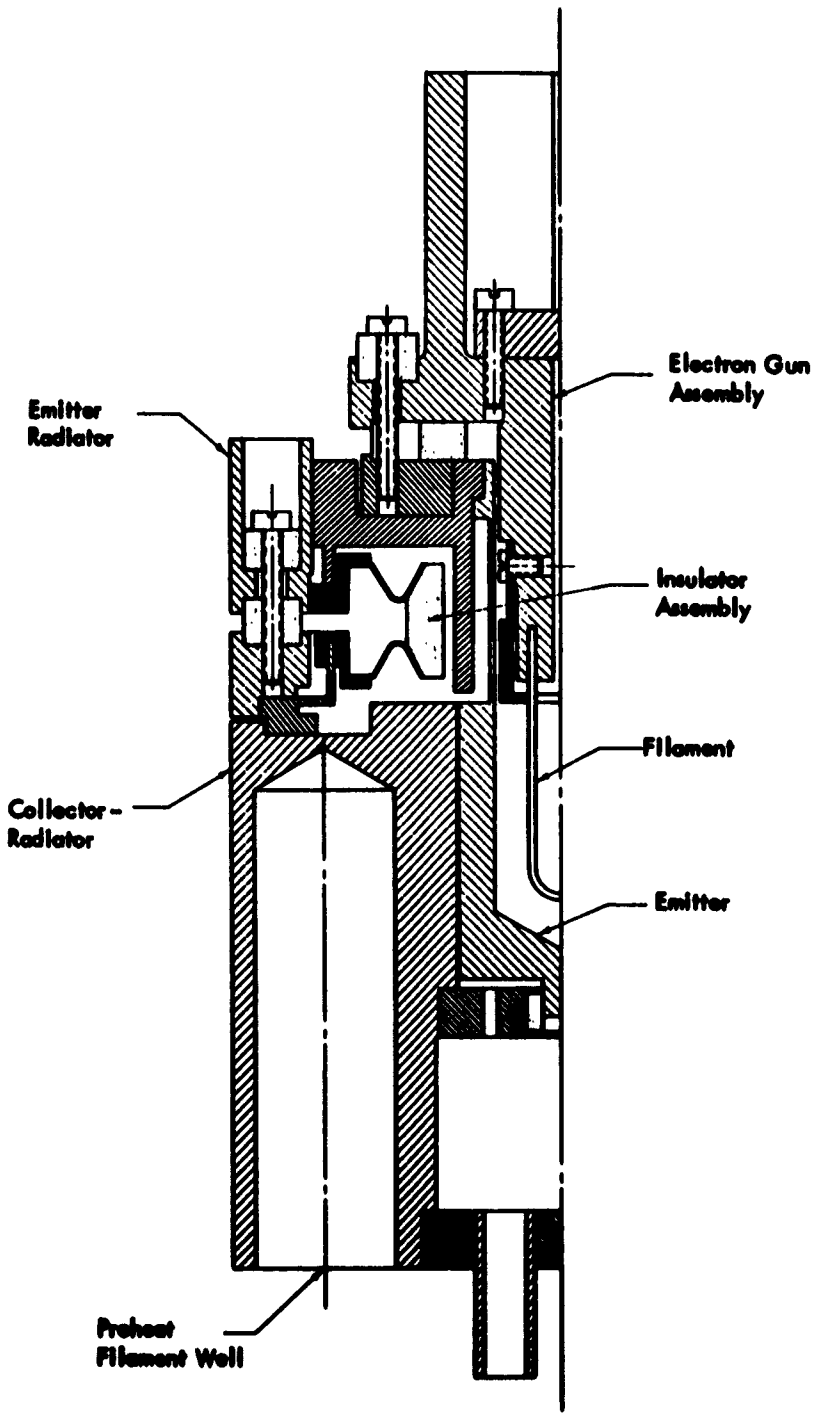

Fig. 3.1.11

EI CHARACTERISTICS, UNIT # 1, 1720 WATT INPUT POWER

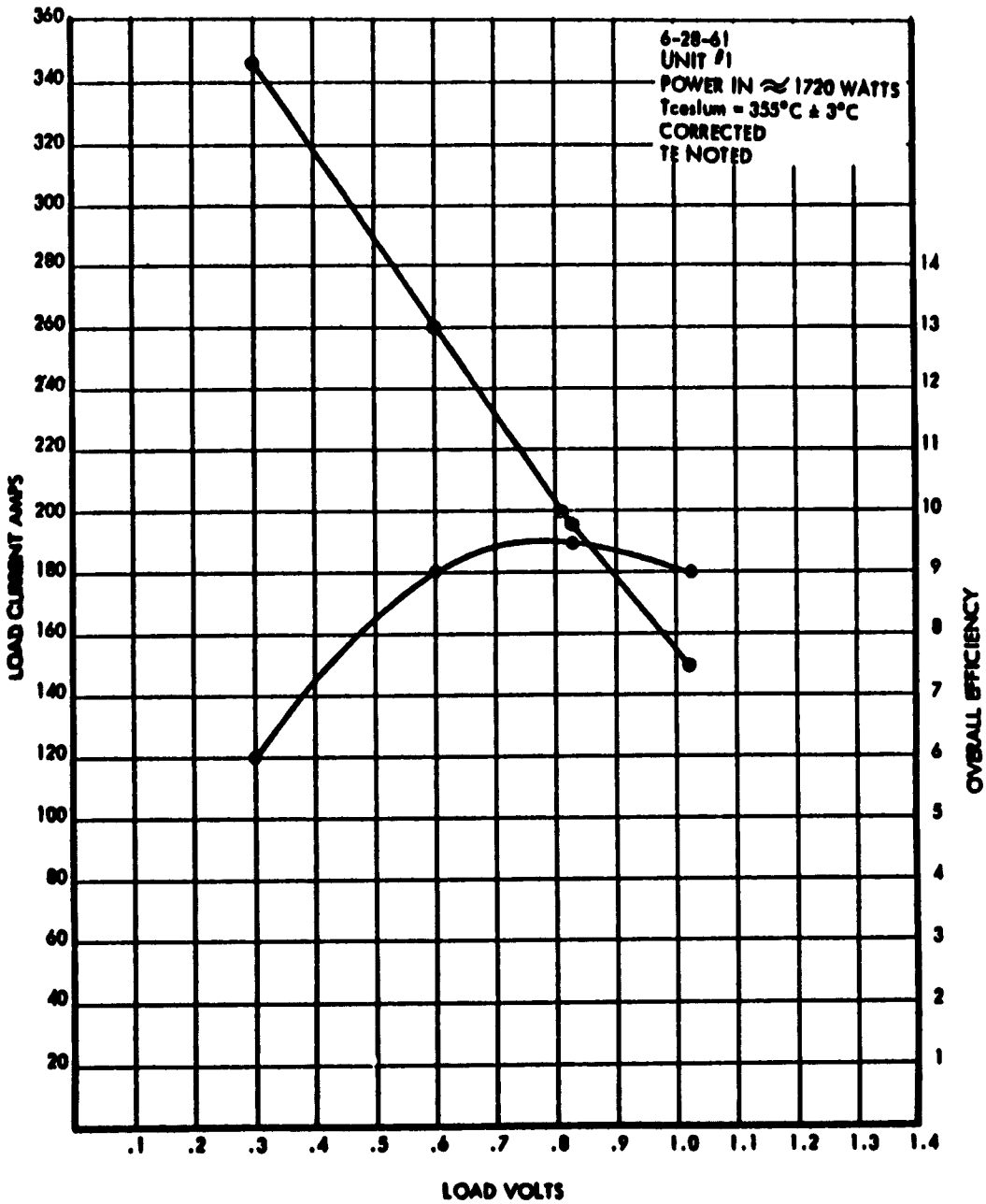

Fig. 3.1.12

EI CHARACTERISTICS,UNIT # 1, 1425-WATT INPUT POWER

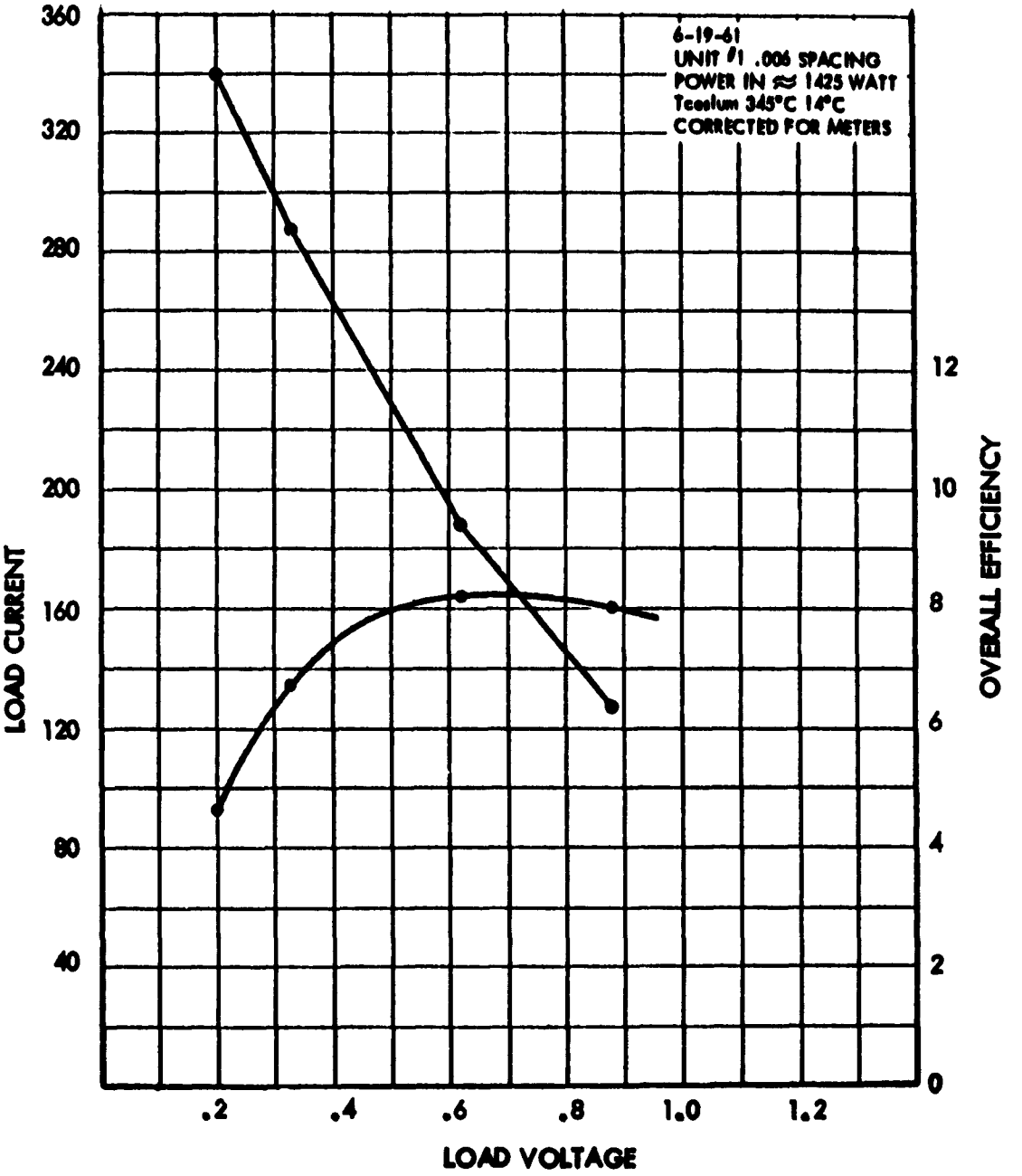

Fig. 3.1.13

EI CHARACTERISTICS,UNIT # 2, ACCEPTANCE TEST

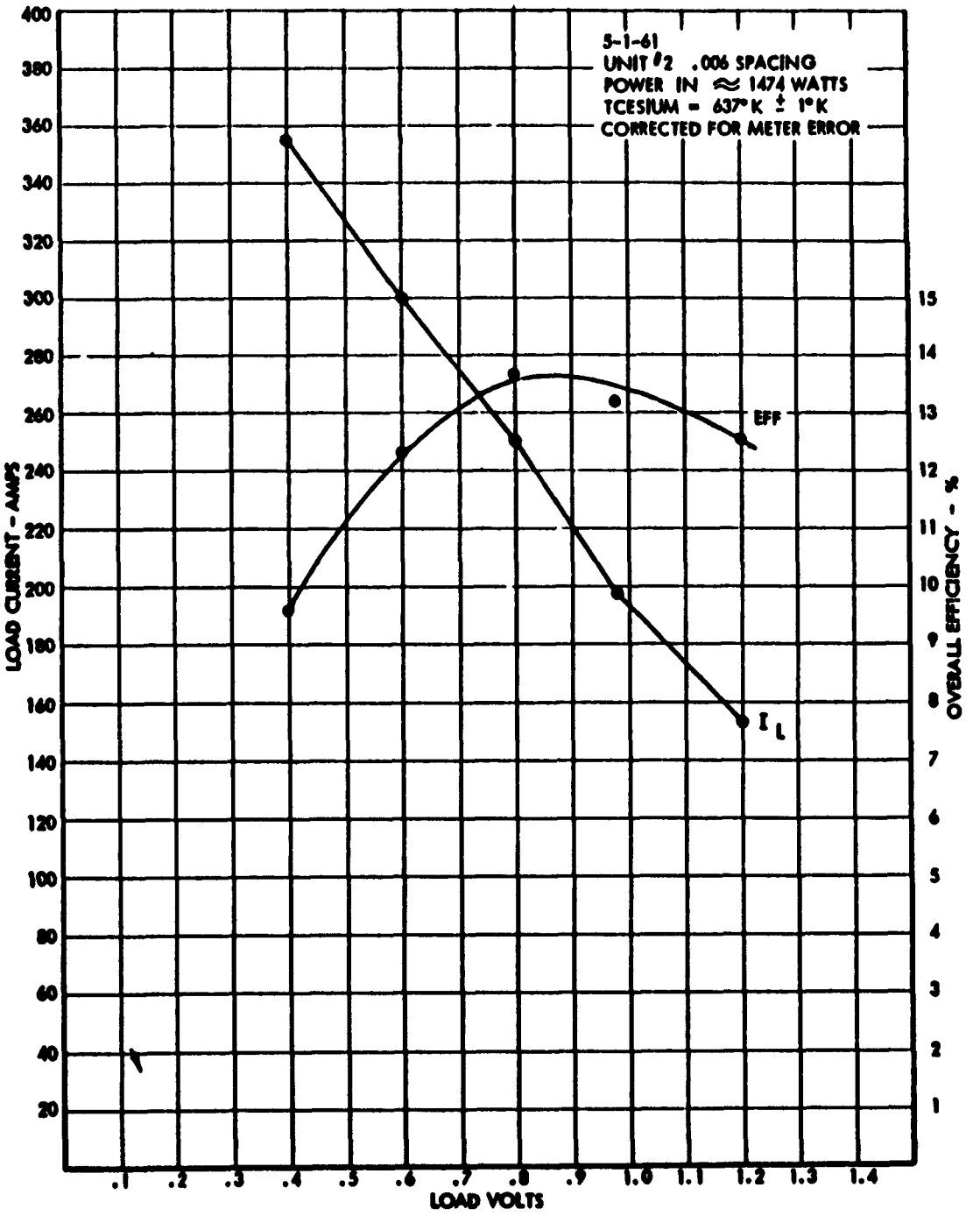

Fig. 3.1.14

COMPOSITE PLOT - UNIT #2 - VARIOUS Tcs VALUES

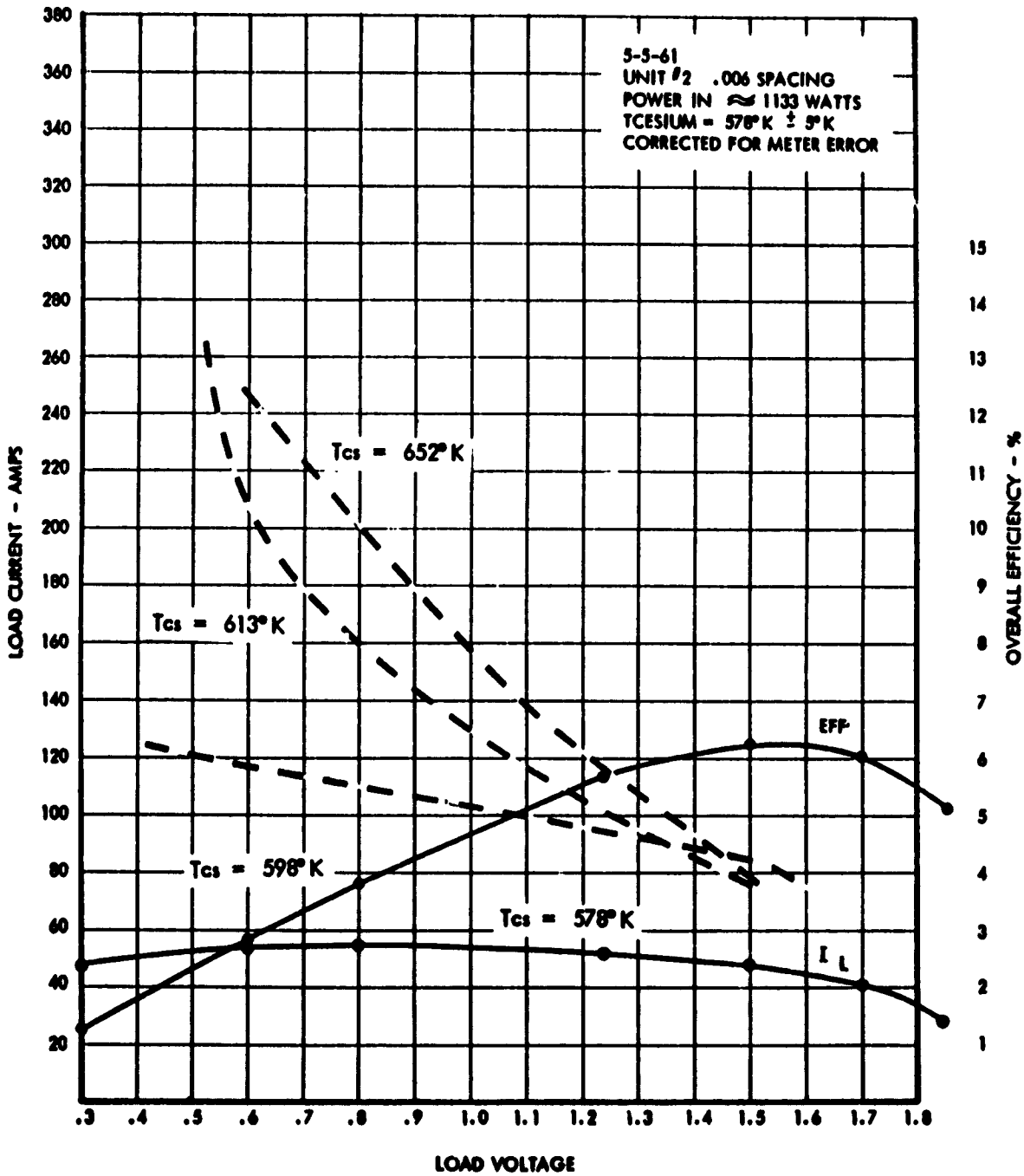

Fig .3.1.15

COMPOSITE DATA PLOT

OPTIMUM CESIUM TEMPERATURE VERSUS EMITTER TEMPERATURE

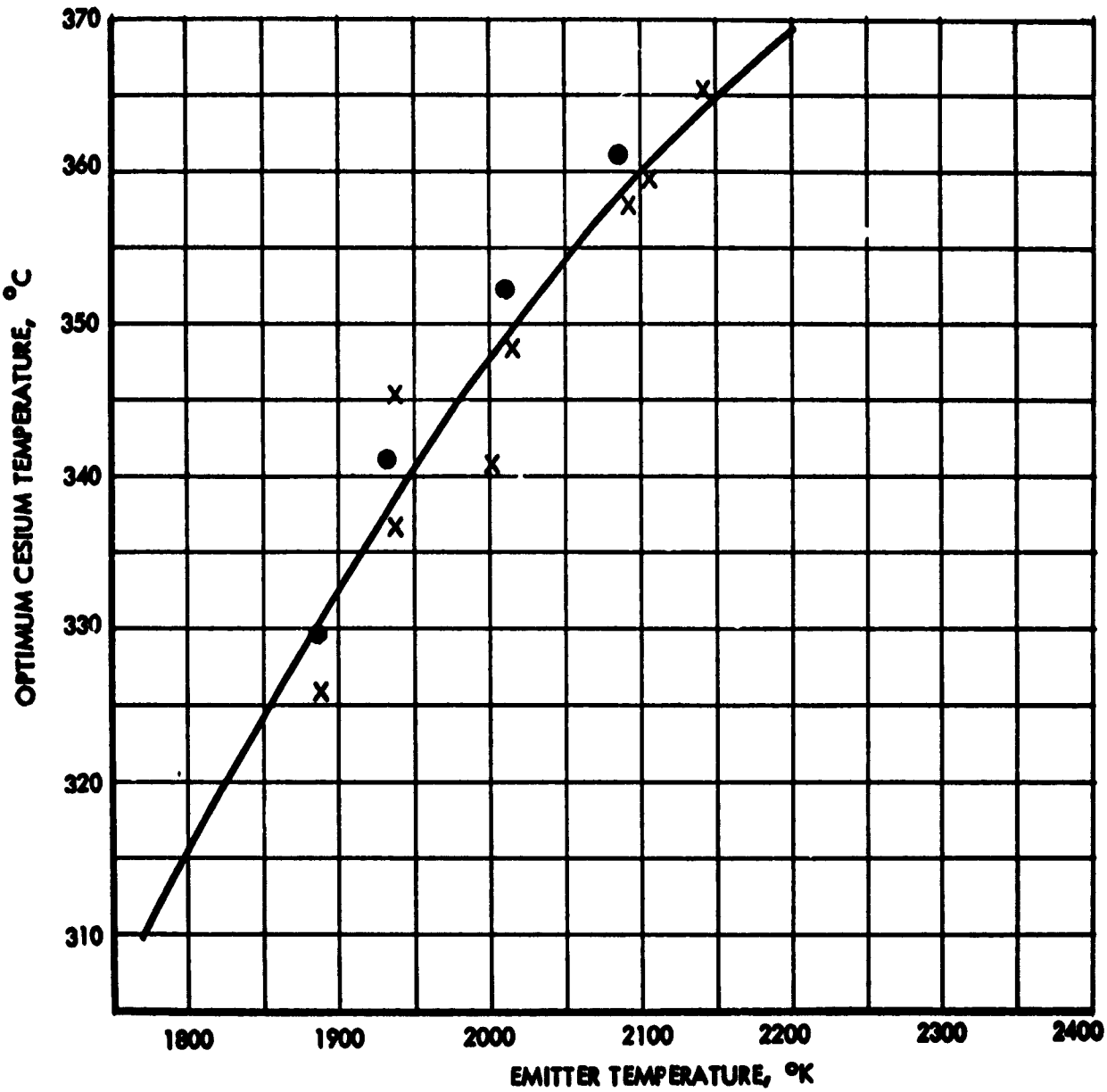

Fig. 3.1.16

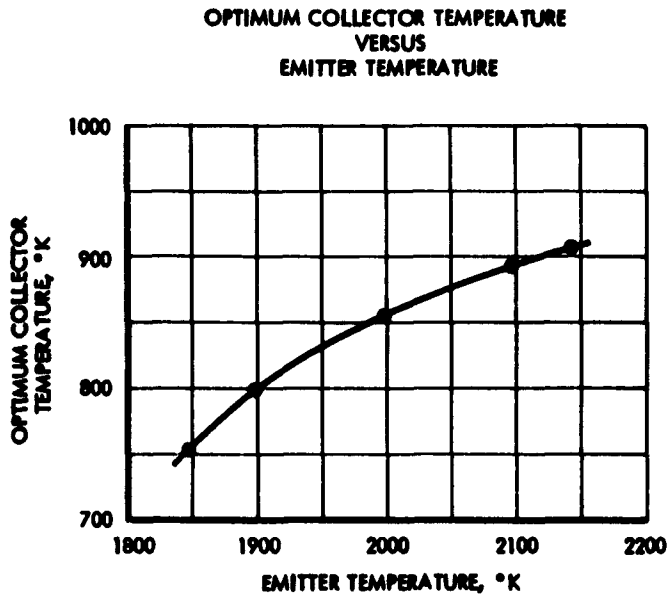
OPTIMUM COLLECTOR TEMPERATURE
VERSUS
EMITTER TEMPERATURE
OPTIMUM COLLECTOR TEMPERATURE, °K
1000
900
800
700
1800
1900
2000
2100
2200
EMITTER TEMPERATURE, °K

Fig. 3.1.17

OPTIMUM LOAD VOLTAGE VERSUS EMITTER TEMPERATURE
FOR .006 SPACING

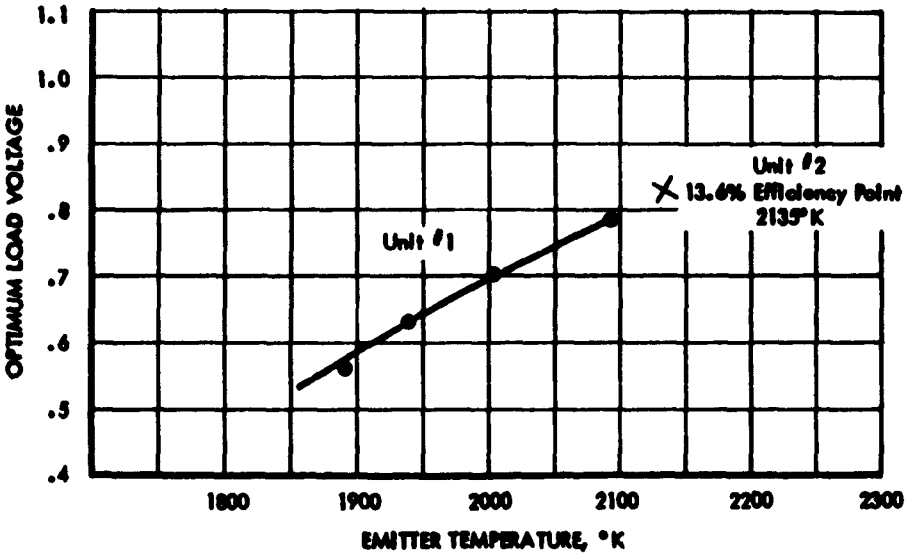

Fig. 3.1.18

Universal Characteristic Performance Map

From the data relating temperature, power input, and load current, a universal performance map was developed. By plotting the load voltages measured at the various current levels for each power input, as shown in Figure 3.1.19, a well defined picture of converter characteristics emerges. As shown in Figure 3.1.20, a plot of temperature versus voltage can be generated with current on a per square centimeter basis as a parameter. With this second figure, it is possible to determine the load characteristics of a converter for any given temperature. These data are applicable to any converter design and will indicate the optimum performance if the same materials, spacing, and optimum or near optimum values of cesium and collector temperature are used.

Series Operation of Two 200-Watt Cesium Vapor Converters

At the completion of individual testing, both units were connected and operated in series. The converters were made to operate satisfactorily at a reduced overall efficiency, but a basic problem connected with series operation was uncovered. The solution to this problem was to operate the converters at other than optimum cesium pressures with some sacrifice in performance.

Both converters were series connected and brought up to what had been optimum conditions in previous tests. Measurements showed that under these conditions very little power was actually delivered to the load. In fact, one converter, Unit #2, seemed to be acting as part of the load. The polarity of the voltage across this unit had reversed. Unit #1 had a + 0.8 voltage, Unit #2, a - 0.6 volts with + 0.2 volts appearing across the load at a 200-amp current level. Overall efficiency in this condition was less than 2%.

By increasing cesium pressure or reducing the emitter temperature in Unit #2, the polarity could be made positive and the load power greatly increased. It is apparent that the cause of the voltage reversal is associated with emitter work function, and, in particular, with an increase in work function due to a deficiency in cesium coverage. Subsequent adjustments in cesium temperature gave a new set of optimum conditions for series operation. Peak outputs of nearly 310 watts at 9.5% overall efficiency were obtained.

THERMIONIC CONVERTER UNIT # 1
PERFORMANCE CHARACTERISTICS

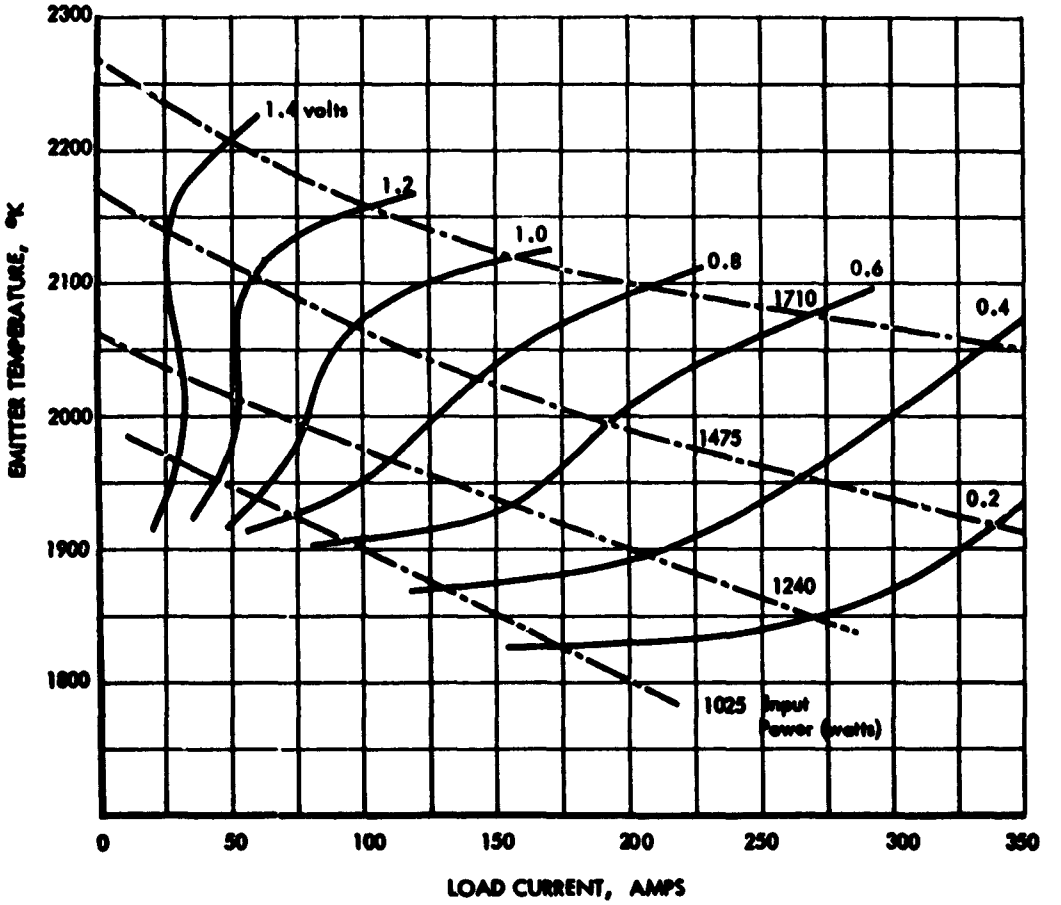

Fig. 3.1.19

THERMIONIC CONVERTER PERFORMANCE WITH
CURRENT AS THE PARAMETER

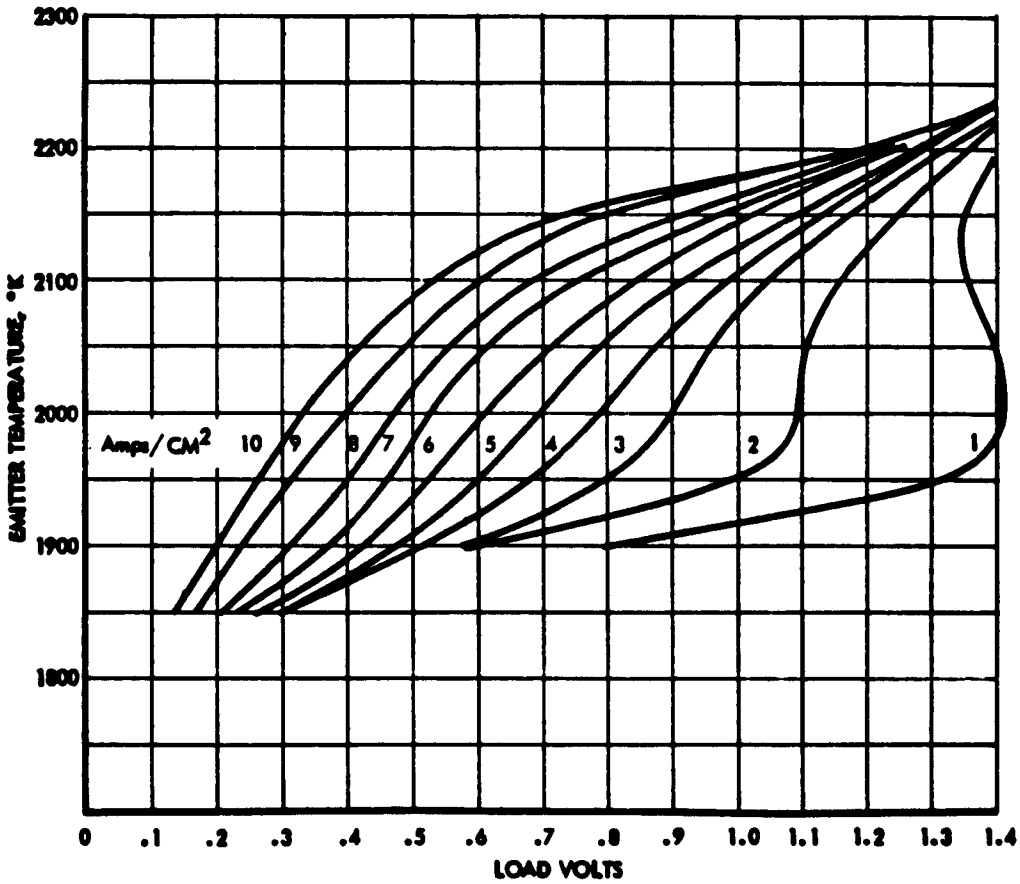

Fig. 3.1.20

The plot of the series data presented in Figure 3.1.21 is a composite of data obtained during tests conducted on two separate days. The cesium pressure and input power levels are nearly the same for all points, however, and the voltages noted for each individual converter were approximately the same. Unfortunately, the premature failure of converter #2 under test restricted a further examination of factors affecting series operation.

At first it was concluded that the previously noted difference in efficiency between Unit #1 and #2 was responsible for reversion to the passive mode of operation. It appeared that Unit #2 had to be deliberately operated at a non-optimum point as indicated by the fact that a 380° cesium temperature was required to obtain a condition where the voltages were approximately equal and additive. Closer examination of the data sheets, however, disclosed that it is quite possible that a leak in Unit #2 was causing a reduction in the plasma pressure.

It was noted on the data sheet of this test that the vacuum in chamber #2 had risen to 4×10^{-5} mm Hg. This would indicate the possible introduction of a high-vapor-pressure substance such as would be experienced with a cesium leak. It follows that if cesium vapor were leaking out of the converter a higher pressure would be required in the cesium reservoir to insure a sufficient quantity of cesium vapor in the interelectrode space,and to make up for the decline in pressure that would be associated with a leak into the vacuum chamber.

The test carried out on the 200-watt converters covering a wide variety of loads such as motor, resistive, static converter and others under steady state and transient or cyclic conditions demonstrated the feasibility of using thermionic converters for orbital applications. The relatively high failure rate associated with the cylindrical geometry generators also indicates the need for further development and improvement to make the utilization of this highly efficient configuration practical.

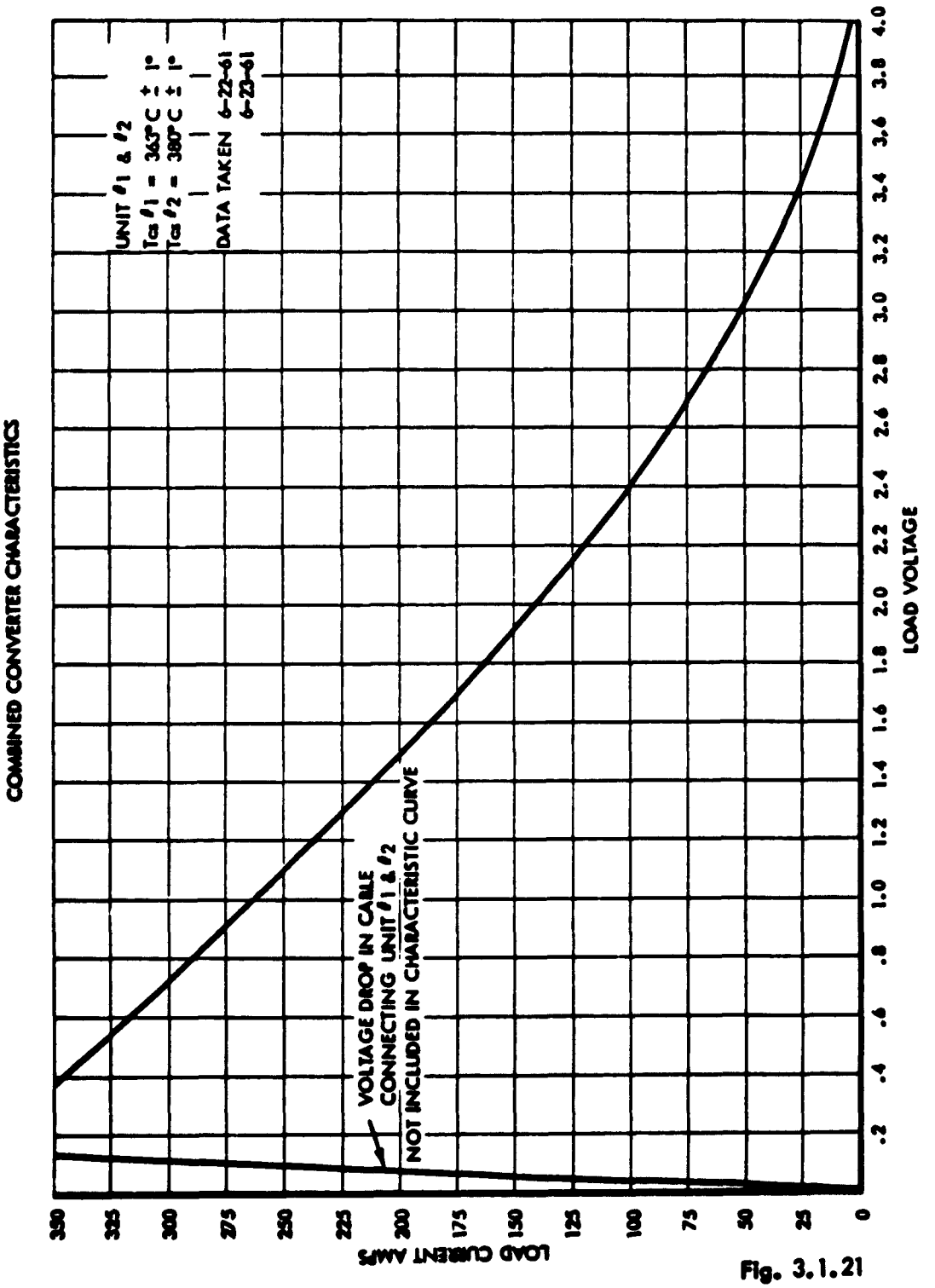
COMBINED CONVERTER CHARACTERISTICS
UNIT #1 & #2
Tca #1 = 365°C ± 1°
Tca #2 = 380°C ± 1°
DATA TAKEN 6-22-61
6-23-61
VOLTAGE DROP IN CABLE CONNECTING UNIT #1 & #2 NOT INCLUDED IN CHARACTERISTIC CURVE
LOAD CURRENT AMPS
350
325
300
275
250
225
200
175
150
125
100
75
50
25
0
.2
.4
.6
.8
1.0
1.2
1.4
1.6
1.8
2.0
2.2
2.4
2.6
2.8
3.0
3.2
3.4
3.6
3.8
4.0
LOAD VOLTAGE

Fig. 3.1.21

The Cubical Cavity Generator

The concept of a cubical cavity generator was the result of a desire for a thermionic generator which would have an output potential of about five volts from a single solar concentrator, single generator configuration. Therefore, if the above stated objective is to be achieved, it is necessary to arrange a group of converters so that the emitter of each is close to the focal point of the concentrator and so that the converter leads may be connected in series. The arrangement must be such that the maximum amount of energy which is directed to the focal point by the concentrator is absorbed by the converters.

By arranging five flat converters to form a cubical cavity, the heat losses are reduced with a minimum of complication to the converter. The sixth side of the cubical block faces the solar concentrator and admits the concentrated solar energy. The system is designed so that the focal plane of the concentrator is coincident with cavity aperture.

Initially, the objective was the development of a laboratory prototype generator to be heated by electron bombardment. The design goals for the converters to be used in this generator are given in Table 3.1.1. A generator design was prepared and development was begun. The result of this work was the converter which is shown in Figure 3.1.22.

Over 100 hours of testing were accumulated on this converter. The most significant results are given in Table 3.1.2. These tests taken together with data from other programs showed that a number of improvements could be made in both the converter and the generator design. At the same time it became desirable to fabricate a generator which could be solar tested in the TRW solar test facility. A complete redesign was, therefore, instituted.

The generator which resulted from the redesign is shown in Figure 3.1.23. This design allows solar flux from a 60° rim angle concentrator to reach the cavity and has a sufficiently massive support structure to permit conduction cooling of the block during solar test. The converter which was developed for this generator is shown in cross section in Figure 3.1.24. The reentrant emitter design is maintained but a simple tantalum emitter is used instead of tungsten. This change was made to simplify fabrication and improve reliability. The seal

TABLE 3.1.1

DESIGN GOALS FOR LABORATORY PROTOTYPE CONVERTER FOR CUBICAL CAVITY GENERATOR

Emitter Temperature	2000°K
Collector Temperature	1000°K
Cesium Reservoir Temperature	650°K
Emitter Area	4.12 cm^2
Interelectrode Spacing	4 mils
Output Voltage	1 volt
Output Current	41.2 amperes
Power Density	10 $watts/cm^2$
Power Output	41.2 watts

Fig. 3.1.22 40 WATT THERMIONIC CONVERTER

TABLE 3.1.2

LABORATORY PROTOTYPE CONVERTER CHARACTERISTICS

Emitter Material: Tungsten
Emitter Area: 4.28 cm^2
Emitter Temperature: 2048°K
Collector Material: Molybdenum
Collector Area: 4.28 cm^2
Collector Temperature: 923°K
Interelectrode Spacing: .004"

Voltage:	0.9 volt	1.0 volt
Power:	30.6 watts	27 watts
Power Density:	7.15 w/cm^2	6.35 w/cm^2

Cesium condensation temperature 645°K

$$\text{Efficiency} = \frac{\text{Measured Output}}{\text{Calculated Heat Rejected + Output}}$$

$$= 13.6\%$$

Operation: 116 hours, 23 cycles with no degradation

Specific Power: 12.25 watts per lb.

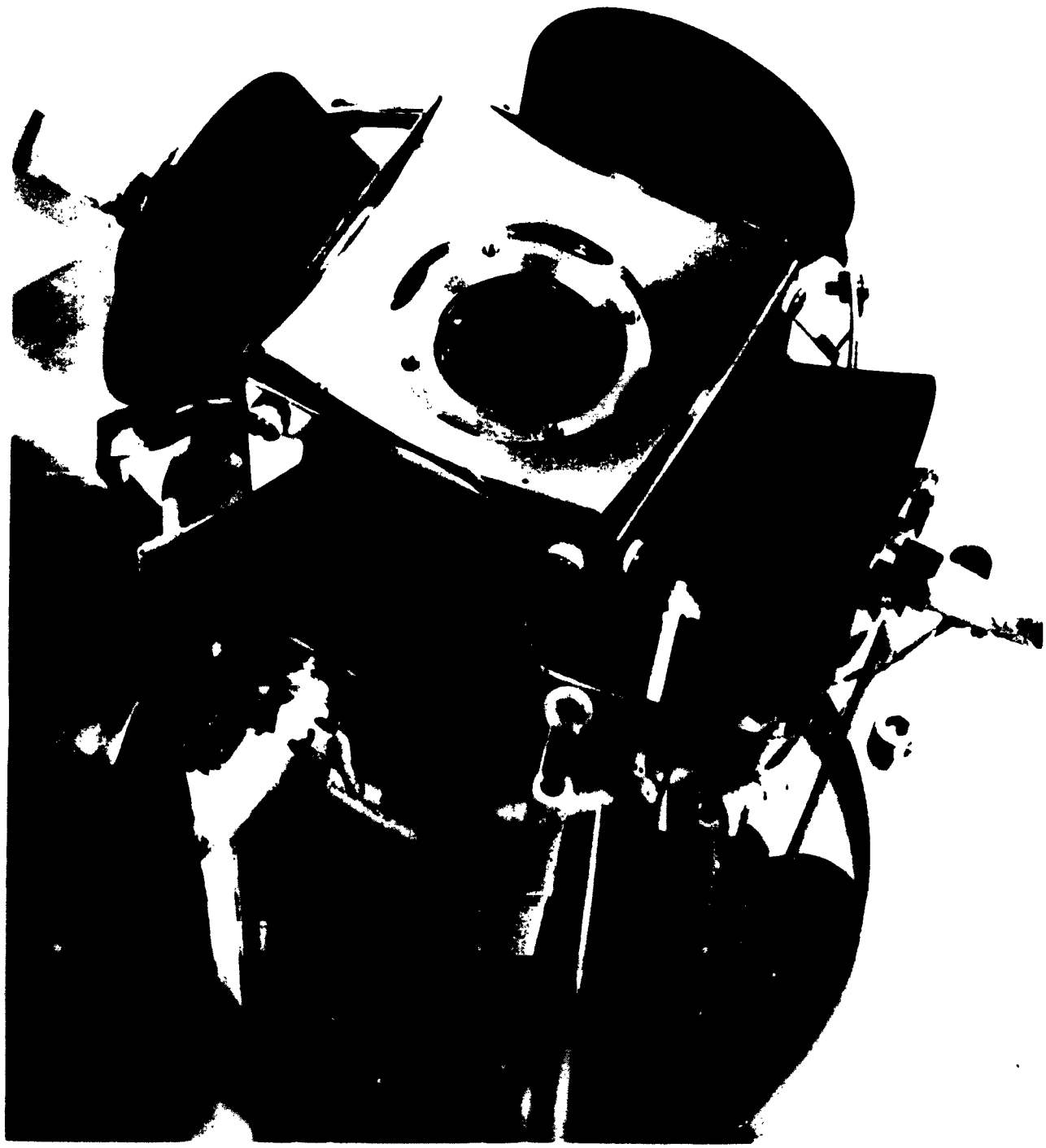

CUBICAL CAVITY GENERATOR ASSEMBLY

Fig. 3.1.23

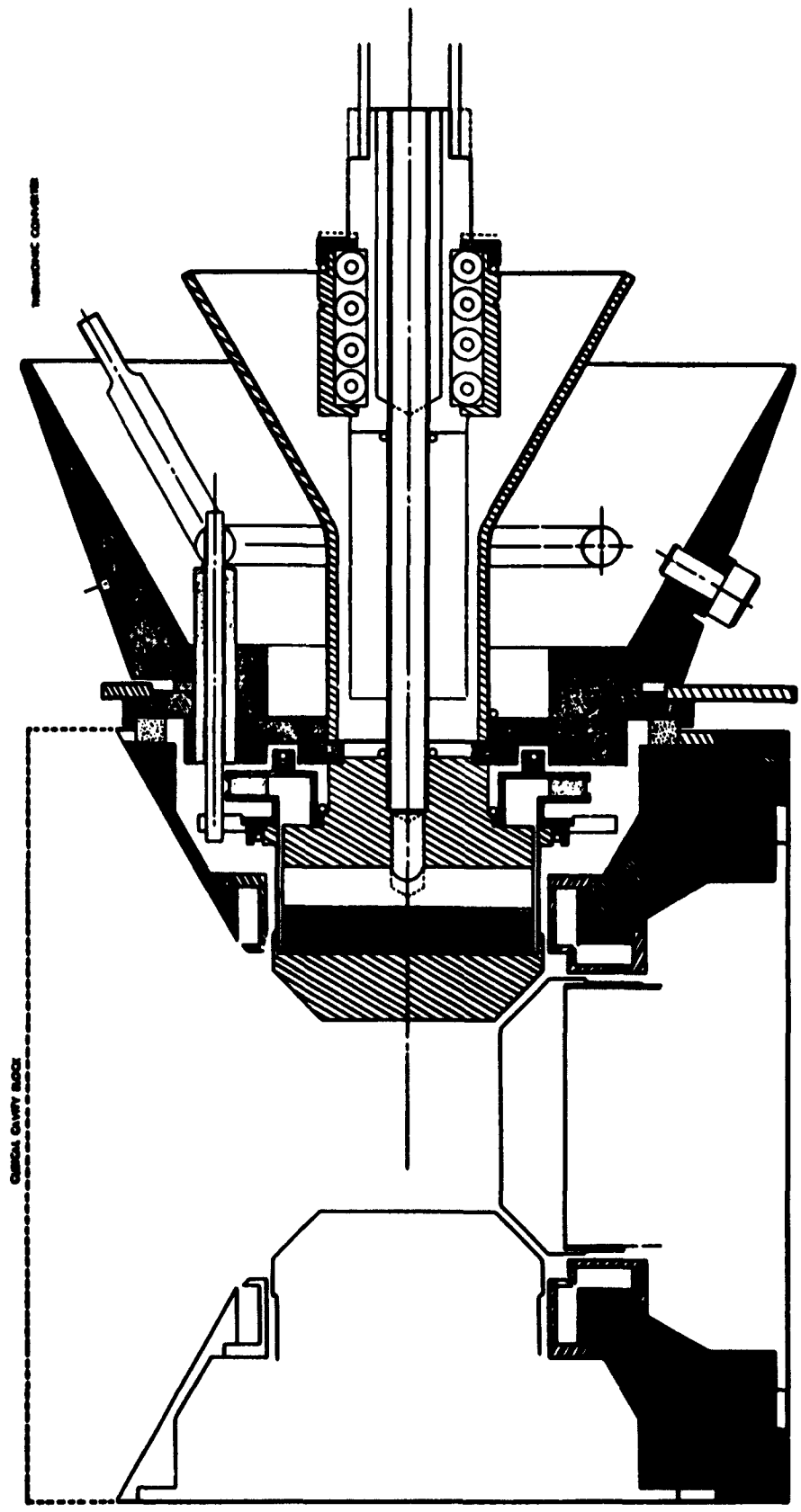

Fig. 3.1.24 Thermionic Converter and Clinical Cavity Block Assembly

structure is more compact and eliminates the space required by a floating type seal. Thus, the entire converter is smaller in diameter and the 60° rim angle for the aperture plate is obtained. The cesium reservoir is of such a nature that the converter can be operated in any position without difficulty. Even when the converter is inverted, the cesium will remain in the reservoir. Table 3.1.3 gives the design goals for the converter to be used in the cubical cavity generator. The actual converter is shown in Figure 3.1.25.

Preliminary tests were carried out on each of the five converters used in the cubical cavity assembly to determine individual characteristics and assure proper operation in the assembly. These preliminary tests indicated some differences in converter performance existed because the converters were found to develop different power outputs and to require slightly different cesium temperatures for proper operation with nearly the same emitter temperatures prevailing. These differences were small, however, and not of serious consequence so far as the generator performance was concerned.

The generator was found to function well under test. The generator demonstrated a performance capability comparable to the cylindrical geometry generator with the advantage of a higher output voltage available to the load. No deterioration in performance was experienced during more than 72 hours of laboratory tests. Also, the design was so nearly optimized as to permit operation near the design point without the need for cesium heater power input.

The nature of the electron bombardment heater circuits used in the laboratory test of this five-converter assembly precluded rapid start-up and cyclic testing. This is not felt to be a serious defect, however, since a prototype converter of identical design but not charged with cesium was capable of withstanding hundreds of on-off cycles without loss of structural integrity when tested alone. All other types of tests could be conducted satisfactorily with the cubical cavity generator assembly.

All pertinent data, including a reasonably good measurement of emitter temperature, was taken satisfactorily throughout the testing. It became apparent that there were some defects in the thermocouple instrumentation used to measure cesium and radiator temperature, but the errors introduced can be adequately accounted for.

TABLE 3.1.3

THERMIONIC CONVERTER SPECIFICATIONS FOR

100-WATT CUBICAL CAVITY GENERATOR

Emitter Temperature	2000°K
Collector Temperature	950°K
Cesium Reservoir Temperature	650°K
Emitter Area	3.08 cm^2
Interelectrode Spacing	2 mils
Output Voltage	1 volt
Output Current	20 amperes
Power Density	6.5 w/cm^2
Power Output	20 watts

20 WATT CUBICAL CAVITY CONVERTER

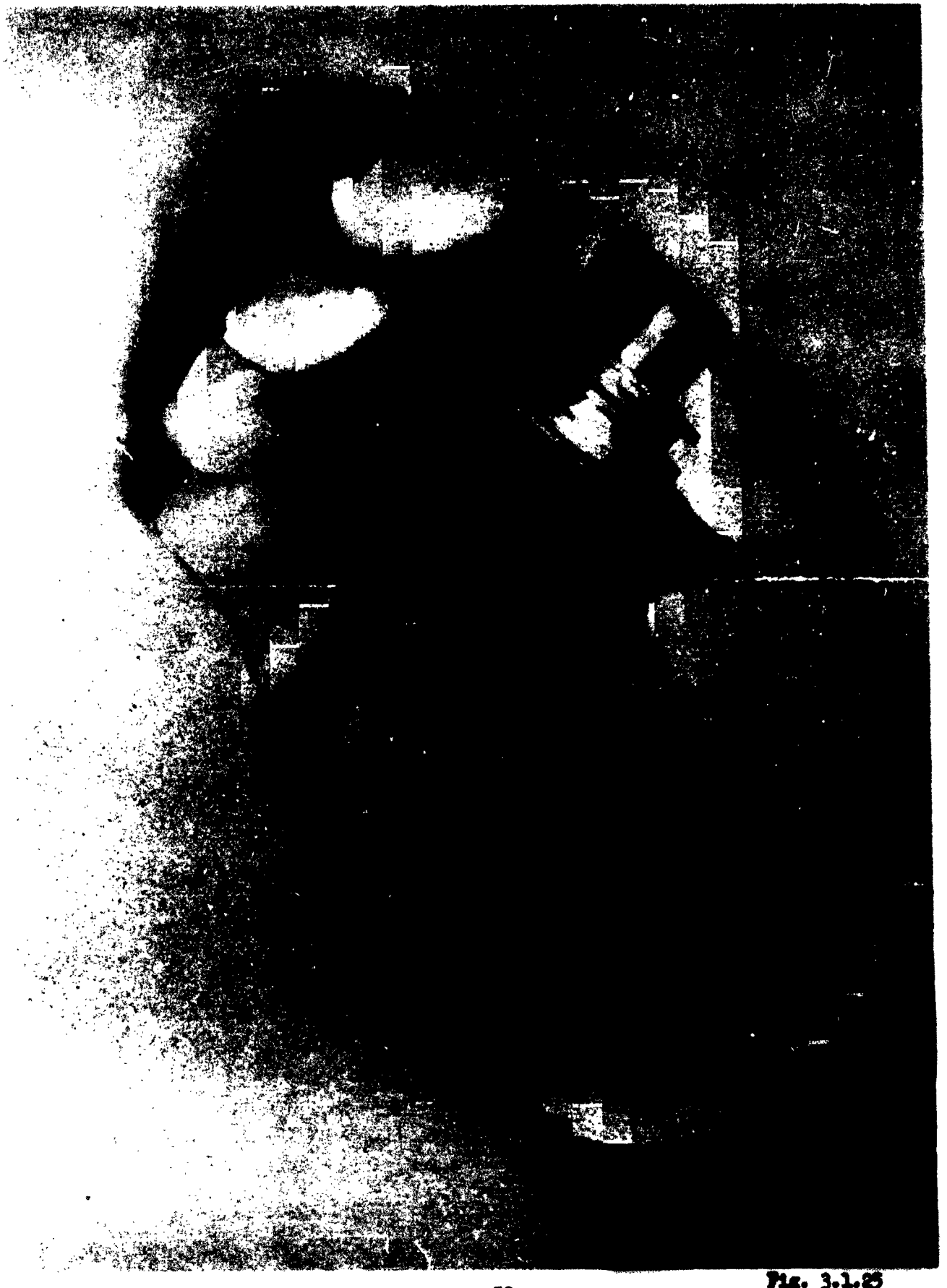

Fig. 3.1.25

Measurements of voltage and current are accurate and meaningful due to a novel loading technique which was employed in obtaining characteristic curves.

It was found that most of the data acquired on the two cylindrical generators was verified by the measurements made with the cubical cavity generator. In some instances, however, there were significant differences found in the operating characteristics of each generator type. The cubical cavity generator, for example, was found to be far less sensitive to cesium temperature variations, and the shape of the typical load curves does not change greatly from low cesium vapor pressure to relatively high vapor pressures for a given power input.

The complete generator, including all associated leads, electron gun assembly and vacuum feed through base plate, is shown in Figure 3.1.26.

The generator is shown mounted on the vacuum test stand along with other associated support equipment and instrumentation in Figure 3.1.27. The test set-up includes a vacuum system capable of maintaining vacuums of about 2×10^{-6} under operating conditions, a control and meter console with internal resistive loads, two DC and one AC power supplies, a dual channel recorder, XY plotter (not shown), a CVC cold cathode vacuum gage, and a 20-power Pyro Micro Optical Pyrometer. A multi-point switch is also used to select individual thermocouple readings on the generator for entry into one of the dual recorder channels. The vacuum system is also fitted with a liquid nitrogen cold trap and four auxiliary cooling fans directed at the bell jar enclosure.

Test Results - Cubical Cavity Generator

Numerous load characteristics curves were generated during the test activity. A series of typical I-V and efficiency curves are shown in Figure 3.1.28 to Figure 3.1.30. These curves were obtained for three different power inputs with optimum or near optimum cesium temperatures. The data points were obtained by the load-switching technique with the generator performance under nearly constant temperature conditions and under conditions of nearly constant cesium coverage.

One of the most gratifying features of the generator tested is its reduced sensitivity to variations in cesium coverage or reservoir temperature. Also, the generator was found to work reasonably well even when one or more of the con-

CUBICAL CAVITY GENERATOR & BASE PLATE ASSEMBLY

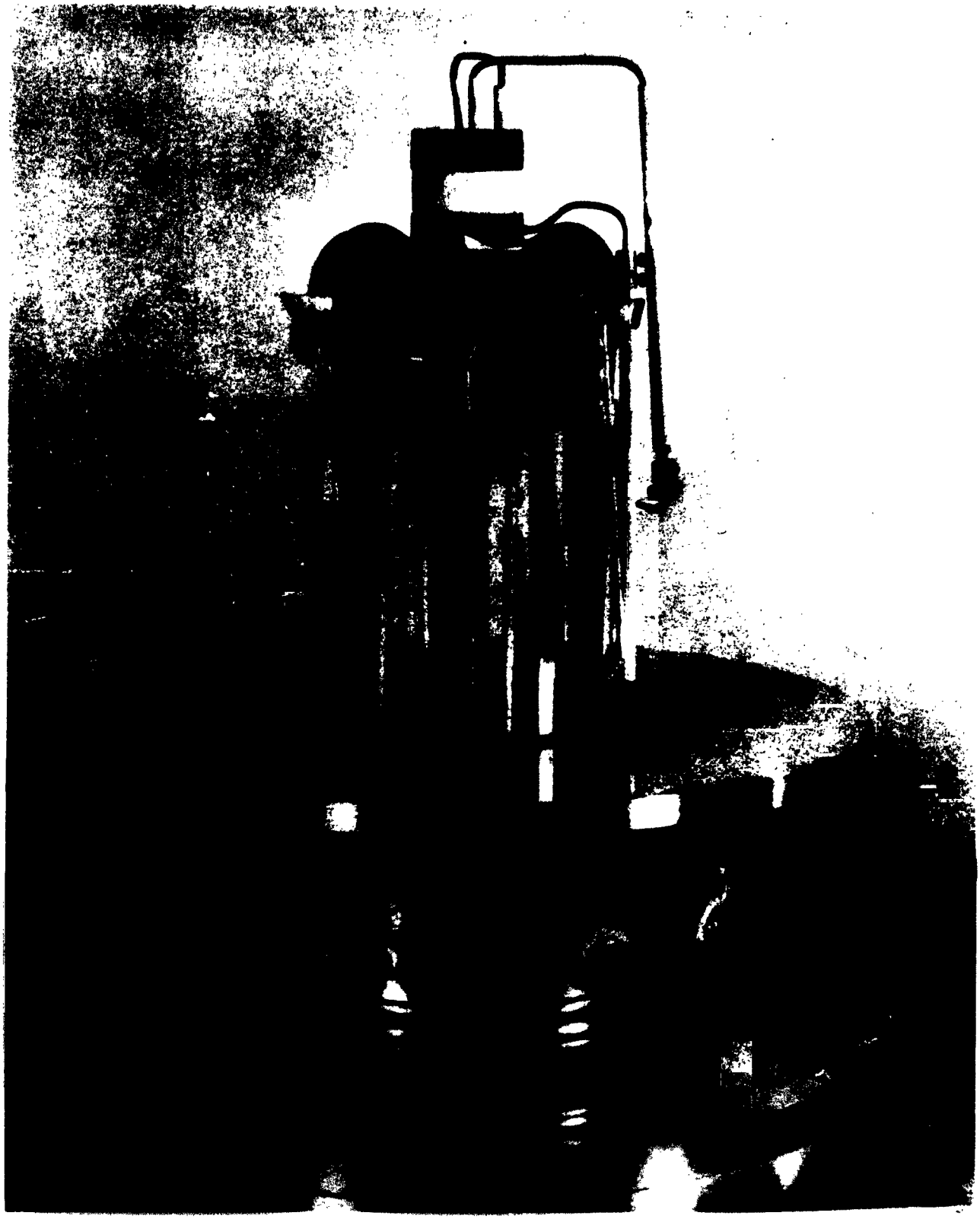

Fig. 3.1.26

Fig. 3.1.27 GENERATOR ON TEST STAND WITH ASSOCIATED SUPPORT EQUIPMENT AND INSTRUMENTATION

LOAD CHARACTERISTIC CURVES

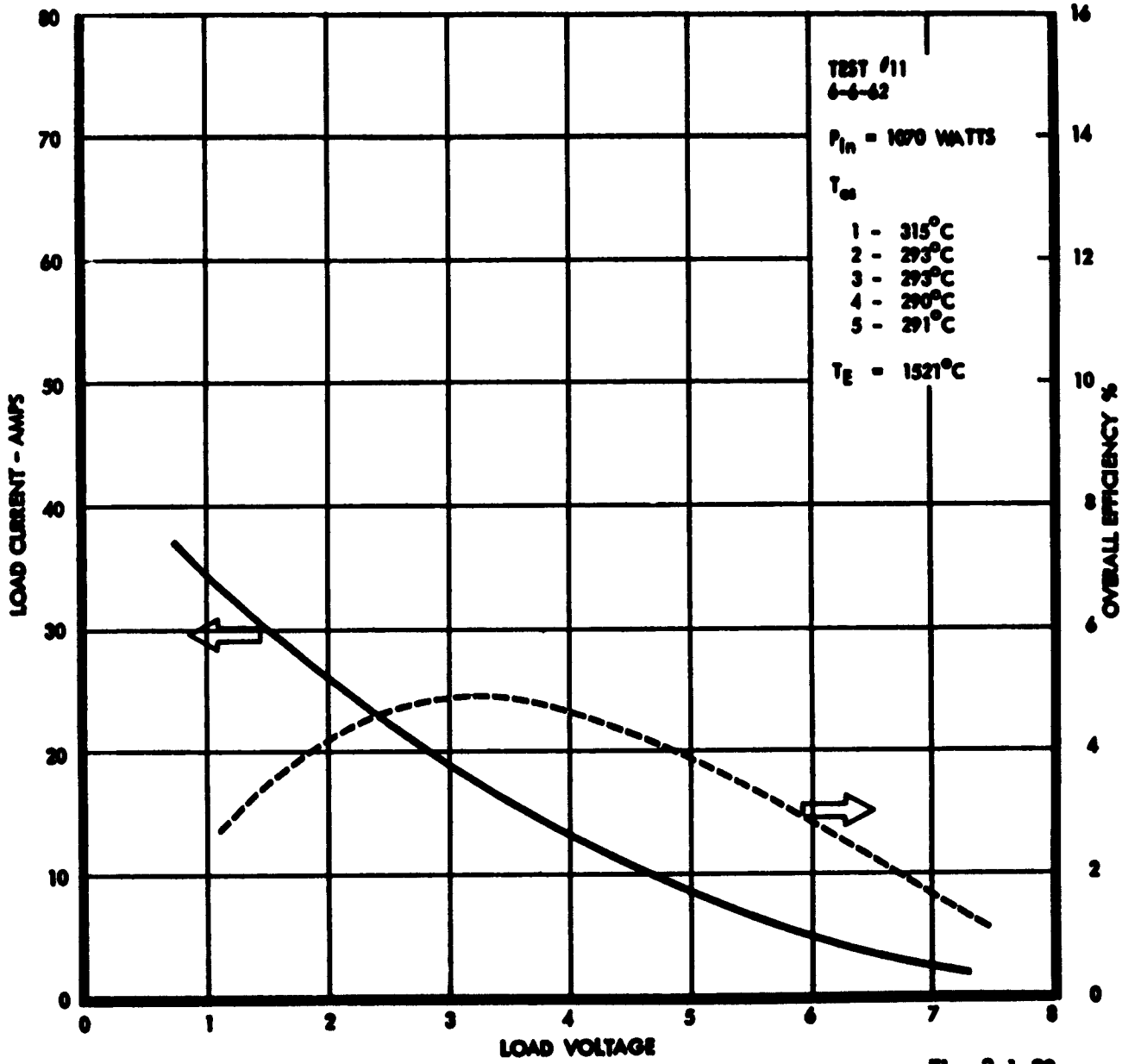

Fig. 3.1.28

LOAD CHARACTERISTIC CURVES

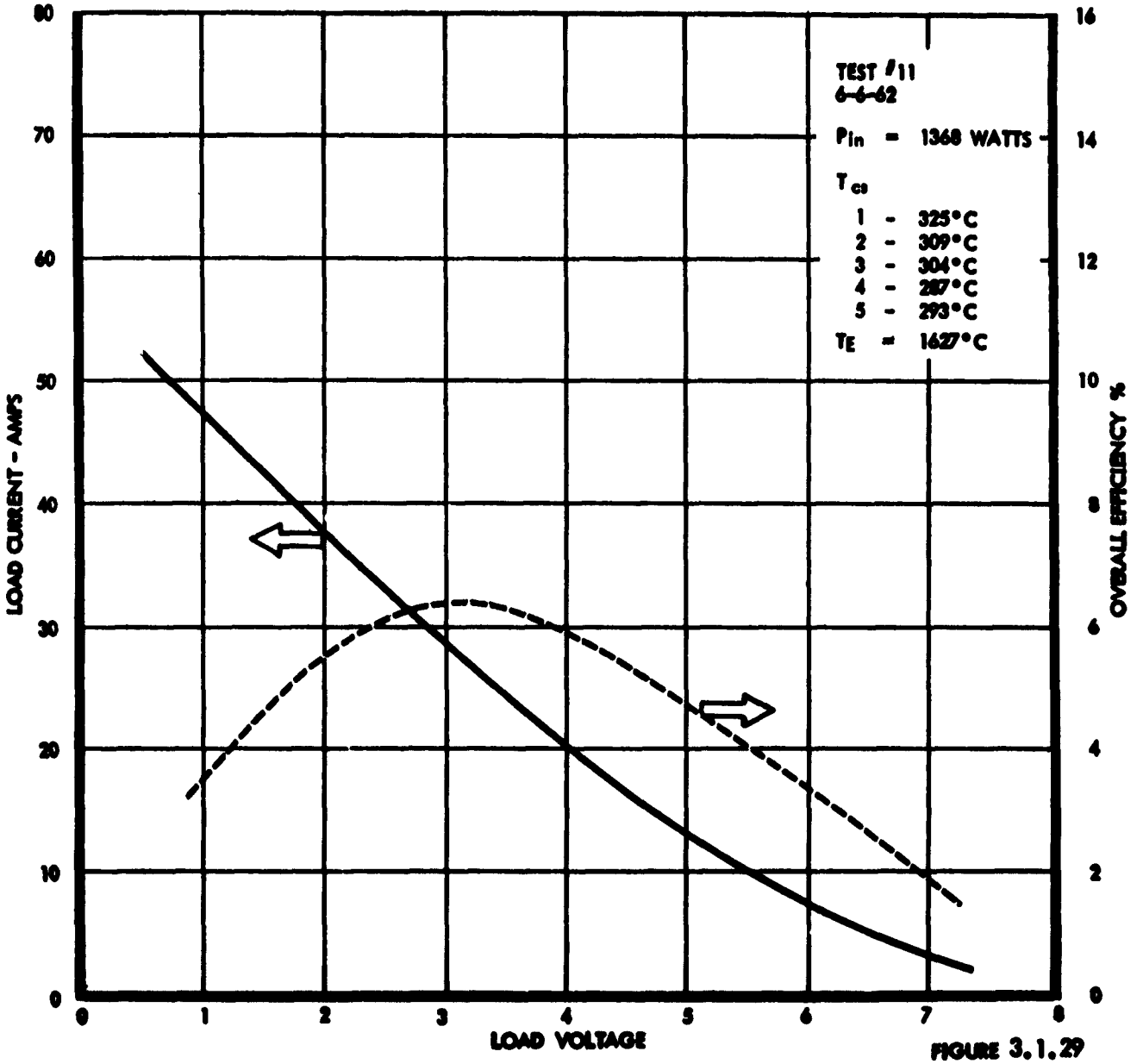

FIGURE 3.1.29

LOAD CHARACTERISTIC CURVES

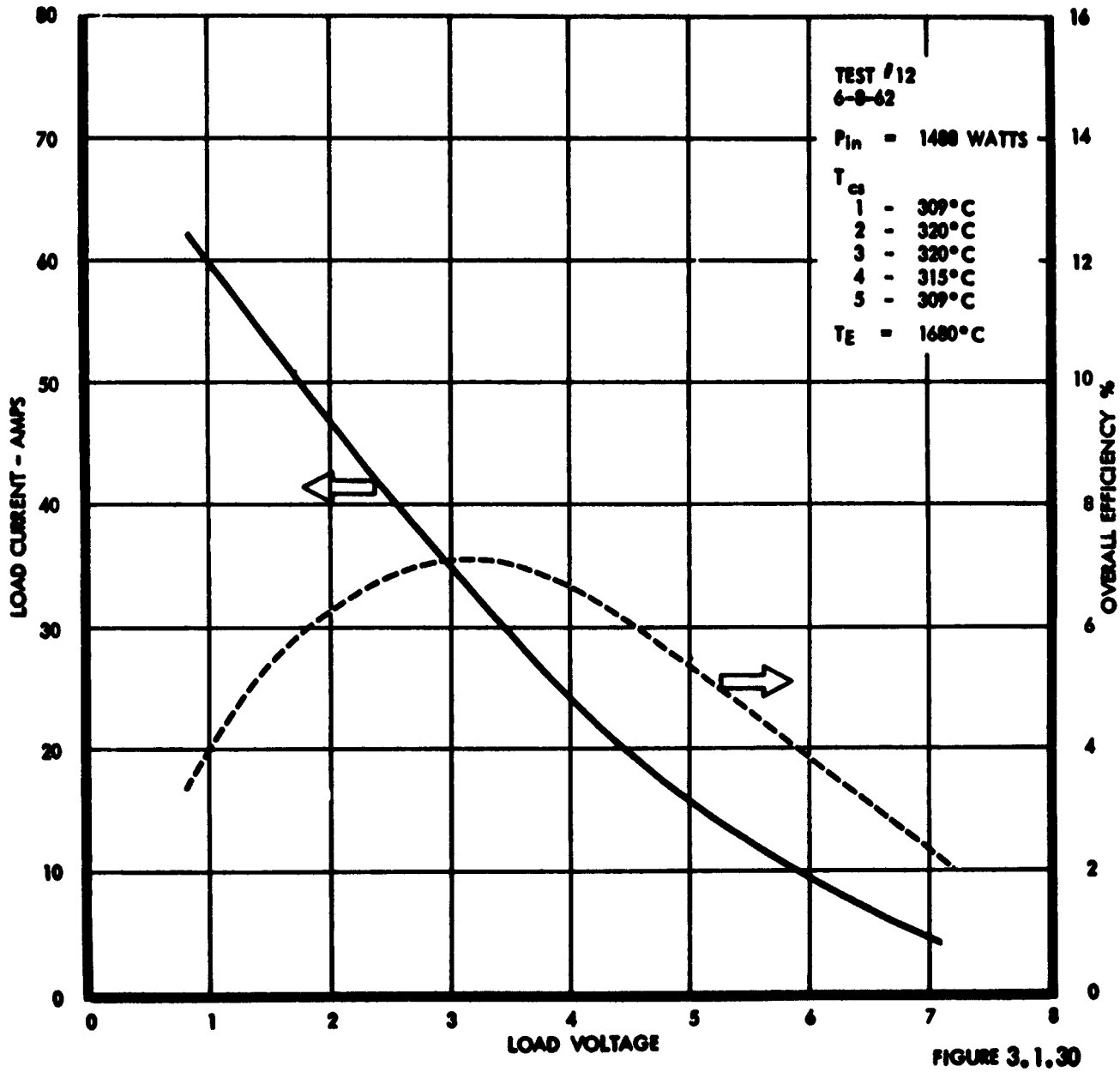

FIGURE 3.1.30

verters was poorly optimized. In many instances it was very difficult to detect improper cesium temperature from the shape of the generator curve. Figure 3.1.31, for example, shows a plot of four I-V curves which, from initial appearance, might be considered a family generated under different input power conditions. Curves #1 and #3 are taken at the same power input however and the difference in slope and efficiency is a function of cesium coverage only. Curves #3, #4, and #6 are taken at different power inputs with nearly optimum cesium coverage. Curve #1 however was taken during the warm up period before proper cesium temperature was reached by the reservoirs. All converter voltages were well matched for each of the four curves.

The determination of an optimum cesium temperature as a function of emitter temperature is very difficult. With five converters to monitor and with the introduction of errors in the thermocouple data due to the junctions established by the feed-through arrangement, it is not possible to present a concise picture of cesium temperature optimization. The picture is further obscured by the fact that all converters are not exactly alike, nor is it certain that all emitters are at the temperature observed in emitter #4. It is, in fact, very fortunate that a generator has been found to operate so well considering the lack of precise control and measurement in the areas mentioned.

The best approach that can be made based on the data available is to present a composite plot of average cesium temperature versus emitter temperature. A comparison between this data curve and the optimum curve obtained from the tests of the 200 watt generators is shown in Figure 3.1.32.

It appears that a somewhat higher optimum cesium temperature is required for the cubical cavity generator. This requirement is felt to be justified because the decrease in electrode spacing would necessitate a slightly higher cesium pressure to provide the required number of ions needed in the reduced volume to assure proper space charge neutralization. Again however, because of the lack of precise data, no positive conclusions can be drawn. The data shown here is sufficient to provide reasonable design data for future generator development, but most certainly should be supported by additional test results.

The optimization of generator or converter voltage as a function of emitter temperature is obtained by plotting the voltage at points of peak efficiency at several different power inputs versus emitter temperatures. Several points from test run

CHARACTERISTIC CURVE SHAPES INFLUENCED BY
CESIUM COVERAGE AND POWER INPUT

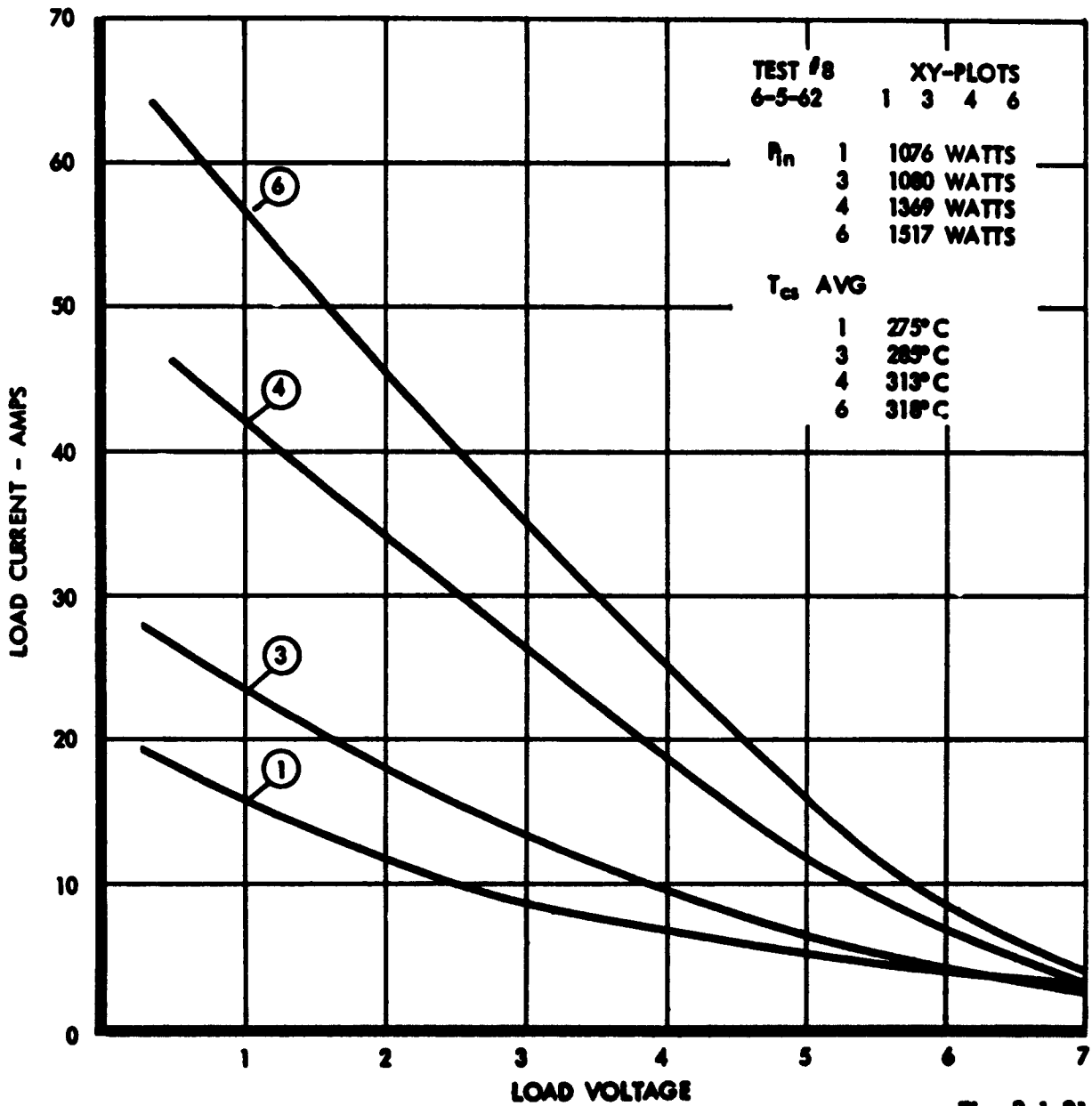

Fig. 3.1.31

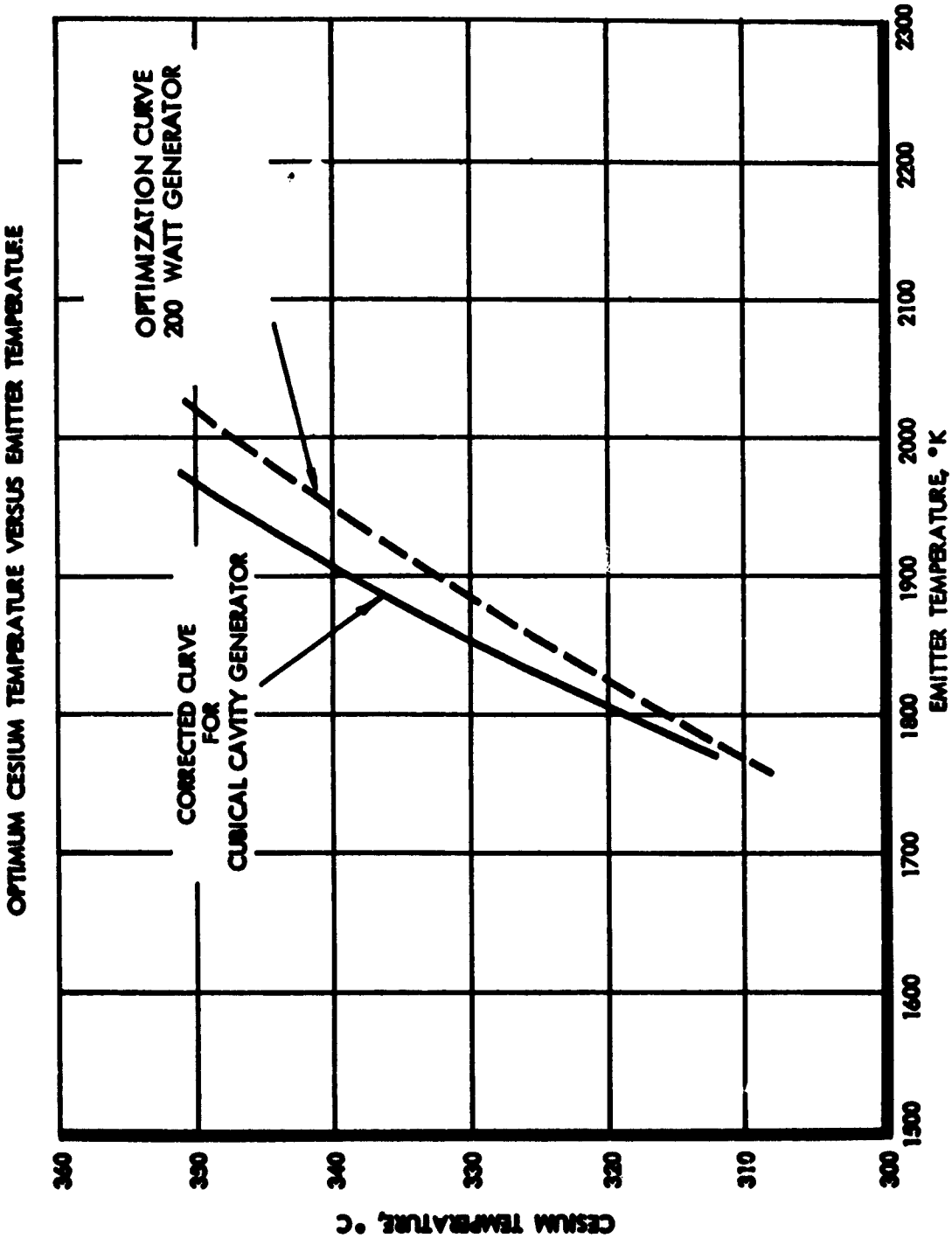
OPTIMUM CESIUM TEMPERATURE VERSUS EMITTER TEMPERATURE
OPTIMIZATION CURVE
200 WATT GENERATOR
CORRECTED CURVE
FOR
CUBICAL CAVITY GENERATOR
CESIUM TEMPERATURE, °C
360
350
340
330
320
310
300
EMITTER TEMPERATURE, °K
1500
1600
1700
1800
1900
2000
2100
2200
2300

Fig. 3.1.32

#13 are shown in Figure 3.1.33. Also shown in this figure is the optimization curve for the 200-watt converter. It appears that the closer spacing results in a reduction of the optimum voltage for a given emitter temperature. The exact reason for this reduction is not clear. Neglecting the possibility that this discrepancy may be due to errors in the data, it is suggested that the reduction may be due to a compression in the barrier sheath at the collector surface. A second possibility is that the collector itself was not optimized to permit proper cesium coverage and maximum output voltage. The amount of the discrepancy is slight and the data very limited. It is therefore felt that no sound conclusions can be drawn at this point.

Maximum obtainable efficiency with the cubical cavity generator is developed by plotting peak efficiency from various tests against the related emitter temperature in Figure 3.1.34. The crosses and dots represent data taken with the cubical cavity generator. The solid line is taken from the efficiency curve generated by the data from the 200-watt generators. The distinction made between the data represented with the crosses and dots is that the cross data was obtained with the generator optimized at about 5 volts, as compared with a more ideal 3 to 3.5 volts for the dots. This illustrates the advantage of optimizing the generator at something less than its design value, with a corresponding increase in performance at lower input power levels or lower emitter temperature.

The significance of the efficiency plot shown here is that it indicates very strongly that both generator configurations will be equally efficient for a given emitter or cavity temperature. Therefore, it might be that the same power output could be expected for a given solar energy input in a system application. This, of course, assumes the effective emitter areas are similar and the cavity absorber efficiency will be identical for each generator. If this is the case, then the cubical cavity generator will have a decided advantage in a systems application because of its inherent higher voltage output and lesser I^2R losses. Also, the higher voltage generator may have additional advantages due to the fact that in a system it is likely several generators would be operated in parallel for higher reliability. With the single converter generator, it is mandatory that all system modules be series-connected to obtain higher voltage and system

OPTIMUM CONVERTER VOLTAGE
VERSUS EMITTER TEMPERATURE

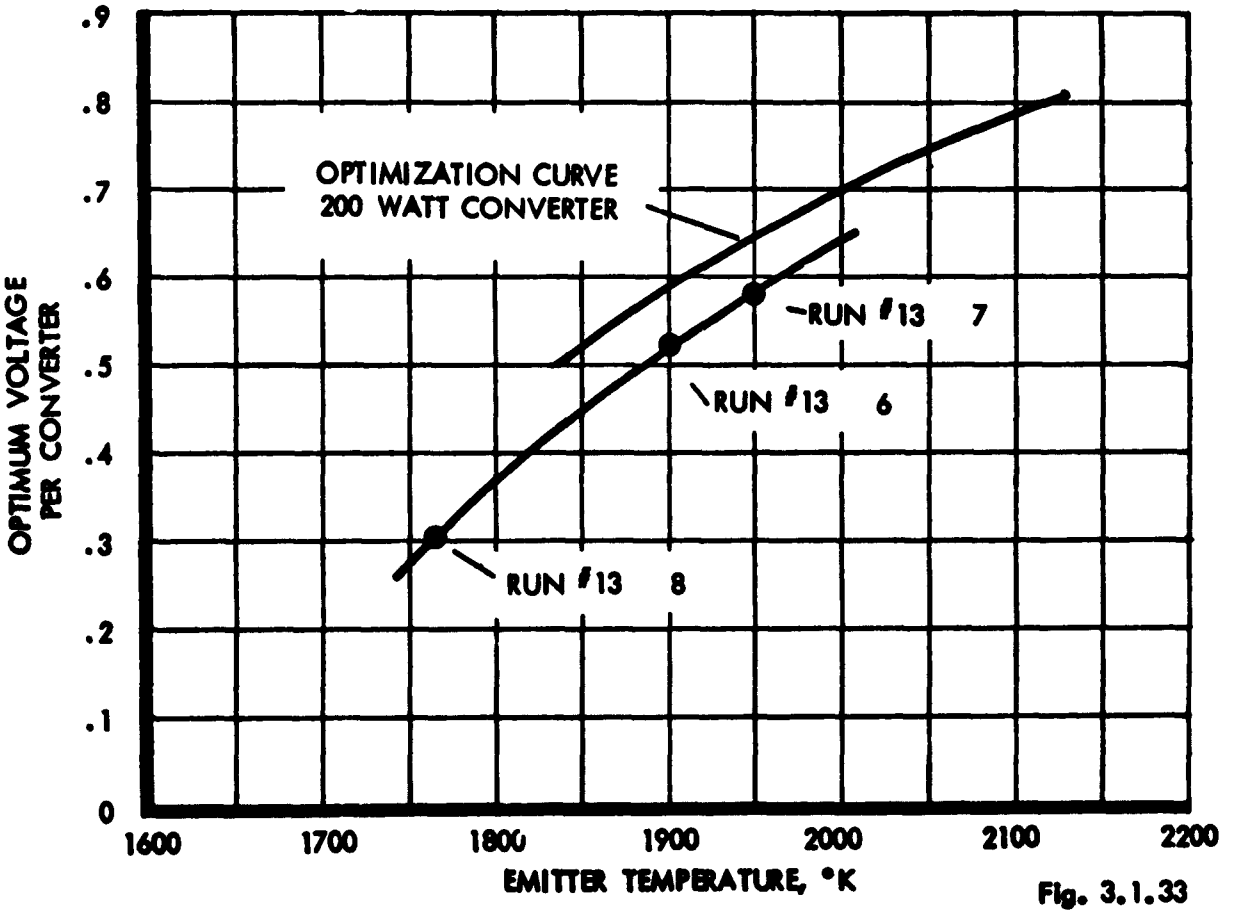

Fig. 3.1.33

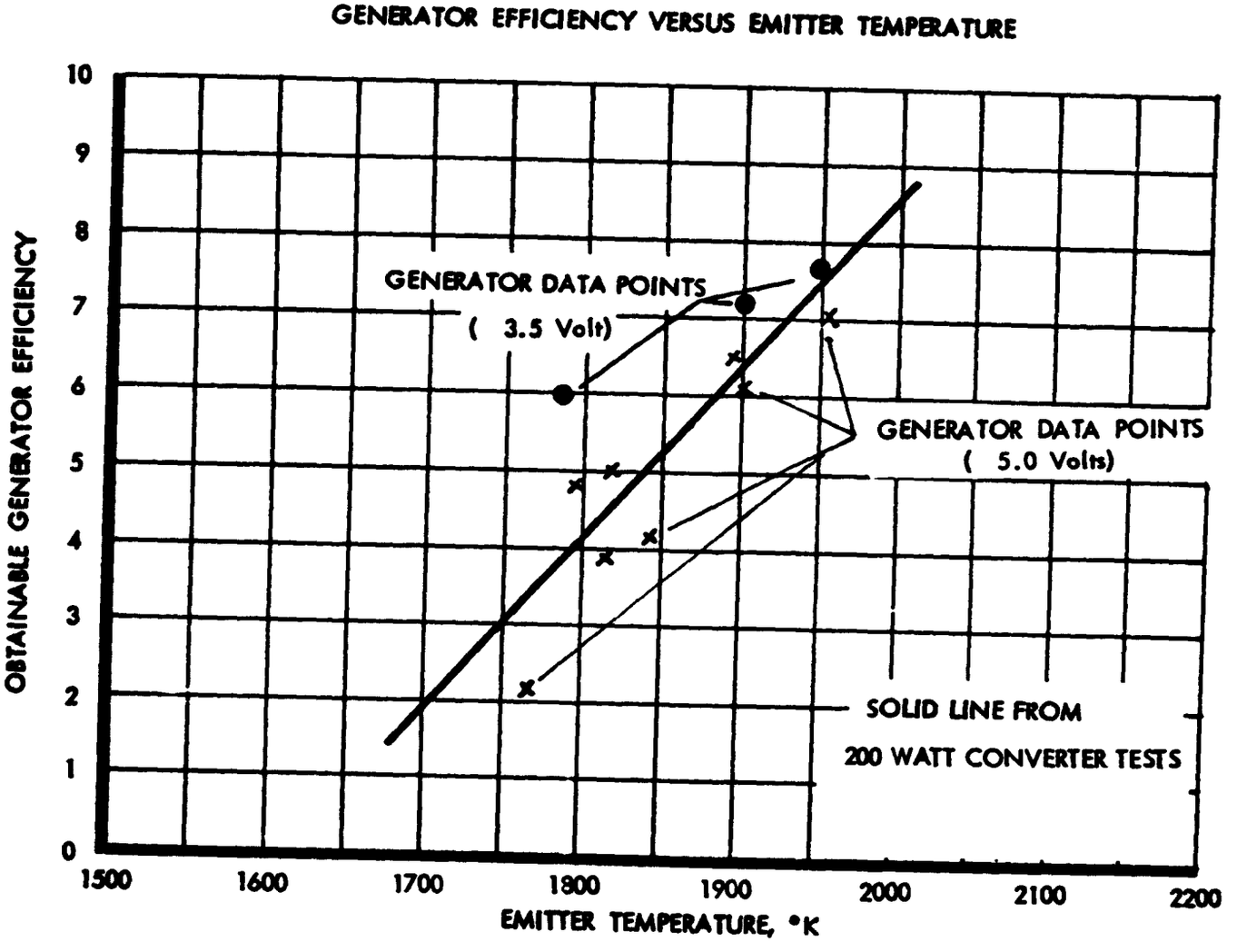
GENERATOR EFFICIENCY VERSUS EMITTER TEMPERATURE
OBTAINABLE GENERATOR EFFICIENCY
EMITTER TEMPERATURE, °K
GENERATOR DATA POINTS
(3.5 Volt)
GENERATOR DATA POINTS
(5.0 Volts)
SOLID LINE FROM
200 WATT CONVERTER TESTS
0
1
2
3
4
5
6
7
8
9
10
1500
1600
1700
1800
1900
2000
2100
2200

Fig. 3.1.34

The cubical cavity generator did not attain the maximum efficiency of 12 to 13.6 percent reported for the 200-watt generators, but it has developed comparable efficiencies based on emitter temperature. It appears that it is quite reasonable to expect improvements in performance equal to or in excess of those reported for the 200-watt converters at higher input power levels and emitter temperatures. The testing carried out with the cubical cavity generator was intentionally limited to insure its survival for a subsequent solar test without necessitating expensive repair or rebuilding. The data taken at more modest power inputs is sufficient for comparison with the 200-watt converters and at the same time provides data which it is hoped will be capable to the solar test data.

In order to permit a valid comparison of the 200-watt and cubical cavity generators, it is necessary to make a calculation of corrected obtainable efficiency. This calculation is carried out to permit a separation of the losses associated with the electron bombardment heating assembly. This includes only heat lost in the gun assembly by radiation and in the I^2R and thermal conduction losses associated with the heater lead lines. Since a similar calculation was carried out for the 200-watt converters, it will then be possible to weigh the performance of the two generators exclusive of any losses peculiar to the laboratory test set up and not inhernent in the generator assembly. The cavity absorbers would in each generator contribute additional losses in a solar systems application. Because these losses would be nearly identical for a given solar concentrator, which would fix the power level and aperture size, it is possible to evaluate the generators on the basis of intrinsic efficiency alone for any given emitter temperature.

A comparison of the corrected efficiency for each generator type shows almost identical performance. Maximum efficiency obtainable is plotted in Figure 3.1.35.

Parametric Performance Characteristics

The multiconverter generator assembly does not lend itself well to a study of individual converter characteristics. It is not possible to insure that all emitters are at the exact same temperature nor that all converters are optimized at the same point. It is likewise impossible to say that electrode spacing is .0020 inches in all cases. Recognizing that there are some variations in the operating conditions attributed to the converters, and in the inherent performance characteristics of the five converters, a technique using average values and near optimum conditions (as can best be determined) is employed to generate a parametric performance curve.

MAXIMUM OBTAINABLE EFFICIENCY WITH
STATE-OF-THE-ART CONVERTERS

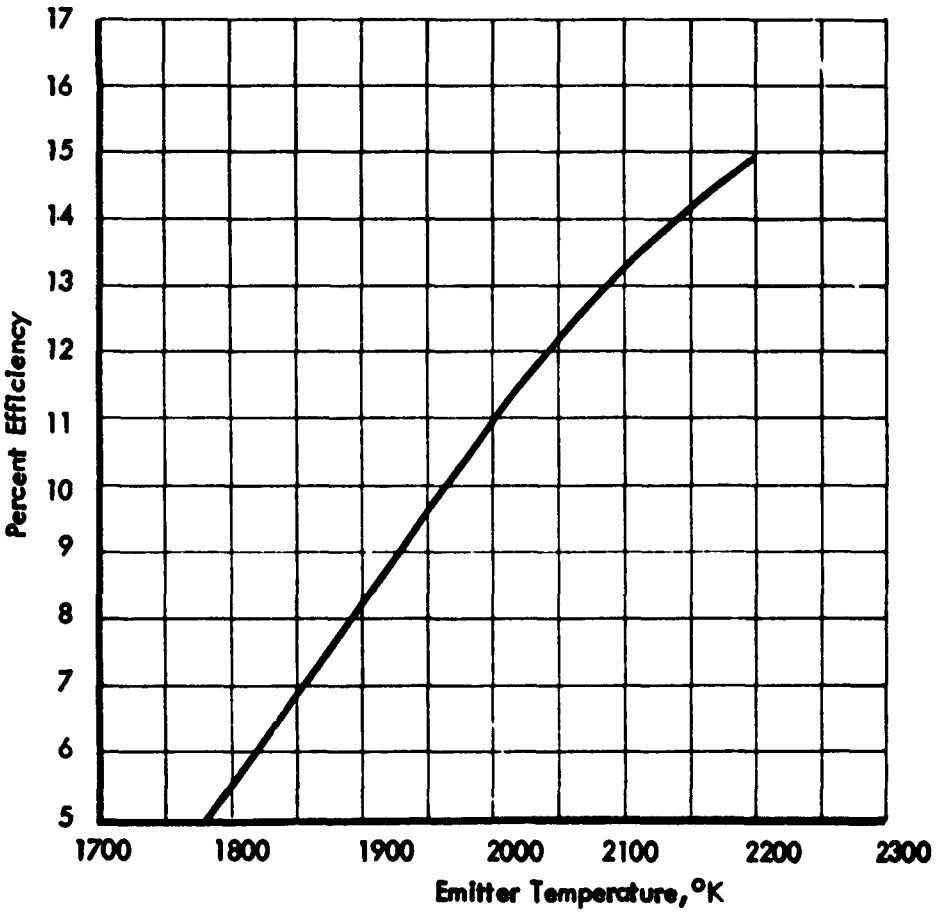

Fig. 3.1.35

Having learned that optimum performance occurs at about 3 volts, a set of four curves taken during test #13 is used to develop the parametric curves. The preparation of this parametric data is greatly simplified in this test series because of the point by point technique for obtaining data at constant power input and temperature.

Using current as the abscissa and emitter temperature as the ordinate, voltage is plotted as a parameter. This plot is shown as Figure 3.1.36. There is reason to believe from the shape of the curves at the higher temperature and voltage that the original data taken was not acquired under truly optimum conditions. If this is not the case, then the difference between the shape of these curves and those shown for the cylindrical generator must be attributed to the change in spacing.

Special Test Results

The various types of loads specified in the contract work statement were applied to the cubical cavity generator. These loads include the application of resistive, inductive, solenoid, motor DC-DC converter, and inverter loads. Also, several of the loads were operated with the generator placed in series with, or in parallel with, an automotive battery.

In no instance was any unfavorable response noted in the generator. Loads of any type, when properly matched to the generator, will result in performance and response identical to that experienced with simple resistive loads. The generator, when properly matched with a battery in either series or parallel connection, will function normally. In series operation, a generator and battery aid each other according to their current and voltage characteristics. Parallel operation is equally dependent on these characteristics in obtaining a division of load power.

Conclusions

Much has been learned about the performance capability of thermionic generators from the tests carried out in this program. Earlier in the program it had been established that the vacuum close spaced converters were not competitive with cesium vapor types from a structural reliability, or performance standpoint. To make the program more meaningful, the efforts had been redirected from carrying out a comparative evaluation of the vacuum and the cesium vapor type converters

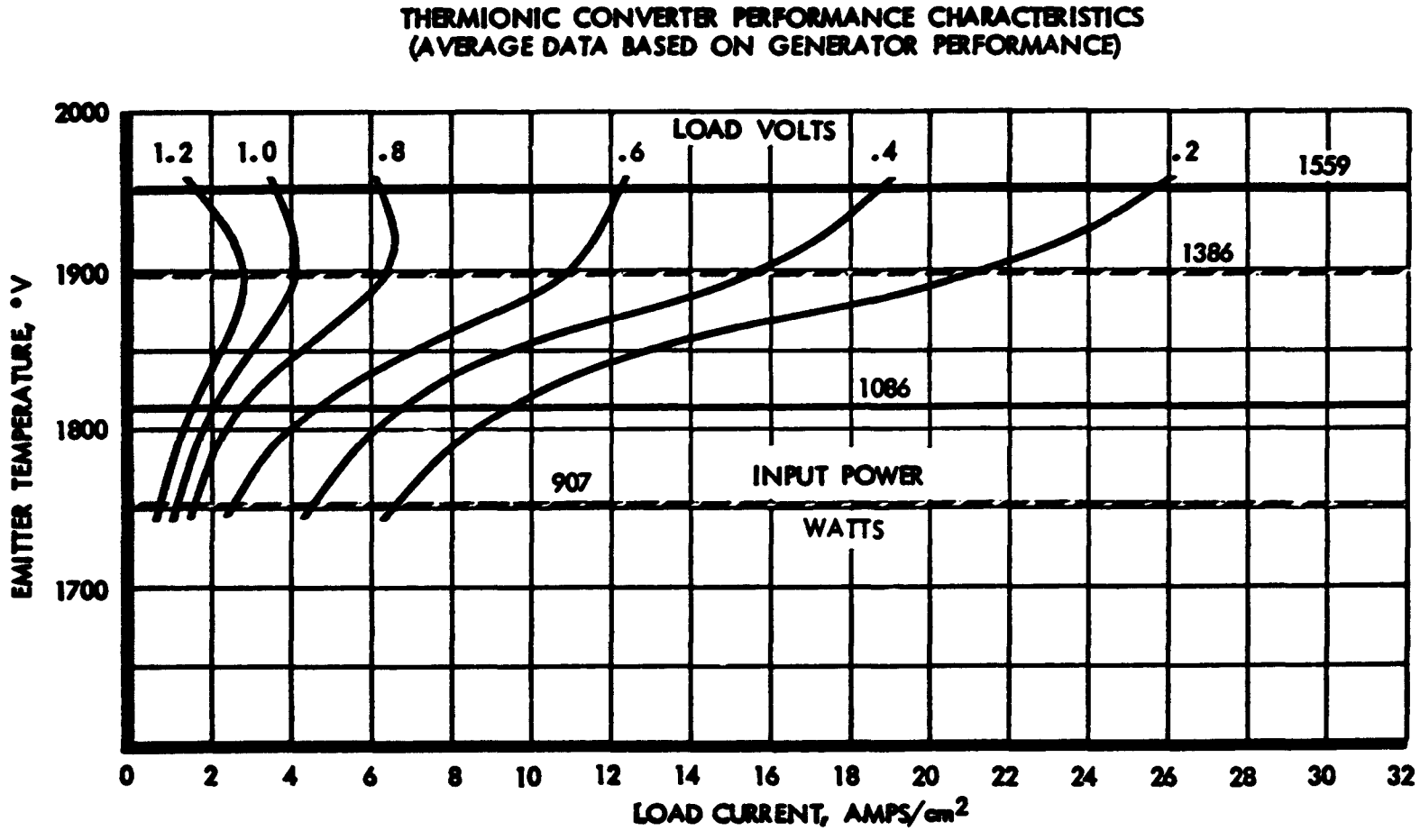
THERMIONIC CONVERTER PERFORMANCE CHARACTERISTICS
(AVERAGE DATA BASED ON GENERATOR PERFORMANCE)
LOAD VOLTS
1.2
1.0
.8
.6
.4
.2
1559
1386
1086
907
INPUT POWER
WATTS
EMITTER TEMPERATURE, °V
2000
1900
1800
1700
0
2
4
6
8
10
12
14
16
18
20
22
24
26
28
30
32
LOAD CURRENT, AMPS/cm²

Fig. 3.1.36

to a comparison of two promising cesium converter configurations. To make the test evaluations directly applicable to the development of a useful power-generating system, the configurations were realistically sized and designed for heating with a precision solar concentrator. The designs were further restricted by specifying that the systems application would be that of providing power for a space vehicle operating in a 35-55 minute shade-sun orbit. Based on these objectives two generators were developed. The first design concept utilizes a cylindrical configuration, with the emitter in the form of a closed cylinder, the collector completely enclosing the cylinder walls, and only a small annular cesium gap between the two. For solar operation, one end of the cylinder assembly is closed off with a thin tantalum membrane to contain the cesium vapor while at the same time permitting solar flux access to the cylinder cavity abosrber. The second geometry uses five smaller converters arranged to form a cavity absorber for concentrated solar energy with the back side of the emitter faces. In the second assembly each converter is self-contained with its own cesium reservoir. With small changes, both generators could be incorporated in a solar module and used as part of a system.

The tests carried out on the two configurations have shown that each is capable of producing sizable power outputs of from 100 to 200 watts. In both cases the limitations imposed by the electron bombardment heating equipment made it somewhat difficult to exploit the full capability of the generators. The technique employed did however demonstrate that both configurations are responsive and are capable of generating power under various conditions, including many types of loads and cesium pressures and at different input power levels. The actual performance characteristics obtained were nearly identical when related to a given emitter temperature. The small variations which were noted can be attributed to the reduction in spacing between the emitter and collector in the second cubical cavity assembly. No insurmountable difficulties have been experienced with either generator. All types of resistive, motor, inductive, inverter, and converter loads were easily accepted by the generators. The dynamic response to step changes is almost instantaneous and, except for problems associated with the bombardment heating techniques, no problems were encountered. The thermal response of the generators is, of course, related to the size and mass of the individual units and the given system requirements. With the generators tested it appears there would be only a small percentage of power output lost due to

the warm-up characteristics in an orbital application. To insure long life the generators should normally be protected for sudden and total loss of load which will cause high emitter temperatures and thermal stresses.

The 200-watt cylindrical geometry converters have produced more power and higher over-all efficiencies of over 200 watts and 13.6% as compared to 122 watts and 7.6% for the cubical cavity generator. This does not indicate a superiority on the part of the cylindrical geometry however. When the two 200-watt converters were operated in series the maximum output power was 310 watts. The efficiency was 9.6%. With the data taken from both generators compared on the basis of emitter temperature, it is found that only a few tenths of a percent difference in performance exists. (And when the losses associated with the cavity absorbers are taken into account, it may even be possible the cubical cavity generator will show a marked superiority.) Very sizable losses are certain to be associated with the support membrane required to hold the emitter in place and retain the cesium in the cylindrical assembly. Further, it is shown that an improvement in performance is attained with the cubical cavity converters due to the ability to reduce interelectrode spacing. The actual watt density is shown to be twice that of the cylindrical geometry at a given temperature. In summary, it is stated that the apparent superiority shown by the cylindrical geometry is due only to its having been operated at higher temperatures with a correspondingly greater efficiency, and due to an improved loss picture which is associated solely with the electron bombardment heating arrangement. Discounting these two factors, the generators are equally efficient, with perhaps the greatest opportunity for improvement lying with the small planer converter configuration used in the cubical cavity generator.

In several other respects the cubical cavity generator is more satisfactory. From a reliability standpoint the smaller converters used in the cubical cavity generator are better. Converters of this and similar designs have shown a tolerance to hundreds of hours of operation and cyclic tests. The 200-watt converters were each rebuilt during the test program to permit the completion of the tests required over a period of only 40 hours. The cubical cavity generator had had over 72 hours of testing plus the hours accumulated on individual converters prior to assembly with no loss or reduction of output. The principal areas which currently limit life expectancy are the alumina seals and the thin tantalum emitter support

sections. The improvement in the seal assembly in the cubical cavity converters is largely responsible for its longer life. The susceptibility of the thin tantalum support sections to carburization and cracking is equally present in both units although somewhat less severe in the larger assembly which can tolerate a heavier wall section. High purity metals and clean hard vacuums will eliminate this area as a source of failure.

The higher voltage output of the multiconverter generator may also be advantageous in systems applications requiring modest power output. The cylindrical converters must be series-connected to produce higher voltages. This requires a larger number of concentrators than would be needed if the multiconverter configuration is used. It is recognized that this need not always be true but generally it is more efficient to work with higher voltages and less currents. This is particularly true if a DC-DC converter is to be employed in the system.

The shape and size of the smaller converters also lends itself to mass production and assembly into a number of alternate generator configurations with more or fewer converters. Also, the geometry is such as to permit close control over spacing, a factor which will probably contribute more than anything else to improvement in performance.

It is recommended that the multiconverter assembly be the subject of further development and improvement for incorporation into aerospace systems. Additional tests of individual converters to further explore performance characteristics and the effects of changing spacing and materials should be undertaken. Testing of the completed generators at higher power and temperatures with improvements in instrumentation and access to all pertinent temperature points is very desirable to substantiate the findings of this report. Additional efforts to improve cavity geometry and absorber efficiency will also contribute greatly towards the development of a space-worthy system. Reductions in radiator size and weight and the development of suitable automatic cesium reservoir temperature controls and flux or emitter temperature controls will be necessary for a prototype system. Developments in these areas, combined with improvements in fabrication and assembly techniques and the selective assembly of matched converters into generator clusters, can be expected to yield generators capable of efficiencies above 12% for solar applications.

3.2 Solar Receivers

A solar receiver may be classified as either a flat plate type or a cavity type. The function of the receiver, placed at the focal point of a solar concentrator, is to absorb a large fraction of the energy incident upon it and to limit the amount of energy reradiated so that the net useable thermal energy is a maximum. The receiver may be either a flat plate selective absorber or a black body cavity.

Advancement of the state-of-the-art of selective absorbers has been limited to absorbers which are considerably below thermionic converter operating temperatures. The choice of materials for use at the anticipated operating temperatures is very limited. None of the high temperature materials has promising properties as a selective surface absorber. The use of cover glasses does not appear promising because: (1) the increase in efficiency is marginal and (2) the glass may become coated with metal evaporated from the receiver surface.

The state-of-the-art of cavity receivers has barely begun to advance. Some experimental and theoretical investigations have been conducted to determine the effective emissivity of the simplest cavity geometries. However, investigations of the more important property, solar absorptance, have been very few. The investigations which have been made have been theoretical and have required gross assumptions as to the specularity of the interior walls of the cavity.

The need for a receiver of the cavity type for solar thermionic systems in order to obtain high overall system efficiencies is clearly illustrated in the following consideration. Receiver efficiency may be defined as the ratio of the power retained by the receiver to the power incident upon the receiver. The incident power is:

$$P_{inc} = q\, A_c\, N_c \qquad (9)$$

where: q = solar flux incident on the concentrator
A_c = area of the concentrator
N_c = concentrator efficiency

The power absorbed by the receiver is:

$$P_{abs} = \alpha\, q\, A_c\, N_c \tag{10}$$

where: α = receiver absorptivity

The reradiated power is:

$$P_{rer} = A_r \varepsilon \sigma T^4 \tag{11}$$

where: A_r = receiver area

ε = receiver emissivity

σ = Stephan-Boltzman radiation constant

T = receiver temperature

Receiver efficiency is then: $N_r = \dfrac{P_{abs} - P_{rer}}{P_{inc}}$ (12)

$$= \frac{\alpha\, q\, A_c\, N_c - A_r \varepsilon \sigma T^4}{q\, A_c\, N_c} \tag{13}$$

A_c/A_r is the area concentration ratio, C_a

Then,

$$N_r = \alpha - \frac{\sigma T^4}{q\, C_a\, N_c}\, \varepsilon \tag{14}$$

Therefore, the receiver efficiency is a linear function of the parameter $\sigma T^4/q\, C_a\, N_c$ for any particular material with a constant absorptivity and emissivity, as shown in Figure 3.2.1. The curve intersects the black body ($\alpha = \varepsilon = 1$) efficiency curve at an efficiency of $\alpha - \varepsilon / 1 - \varepsilon$, which corresponds to $\sigma T^4/q\, C_a\, N_c = 1 - \alpha / 1 - \varepsilon$. This means that the black body receiver is preferable if efficiencies greater than $(\alpha - \varepsilon)/(1 - \varepsilon)$ are desired. Furthermore, for a black body receiver to be advantageous, $\sigma T^4 / q\, C_a\, N_c < 1 - \alpha / 1 - \varepsilon$, i.e., the area concentration ratio must be at least $(1 - \varepsilon / 1 - \alpha)(\sigma T^4 / q\, N_c)$.

RECEIVER EFFICIENCY FOR BLACK BODY AND
SELECTIVE ABSORBERS

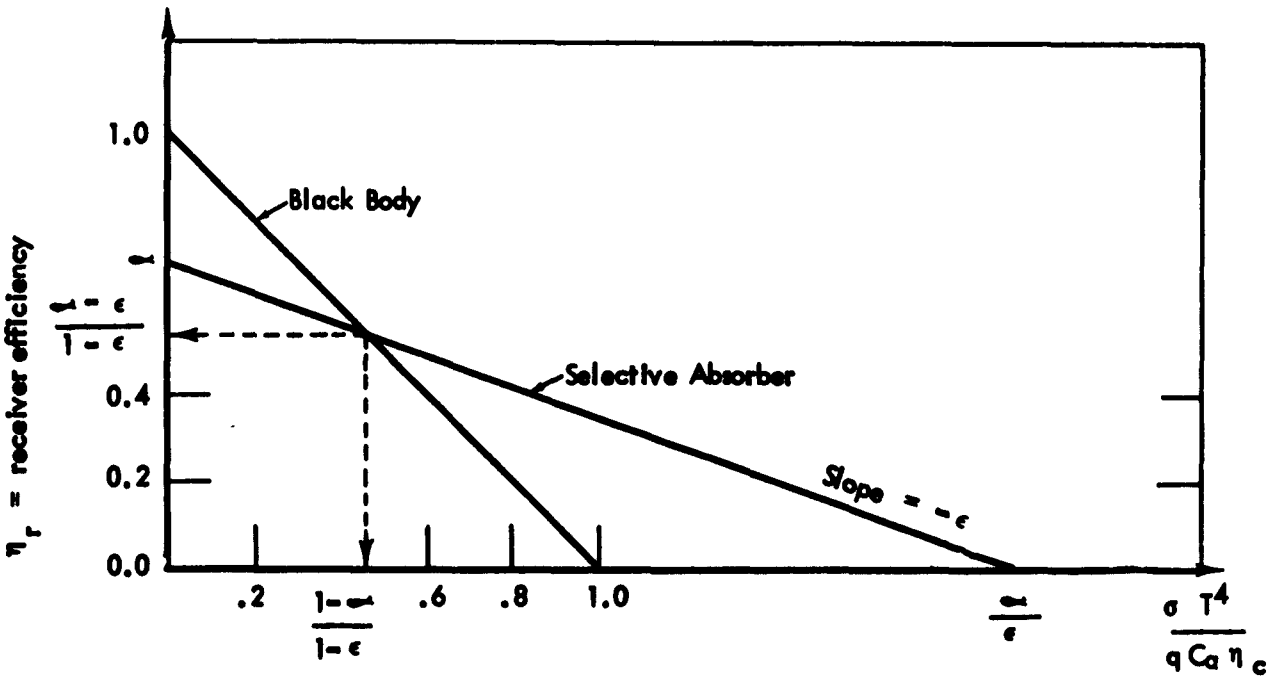

Fig. 3.2.1

RECEIVER EFFICIENCY FOR BLACK BODY AND
TANTALUM ABSORBER AT 2000°K

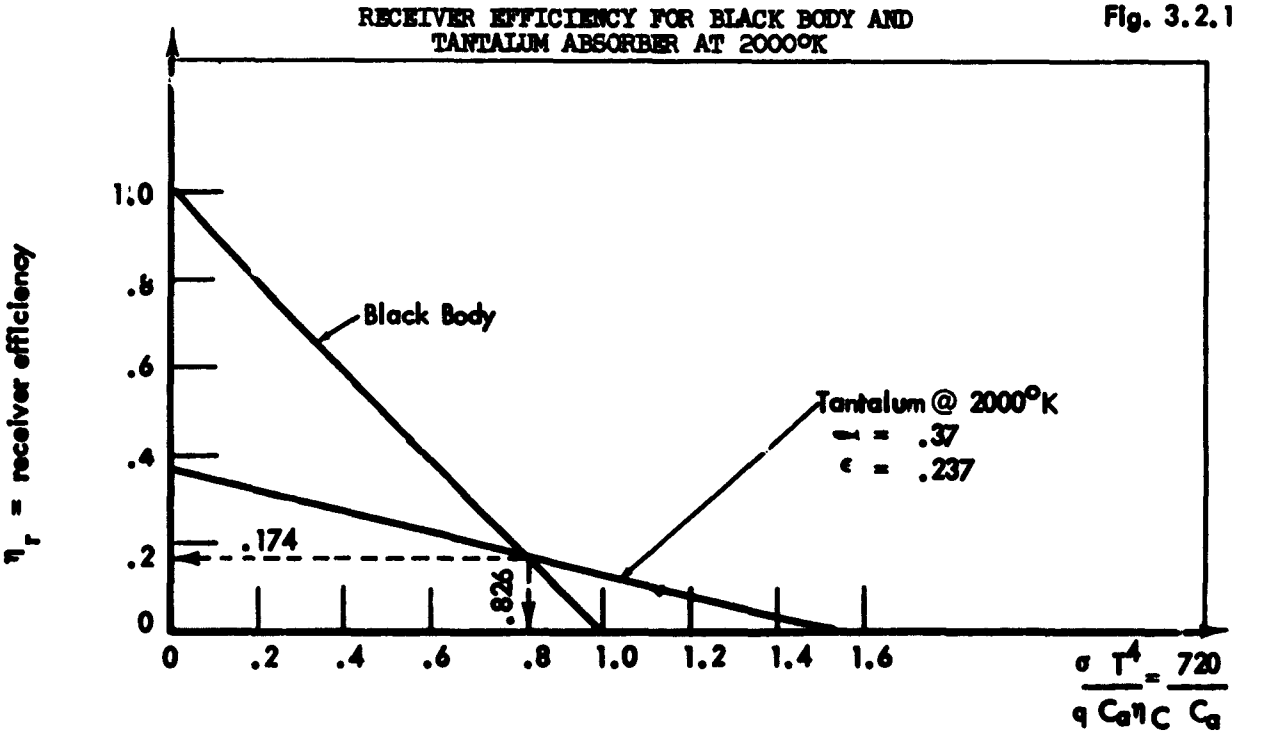

Fig. 3.2.2

For example, in Figure 3.2.2, the curves for a black body and a tantalum receiver are plotted for T = 2000°K, q = .140 w/sq. cm, N_c = 0.9. For tantalum at 2000°K, α = .37, ε = .237. A black body receiver is preferred if a receiver efficiency greater than 17.4% is desired. The selective absorber is advantageous only for area concentration ratios less than 870, whereas the cavity receiver used with properly sized apertures and high precision concentration can provide receiver efficiencies suitable for thermionic systems.

3.2.1 Thermionic Generator Cavity Absorbers

General Considerations

The absorptive and emissive characteristics of cavity absorbers are dependent on the following factors:

1. Wall-to-Aperture Area Ratio
2. Absorber Geometry
3. Wall Materials and Surface Finishes
4. Temperature of Walls
5. Concentrator Parameters

A clear understanding of the effect of these factors is necessary in order to design, fabricate, and test solar thermionic generators. A general discussion of these factors follows.

1. Wall-to-Aperture Area Ratio

   Heat flux at the wall is primarily determined by the thermionic converter requirements, while the heat flux at the aperture is primarily determined by the solar intensity and various attenuation factors such as reflectivity of the reflector, vignetting, etc. Since the thermionic converter requirements can be expected to remain relatively fixed and the attenuation factors are constant for all space applications, the wall-to-aperture area ratio can be expected to remain essentially the same for all space missions. Atmospheric attenuation, however, has a drastic effect on this ratio. Therefore, the geometry most suitable for ground operation will differ from the best geometry for space. Since all of the useful applications contemplated for the solar thermionic generator are for space, it must be recognized that some compromises must be accepted in the design for ground test if both efficiency and ground-to-space performance correlation are to be design and test objectives.

Let

A_c = converter emitter area = wall area

A_a = aperture area

ϕ_c = heat flux required by the converters

ϕ_a = average heat flux entering aperture

ϕ_r = average heat flux reradiated through aperture

α = cavity absorptivity.

The basic heat balance equation may be written:

$$A_c \cdot \phi_c = A_a (\alpha \phi_a - \phi_r). \tag{15}$$

The cavity wall-to-aperture area ratio is then:

$$\frac{A_c}{A_a} = \left(\frac{\alpha \phi_a}{\phi_c}\right) - \left(\frac{\phi_r}{\phi_c}\right) \tag{16}$$

It may be argued that there are certain factors present only in space which tend to decrease the aperture flux and thereby compensate for this inconsistency. These factors are geometric inaccuracies associated with lightweight concentrators and orientation errors associated with space vehicles. While there is some logic to this argument, the fact remains that the effect of these factors on generator performance cannot be evaluated by ground test when successful operation depends on their being eliminated. Furthermore, it cannot be assumed that the heat distribution in the absorber will be the same when the intensity is increased by increasing the concentrator precision.

Because of the above consideration, absorber studies should be concentrated on absorbers having the wall-to-aperture area ratio expected to be used in a space generator. The flux level will be lower than that expected in space, requiring the use of correction factors to determine the performance

in space. This approach is considered to be the most accurate one, since absorption can be expressed as a fixed fraction of the incident energy and emission can be expressed as a proportion of the fourth power of temperature with a minimum error.

2. Absorber Geometry

Ideally, each and every thermionic converter in the absorber cavity should have the same "view" of the solar image. Each converter will then receive an equal amount of solar radiation.

Also, the absorber walls should consist completely of surfaces which are connected to the thermionic emitter surfaces by a good thermal conductor.

These two design objectives are not readily achieved in a single design. The first objective may be met by locating the converters in a ring about the absorber axis. This, however, will leave an unfilled space in the bottom of the absorber. This space may be (1) filled with an additional converter, (2) filled with a reflective plug, or (3) closed by extending the absorber wall surfaces.

Filling the space with an additional converter requires that steps be taken to insure that the extra converter receives its proportionate share of solar energy.

The cubical cavity generator described in Section 3.1.2 is a design of this type. In order to establish what power distribution exists within the cubical cavity absorber, solar tests were conducted using a mock cavity calorimeter, consisting of five individual power abosrbing devices which closely simulate the thermal characteristics of the thermionic converters used in the cubical cavity generator. Evaluation of test results of the mock cavity (and subsequently of the generator itself) show a non-uniform power distribution between the side absorbers and the bottom absorber. Table 3.2.1 shows the power distribution measured between absorber sides S_1, S_2, S_3, S_4 and the bottom

TABLE 3.2.1

POWER DISTRIBUTION CALORIMETER TEST DATA
FOR CUBICAL CAVITY CONFIGURATION

Calorimeter Unit #	T_{2f} (°C)	T_{3f} (°C)	Power Absorbed
S_1	1025	745	94.0
S_2	1025	685	111.0
B	940	665	90.5
S_3	1035	720	102.0
S_4	1035	750	97.0
Total Power (Watts):			494.5
Solar Constant (W/ft^2):			71.2
Aperture:			(5/8" Dia.in Focal Plane)
Baseplate Temp (°F):			76.0
Run Time (Min.):			27.0

absorber B during a typical test run. The bottom calorimeter absorbed less power.

During the solar test of the generator the bottom converter produced less power output than the side converters. This again indicated a maldistribution of power within the cavity.

Filling the bottom of the cavity with a reflective plug will cause an additional thermal loss in the generator. The energy absorbed by the plug will raise its temperature to a level higher than the surrounding absorbers. Some of the heat absorbed by the plug will leak through its back side insulation and supports, some will be radiated through the aperture, and a small portion will be radiated to the surrounding absorbers. The design of this plug must be verified by test.

Closing the space at the bottom of the cavity by extending the absorber wall surfaces to meet the absorber axis presents some difficulty from an arrangement standpoint, but this is not serious. The chief difficulties are the prevention of heat leaks from the extended surface and the conduction of heat to the emitter surface with a reasonable temperature gradient. Assuming these problems can be solved, the advantages of a symmentrical configuration which insures uniform power distribution and a more efficient cavity absorber geometry makes this configuration preferable in future designs.

Within the confines of wall-to-aperture area ratio limitations and the limitations imposed by the above arrangement considerations, there exist many possible absorber geometries. From an absorber standpoint, the most significant property is its absorptivity. The absorptivity of the cavity is that fraction of the energy entering which is not reflected back out of the cavity. It is important therefore that the geometry be such that the first few specular reflections are confined within the cavity. This task is made difficult by the wide variation of incoming rays.

3. Wall Materials and Surface Finishes

Since absorptivity is the most important property of the absorber, the walls of the absorber should have as high an absorptivity as practical. Unused portions of the cavity such as the aperture plate and the reflective plug should have as low an absorptivity as possible in order to minimize heat leaks.

There are limits to which the wall absorptivity can be increased by the choice of wall material. This is true chiefly because the choice of wall materials is limited to the refractory metals. However, the wall surface can be grooved or roughened by grit-blasting in order to increase the number of reflections at the surface and thereby increase the absorptivity. The effect these steps have on the flux distribution in the cavity and the overall performance of the generator can be only approximated and should be verified by test.

Unused surfaces in the cavity should be made as reflective as possible.

The fraction of the incident energy absorbed by these surfaces can be utilized only by radiative heat transfer from them to the thermionic converters. In order to effect such a transfer, these surfaces must reach a temperature higher than the converter temperature. These surfaces, however, cannot be allowed to reach a temperature where material evaporation becomes a problem.

4. Wall Temperature

The temperature of the cavity walls is important in the design of the generator in that thermal radiation from the cavity constitutes a major generator loss. The temperature differential required to conduct heat from the solar absorber surface to the thermionic emitter surface increases the absorber temperature and raises the cavity radiation loss. It is important therefore to minimize the length of this conduction path. This consideration is especially important in systems utilizing thermal energy storage.

It is also important that the temperature of the absorbing portions of the walls be uniform. Local overheating will increase heat losses and shorten the life of the thermionic converters. Local underheating will reduce the output of the generator because of its effect on the thermionic conversion process.

5. Concentrator Parameters

The chief concentrator parameter affecting cavity absorption characteristics is the rim angle. High rim angles direct more energy to the cavity side walls and less to the bottom of the cavity. The more oblique rays also have less tendency to be reflected back through the cavity aperture. In general, the high rim angles are to be preferred as long as they are not so high as to affect the performance by requiring an excessively large cavity aperture.

Using an oversize concentrator to compensate for the attenuation factors associated with ground testing will increase the solar image size and will have an effect on the distribution of energy within the cavity as compared to a space-sized concentrator. The effect will be to direct more energy to the side walls and less energy to the bottom face of the cavity. Reradiation losses will also be disproportionately large with an oversize concentrator.

Basis for Selection of Generator Component Materials

The design of a thermionic generator absorber requires a knowledge of various high-temperature properties of materials proposed for use in the construction. The properties of interest may be categorized as follows:

1. Optical
   - Absorptivity
   - Emissivity
   - Specularity

2. Thermal
   - Specific Heat
   - Conductivity
   - Expansion

3. Structural
   - Strength
   - Density
   - Dimensional Stability

4. Chemical
   - Vaporization
   - Compatibility

1. Optical Properties

To achieve maximum absorber performance, the absorbing surfaces in the cavity should have as high a solar absorptivity as possible, and the reflecting surface should have as low an absorptivity as possible. Because of the scarcity of applicable absorptivity data and the strong dependence of this property on the method of fabrication, tests must be made to properly evaluate various materials.

Total emissivity is also an important factor affecting absorber performance. This data is similarly scarce and dependent on fabrication methods.

Solar absorptivity and total emissivity of materials and surface finishes being considered for use in the thermionic generator can be determined by test in an arc-imaging furnace. The spectrum from the arc-imaging furnace simulates the solar spectrum very closely and allows solar absorptivity to be determined directly by simple heat balance methods. This eliminates the need for monochromatic absorptivity determinations which must be subsequently integrated over the solar spectrum. Total emissivity can also be determined during these tests.

Surface specularity is the extent to which solar energy incident on a surface is specularly reflected. There is no quantitative measure of specularity per se, but the reflected energy may be roughly divided into a specular

reflection, a flare reflection (nearly specular), and a diffuse reflection. Some knowledge of this division is necessary to appraise the optical analysis of an absorber cavity. Since the division is chiefly a function of microscopic surface geometry, observations at room temperature with an integrating sphere reflectometer using white light will provide sufficient information for the design of a generator cavity.

2. Thermal Properties

The thermal properties of most materials being considered are available from the literature. They are not very dependent on the method of fabrication, with the possible exception of the refractories. Where refractoreis are to be used in the generator, they can be tested to determine their thermal shock resistance before being accepted in a design. This property is a combination of other thermal parameters for this type of material.

The selection of materials to be used in construction of thermionic converters and generators is generally based on properties other than thermal properties. However, the specific converter or generator performance characteristics desired for a given application will dictate the thermal properties of the construction materials.

3. Structural Properties

The structural properties of importance in the thermionic generator are high temperature strength, dimensional stability, and impermeability to cesium. Suitable materials have been selected and proven during thermionic converter development to date. Any new materials will be required to equal or excel present standards.

4. Chemical Properties

Probably the most critical materials properties for thermionic generators are compatibility and evaporation. The materials containing cesium must be compatible with it. Evaporation of materials in a space environment will limit the life of the generator and could also cause a degeneration of performance by coating electrical insulators or the reflective surface of the concentrator. The refractory metals have demonstrated their suitability in these respects.

3.2.2 Cavity Absorber Analysis

Introduction

Several cavity absorber analyses have been made for solar-powered thermionic systems using high-precision solar concentrators. The analyses were made for cavity absorber receivers having the following geometric shapes: (1) Cube, (2) Right Square Prism, and (3) Right Circular Prism (Cylinder). The analyses are based on a ray tracing method which assumes specular reflection at each surface within the cavity. This assumption may be far from accurate in many cases but it was believed to be accurate enough to obtain realistic results and to determine the relative importance of various parameters. The actual surface characteristics lie somewhere between a specular reflective surface and one which gives a hemispherically diffuse reflection. Although there is some justification for use of the "specular" assumption in that surfaces tend to "brighten" in vacuum at thermionic temperatures, further computational analysis and tests should be made to determine the performance band between these two extremes.

Cubical Cavity Absorber

The selection of the cubical cavity absorber configuration for one of the generators built under this program was based on the results obtained from the analysis conducted for this type of cavity receiver.

There are several limitations to the design of the cavity absorber however, which prevent the achievement of ideal performance. First, the cavity aperture size is essentially a function of solar image size. Second, the cavity wall area is determined by the thermionic generator emitter area required. Third, cavity geometry is limited by emitter geometry limitations. Practical considerations dictate the use of one material to serve the dual purpose of thermionic emitter and cavity absorber.

In the cubical cavity generator, uniform distribution of the concentrated solar energy to the five emitters is required. Energy variations in the cubical cavity can be compensated by changing the effective emissivity of the bottom wall converter as compared to the side wall converter, but extensive testing with this geometry is required to establish the degree of improper energy distribution. At first it might appear that the surface at the bottom of the cavity will receive more than its share of the radiation; however, analysis (as well as subsequent generator test)

has shown that the flux attenuation at a point 1.5 cm from the focal plane is more than sufficient to prevent overheating of the bottom surface. Any variation which may exist will be minimized by the high rate of radiant energy interchange between wall surfaces which takes place at the high operating temperature (2000°K). (This was also confirmed during mock converter tests. See Table 3.2.1)

The effective cavity absorptivity was obtained by calculating the amount of concentrated incident flux reflected from the cavity after once having entered the cavity. The cavity has a circular aperture. Incident radiation passing through the cavity aperture is weighted with respect to the total energy received from a given direction (i.e., from a given incremental ring on the solar concentrator paraboloid surface). A relation is obtained for the number of multiple reflections within the cavity experienced by a single ray as a function of the ring angle from which it emanated. Figure 3.2.3 presents the results of the computer evaluations of this relation. For the cubical cavity generator which uses tantalum emitters at 2000°K and a reflectivity of 0.55, an effective cavity absorptivity of 0.94 is obtained.

The effective emissivity of a cubical cavity absorber with a circular aperture in one face was determined by the Michaud equation which has been experimentally verified. Michaud gives the emissivity as:

$$e_o = \frac{e\left[1 + (1-e)\left(A/A_c - \sin^2 \Phi\right)\right]}{e\left(1 - A/A_c\right) + \left(A/A_c\right)} \qquad (17)$$

where e = surface emissivity
A = area of aperture
A_c = area of cavity
Φ = arc-tan of aperture radius/cavity depth

The results of this equation are plotted in Figure 3.2.4 where effective emissivity is shown as a function of the relative aperture size.

For the tantalum cubical cavity, therefore, a geometric selective effect is obtained which improves the solar concentrator-absorber efficiency to a level higher than could be obtained with either a tantalum selective surface absorber or a black body absorber. Hence the selection of the cubical cavity absorber

ABSORPTIVITY OF CUBE CAVITY

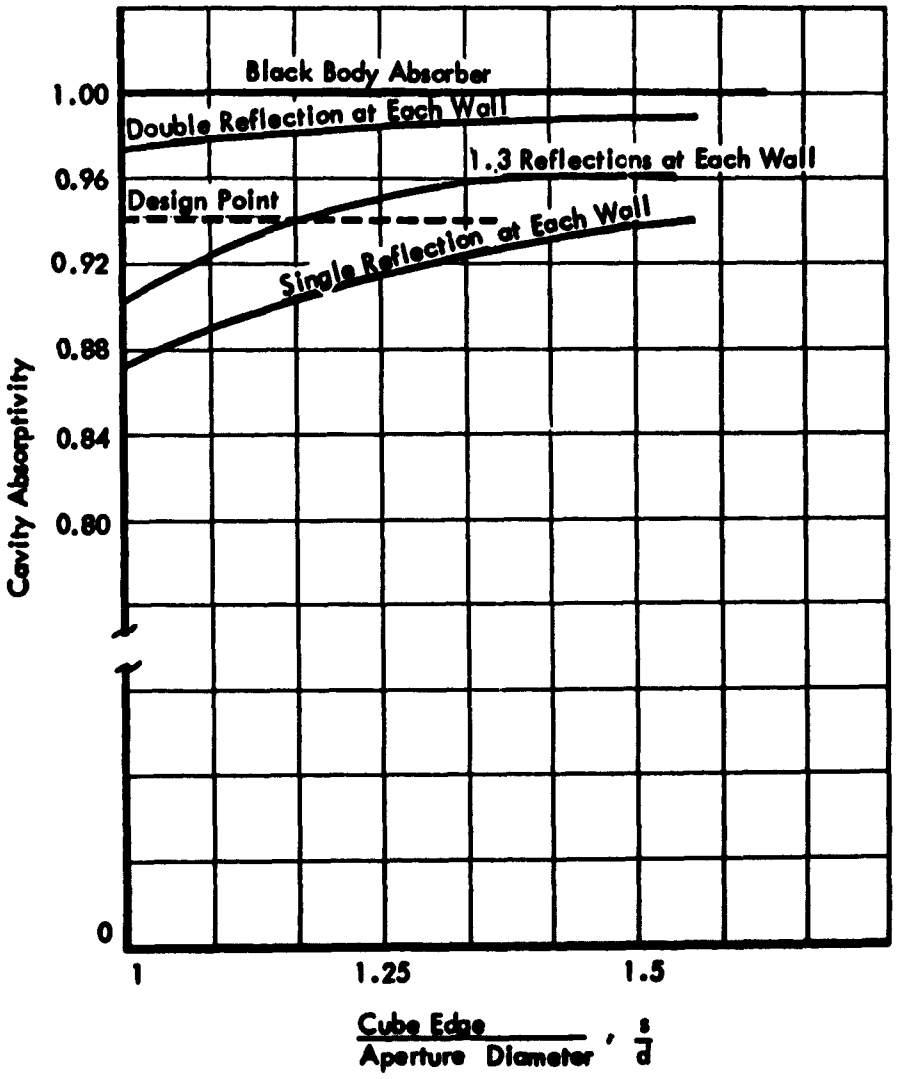

FIGURE 3.2.3

EFFECTIVE EMISSIVITY OF A CUBE CAVITY WITH A CIRCULAR APERTURE

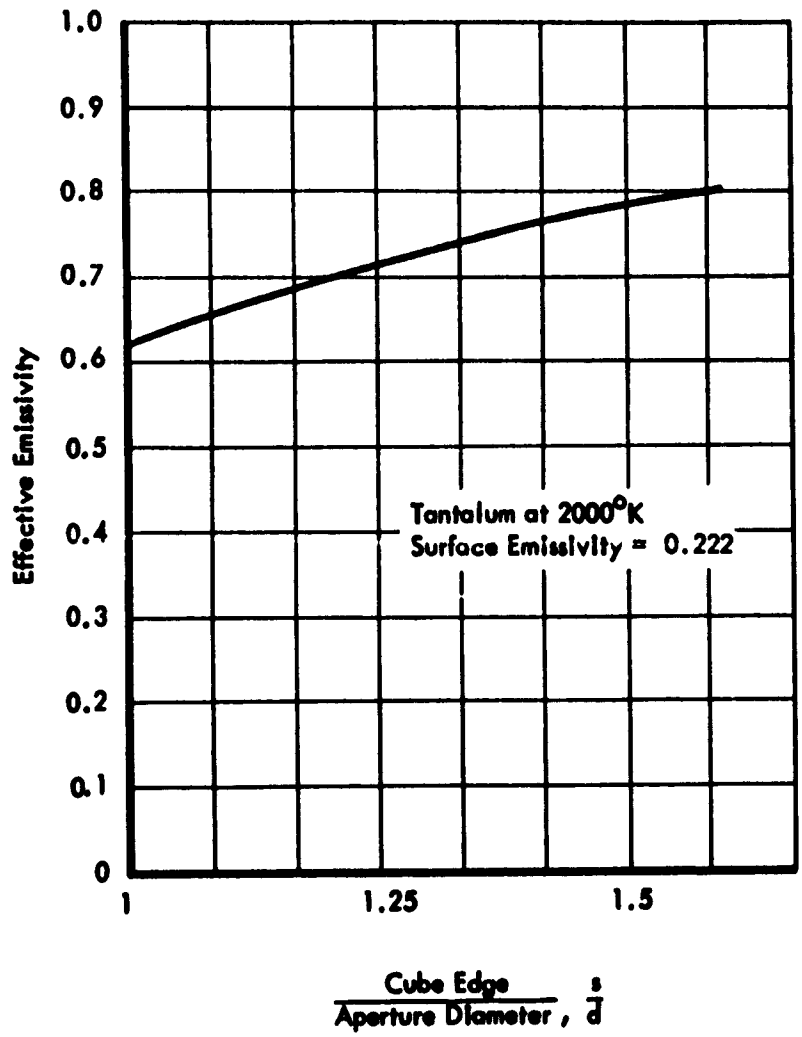

FIGURE 3.2.4

geometric configuration for the thermionic generator built under the program.

Absorber Efficiency

A parametric analysis was made for a cylindrical cavity absorber to determine absorber efficiency as a function of variations in the following parameters.

1. Cavity wall surface absorptivity, α_o
2. Solar flux concentration ratio, C_f
3. Solar concentrator aperture ratio, D/f
4. Cavity depth-aperture ratio, d/r
5. Cavity surface emissivity, ε_o
6. Cavity surface power density, q_g
7. Cavity surface temperature, T

The results of this analysis are plotted in Figure 3.2.5.

The following conclusions have been drawn from an examination of these curves.

1. The most promising methods of increasing absorber efficiency appear to be (a) increasing cavity surface absorptivity, and (b) increasing cavity surface area.

2. Increasing concentrator aperture ratio will increase efficiency, but will also have an effect on flux concentration ratio. The net effect remains to be investigated.

3. Efficiency exhibited a minimum change in the range of cavity depth-to-aperture ratio investigated. Variations of this parameter to obtain a significant increase in efficiency appear to be impractical because of geometry limitations associated with the thermionic energy converters presently being used or considered.

DEPENDENCE OF ABSORBER EFFICIENCY ON VARIOUS PARAMETERS
FOR A CYLINDRICAL CAVITY AT 1 A.U.

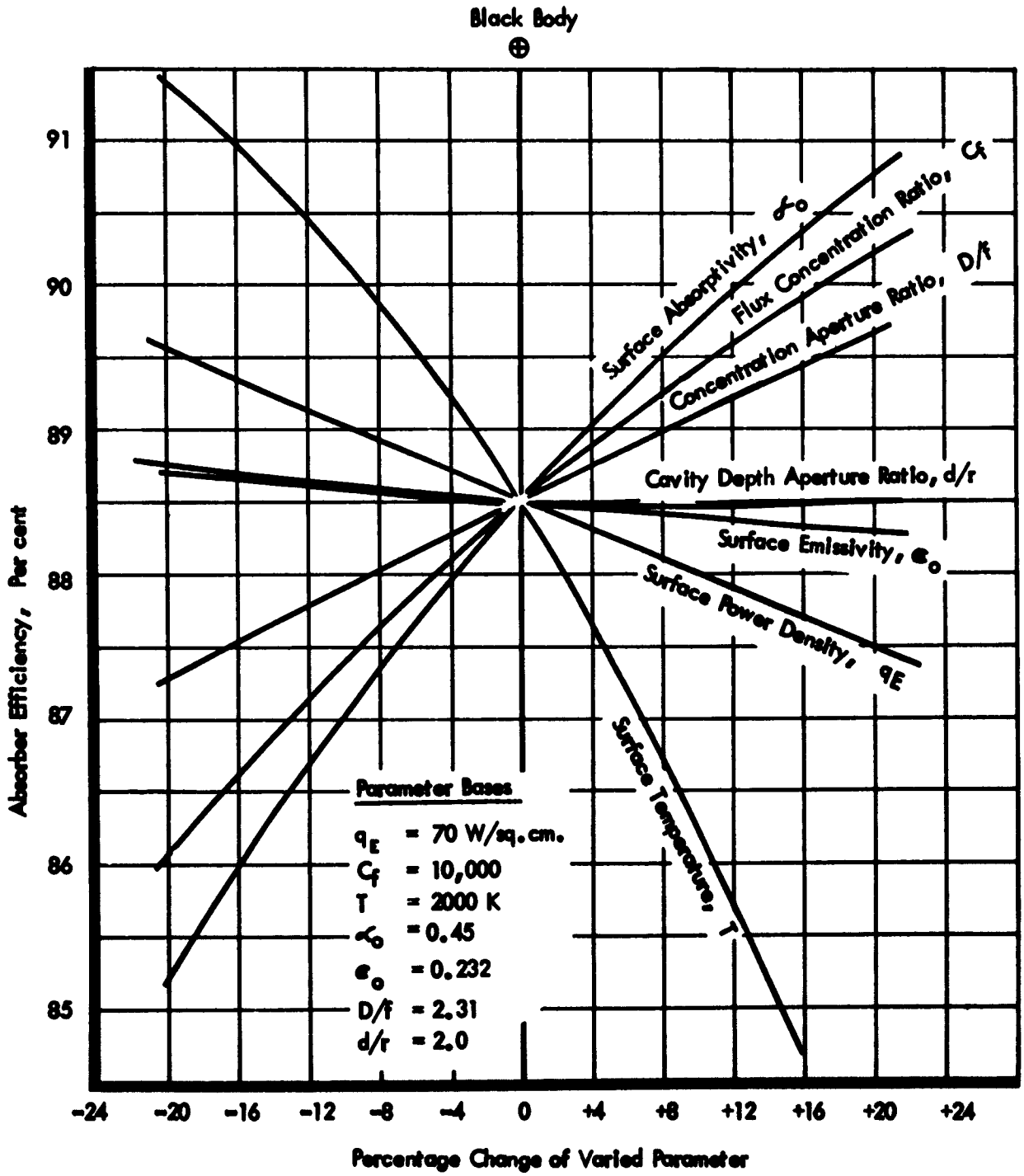

Fig. 3.2.5

3.3 Solar Concentrators

Because of the high energy density required to operate thermionic converters efficiently, only a very precise solar concentrator is suitable for use in a solar thermionic power system in which efficiency is a chief criterion of performance. The concentrator selection is therefore limited to a precision paraboloidal reflector which can be inspected on the ground and stowed on a launch vehicle without folding or deflating. Other types of concentrators may be made sufficiently accurate to produce thermionic power, but the system utilizing them will not compare favorably on an efficiency basis. Some of the less precise types are described below.

The Fresnel reflector offers the advantage of a nominally flat surface for easier stowage. However, steps between the reflecting surfaces form large areas which do not concentrate incident solar flux, and efficiency is considerably reduced. Fabrication is also difficult.

The Petalline reflector can be folded for stowage in its vehicle to obtain low volume requirements, but the loss of precision associated with the folding mechanism is a serious drawback. Dimensional control of petal-shaped reflectors is far more difficult than for shell-shaped reflectors.

The Fresnel lens is not as sensitive to distortion as reflectors, but it has a step loss similar to Fresnel reflectors. Glass lenses are subject to breakage and plastic lenses are susceptible to ultra-violet damage.

Low concentration systems which do not approach thermionic requirements include: the hemispherical concentrator, the "umbrella" type concentrator, and the parabolic cylinder concentrator.

3.3.1 Solar Concentrator Materials

The chief criteria by which solar concentrator materials should be judged are:

1. Density
2. Rigidity
3. Strength
4. Dimensional stability
5. Formability
6. Surface finish attainable
7. Vapor pressure

Table 3.3.1 summarizes many of these properties for materials which have been considered. The materials listed are good in most respects but all seem to have at least one major drawback.

Aluminum is very good in all respects except that it is difficult to obtain a satisfactory mirror-like surface finish by standard polishing methods.

Beryllium is attractive because of its high strength-to-weight ratio. Because of its high cost, it has not been used in the fabrication of large shapes, and the fabrication of solar concentrators from Beryllium would require a development of fabrication techniques. The seriousness of the toxicity problem associated with Beryllium is largely a matter of opinion.

Copper and its alloys are readily electroformed and easily polished. Copper suffers the disadvantage of a very low strength-to-weight ratio.

Nickel is easily electroformed and easily polished. Much work has been done on the development of nickel electroformed solar concentrators. (See EOS Report 1587 - Final; prepared for NASA under Contract NAS 7-10.) The chief disadvantage of nickel is its high density. The magnetic properties of nickel may also be a disadvantage for some applications.

Steel may be fabricated with high strength, but it has the disadvantage of high density. Special finishing techniques are probably needed to obtain a mirror-like finish.

Titanium and its alloys have high strength and low density. Forming techniques in their present state are inadequate for the production of solar concentrators.

Epoxies and plastics present a variety of difficulties depending on the particular compound considered. In general, they offer little advantage over the metals and present the additional problems of dimensional instability, and thermal distortion due to low thermal conductivity.

3.3.2 Methods of Fabrication

Several fabrication methods for achieving high-precision solar concentrators have been evaluated during the course of this program to establish the advantages and disadvantages of each. Although minimum weight is a major design objective

Table 3.3.1 Physical Properties of Solar Concentrator Materials

Material	Density g/cc(20°C)	Coefficient of Expansion x 10^{6} (0 - 100°C)	Strength	Modulus of Elasticity (x 10^{-6})	Formability	Attainable Surface Finish	Vapor Pressure 1000°K-mmHg
Aluminum	2.70	23.5	Moderate	10	Good	Good	7×10^{-8}
Beryllium	1.848	13.0	High	43	Poor	Good	2.5×10^{-8}
Copper	8.96	17.0	Low	17	Excellent	Poor-Must Be Plated	9×10^{-9}
Nickel	8.90	13.3	Moderate	30	Excellent	Excellent	7×10^{-11}
Steel	7.8	6.3	High	30	Good	Fair	2×10^{-10}
Titanium	4.5	8.8	High	16	Poor	Fair	1×10^{-11}
Epoxies	—	Poor	Low	—	Good	Good	—
Plastics	—	Poor	Low	—	Good	Good	—

considered during the investigation of materials, structural concepts, and fabrication techniques, the optical properties of a particular concentrator structure determine how much area is needed to provide the required input power through a given cavity aperture for use by the conversion device. Therefore, surface quality as well as weight must be included in the criteria used to judge material selection and fabrication technique. In brief, the chief criteria by which fabrication methods should be judged are: (1) dimensional accuracy of the fabricated part, (2) surface finish of the reflecting surface, (3) suitability of the fabrication process for the size of concentrator to be fabricated, (4) compatibility of the process with the material being fabricated, and (5) cost of the process. Electrodeposition onto an optically ground master surface provides excellent reproduction of the master. Nickel, copper and silver can be deposited, but nickel gives the best strength properties due to its high yield stress value. The electroforming process can provide a completely integral structure with reflecting surface, supporting ring, point of attachment brackets, etc., all produced from one common material. In this process there is no need for adhesives, welds, brazes, etc. This fabrication process is extremely desirable for the production of space-type concentrators. A possible disadvantage is its higher specific weight as compared to aluminum and its magnetic properties.

The stretch forming process using aluminum does hold promise for a lighter weight concentrator. In this process, the controlled yielding of a metal sheet over a master surface provides parts having a minimum springback from the tool. Large concentrators can be formed by joining several sectors or by overlapping several stretch-formed paraboloidial strips. The pieces, however, must be held in shape with an adhesive bond. Weights of 0.6 pounds per square foot including a support ring are attainable by this process as compared to 0.75 pounds per square foot for the electroformed concentrators.

Because of its lighter weight and adaptability to the stretch forming process, aluminum, stretch-formed concentrators are under development. To date, it has been shown that the process holds promise if refinements in the stretch operation and subsequent epoxy surface finish operation can be developed. It must be concluded, however, that only the electroformed concentrator is currently suitable for use in solar thermionic space power systems.

3.3.3 Solar Concentrator Analysis

In attempting to utilize the usual approximations for determing a focal plane flux distribution, it was found difficult to superimpose the effects of concentrator misalignment, monochromatic limb darkening, non-parallel nature of solar radiation, concentrator surface roughness, inequalities in concentrator surface reflectivity, et al. It was therefore desired to derive a mathematical formulation and numerical computational procedure that would permit the accurate, simultaneous consideration of the various effects on the collected flux distribution. The characteristics of concentrator surface roughness and solar limb darkening are the most important constituents of an observed flux distribution.

Formulae and associated numerical analysis for computing flux distributions have been derived. This mathematical formulation permits considering simultaneously roughness of the concentrator surface, misalignment of the concentrator, misalignment of the focal surface, irregularities from the finite disk of the sun which does not emit parallel rays, monochromatic solar limb darkening, et al. A dispersion function is attributed to the concentrator surface. In particular, a dispersion function is computed by considering surface imperfections to be described by a double Fourier series which has been approximated by its first harmonic. This concept has yielded computed flux distributions very nearly those observed, whereas other methods (e.g., a Gaussian distribution of concentrator surface normals) have failed to preserve the essential nonmonotonic radially-decreasing flux distribution which, from these calculations, appears to be characteristic of a dispersing surface. This model for surface roughness, not necessarily microscopic, possesses one parameter (δ/λ, which is the height-to-width ratio of an individual sinusoidal surface imperfection) which alone proves to be the fundamental parameter for the computation of the correct flux distribution. This parameter is simply related to the "circle-of-confusion" and can be used as a design parameter for specifying mirror accuracy throughout its surface. The general formulation of the flux distribution involves a quadruple integration in which the limits and integrand present an imponderable problem analytically and a problem not amenable to conventional numerical integration. The integrand and subsequent numerical evaluation are greatly simplified, without additionally complicating the limits of integration, by the introduction of the

pseudosun concept and a matrix algorithm for its numerical computation. The pseudosun is a radiating disk replacing the sun, which has the proper law of monochromatic limb darkening so as to absorb the effect of surface dispersion and hence permit the concentrator to be treated as being perfectly smooth. (Hence, by this definition the formulation of the surface roughness is absorbed in the formulation of the pseudosun.) In order to calculate an accurate and realistic pseudosun, an accurate intensity function for the monochromatically limb-darkened sun has been obtained by fitting a large amount of precise data to an astrophysical formula for this function. The solar surface temperature and wavelength-integrated central intensity have been determined from this data as boundary conditions. Flow charts for the numerical computational procedures for calculating a pseudosun and the resulting flux distribution for a parabolic concentrator were developed and applied, with a digital computer, to a specific concentrator.

The results of these computations (See Figure 3.3.1) when compared to observed flux distributions indicated the general applicability of these methods and demonstrated the fundamental importance of the surface imperfection, b/λ, as a means of faithfully computing flux distributions as are observed and as a design parameter for concentrator surfaces.

These results strongly suggest that further work should be done with the dispersion function. Modifications of the sinusoid surface imperfection should be investigated from which fundamental parameters similar to b/λ could be determined. As a further refinement, a probability distribution should be given to these fundamental parameters, and in particularl b/λ, to improve the accuracy of the flux distribution determination.

Determination of Pseudosun Intensity Distribution

The pseudosun used in the above analysis which resulted in the intensity distribution given in Figure 3.3.1 was based strictly on a hypothetical surface dispersion model. Therefore, a further analysis was made to determine the pseudosun intensity distribution from experimental data so that a comparison could be made with the hypothetically determined pseudosun. The experimental flux profile data was obtained on a 31.5 inch diameter solar concentrator.

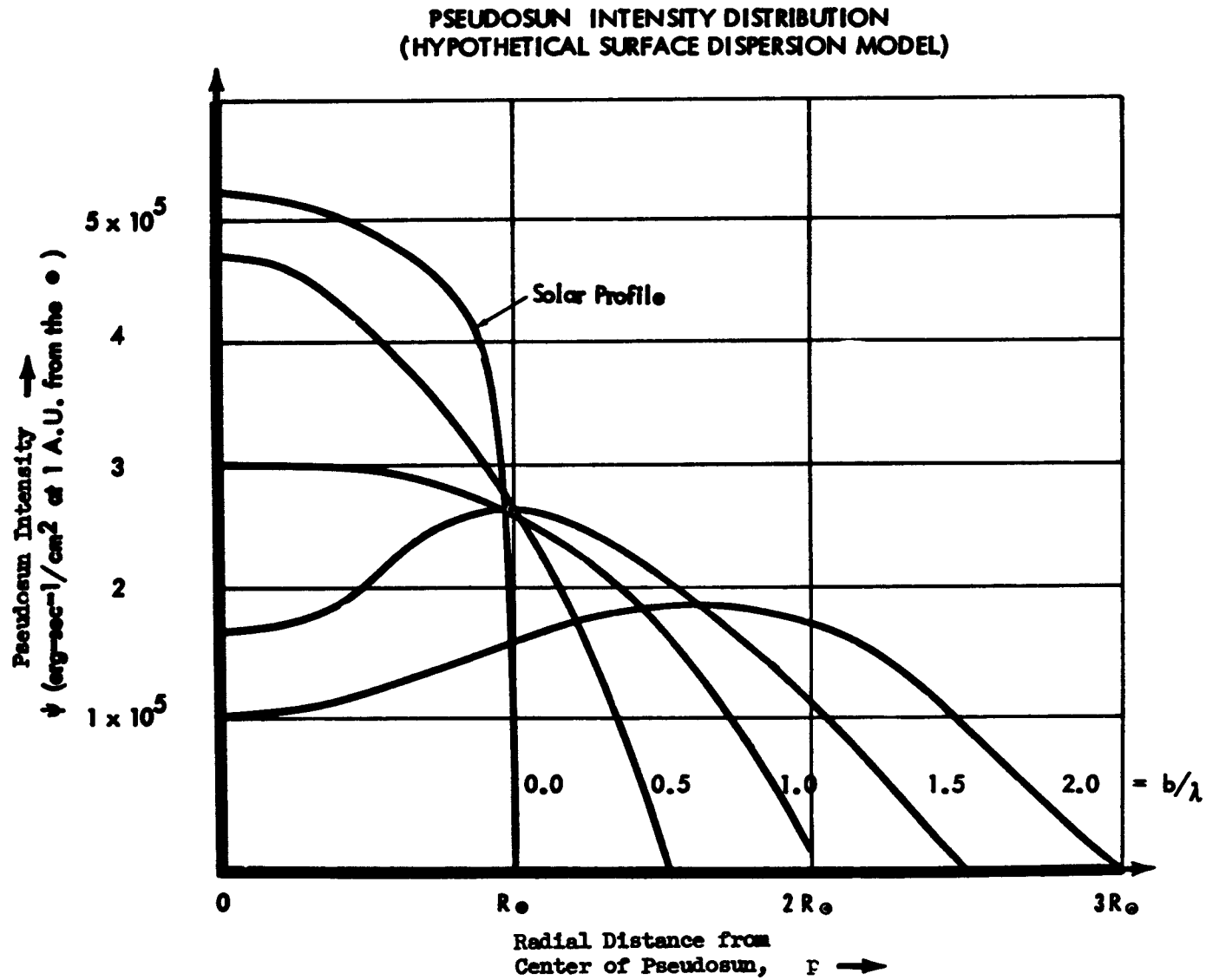
PSEUDOSUN INTENSITY DISTRIBUTION
(HYPOTHETICAL SURFACE DISPERSION MODEL)
Pseudosun Intensity → (ergsec⁻¹/cm² at 1 A.U. from the ⊙)
5 x 10⁵
4
3
2
1 x 10⁵
Solar Profile
0.0
0.5
1.0
1.5
2.0
= b/λ
0
R⊙
2R⊙
3R⊙
Radial Distance from
Center of Pseudosun, r →

Fig. 3.3.1

If the pseudosun is assumed to be made up of incremental circular suns of various intensity, the sum of the focal plane flux distributions corresponding to these incremental suns must equal the focal plane flux distribution obtained with an actual concentrator. The latter was obtained from the 31.5 inch diameter concentrator and the distribution corresponding to circular uniform sun was determined by calculation, using a method similar to that employed by Hukuo and Mii. For this analysis, rather than using the curves of flux versus radius, the curves of integrated power versus area were used. This choice was based on the desirability of working with functions without sharp discontinuities. The power versus area curve for the 31.5 inch concentrator is shown plotted in Figure 3.3.2 and the power versus area curve for a uniform circular sun is shown plotted in Figure 3.3.3. It will be noted that the ordinates have been normalized so that the total reflective power is equal to unity. The incremental suns were chosen such that the areas of succeeding suns increased in geometric progression by a factor of 1.259, which is the tenth root of 10. Intensities for the incremental suns were chosen such that when the incremental suns were subtracted from the power associated with the true mirror, the remaining power was 0 or as near to 0 as could be achieved. The maximum deviation from 0 was 8 parts in 1000 and the average was between 1 and 2. The intensities of these incremental suns are shown plotted in Figure 3.3.4 such that the combination of them shows the intensity distribution of the pseudosun.

The shape of the pseudosun as shown in Figure 3.3.4 does not agree very closely with any of the shapes shown in Figure 3.3.1. It seems, therefore, that the hypothetical surface model assumed is inadequate. Other surface models should be examined to find one which will approximate the results of these calculations. An alternative would be to use the experimental data developed and work back to determine a surface dispersion characteristic and possibly the surface model which will yield the desired pseudo sun intensity distribution.

It will be noted in Figure 3.3.4 that the tail end of the curve is negative. There is, of course, no dispersion characteristic which will yield a pseudosun with a negative portion. The negative portion of the curve is attributed to an error caused by loss of sensitivity of the radiometer in determining

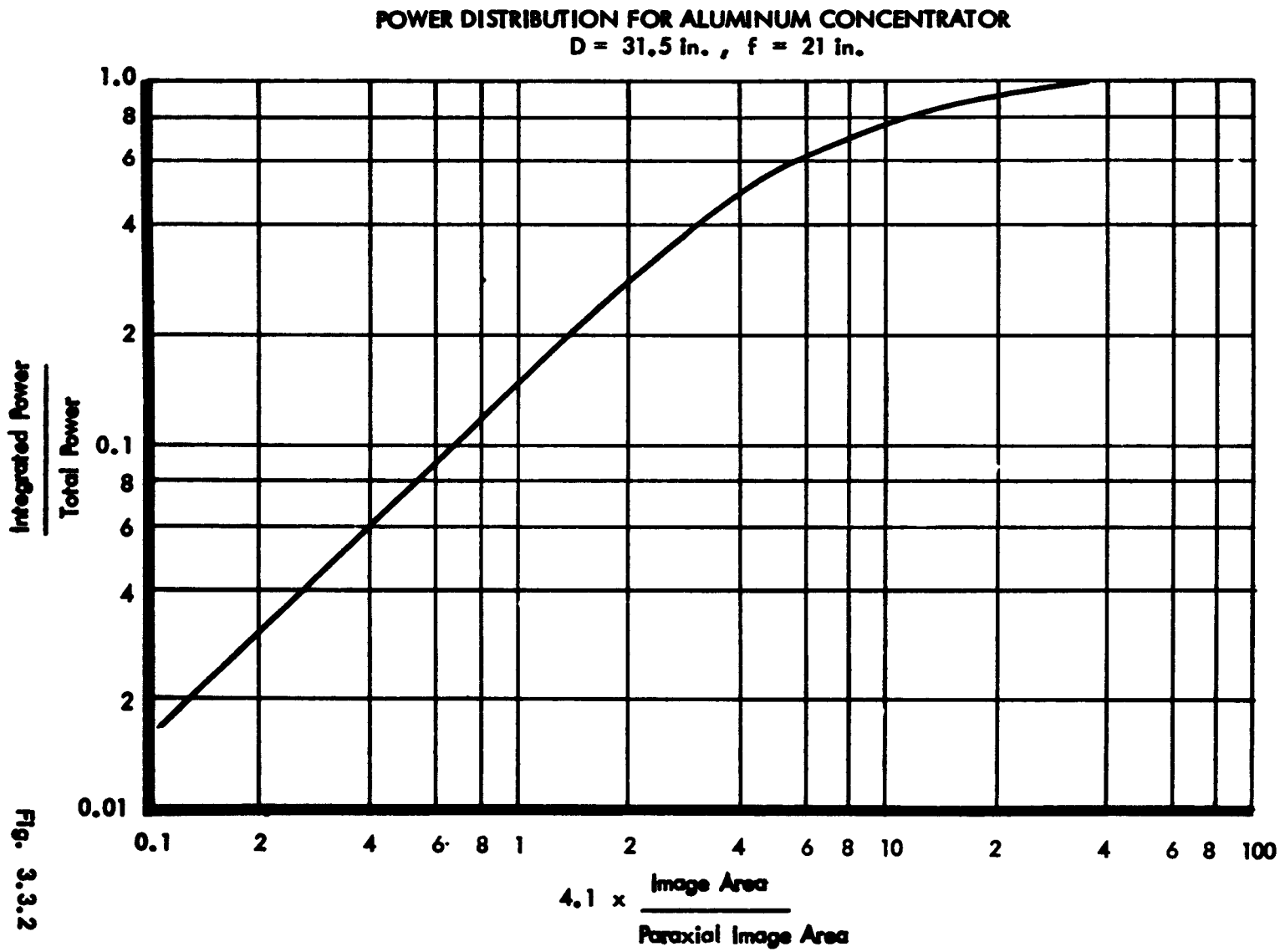
POWER DISTRIBUTION FOR ALUMINUM CONCENTRATOR
D = 31.5 in. , f = 21 in.
1.0
8
6
4
2
0.1
8
6
4
2
0.01
Integrated Power / Total Power
0.1
2
4
6
8
1
2
4
6
8
10
2
4
6
8
100
4.1 x Image Area / Paraxial Image Area

Fig. 3.3.2

POWER DISTRIBUTION FOR A PERFECT PARABOLOID
D/f = 1.5
AND A UNIFORM CIRCULAR SUN

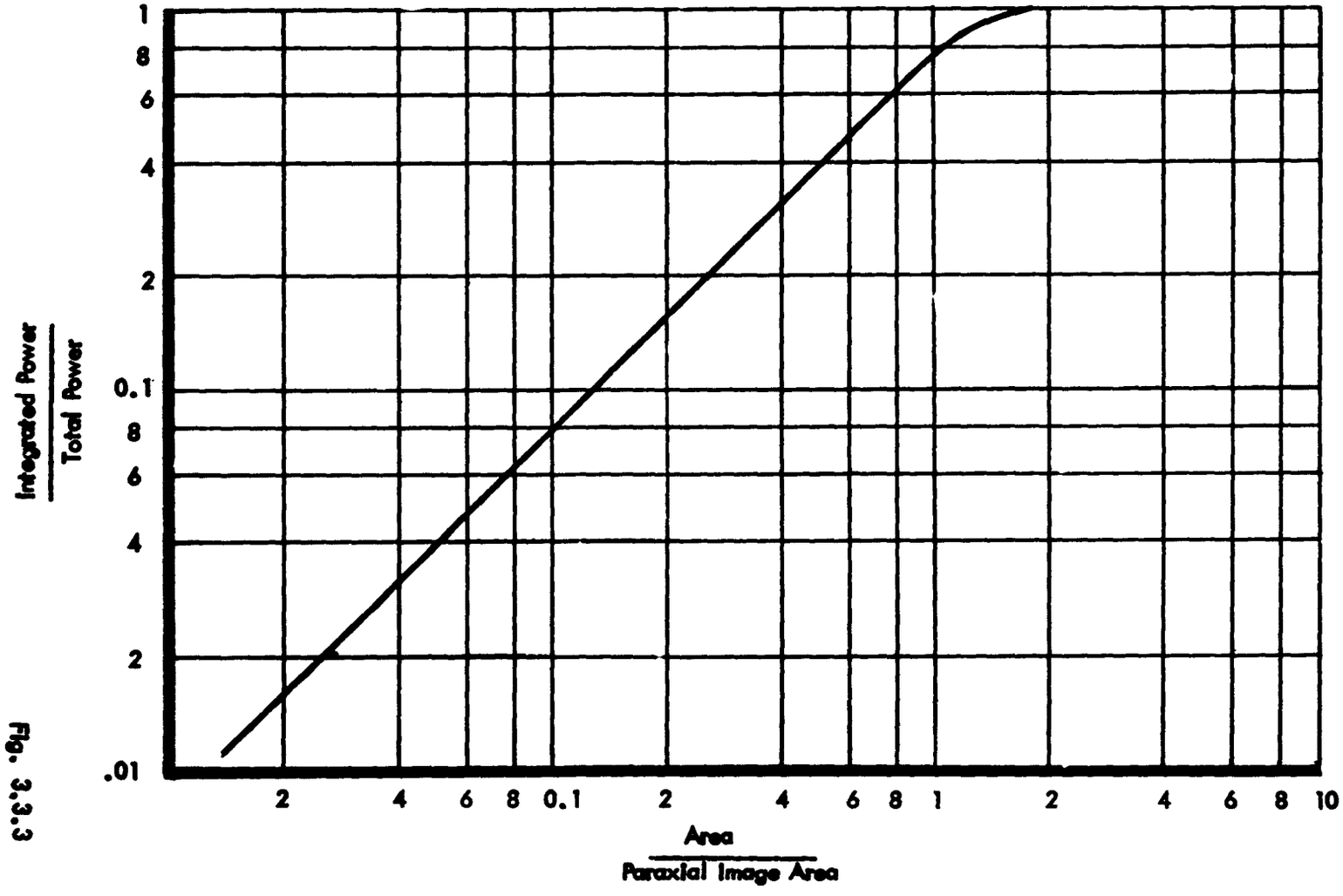

Fig. 3.3.3

100

PSEUDOSUN INTENSITY DISTRIBUTION - 31.5" ALUMINUM CONCENTRATOR

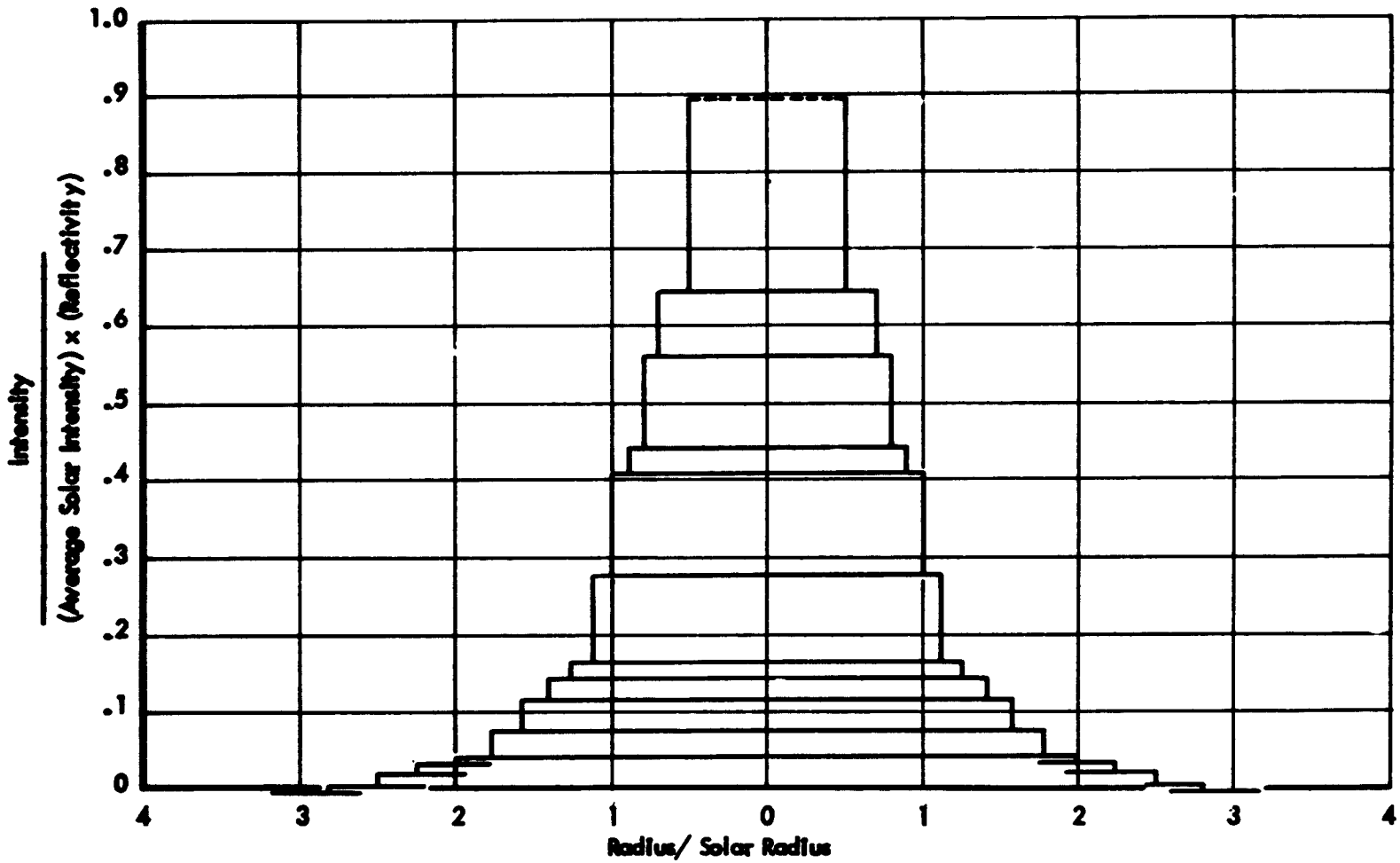

Fig. 3.3.4

the low intensity portion of the flux profile of the 31.5" diameter concentrator.

Solar Concentrator Misorientation Effects

The focal plane power and flux functions for the case of the misoriented concentrator proved to be obtainable only through an extremely lengthy computer calculation. A sample calculation was made for the case of a solar concentrator with a misorientation of one-third of the solar diameter (10.67 minutes). Concentrator rim angles of 50°, 53°, and 60° were used. The results of this calculation showed that negligible error would be incurred by assuming that the optimum cavity aperture radius for the misoriented case is larger than the optimum cavity aperture radius for the oriented case by an amount equal to the paraxial image translation; and further that the same amount of power will fall within the aperture in both cases. Reradiated power will, of course, increase with an increase of aperture area.

Figure 3.3.5 gives the percentage focal plane power in the cavity-absorber aperture, (P_c/P_f), as a function of the normalized aperture diameter $(d_a/f\ s)$ for concentrator rim angles of 50°, 53°, and 60° and for 0.0' and 10.67' misalignment of the concentrator with the sun's direction. It has been shown that this relation is dependent only on the concentrator rim angle and is independent of concentrator diameter. It can be seen from Figure 3.3.5 that when 10.67' misalignment occurs, the maximum P_c/P_f is always given by the 60° rim angle concentrator.

Figure 3.3.6 gives the percentage focal plane power retained by the cavity, (P_n/P_f), (assuming the cavity absorptivity to be constant, independent of temperature) as a function of normalized aperture diameter for a 60° rim angle concentrator $(d_a/f_{60^\circ}\ s)$ for effective cavity temperature (Te) ranging from 1900 to $2400^\circ K$. Also given in this Figure is the percentage normalized power reradiated by the aperture for the corresponding T_e's. The maximum P_n/P_f and the corresponding optimum $(d_a/f_{60^\circ}\ s)$ are plotted as a function of T_e in Figure 3.3.7. If S is the percentage of the concentrator surface not shaded and N_r is the concentrator reflectivity, then the maximum concentrator-cavity absorber efficiency as given by $[\text{max. } N_{cc} = S\ N_r\ (\text{max. } P_n/P_f)]$ can be plotted as a function of T_e as in Figure 3.3.8.

FOCAL PLANE POWER VERSUS NORMALIZED APERTURE DIAMETER

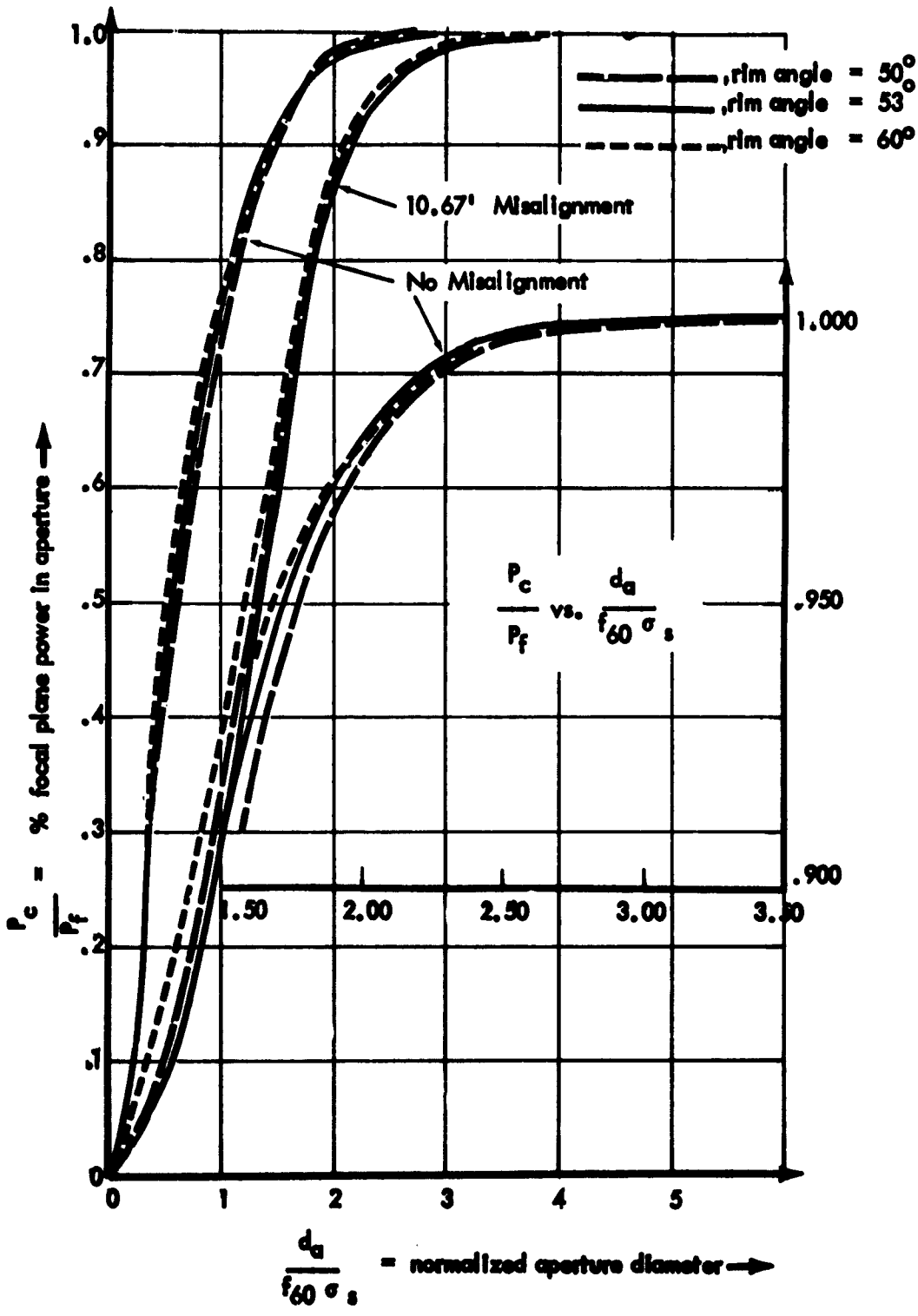

Fig. 3.3.5

CAVITY POWER VERSUS NORMALIZED APERTURE DIAMETER

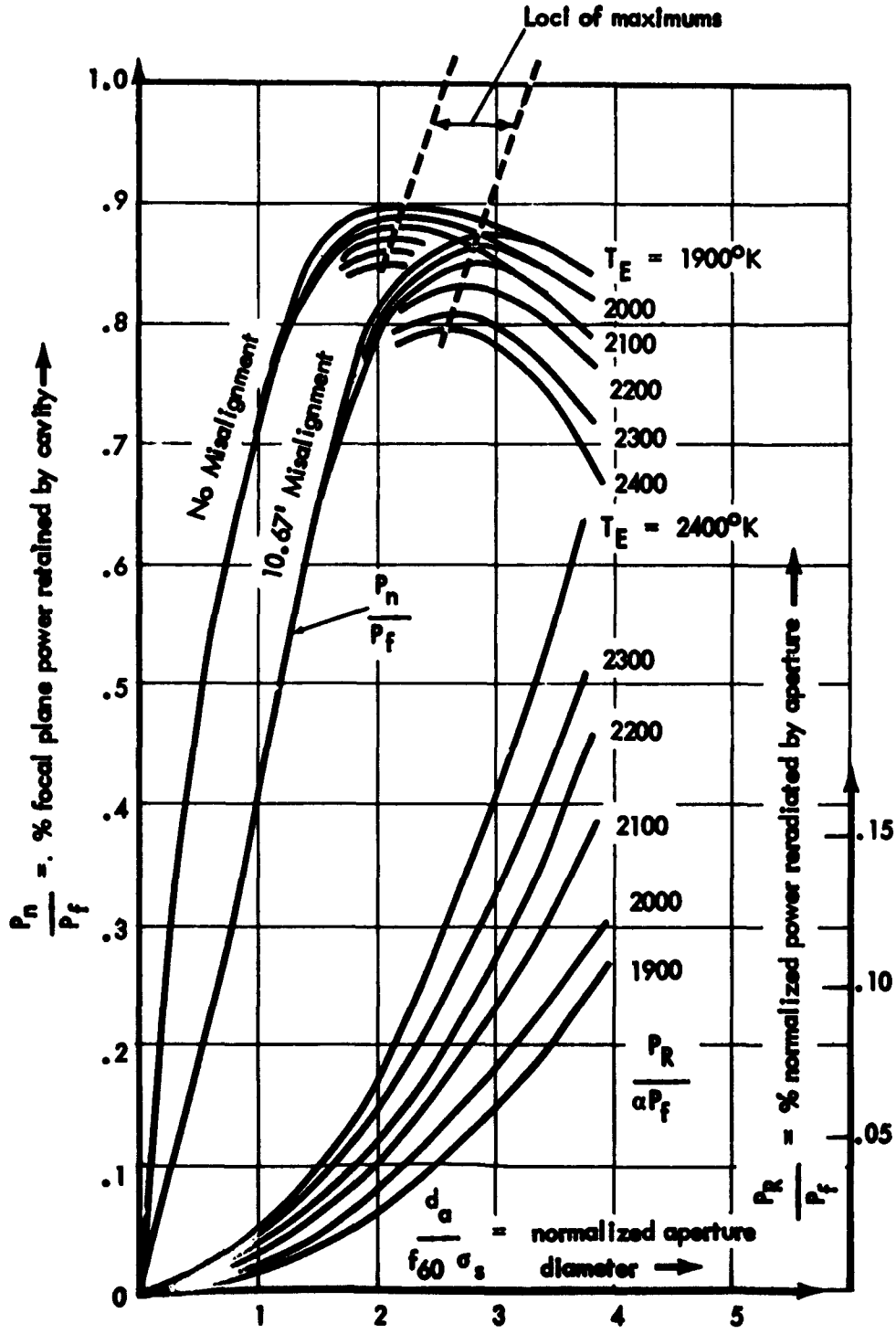

Fig. 3.3.6

CAVITY POWER VERSUS EFFECTIVE CAVITY TEMPERATURE

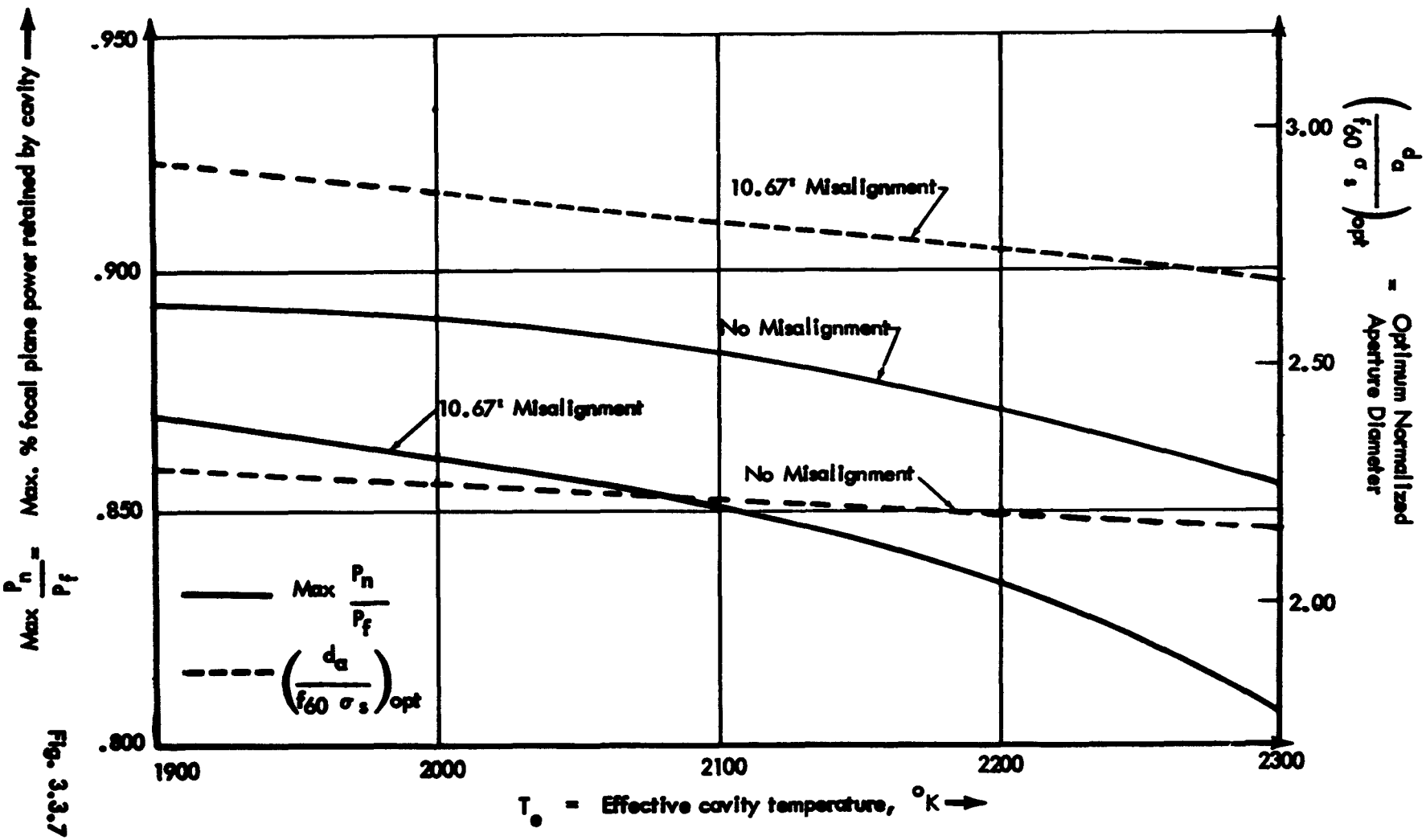

Fig. 3.3.7

MAXIMUM CONCENTRATOR - CAVITY ABSORBER EFFICIENCY
VERSUS EFFECTIVE CAVITY TEMPERATURE

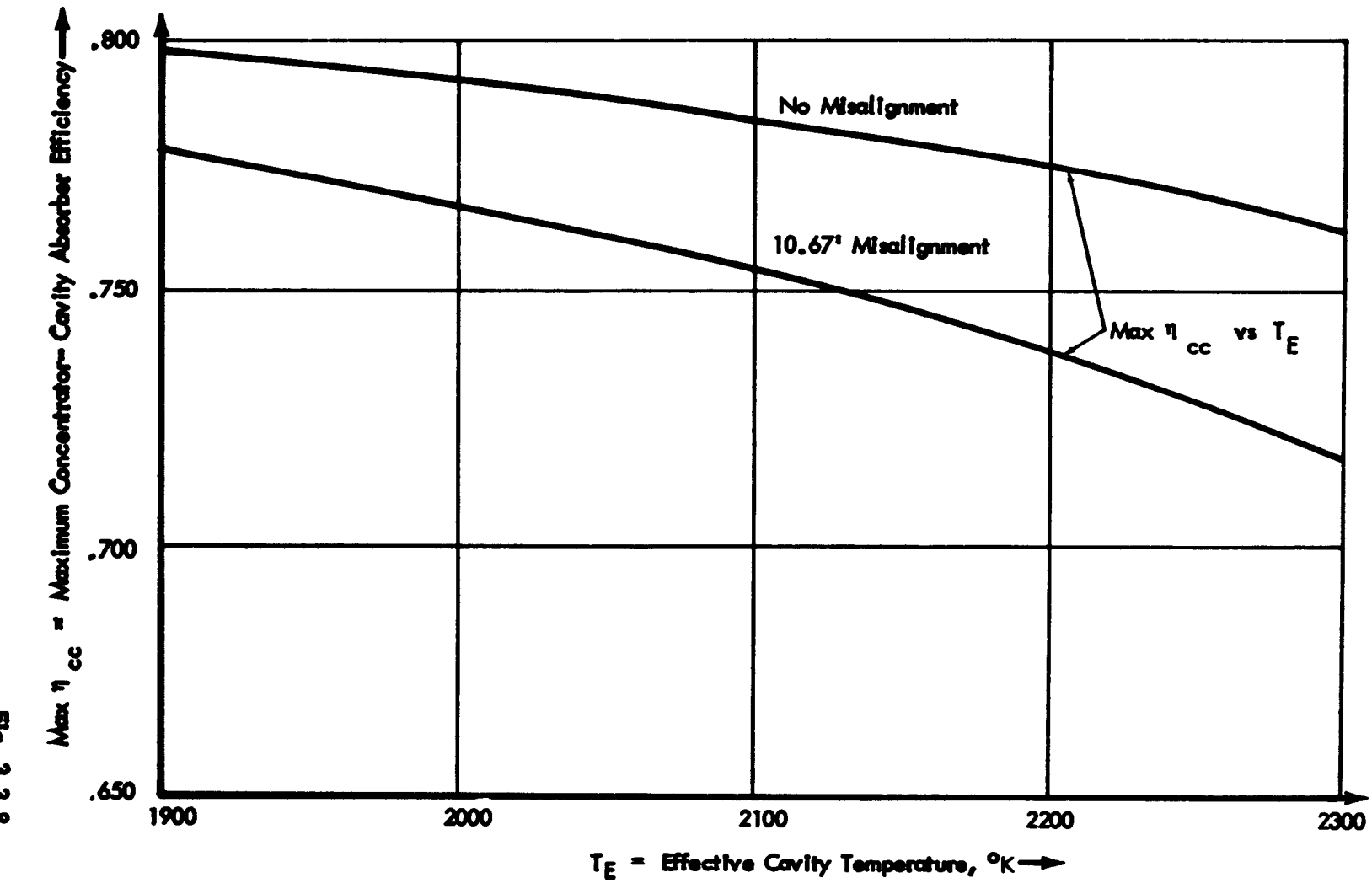

Fig. 3.3.8

3.3.4 Solar Concentrator Structure

In view of the high precision requirements of solar concentrators for thermionic systems, optical errors associated with the concentrator structure must be held to an absolute minimum.

The structure consists of two parts: the paraboloidal shell and its supports.

The experimental determination of the effect of paraboloidal concentrator shell thickness on optics and performance is prohibitively expensive for the purpose of this study. However, a theoretical relationship has been determined which appears very satisfactory when compared with the few lightweight concentrator test results available.

The weight of the solar concentrator is the sum of the shell weight and the weight of the support ring which positions the periphery of the shell. The shell weight is readily obtained from the bowl area, thickness, and density. Bowl area is determined from the equation:

$$A_B = \frac{\pi D^2}{6} \left(1 + \frac{1}{\cos \frac{\beta}{2} + \cos^2 \frac{\beta}{2}}\right) \qquad (18)$$

where β is the concentrator rim angle. A satisfactory expression for ring weight has been obtained by considering the ring to be an extension of the shell having the same thickness. The length of the extension has been made great enough to damp out any distortions induced at its outer edge. If the shell is approximated by a spherical segment of radius,

$$R = D/2 \sin (\beta/2) \qquad (19)$$

then the length of this extension is about $R \times 2/\lambda$ where:

$$\lambda = \sqrt[4]{3(1-\mu^2)}\sqrt{R/t}, \qquad (20)$$

μ = Poisson ratio

The actual support ring will not have the shape of a simple shell extension. The actual shape will be governed by additional considerations of flexural rigidity and stresses, but it has been found that the ring can be designed within the weight and overall size limitations defined by this simple assumption.

The greater the thickness and dish of the shell, the more rigid it will be, and the smaller the surface slope errors will be. Flexural rigidity equations for a sphere show that the surface slope error will be proportional to λ^3/ER (where λ and R are defined as above) for a particular residual stress level.

The weight of the shell expressed in terms of surface slope error is then:

$$W_S = \frac{\pi D^2}{4} \times 2/3\, w \sqrt{3(1-\mu^2)} \left(1 + \frac{1}{\cos \theta/2 + \cos^2 \theta/2}\right)\left(\frac{K^2 D}{2\phi^2 E^2 \sin \theta/2}\right)^{1/3} \quad (21)$$

and the weight of the support ring is:

$$W_R = \frac{\pi D^2}{4} \times \frac{4\, w}{\sin \theta/2} \times \frac{K\sqrt{3(1-\mu^2)}}{\phi E} \quad (22)$$

where: w = density of material

ϕ = surface slope error

E = modulus of elasticity

K = proportionality constant = $\phi ER/\lambda^3$

Thus, it is apparent that shell weight is proportional to $\phi^{-2/3}$

and ring weight is proportional to ϕ^{-1}.

3.4 Orientation Subsystems

General Considerations

One of the major control areas associated with the operation of a solar thermionic power generation system is that of sun acquisition and tracking by the solar concentrators. Acquisition of the sun upon emerging from the earth's shadow must be accomplished as rapidly as possible. This is necessary to provide the greatest number of watt-hours possible for use by the vehicle, and to prevent possible damage caused by improper direction of the concentrated solar energy on some surrounding structural member.

Several approaches may be taken to insure the proper acquisition and subsequent tracking of the sun. The merits of each approach are dependent upon the vehicle application and the orbital altitude. In most instances it can be assumed that a vehicle using a sophisticated solar thermionic power system will have a built-in orientation or guidance system necessary for the proper operation of other vehicle equipment such as television cameras or telescopes. With the vehicle already earth-oriented, for example, it becomes a somewhat simpler task to direct the concentrator array in terms of a vehicle reference. Depending upon the accuracy inherent in the vehicle attitude control system,it may be possible to simply drive the concentrator array at a predetermined rate to insure that the concentrators will always face the sun. This would normally require a vehicle orientation control capable of holding $\pm$ 6 minutes with an error in the drive mechanism of not more than 5 or 6 minutes. Using this approach, the concentrators would be assured of immediate sun acquisition. This type of drive necessitates that the concentrators have freedom to move about two axes.

A similar approach may be used with vehicles possessing only course attitude control systems. Here, however, it would be necessary to include a second sun-seeking system in the concentrator array. Two basic controls may be used in this instance to direct the concentrators. Solar cells or sensors used in closed-loop servo systems would be one method,and the use of bimetallic or vapor pressure heliotropic mechanisms would be the second method. The first method has the advantage of high gain and accuracy but will require some auxiliary power to operate. The heliotropic control allows a slight persistent error to exist but requires no power except the stray radiant energy already present at the converter cavity. Also, the heliotropic control may be built right into

the converter, thereby saving on system complexity. There are two types of control actions which may be used for either method; namely, fixing the concentrator and positioning the converter at the focal point or fixing the converter and aligning the concentrator axis. The selection of a control would be made primarily on the basis of the system configuration. In the case of a low power system with only a few converters, a single sun sensor and servo actuator may be preferred to direct the entire array of rigidly mounted modules. For large, complex arrays with many joints and hinges, it may be impossible to insure the alignment of all concentrators attached to the framework. Here the frame is roughly oriented towards the sun within $\pm 5^{\circ}$ at all points on the frame and the heliotropic mount in each module is used to insure accurate alignment within ± 6 minutes. The rough orientation is accomplished with a scan sensing servo system which aligns either the vehicle or the solar concentrator framework.

The nature of the vehicle mission, the orbital altitude, and the vehicle reference are all pertinent in selecting the type of orientation control most suitable. If, for example, the vehicle is required to maneuver during its orbital life and at the same time maintain power output from the converters, the orientation system may be very complex. By the same token a vehicle that is sun-oriented for its entire useful life will require far less in terms of system complexity. Also, it becomes apparent that much less power will be required to maintain vehicle orientation under some conditions. Ideally, it would be best to consider a sun-oriented vehicle with the power conversion system designed to trim the alignment of the concentrators with the heliotropic mounts. The concentrators should be deployed so as to produce the least moment of inertia, thereby requiring the least amount of energy to maintain vehicle orientation. Also, it can be seen that by having each concentrator mass individually trimmed with the heliotropic mounts there is less danger of the vehicle alignment being disturbed by inertial forces resulting from motion in the entire concentrator array.

Feasibility test models designed and built by TRW have shown that heliotropic mounts can provide the type of control action required to orient solar concentrators without using complex electronic or electromechanical devices. The TRW models demonstrated that mount power requirements are very small, representing only the energy normally lost outside a thermionic generator cavity due to the

image spread associated with large-aperture reflectors. The simplicity of the design concept and the small number of parts in a heliotropic mount promote high performance and reliability.

TRW Heliotropic Development Program

In the early part of 1959, TRW developed the concept of the simple bimetallic heliotropic mechanism shown in Figure 3.4.1. Figure 3.4.2 presents a second, somewhat more sophisticated concept. Examination of these figures will reveal the basic operating principles of the heliotropic mount.

The major difference between the two mount concepts developed by TRW is the relative position of the solar concentrator and thermionic generator. In the first concept (Figure 3.4.1), the concentrator is rigidly mounted to the vehicle and oriented toward the sun. In the second concept the thermionic generator is rigidly attached to the vehicle structure and the solar concentrator is suspended from bimetallic members also fixed to the generator assembly. The two concepts are compared below:

Concept 1	Concept 2
Small alignment errors will cause uneven heating of the thermionic converter and the bimetallic elements; therefore the converter cavity will try to center itself on the focal point to eliminate the temperature difference in the elements.	Displacement of the focal spot produces uneven heating of the elements which produces a torque or couple to swing the concentrator until the spot returns to the center of the generator. This will reduce the temperature difference in the actuator elements and by proper adjustment in sensitivity, allow only a small persistent mislocation of the spot.

Concept 2 seems to offer the greatest number of features and advantages:

1. Each concentrator can be directed independently, thereby reducing inertial coupling of the concentrator mass with the vehicle.

SELF-ALIGNING CONVERTER MECHANISM

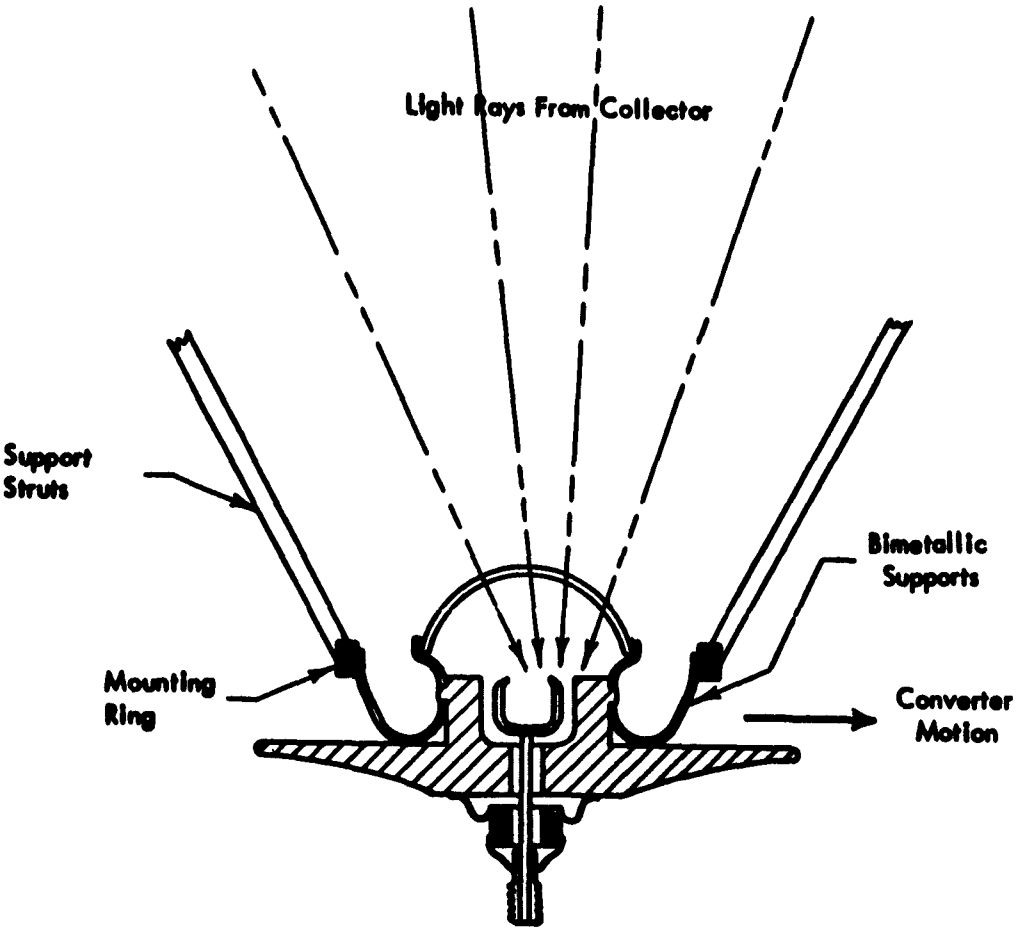

NOTE: Mislocation of focal spot causes uneven temperature distribution around anode rim. Bimetallic elements react to move converter cathode toward the focal point. This self-compensating action helps to reduce requirements for orientation accuracy.

Fig. 3.4.1

HELIOTROPIC ORIENTATION SYSTEM SCHEMATIC

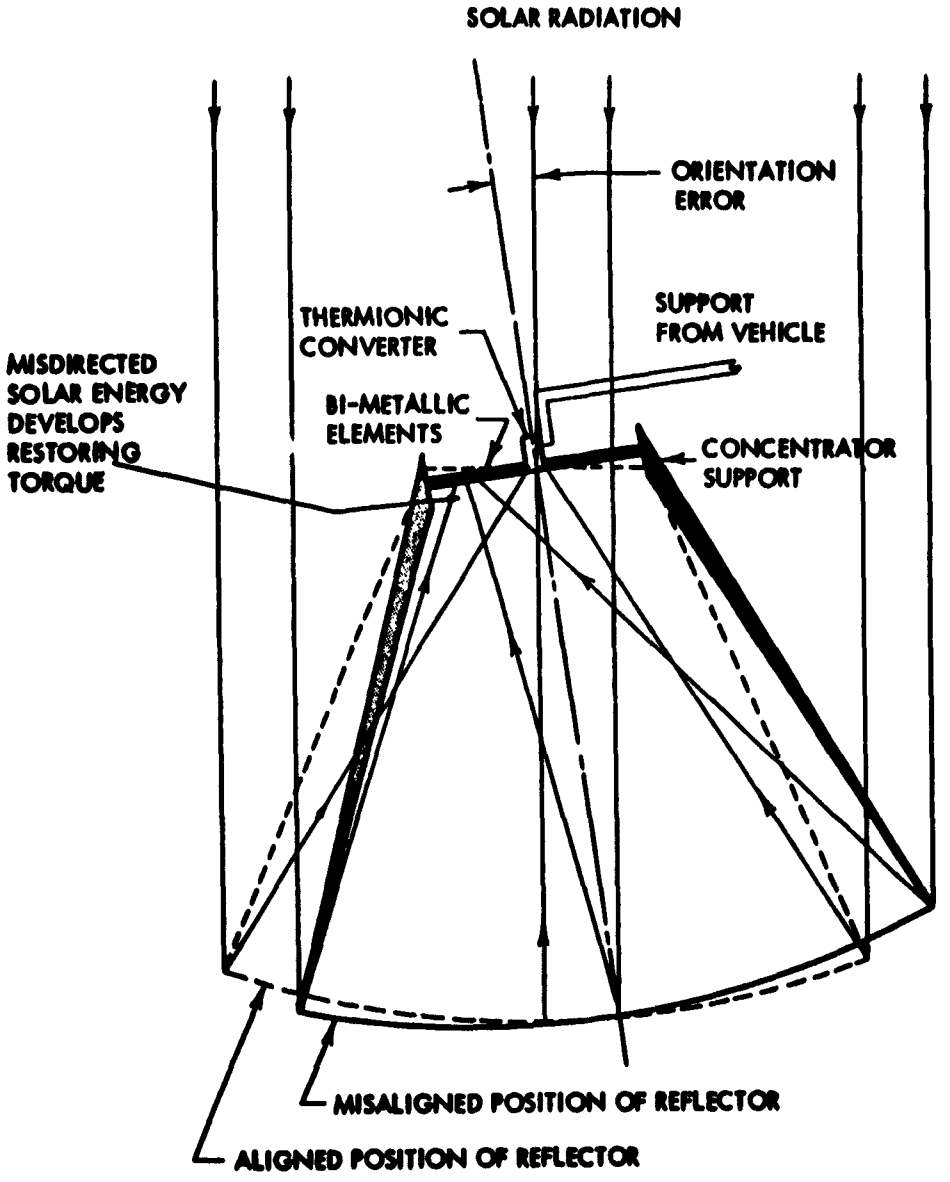

Fig. 3.4.2

2. Each mount can correct independently for structural inaccuracies in the generator array or deployment mechanism.

3. Several unique stacking arrangements for stowing the generating array in a vehicle in the least possible volume are possible.

4. The concept is ordinarily used in conjunction with a pair of gimballed rings which retain the thermionic generator in the focal plane while permitting rotation of the concentrator.

5. Gain can be easily adjusted and made very effective in controlling orientation with only a few watts of stray radiant flux.

A feasibility model is shown in Figure 3.4.3. This model also includes a calorimeter to measure total flux entering the cavity between the element tips. A water boiler on the rear end of the calorimeter provides a constant temperature heat sink at approximately 210°F. A differential temperature measurement was made along a heavy copper post leading from the cavity to the heat sink to permit an accurate determination of heat conduction. During tests this calorimeter provided a very satisfactory means of determing power input to the cavity and to the elements.

The model shown in Figure 3.4.3 was mounted in TRW's arc-imaging furnace for testing. The arc furnace was set up to permit the simulation of a variety of solar concentrator geometries; that is, the flux levels, spot size, and rim angle could all be varied at will within the furnace installation. The furnace was also mechanized to permit moving the heliotropic mount to introduce any desired persistent error in spot alignment to allow study of all mount characteristics.

A significant omission in this feasibility test effort was that no provision was made to produce the vacuum environment found in space. A vacuum environment results in a tremendous reduction in temperature in the sensing elements and in

HELIOTROPIC TEST ASSEMBLY

Fig. 3.4.3

the gain measurements for various power inputs. Heat loss from convective cooling of the sensing elements in a normal atmosphere is relatively large. A second omission of lesser importance was the lack of a representative ambient temperature in the cavity and what would normally be the thermionic converter radiator. With a thermionic generator these regions would be quite hot and the proximity of the sensing element to these hot radiation surfaces would make a significant difference in the temperatures attained by the elements. The calorimeter was designed to operate at lower temperatures to minimize radiation losses and therefore does not truly simulate a thermionic device in the heliotropic mount assembly.

Figure 3.4.4 is a plot of some typical test results for two rim angles. Other useful measurements, such as the thermal time constant which appeared to be about 1.5 minutes, were also made.

The first feasibility test program conducted in air demonstrated that a simple bimetallic control can give the required corrective action for a misoriented concentrator in a thermionic system. The gain normally required (assuming a maximum correction of 5 degrees and a persistent error of 0.1 degree) is 50, as opposed to the gain of 4 demonstrated in the test. However, this apparently large difference is easily accounted for by the excessive convection losses encountered in atmosphere and other mechanical defects found in the mount design. In the latter instance it immediately became obvious that excessive drag was present at the contact point between the elements and the aperture ring and that the size and shape of the elements were not optimum. Also, the use of six elements produced counter-torques about the gimbal axis which greatly stiffened and limited the motion of the gimbal rings. The results given in Figure 3.4.4 were obtained using only four elements placed 90 degrees apart and located on each gimbal axis.

Improved Heliotropic Test Model

Following an evaluation of the data obtained from the feasibility models and the investigation of other concepts, an improved mount was built and bench tested. The improved mount was designed around a 40-watt thermionic generator configuration which was intended for use with a 31.5 inch mirror. The generator cavity size and the 45-degree rim angle of the concentrator were used to fix the heliotropic mount geometry.

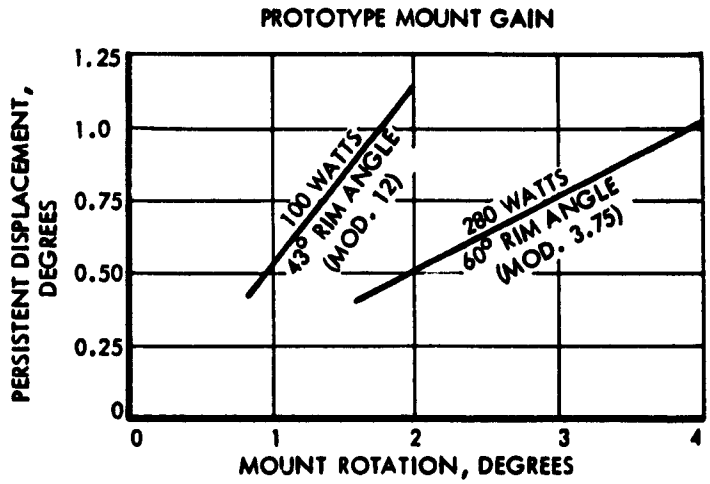

Fig. 3.4.4

Figures 3.4.5 and 3.4.6 are of the improved heliotropic mount. Figure 3.4.5 shows the complete assembly installed on a vacuum plate and equipped with heaters and other instrumentation. The large ring shown with the bell jar is mounted above the heliotropic assembly to counterbalance the weight of the mock generator. This renders the mount insensitive to gravity and permits operation in any attitude.

The mount operates as follows: The thermionic generator (parts 1, 2, and 17) is fixed to the vehicle frame and the concentrator is suspended from the lower gimbal ring. The properly-oriented solar concentrator directs concentrated flux into the cavity within the limits indicated by the included rim angle. A small fraction of this flux is intercepted by each bimetallic sensor. With proper orientation the heat input to each bimetallic element is equal and no deflection occurs. With a small vehicle misorientation, the heat input to one or more elements is increased and the elements on the opposite side of the mount receive less heat input. This differential in heat input causes the hotter elements to lift off their bearing point on the generator and the cooler elements to exert greater pressure at their bearing point. The gimbal ring to which the elements are attached then rotates, thereby restoring the force balance within the assembly. This rotation swings the concentrator so as to

COMPLETE HELIOTROPIC MOUNT ASSEMBLY
INSTALLED ON A VACUUM PLATE

Fig. 3.4.5

IMPROVED HELIOTROPIC MOUNT

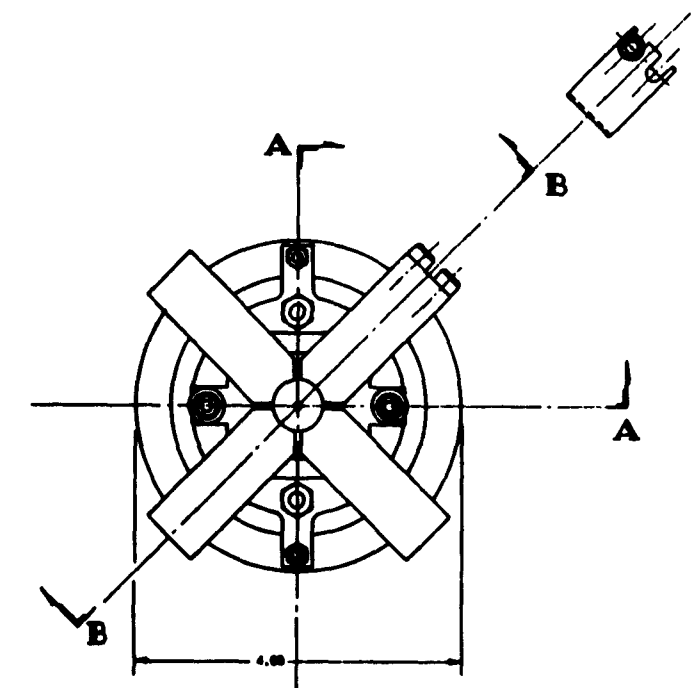

NO.	NAME	MATERIAL	NO. REQ'D
23	HEAT SHIELD, LOWER		1
22	HEAT SHIELD, INNER		1
21	SPACER		2
20	HEAT SHIELD, OUTER		1
19	JAM NUT #10 - 24		4
18	SET SCREW #10 - 24 x 1		2
17	CELL		1
16	WASHER, STD. PLAIN #10		2
15	DOG SET SCREW FL. #10 - 24 x 0.38		3
14	SOC. HD. CAP SCREW 1/4 - 28 x 0.5		1
13	SOC. HD. CAP SCREW #10 - 24 x 0.5		14
12	PIVOT BALL - 0.125 DIA.		4
11	BI-METALLIC ACTUATOR		4
10	SPACER BLOCK		6
9	LOWER GIMBAL RING		1
8	PIN BRG., LOWER		2
7	UPPER GIMBAL RING		1
6	BRG., SOCKET		4
5	JAM NUT #5 - 40		4
4	PIN BRG., UPPER		2
3	GIMBAL SUPPORT PLATE		1
2	GIMBAL SUPPORT		1
1	BOTTOM PLATE		1

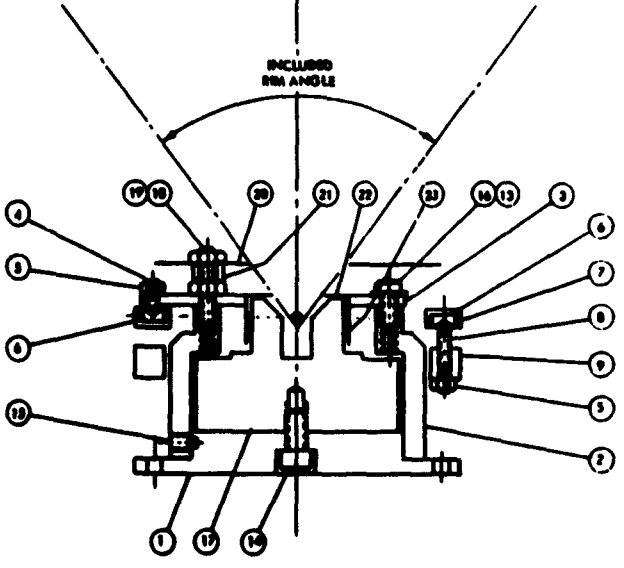

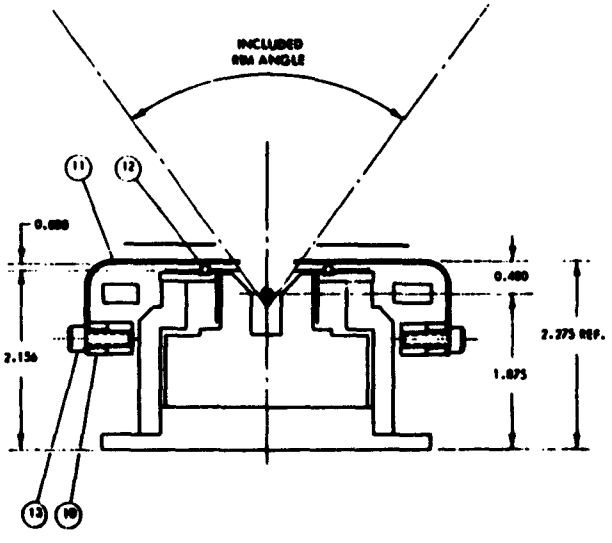

Fig. 3.4.6

relocate the focal spot at the center of the sensing elements. A small persistent imbalance in power input to the bimetallic elements remains to keep the concentrator properly oriented.

Test Results

In the-improved mount test program, the environment created was sufficient to permit a reasonable determination of what could actually be expected in a space application. Also, the instrumentation was adequate for accurate measurement and interpretation of mount performance. In particular, the following performance characteristics were carefully investigated in the course of testing:

1. angular deflection versus element temperature,
2. angular deflection verus element power input,
3. vector summation of single element motions,
4. hysteresis,
5. position or inclination sensitivity in a 1 g environment,
6. thermal time response,
7. idealized mount gain, and
8. mechanical performance factors and limitations.

Typical performance curves shown in Figures 3.4.7 and 3.4.8 indicate the satisfactory characteristics of the improved mount design. The determination of gain for this assembly was accomplished analytically using the power distribution characteristics of a 31.5 inch concentrator and the test data obtained with the mount. A gain of over 97 degrees per degree, or nearly twice the nominal value specified for a solar thermionic system, was obtained. All other pertinent factors concerning mount performance and design were deemed acceptable for a thermionic systems application.

It is a certainty that adequate heliotropic mounts for moderate size modules can be developed for any system. The development will, of course, be tempered by many factors which cannot be considered on a generalized basis. Problems of inertial effects on the vehicle, stowage problems associated with vehicle geometry, the requirement for vehicle orientation changes, etc., must be considered for a particular system. For systems in the 1 to 10 KW range, it is practical to consider the use of the heliotropic mount assuming the use of a moderate module sized with concentrators on the order of 3 to 8 feet in diameter.

DEFLECTION VERSUS POWER INPUT

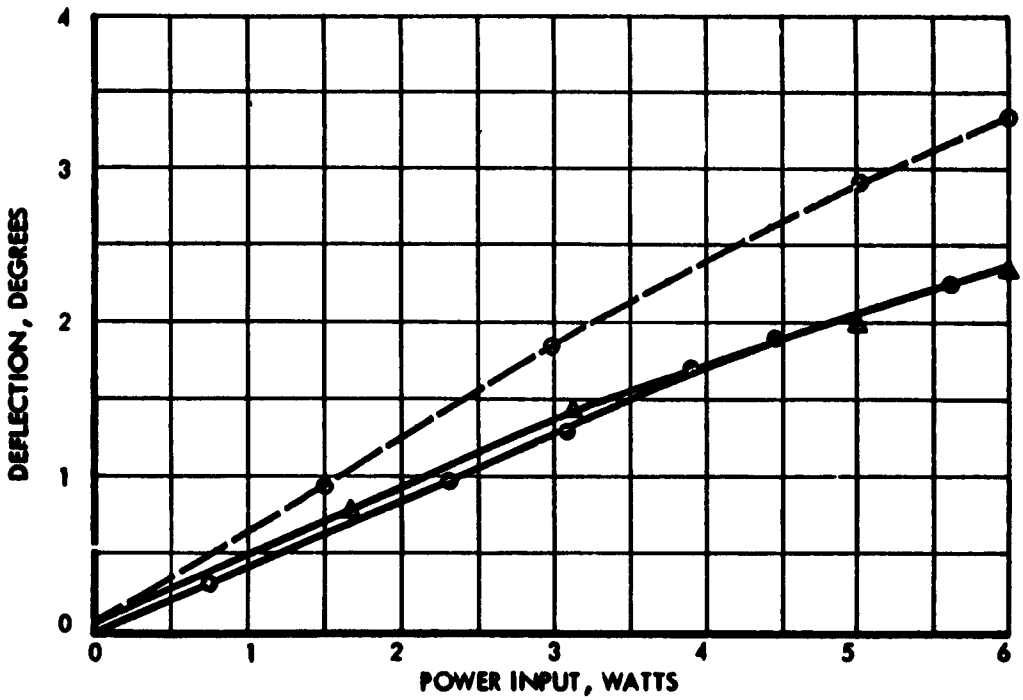

Fig. 3.4.7a

DEFLECTION VERSUS TEMPERATURE AND HYSTERESIS

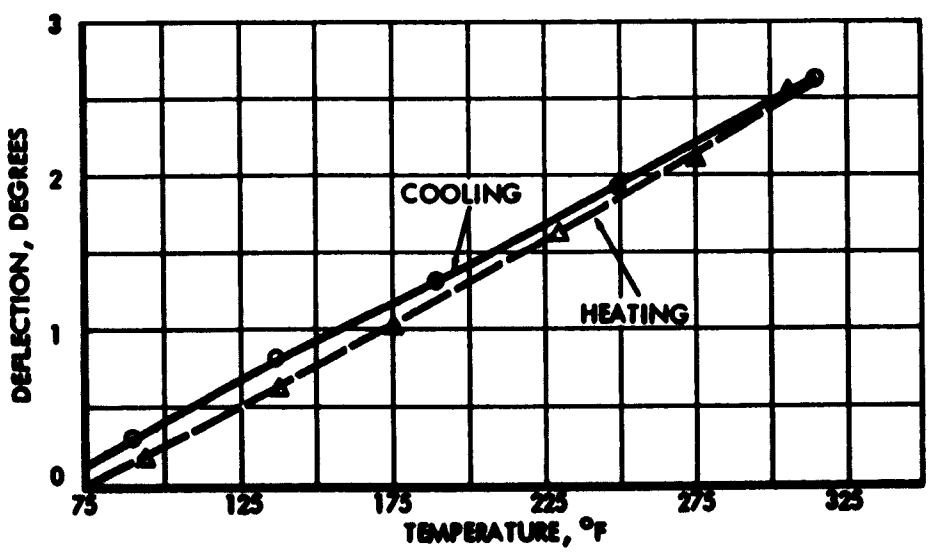

Fig. 3.4.7b

TOTAL DEFLECTION VERSUS ELEMENTAL POWER INPUT

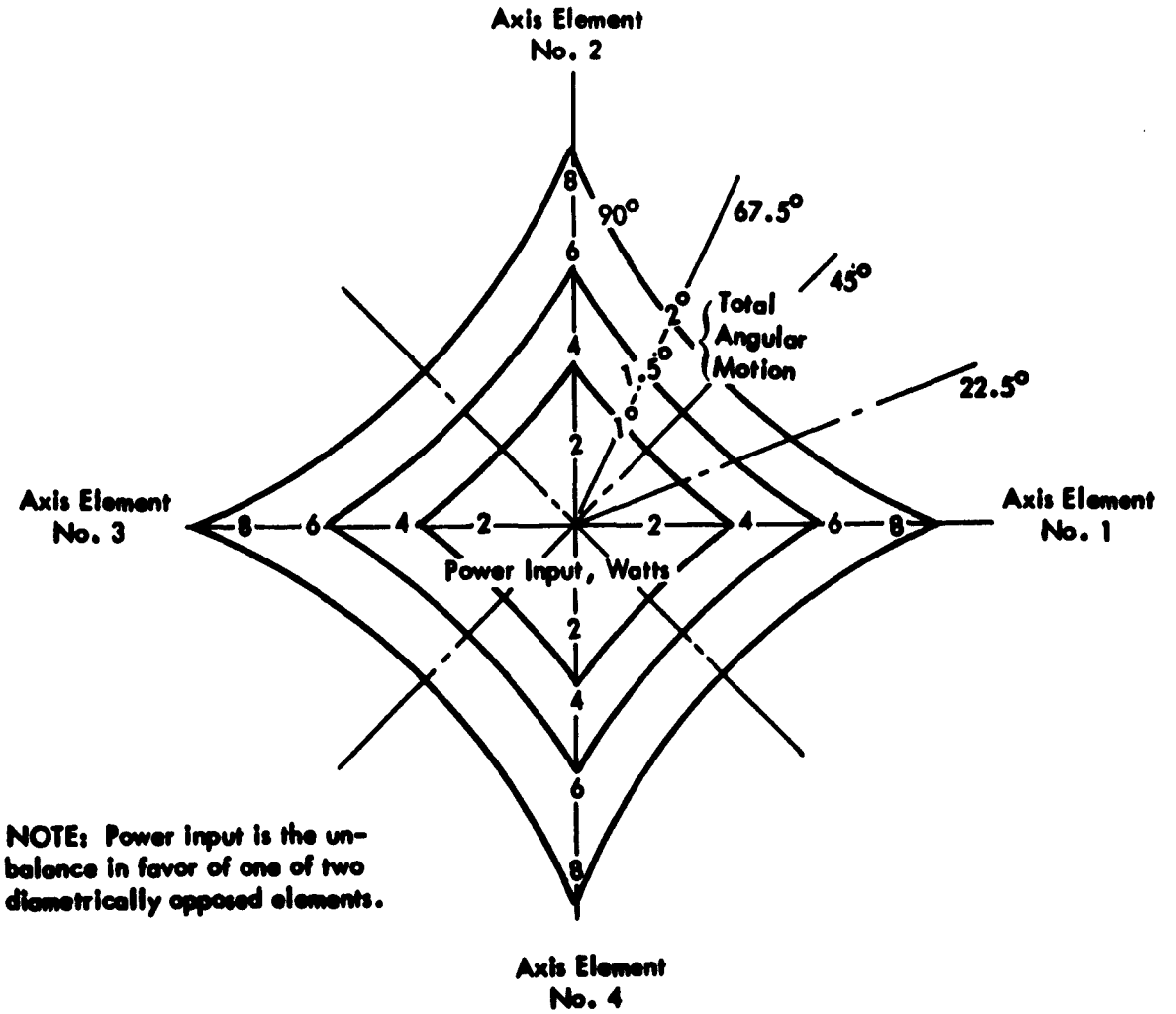

NOTE: Power input is the unbalance in favor of one of two diametrically opposed elements.

Fig. 3.4.8

3.5 Energy Storage Subsystems

Continuous operation of a solar-powered system over a complete sun-shade cycle requires some form of energy storage. Energy can be stored in many ways, but, unfortunately, most of these are not compatible with a solar thermionic system in a 1 to 10 KW range that utilizes higher temperature thermionic converters. Energy is usually stored in the form of electrochemical, mechanical or inertial, thermal, or pneumatic energy. Mechanical or inertial storage is precluded from a solar thermionic system since the mechanism would offset all weight advantages for the system and would introduce moving parts into what is now a static system. Further, the use of such storage mechanisms would most likely have an undesirable interaction with the vehicle orientation system. The use of pneumatic-type energy storage would require large and heavy tankage to provide sufficient energy for the 35-minute shade period, and complicated heavy rotating machinery to extract and convert this energy to a useful electric output.

The two methods that do hold promise are electromechanical storage and thermal storage. These two methods have been examined in detail to determine their feasibility in solar thermionic applications.

3.5.1 Thermal Energy Storage

Energy must be stored in either thermal or electrical form to maintain power during dark periods when solar thermionic generators are used to provide space power for earth orbit missions. The following properties of storage materials must be considered to select a suitable material:

1. heat capacity,
2. energy release with phase change and crystallographic transitions,
3. specific heat per unit volume,
4. melting temperature near 2000^{o}K,
5. heat of fusion,
6. anisotopic thermal conductivity to minimize thermal gradients which would decrease absorber efficiency,

7. non-corrosive to structural materials over long time periods,
8. not subject to dissociation or large pressure increases with temperature,
9. not chemically reactive with structural materials to form compounds that are solvents for the heat storage material itself.

Due to the general applicability of solids for thermal energy storage at high temperatures in space applications, attention will be focused below primarily on the factors which affect the heats of fusion and heat capacities of solids.

Considerations for Integrating Heat Storage Capability in Solar Thermionic Generator Systems

The high operating temperature of thermionic converters requires that the individual converters be arranged in a cavity geometry in order to minimize heat loss by reradiation. In general, this results in a very compact generator configuration. It is therefore necessary that the thermal energy storage material and container also be of a small volume since it will have to be placed in close proximity to the thermionic converter emitter. The mode of heat transfer from the storage material to the emitter will be radiation and/or conduction, since body forces are absent in space, and employing forced circulation at these high temperatures is improbable. Thus the thermal conductivity of the heat storage material and the surface characteristics of the container are important considerations.

Heat losses being proportional to the fourth power of the temperature indicates the desirability of minimizing temperature differences between the solar energy absorber and the thermionic emitter. A high thermal conductivity in the heat storage material will minimize temperature gradients and, consequently, the maximum temperatures within the cavity. The emissivity and absorptivity of absorber surfaces are important design variables over which the designer may have some control. For example, it would be desirable to obtain a surface with a high absorptivity to the incoming solar radiation and a low emissivity for radiation of the wavelengths corresponding to the temperature of the absorber. However, if the mechanism for heat transfer from the absorber to the emitter is also radiation, then a high emissivity would be desirable. This apparent inconsistency can be circumvented through proper geometric considerations in placing

the heat storage material within the thermionic generator package. An illustration of this would be to transfer heat into the storage material through one surface and from the storage material to the emitter through another surface, thus allowing each surface to have different radiative properties. A great deal of work in the field of coatings for space radiators is presently being done, but this is for a temperature range considerably below that of concern for thermionic devices. The problem of coating deterioration with time due to high temperature and vacuum will require investigation.

Utilization of sensible heat in addition to latent heat requires analysis of the thermionic system performance when the emitter temperature is allowed to decrease in order to obtain the sensible heat from the cooling heat storage material. An optimization will indicate the amount of sensible heat contribution desired in order to obtain the best overall power-to-weight ratio for the solar thermionic system. If a decrease in thermionic generator power output is allowable, it is possible to utilize additional sensible heat. However, this will result in an increase in the temperature cycle band width below that of normal operating temperatures. If the temperature cycle band width is permitted to increase above that of normal operation, greater solar concentrator precision is required. In addition, heat losses will increase rapidly with temperature as stated above.

Consideration of containment of the heat storage material demands equal consideration to the heat storage material itself, since the weight and volume of the container could be of the same magnitude as that of the heat storage material. Material compatibility is necessary for durations up to one year. Corrosion and alloying between the heat storage material and container material must be investigated. Therefore, the merit of a heat storage system must be evaluated on either a volume or weight basis which includes both the storage material and container material. Volume changes due to thermal and phase change will influence the container design. The strength of the container must be sufficient to withstand the partial pressures of the heat storage material components. Further, the container material must limit, if not prevent, diffusion through the container walls.

The feasibility of thermal energy storage therefore cannot be decided solely on the basis of the thermodynamic properties of the storage material but on

its integration in the solar thermionic generator system. These requirements may be mutually contradictory. It is not a priori evident that high specific heat materials possessing desired thermal conductivity properties also have high heats of fusion. Further, it is not obvious that low density materials for thermal storage will, of necessity, result in the lowest-weight heat or energy storage system. Thus, it may be advantageous to examine the higher density materials to determine whether or not they may result in more optimum thermal storage systems.

The energy storage system under consideration should be that which results in the lightest weight system subject to the various operating constraints imposed by the operating environment. The greatest bulk advantage for a thermal energy storage system will in all probability accrue by maximizing the heat of fusion, on a unit weight basis, of the thermal storage material. The energy storage capacity which results from a high specific heat is, as a rule, two or three orders of magnitude below the thermal capacity inherent in a phase change and is not available as constant temperature energy. The greatest energy storage capacity of presently known materials will come about in conjunction with the heat of vaporization, however, containment problems inherent in the transition to the vapor phase from the liquid phase may be difficult to solve. An appreciable amount of energy is, however, stored in the material in the process of raising its temperature to that level where melting occurs. Large specific heats, if not obtained at the expense of the heat of fusion, are also desirable. Since the energy must be added to the material in the form of an incident energy flux, the thermal conductivity properties of the material are also of interest.

A preliminary survey of high temperature materials has been conducted in an attempt to select promising heat storage materials for advanced thermionic generators. Table 3.5.1 presents the results of the survey. These materials demonstrate the following basic properties: (1) solid state, (2) chemically stable in the temperature range 1500°K to 2000°K, (3) high heats of fusion, and (4) high melting temperatures with low diffusion.

Gases and liquids or the alkali halides and hydrides were not considered. Although these materials demonstrate high heats of fusion (e.g., LiF,

THERMAL PROPERTIES OF PROMISING HEAT STORAGE MATERIALS

TABLE 3.5.1

Heat Contents, Cal/Mole (Based on Material at 298.15°K)

Number	Material	State	Melting Point, °K	Molecular Weight	1500°K	1600°K	1700°K	1800°K	1900°K	2000°K	2100°K	2200°K	2300°K	2400°K	2500°K	2600°K
1	Al_2O_3	C	2323	101.96	33890	36990	40100	43220	46350	49490						
2	$LiAlO_2$	C		65.92	28080	30710	33370	36060	38780	41530						
3	$MgAl_2O_4$	C		142.28	48620	53230	57850	62480	67120	71770						
4	Al_2TiO_5	C		181.86	55260	60370	65490	70620	---	---						
5	Al_2SiO_5	C		162.05	52700	57700	62800	---	---	---						
6	Be	C, L	1563	---	7480	11050	11800	12550	13300	14050						
7	BeO	C, L	2823	25.013	525.41°	576.10°	627.23°	678.77°	730.58°	782.71°						
8	B	C	2300	10.82	6410	7080	7765	8460	9165	9880						
9	B_2O_3	C, L glass	723	69.64	38160	41210	44260	47310	50360	53410						
10	W	C, L	3300	170.90	8200	8960	9740	10510	11310	12120	12940	13770	14610	15460	16300	23870
11	WO_2	C,	2012	210.90	22220	24260	26320	28400	30500	32630						
12	HfN	C		192.51	14220	15550	16900	18270	19670	21090						
13	HfC	C	2397	190.51	13250	14670	16020	17400	18810	20060						
14	$LiAlO_2$	C		65.92	28080	30710	33370	36060	38780 39.140 1820°	41530						
15	Li_2TiO_3	C(d), C B, L	1830	109.78	45230	49490	53830	58250	86.910 1850°							
16	$MgAl_2O_4$	C	2135	142.28	48620	53.230	57850	62480	67120	71770						
17	$KMg_3AlSi_3O_{10}F_2$	C, L	1670	421.31	133.980	146.630	1670(C)- 155.630	25970 1670(L)- 229.430	---	---						
18	Mg_2TiO_4	C		160.54	50760	55600	60470	65370	70300	75250						
19	$MgTi_2O_5$	C		200.12	56.850	62370	67940	73530	79130	84740						
20	MgO	C	2800	40.32	13830	15.090	16350	17610	18870	20.130 21.390 2100°						
21	Mg_2SiO_4			140.73	47950	52470	57000	61540	66090	70.650						
22	Ti	C (L), C (B)	1800	47.90	9680	10350	11100	11850	12600	1900(B) 12980 1900(2) 17260		19440		21040		22640
23	TiO	C(L), C(B)	1750	63.90	17050	18780	20380	22090	23830	25600						
24	Al_2TiO_5	C		181.86	58360	60370	65490	70620								
25	Li_2TiO_3	C(L), C(B), L		109.78	45230	49490	53830	58250 1850°	86910/ 1820(B) 59140 1820(L) 83470							
26	$MgTiO_3$	C		120.22	38660	39040	42450	45980	49680	53390						
27	Mg_2TiO_5	C		200.12	56850	62370	67940	73530	79130	84740						
28	$MgTi_2O_6$	C		160.54	50760	55600	60470	65370	70.300	75230						
29	TiN	C	3220	61.91	14980	15870	17190	18540	19840	21170						
30	W	C	3370	183.86	7720	8420	9120	9840	10550	11270		12720		14190		14.650
31	WO_2	C														
32	WO_3	C(L), C (B), L														
33	Zr	C(L), C (B)	2130	91.22	9890	10680	11470	12260	13050	13840	21300(C) 14850 21300(C) 19770	20830		21920		22830
34	$ZrSiO_4$	C		183.31	39990	42630	47290	50980	54690	58430						

*Cal/gram; C, Crystalline; L, Liquid; B, Beta; d, decomposed

Fig. 3.5.1

450 Btu/lb at 1117°K, and LiH 1250 Btu/lb at 958°K), their relatively low boiling points and instability at temperatures required for this application does not at first approximation suggest further study. LiH, for example, decomposes at 1331°K into lithium and hydrogen. Due to large diffusibility of hydrogen in materials, the containment problem may be quite severe from an engineering standpoint. The problem associated with using such a material for heat storage at temperatures of 2000°K is further complicated when one considers the high pressure differential resulting from the operation in the space vacuum.

Table 3.5.2 presents heat contents between 1500°K and 2800°K for several potential heat storage materials.

An examination of the lists of materials indicates that several materials may have heat storage properties suitable for use with thermionic generators. The suitability of any of these materials cannot be definitely determined, however, without recourse to an extensive development and evaluation program. It has been proposed that a heat storage materials study be made. Such a study may prove the feasibility of using one or more of the better materials, such as beryllium oxide with thermionic generators, but as of this time it appears impractical to utilize thermal storage in any proposed thermionic system. Calculation of the heat storage capacity of BeO shows that 1780 Btu/lb can be realized over a temperature range of 2000°K to 2820.9°K; but it is very doubtful if the necessary storage material could be packaged in the quantities required, considering the geometries associated with our present thermionic generator concepts.

Also, there is little certainty of the necessary heat transfer taking place or that the materials involved would be compatible for long-term operations.

TABLE 3.5.2

HEATS OF FUSION AND TRANSITION FOR HIGH TEMPERATURE HEAT STORAGE MATERIAL

Material	ΔH fusion (or transition), Cal/mole	Melting Temperature, °K
Be	2,800	1563
BeO	13,500	2823
B	5,300	2300
B_2O_3	5,500	723
Hf	5,790	2495
Li_2TiO_3	2,750 (Transition) 26,330	1485 1820
$K Mg_3Al Si_3O_{10}F_2$	73,800	1670
Mgo	~15,000	2800
Ti	950 (Transition) 4,460	1155 1940
TiO	820 (Trans)	1264
Li_2TiO_3	2,750 (Trans) 26,330	1485 1820
Zr	915 (Trans) 4,900	1135 2130

3.5.2 Electrical Storage

With the elimination of thermal storage as an energy source for thermionic systems, the selection of an appropriate battery storage system is indicated. The selection of one of the several promising types of secondary batteries for use in a solar power system is dependent upon the particular requirements of the power system and the characteristics of the batteries. For any space vehicle system application, a high specific power and good reliability is mandatory. Further, the nature of the operating environment necessitates a hermetic assembly, and one which is structurally rugged to withstand the stress of launch loading. The inclusion of such a battery in a 90 minute orbital application with a one year life requirement, as is the case for the proposed thermionic systems, also requires that the battery has a high cyclic life. The selection of the most efficient batteries available consistent with good cycle life and minimum weight is essential because the use of secondary batteries for electrical energy storage incurs electrical losses of various types which must be charged against the generating system.

In all batteries there is an ampere-hour loss with each charge-discharge cycle. That is, all of the cahrge put in the battery during charging cannot be extracted from the battery. This loss is not insignificant, but it is often omitted from charge-discharge efficiency determinations, thereby contributing to the variance of quoted performances.

All batteries also require a charging voltage higher than the discharge voltage. This voltage difference is not merely an internal resistance effect but is a function of the state of charge of the battery. The charge and discharge voltages will vary during constant current operation. Battery efficiency is often quoted as the ratio of nominal charging voltages. This method gives very optimistic performance values, not only because it omits the ampere-hour loss, but because all of the discharge power will not be usable if the discharge at a voltage above or below nominal cannot be fully utilized by the load.

Another source of loss associated with secondary batteries is the regulation of charging current and discharge voltage. Because of the inefficiency associated with static DC-DC conversion, it is desirable to have the generators supply the load directly during sunlight and the batteries supply the load directly during

shade. This means that the batteries should fall within the system voltage-regulation specification, otherwise a power-consuming regulator must be added to the system.

Of the various types of batteries currently available, only three appear truly suited to space applications. These are nickel-cadmium, silver-zinc, and silver-cadmium. All three have relatively high specific powers and can be sealed against the vacuum environment of space. The selection of a type for the thermionic system application is then dependent upon the particular requirements for high cyclic life, reliability, insensitivity to launch loading, and minimum size and weight.

A survey of the characteristics of secondary batteries brought forth many conflicting reports on the performance that could be expected from various types of secondary batteries. The amount of actual test data available at this time is very limited and somewhat inconclusive. Further, it appears that the method of rating batteries and calculating performance varies with the manufacturer.

Several general observations can be made concerning the characteristics of the three batteries mentioned. The silver-zinc battery has the highest specific power of the three but is generally limited to a few hundred charge-discharge cycles. The silver-cadmium batteries have second highest specific power but are not so highly developed as the nickel-cadmium batteries nor have they demonstrated under test the ability to withstand as many cycles as nickel-cadmium batteries. The cycle life of nickel-cadmium and silver-cadmium batteries is dependent upon the depth of discharge and operating temperature. Because of this, the silver cadmium battery appears to have a definite advantage over nickel-cadmium where the cycle life is on the order of 5000 cycles. The silver-cadmium has a specific power of about 2.5 times that of nickel batteries and requires limiting of depth of discharge to 40 to 60 percent as compared to 5 to 30 percent for nickel-cadmium, thereby permitting a greater realization of watt-hours per pound of storage hardware.

An additional feature unique to the silver-cadmium cells is that the discharge voltage is relatively high (approximately 1.1 volts) and remains nearly constant

throughout the entire discharge cycle. This constant discharge voltage characteristic helps insure a good regulation of system voltage and eliminates most of the losses that would be associated with the regulation circuitry need for other battery storage systems.

The best available data regarding the three types of batteries may be summarized and readily compared in Figures 3.5.1 and 3.5.2. The first figure readily compares the specific weights of the three batteries and includes the effects of temperature and discharge rate. The second figure is perhaps the most significant in that it represents a summary of test results obtained to date using the three batteries under cyclic test conditions. The data is displayed with battery weight in pounds divided by megawatt-hour cycles as a function of the number of cycles. In this way it is readily possible to compare the performance of the several battery types tested for the number of cycles indicated. The limit of depth of discharge is also indicated. Also, it must be pointed out that the data points do not constitute the failure limit of the batteries but rather the number of cycles they have satisfactorily completed without failure. From the data it is seen that both nickel-cadmium and silver-cadmium batteries have demonstrated life for over 5000 cycles. Also, the reduced weight figure and higher allowable depth of discharge tolerated by the silver-cadmium batteries indicates a definite superiority of the type for high cyclic solar applications.

Manufacturers and other investigating groups have attested to the ability of these batteries to withstand shock and vibration. Nickel-cadmium, in particular, has been tested and found to withstand accelerations up to 11 g's; vibration at 0.5 inch from 5 to 10 cycles per second; 2.5 g's from 10 to 50 cycles per second; 5 g's from 50 to 400 cycles per second; and 7.5 g's from 400-3000 cycles per second;and a shock intensity up to 30 g's.

COMPARISON OF SPECIFIC ENERGY OF SILVERCEL, SILCAD & NICKEL-CADMIUM SYSTEMS

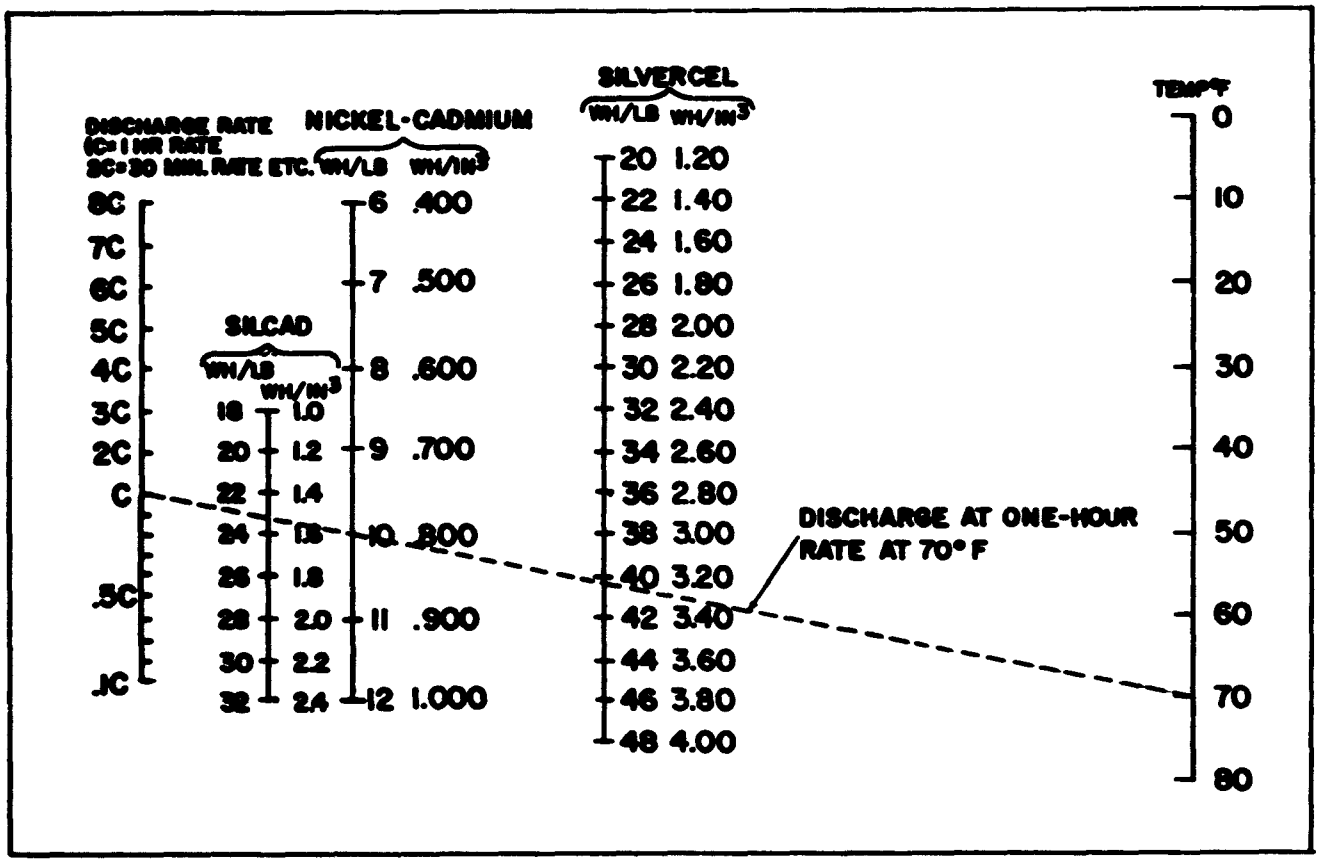

FIG. 3.5.1

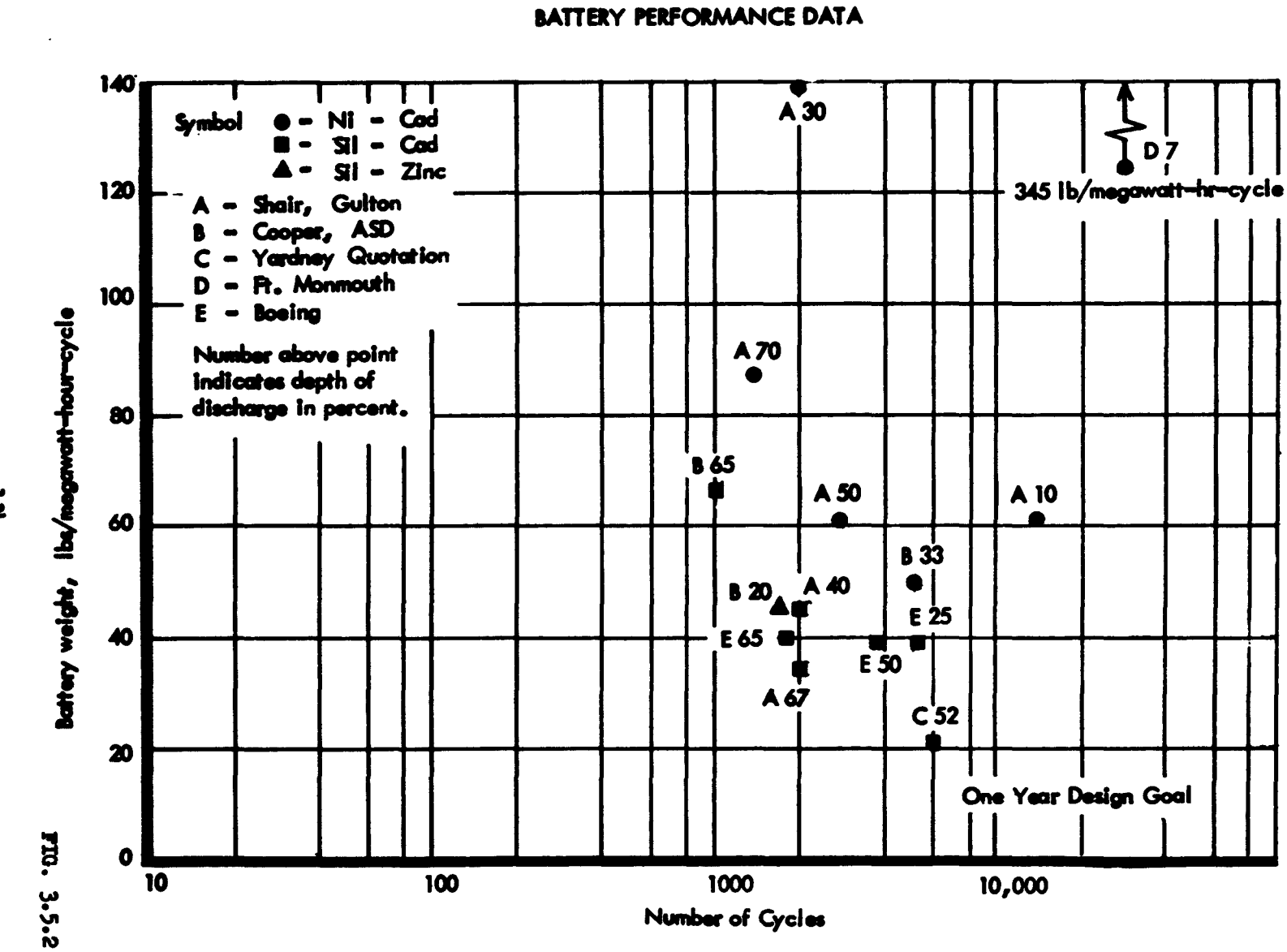
BATTERY PERFORMANCE DATA
Symbol ● - Ni - Cad
■ - SI - Cad
▲ - SI - Zinc
A - Shair, Gulton
B - Cooper, ASD
C - Yardney Quotation
D - Ft. Monmouth
E - Boeing
Number above point indicates depth of discharge in percent.
A 30
D 7
345 lb/megawatt-hr-cycle
A 70
B 65
A 50
A 10
B 33
B 20
A 40
E 25
E 65
E 50
A 67
C 52
One Year Design Goal
Battery weight, lbs/megawatt-hour-cycle
Number of Cycles
140
120
100
80
60
40
20
0
10
100
1000
10,000

FIG. 3.5.2

3.6 Controls

The satisfactory operation of solar thermionic systems is heavily dependent upon the characteristics of the overall control systems. Controls for the generating system can be divided into four major categories, namely:

1. Structure-deployment mechanisms
2. Orientation and startup controls
3. Thermal controls
4. Systems controls

Each category is in its turn vitally important to the overall system, and furthermore, the efficiency of the system and its physical size for a given power level is directly effected.

In summary, the objectives of the overall control systems are as follows:

1. Proper erection or deployment of the system in space.
2. Initial and continuous acquisition of the sun upon emerging from the earth's shadow.
3. Precisely tracking the sun with the concentrator during the sun portion of the orbital cycle.
4. Rapid attainment of full power output from the converters.
5. Stable power generation characteristics throughout the sun portion of the orbital cycle.
6. Protection of the converters from severe transients or improper operational modes which would promote premature failure or reduced reliability and performance.
7. Protection of the batteries from severe transients or improper operational modes which would promote premature failure or reduced reliability and performance.
8. Proper sensing and accommodation of vehicle system load requirements under normal and abnormal circumstances.

In the following discussion an attempt will be made to briefly analyze the system requirements in each of the major areas mentioned and to select the most appropriate approach to meeting these requirements.

3.6.1 Structures and Deployment Mechanisms

Systems requirements such as the need for vehicle stowage, deployment mechanisms, and structural members to insure the accurate positioning of the converters in the focal point may also be considered as part of the systems control problem. These latter items are heavily dependent upon the particular vehicle selected, the purpose of the mission which will dictate the need for other equipment also stowed in the payload area, and the size or type of helionic array selected for the application.

It has been established that the modular concept using moderate-sized concentrators of the rigid high precision variety is indicated. With the state-of-the-art in concentrators currently limited to diameters of five feet or less, it becomes apparent that the structural system selected for deploying and maintaining the modules in space is directly related to how many modules it can satisfactorily accommodate. That is, how many modules can be nested or stacked in the vehicle during launch, and how well can the structure limit stack-up errors which contribute to concentrator misalignment. The deployed structure must not interfere with other vehicle mechanisms nor should it restrain or disturb the vehicle itself due to inertial interactions. Finally, the arrangement must also be satisfactory in terms of the system output voltage requirements and must possess the degree of reliability or redundancy deemed necessary.

Figures 3.6.1 through 3.6.5 present five concepts intended to meet the need of a solar thermionic system from 125 watts to 3 KW. It is immediately apparent that the complexity and the number of modules required for higher power levels increases rapidly. It is this factor more than any other which will limit the size of solar thermionic systems until the state-of-the-art in concentrator fabrication is made to include precision concentrators of significantly larger diameter.

The stowage and deployment of one or even several modules, as shown in Figure 3.6.1, is relatively straightforward. The mechanisms are simple and the structure rugged. Simple hinges, springs, locks, and release mechanisms are adequate once the vehicle is placed in orbit. As the system gets larger, as shown in Figures 3.6.2 and 3.6.3, more attention is directed towards limiting the stowage space

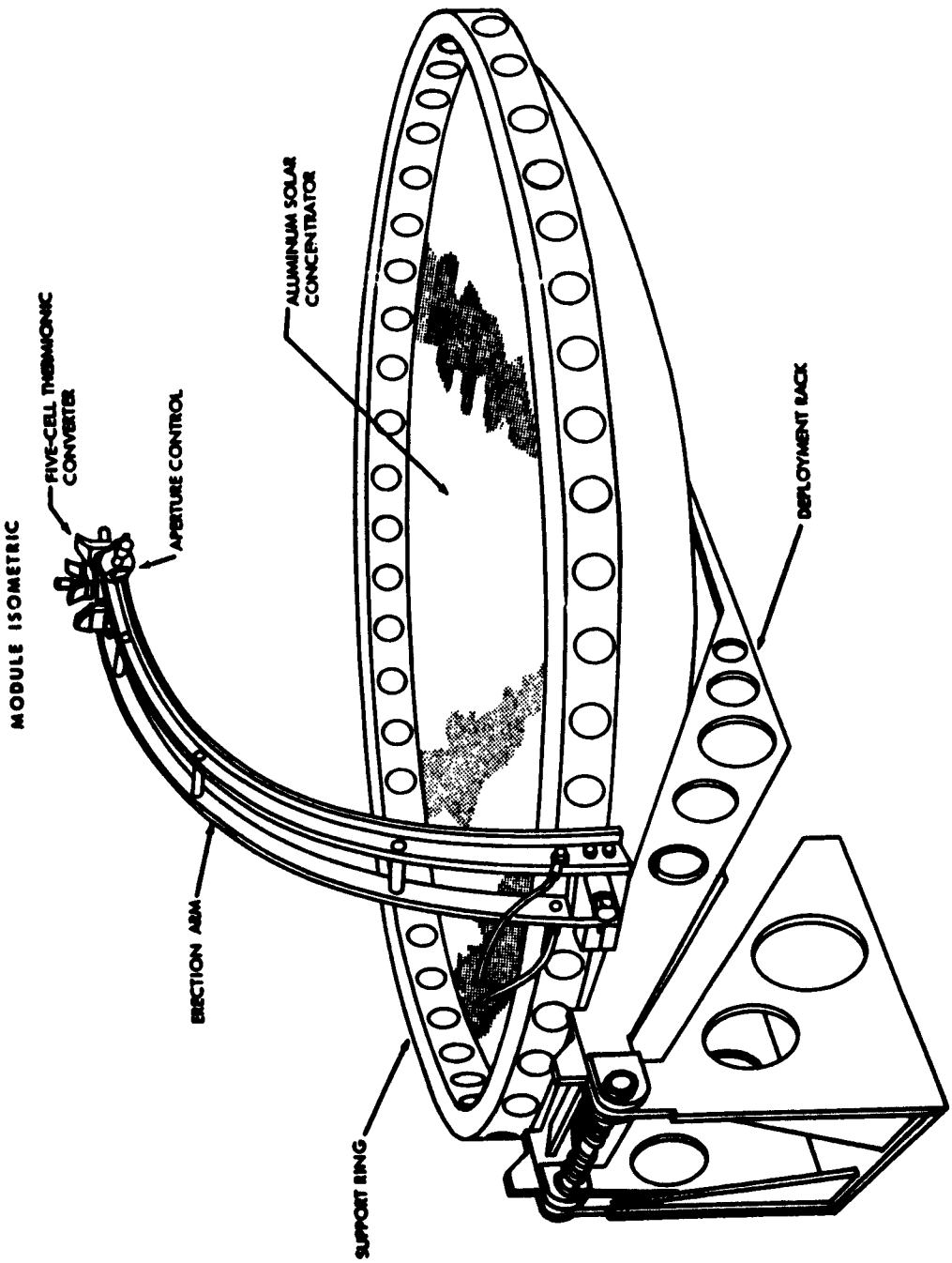
MODULE ISOMETRIC
FIVE-CELL THERMIONIC CONVERTER
APERTURE CONTROL
ALUMINUM SOLAR CONCENTRATOR
DEPLOYMENT RACK
ERECTION ARM
SUPPORT RING

FIGURE 3.6.1

CLASS I CONCENTRATOR MODULE STOWAGE
AND DEPLOYMENT CONCEPT

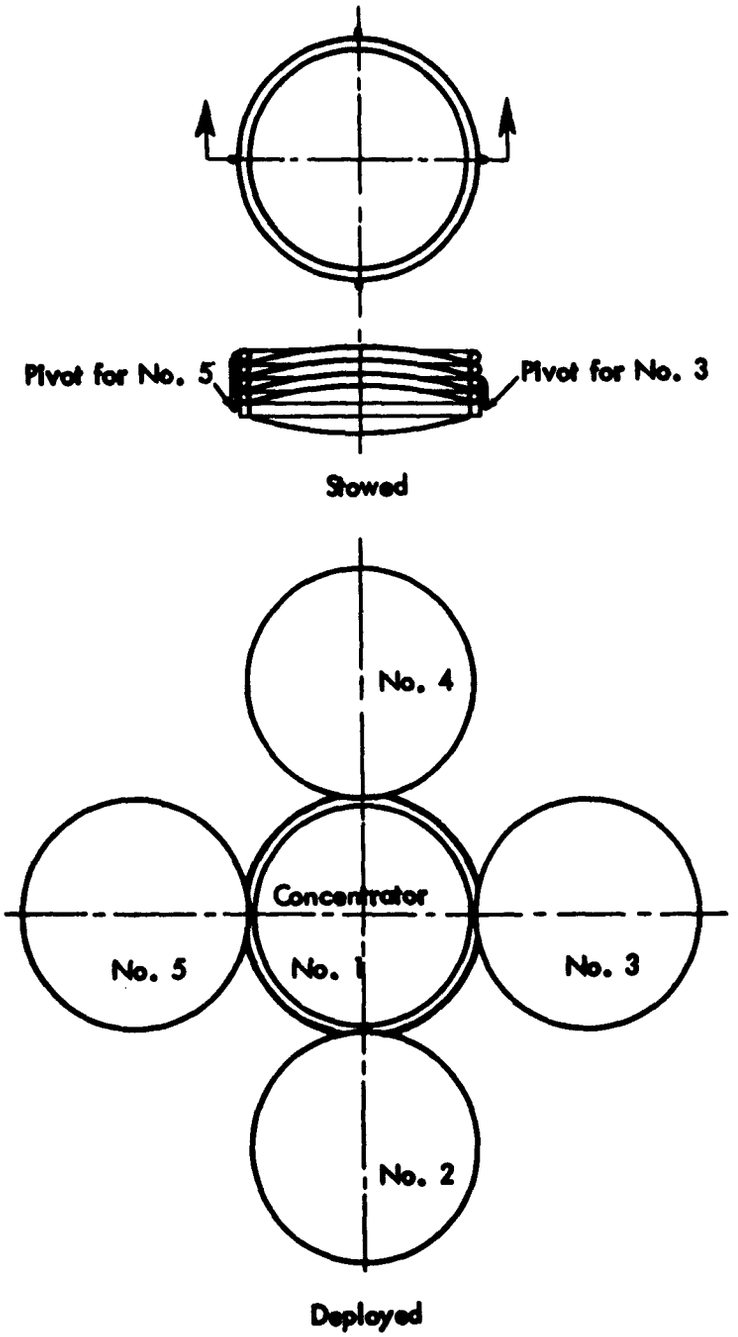

Fig. 3.6.2

CLASS I CONCENTRATOR STOWAGE AND DEPLOYMENT SCHEME

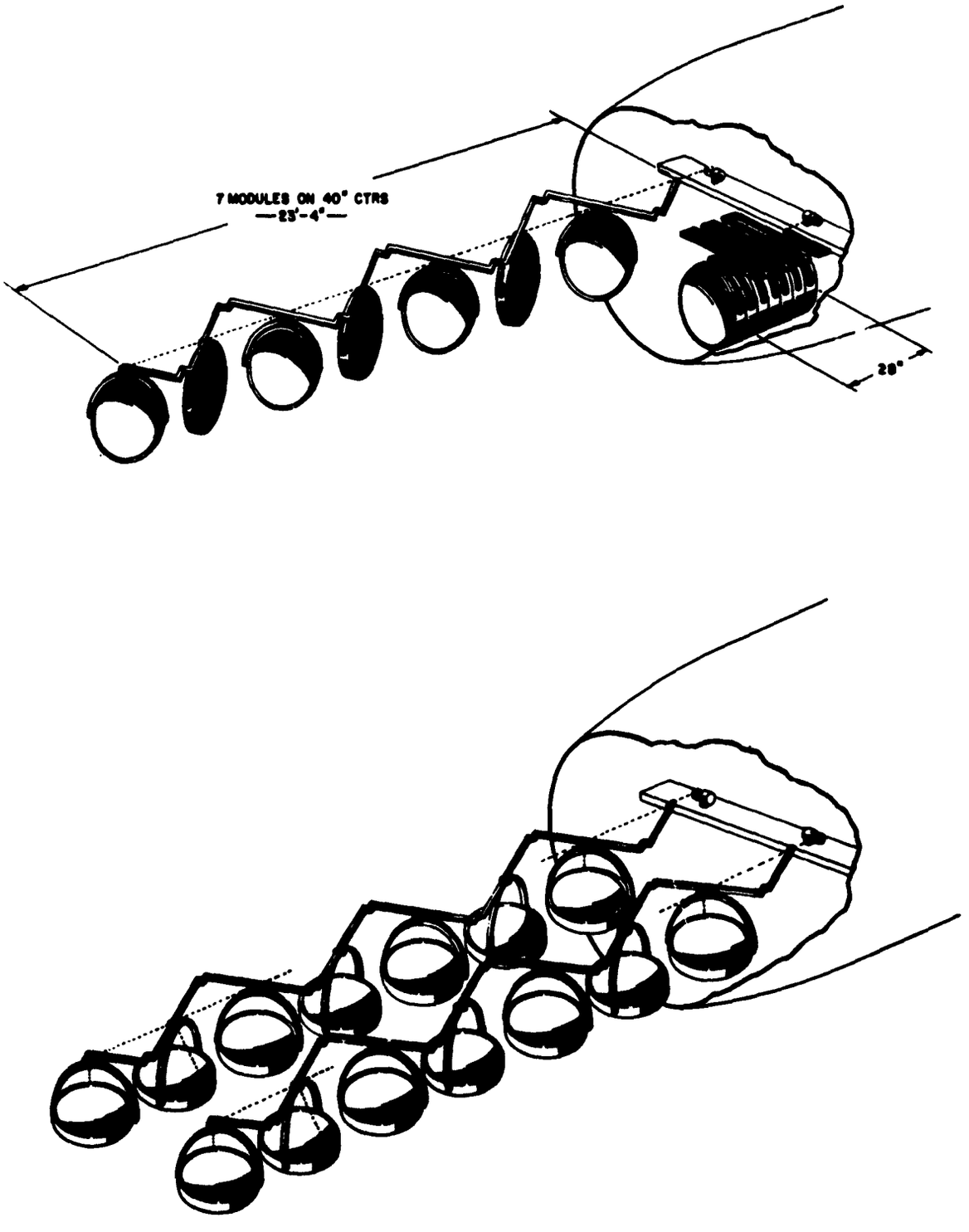

Fig. 3.6.3

SOLAR CONCENTRATOR ASSEMBLY

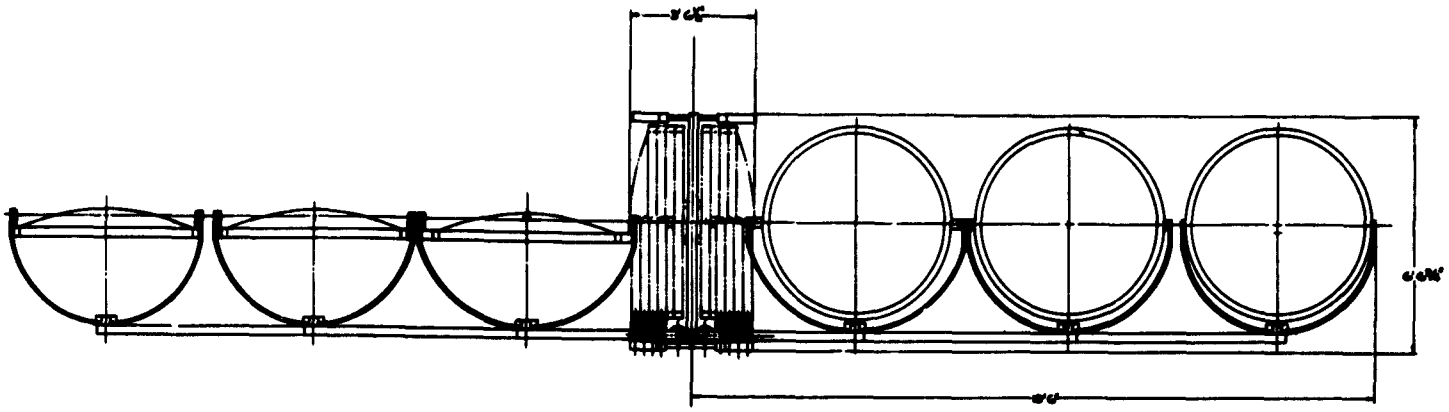

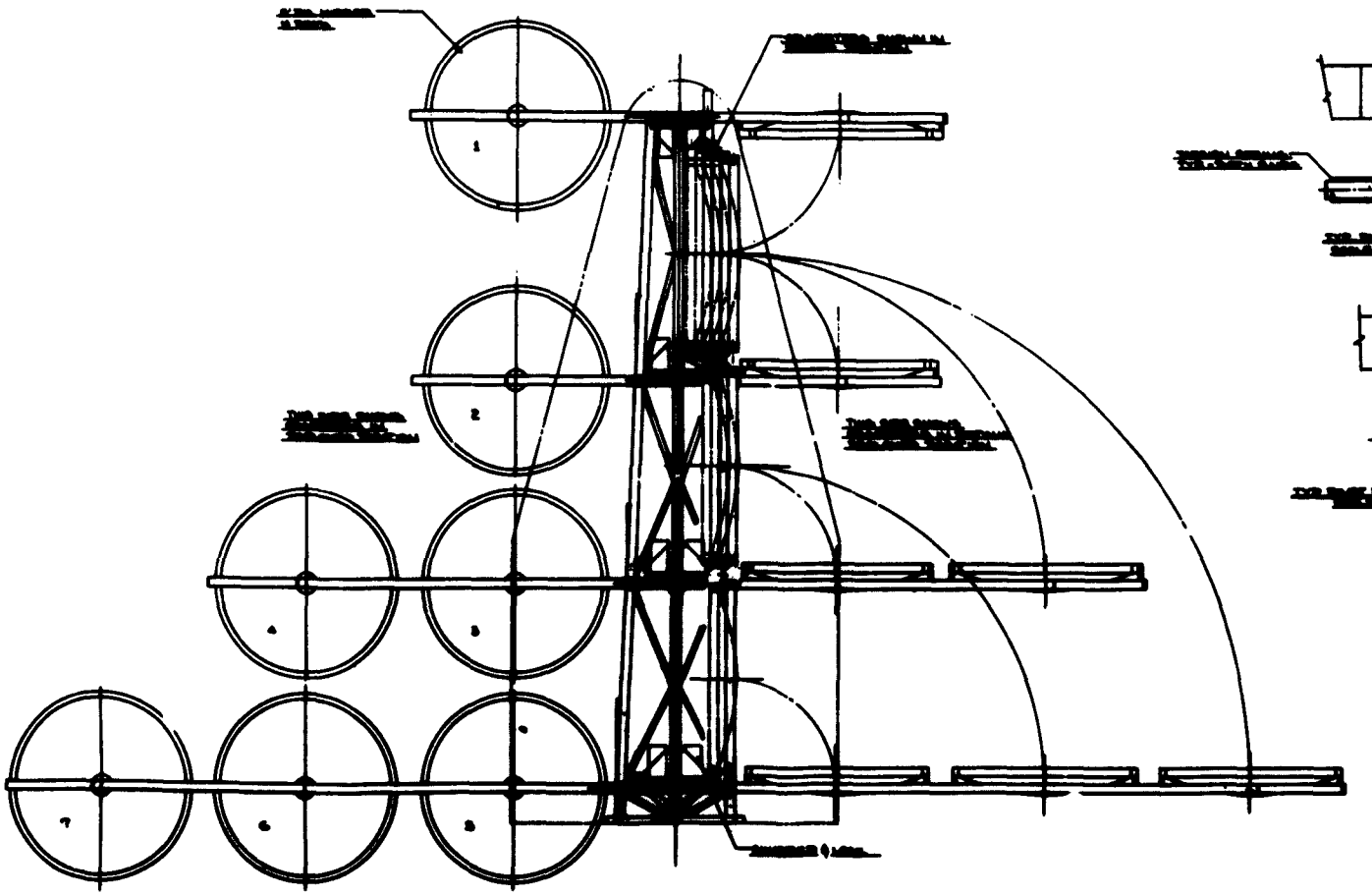

SOLAR CONCENTRATOR ASSEMBLY

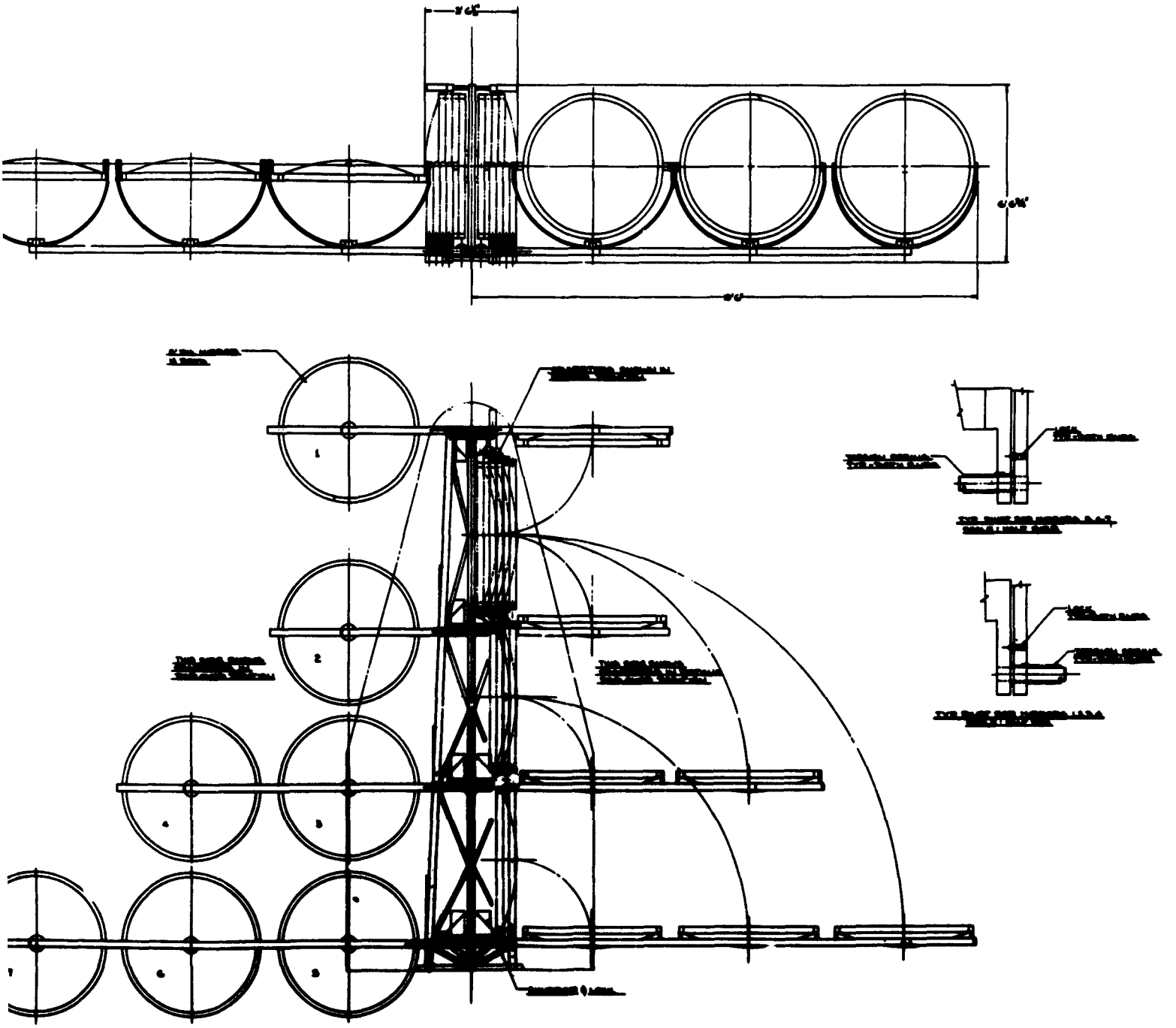

Fig. 3.6.4

FIG. 3.6.5

requirements with an attendant increase in complexity and a marked increase in need for precise alignment of all structural parts along with controlled deployment. Simple extension or unfolding structures are replaced by more elaborate truss work arrays as the size increases to maintain the necessary strength and alignment accuracy and again the deployment programming is made more complicated.

For systems in the 1 to 10 KW range, the array-type deployment structure is necessary. These structures fold compactly into the nose cone and are rigidized by the addition of support structures, locks, and strategically placed prestressed hollow columns fitted with explosive bolts to be released on command. With the vehicle in orbit a timer or radio pulse will command the release of explosive bolt assemblies. The deployment is then controlled by the paying out of a motor-driven cable which restrains the structures against extension springs. These springs are graduated in strength to insure the outermost members are fully extended before the inner members are allowed to move by the payout cable.

With each major segment of the structure moved into position, a release cable allows the module concentrators or the generator erection structures to move into proper position. Here snubbers and locks are employed to insure against shock or deformation and bounce.

The alignment requirements of the solar modules is such that the greatest possible accuracy be built into the structures. With small systems it is possible, by controlling the dimensional accuracy of hinges and structural members, to insure alignment between the vehicle and each module within .1 degree. With this being the case, the system can be rigidized and a single orientation system used to control sun alignment. In larger systems, however, this initial structural alignment seems doubtful and the use of the heliotropic mount with each module and a gross vehicle attitude control seems desirable.

3.6.2 Orientation and Startup Controls

The selection of an orbit also will have a considerable influence on the complexity, weight and efficiency of the conversion system. The lower altitude orbits will generally be the least efficient, most complex, and require the greatest weight. This high weight and low overall efficiency stems from the large shade to sun ratio. This necessitates a larger conversion system to

generate sufficient power in the sun period to accommodate the shade portion of the cycle and imposes the great weight penalty associated with using batteries to store this power. The lower efficiency is also strongly dependent upon the actual period of power generation, which is less than the sun portion of the cycle by the amount of time needed to preheat the converters to establish operating temperatures. The shorter the sun period the more significant will be the preheat period in evaluating overall performance. The fact that batteries are used also imposes a reduction in efficiency because of the charging efficiency of the batteries. It may also be noted that batteries must be derated in proportion to the cycle life expected and that this factor makes a considerable difference in system weight between high and low altitude orbits. Finally, it can be seen that an immediate acquisition of the sun is necessary to insure full utilization of the sun portion of the cycle. This then requires an orientation system which has fast response and stability upon emerging from the earth's shadow or a system which continues to program the orientation of the concentrators during the shade portion of the cycle so that the system is peroperly aligned at the time it enters the sun.

For systems in the 1 to 10 KW range, it will be necessary that the course attitude control system in the vehicle be operational in the shade. That is to say, the array must be properly directed at the instant it emerges from the shade. The accuracy of this direction must be within $\pm$5 degrees. Also because of the large mass and inertia involved in the helionic system, it is most practical to have the system maintained in a sun-oriented attitude at all times, thereby requiring a minimum of fuel or inertial control hardware for the vehicle.

With the $\pm$5 degree direction assured for the modules, it is easily possible for the heliotropic mounts to acquire the sun within the $\pm$6 minute accuracy specified for the modules. Also, there will be no danger of burnout or structural damage due to the concentrated energy being directed on a structural member during the initial sun acquisition.

It has been determined that no startup control as such will be needed for the thermionic generators. With the $\pm$5 degree initial dawn alignment insured, the generator itself can be adequately shielded from burnout during the sun

acquisition by the heliotropic mounts. Also, once the energy is focused into the generator cavity the generator will easily withstand the rapid warmup cycle which will follow.

The generators developed under this program and previous efforts have demonstrated their ability to survive step power inputs without excessive temperatures or stresses being noted in the converter structures. The cubical cavity generator, while not cycle tested in the laboratory, had been subjected to rapid power application in the subsequent solar test effort using the 5 foot earthbound solar tracking rig. The stress of startup can, of course, be of considerable importance in terms of the cycle life of the converters. The proper control of cesium pressure and system load can, however, minimize the extent and severity of such startup.

3.6.3 Thermal Control Systems

Thermionic converter operation depends on the temperature of three parts of the converter being held within certain limits. These three parts are the thermionic emitter, the collector, and the cesium well. Furthermore, in an orbital application utilizing electrical energy storage, the time required to achieve the temperatures necessary for operation is directly translatable into a system performance loss. For example, with a 55-minute orbital sunlight period, each 33 seconds of warmup time results in a 1% drop in system performance. The sunrise period in a 90-minute orbit is 8 seconds. The gradual rise of heat input during this period will reduce the thermal shock on the converters and will lower the warmup time charged against the 55-minute sunlight period.

Operating experience with thermionic converters has shown that the thermionic emitter can be expected to reach operating temperature in less than half a minute. No temperature control is required for the thermionic emitter because:

1. The constant nature of the solar heat source precludes the possibility of large heat input variations.

2. With about 96% of the focused energy being utilized under misoriented conditions, input power variations due to orientation changes cannot exceed 4%.

3. Reradiation loss, being proportional to the fourth power of emitter temperature, has a large stabilizing influence on emitter temperature.

4. The suggested voltage control will keep the generators fully loaded and will thus produce a stabilizing effect on the emitter temperature by increasing "electron cooling" as the temperature rises.

Assuming the application of solar energy is accomplished immediately upon entry into the sun, there is still a period of time required to attain operating temperatures and power output from the generator. There are three parts in a generator assembly which must be maintained at the proper temperatures to insure efficient operation. These are the emitters, the collectors, and the cesium reservoirs. It becomes necessary then to rapidly raise the temperature of the emitters by the direct application of solar flux, to heat the collectors by conduction and radiant transfer from the emitters and later by electron flow from emitters to collectors. With the collectors heated to a reasonable temperature, it is then possible to heat the cesium reservoirs by conduction from the collectors. This warmup sequence, however, may take a considerable amount of time depending upon the masses involved and the amount of energy that can be transferred by conduction, radiation, etc., with the particular configuration used in a generator design. It can be seen that while it may be a simple task to design a generator that will attain the proper equilibrium temperatures under long-term operating conditions with a fixed power input, it is very difficult to design a generator which will attain the same equilibrium conditions very rapidly.

The elevation of the emitters to design temperature may be readily accomplished because the mass involved is relatively small and for an inoperative generator the main source of heat loss in the emitters is by radiation. In the absence of a cesium plasma the emitters will heat rapidly until the radiation loss equals the input power, as is the case with a simple light bulb filament.

A different situation exists for the thermionic generator collectors, however, in that they usually constitute a larger mass which must be strong enough to serve as the mounting base for the converter assembly and must have conduction

paths of sufficient cross section to carry heat from the collecting surface to the radiating surface. For a converter suitable for cyclic operation there are three approaches which may be taken in designing a suitable anode. The first is to make the anode mass very small so as to reduce its heat capacity and keep warmup time to a minimum. The use of high emissivity radiator surfaces to minimize the required area and a metal with light weight, good conductivity, and low heat capacity will greatly assist in rapid warmup. The second approach is to build a large heat capacity into the collector radiator by using large masses of high-heat-content materials or even by using the latent heat content of various elements. With this approach, then, it may be possible to prevent the collector temperature from dropping below the point where reasonable operation can be expected immediately following the shade portion of the orbital cycle. A third approach consists of the use of two members to constitute the collector. In this instance the collector is coupled to a larger radiator mass by the pressure exerted by bimetallic clips. If the collector begins to cool down, the bimetal clip disengages the radiator and thereby retards the loss of thermal energy from the collector. Other methods of shielding the collector-radiator during the shade portion of the cycle may also prove effective in maintaining operational temperatures by limiting radiation losses.

For systems proposed in the 1 to 10 KW grouping, it is more desirable to construct a simple light weight generator. This means the collector-radiator will be built with minimum mass and heat storage capacity. The conduction path will be a minimum consistent with strength and mounting requirements. The radiator shall be designed with the highest possible emissivity surface and minimum area. No thermal control as such need be provided because the converters are relatively insensitive to collector temperature. This simplification and weight saving will more than compensate for the slight attendant loss of performance.

With the strong dependence the converter has on cesium temperature and vapor pressure, this control area requires very careful consideration. While test data has shown that collector temperature may be varied by as much as 200 to 300°K without changing converter efficiency and output by more than a few percent, it has also shown that cesium temperature must be held to within 20 or 30°K to provide the same limits on performance variation. Furthermore, it is very desirable to have the cesium pressure at the desired operating level to

assist in rapidly attaining thermal equilibrium within the converter and to prevent excessive temperatures or thermal stresses from developing in the emitter. It has been pointed out that the emitter heats very rapidly when irradiated. The presence of the proper cesium plasma will permit the immediate transfer of electrons from the emitter to the collector surface. This action greatly limits emitter temperature by the process of electron cooling. Transfer of large quantities of heat to the collector at relatively low emitter temperatures rapidly raise the temperature of the collector and radiator, and,of course, make a significant amount of power available to the vehicle system. With the obvious advantages of being able to limit temperature excursion, reduce temperature gradients and thermal stress, rapidly attain thermal equilibrium and power output, it seems very desirable to have the cesium temperature maintained as closely as possible to the optimum value during startup and operation.

The control of cesium temperature can be approached in many ways. The problem here is somewhat different than with the collector because the mass evolved is much less and the controlled temperature level is much lower. The simplest concept in establishing cesium temperature is to size the conduction path from the converter assembly to the cesium reservoir to transfer sufficient heat to just equal the heat radiated by the reservoir at the design temperature. The approach can be easily achieved if the converter is in equilibrium and the environment is static. This is not at all the case with an orbital application of thermionic conversion where the background radiation, concentrated radiation, converter operation, collector radiator temperatures, etc., are all varying as the system cycles through sun and shade conditions. More sophisticated controls are therefore necessary to maintain proper temperature in the cesium reservoir. As with the collector there are several heat storage techniques that may help limit the excursion in cesium temperature during the shade portion of the cycle. In addition there is the possibility of using a conduction path modulator control or using electrical heating in conjunction with a temperature-sensing or bimetal switching circuit. Another approach is to reduce the heat capacity of the reservoir and place it in a position where it will intercept a portion of the concentrated energy directed at the emitter. With this scheme it would be necessary that the cesium reservoir be heated rapidly to an equilibrium temperature so that sufficient vapor is present by the time the emitter attains operating temperature.

All of the control approaches listed are, of course, dependent upon the converter being at a temperature at least as great as the minimum reservoir temperature encountered in the cycle. It follows then that whatever design is selected for the system,the collector temperature must be maintained above the desired cesium temperature or elevated to that temperature very rapidly.

Actual solar tests with the cubical cavity generator, as shown in Figure 3.6.6, indicate that the temperature of generator collector-radiator will be raised above the critical minimum cesium reservoir temperature of 300°C in less than five minutes after a cold start at room temperature with about a 700 watt input. The cesium reservoir, however, requires almost 30 minutes to reach the same temperature. With the time response of the collector radiator unchanged, a power input with a 130 watt per ft^2 solar constant would permit attaining the minimum 300°C point in approximately two minutes. It follows that nearly full power output can be realized in two minutes if the cesium reservoir temperature can also be elevated to 300°C or better at the same time. To insure this in systems specified for the 1 to 10 KW range, it is necessary to provide electrical heat input for the cesium reservoirs. The heaters will be thermostatically controlled to supply the few watts of power normally required to maintain proper temperature. The thermoswitches will be set at the low end of the cesium reservoir temperature band so that electrical power is added only with the reservoirs slightly below the optimum set point. During full power operation the reservoirs will be designed to reach an optimum equilibrium temperature with the heat conducted down the reservoir connecting tubulation from the collector.

Each reservoir heater and switch will be shunted across its own converter assembly. In this way the converters can provide added power to the heaters to accelerate the warmup process and the batteries can heat all reservoirs during the shade cycle since the generators will remain on the line during this time. The heater and switch circuitry is shown schematically in Figure 3.6.7. With proper design the reservoirs will be held at approximately 280°C to 300°C with the thermoswitch set to operate at 310°C. During the sun portion the reservoir will reach an optimum temperature of 322°C with no electrical power drain.

CUBICAL CAVITY GENERATOR THERMAL RESPONSE

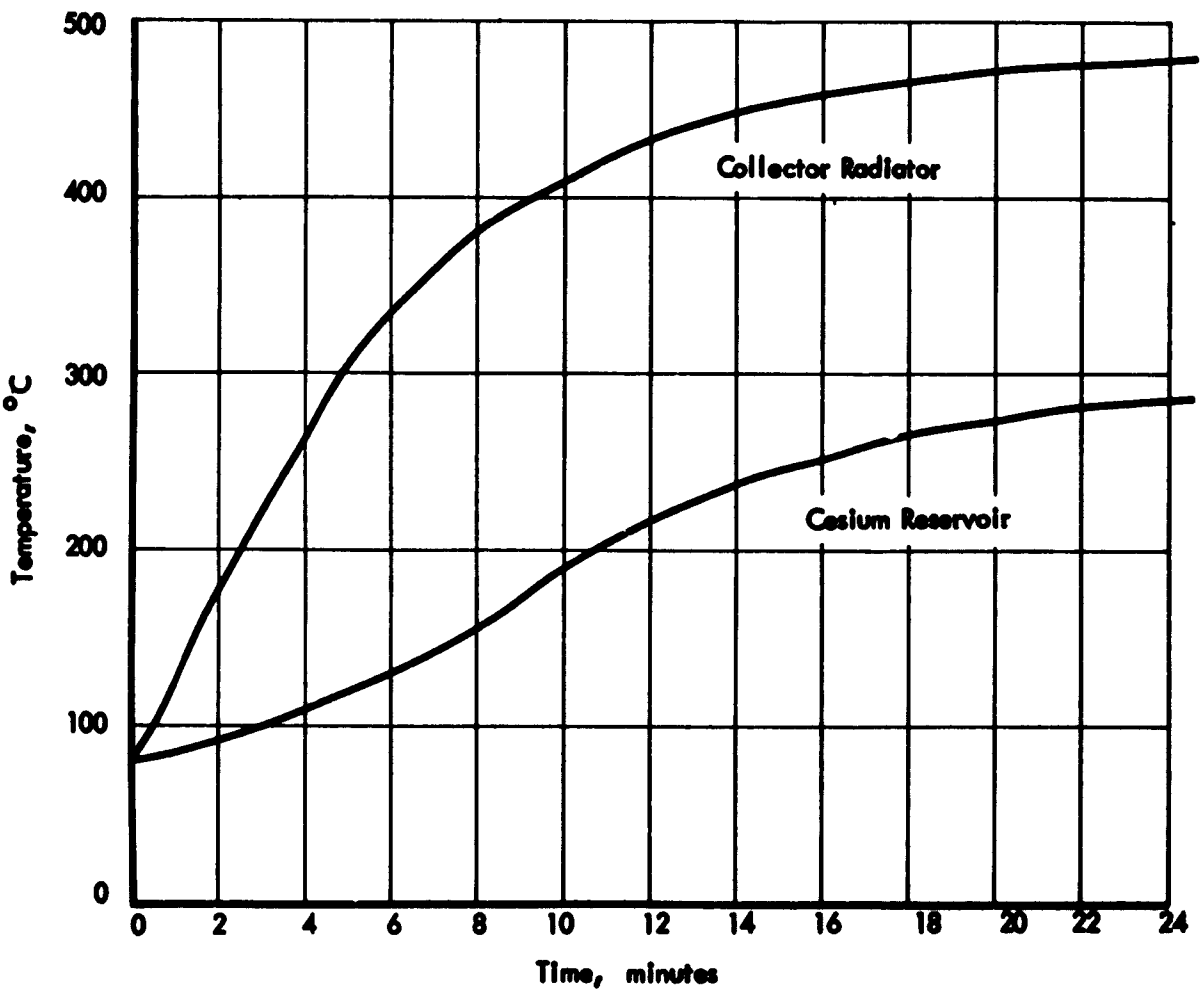

Fig. 3.6.6

CESIUM RESERVOIR HEATER AND SWITCH SCHEMATIC

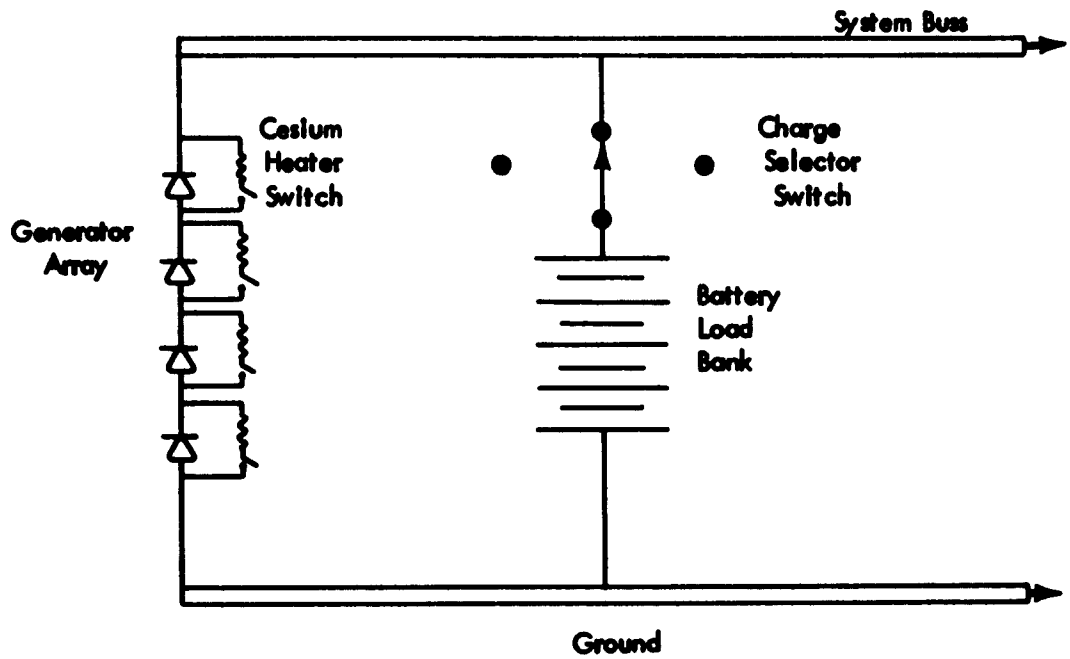

Fig. 3.6.7

The advantage of using electrical heaters is immediately apparent if one considers that for a 1.5 KW system the heater power required at 2 watts per heater for 30 minutes is only 7200 watt minutes, which can be supplied in less than 2-1/2 minutes of sun operation with the thermionic generator output of 2900 watts as would be required for an orbital application with battery storage. Without reservoir heaters an estimated 16 minutes would be required to attain near full power operation which then constitutes a loss of 39,000 watt minutes to the vehicle system.

3.6.4 Electrical System Controls

To function properly, a solar-powered thermionic generating system for an orbital application has need for several electrical control components and control systems. A thermionic power conversion system must be capable of (1) delivering the power necessary to satisfy the vehicle requirements, (2) charging a battery bank needed to sustain the system during shade operation, and (3) making up the power dissipated in any conversion or control equipment. The system is further complicated by the fact that a 55-35 minute sun-shade orbital cycle is involved, and the system load is subject to variations from zero to full power at any time.

To assist in the development of a suitable control system, it is first necessary to evaluate the hardware that is currently available. This hardware includes batteries, DC-DC conversion devices, regulation devices, and power dissipating devices.

The overall electrical control hardware requirements for a typical system with battery storage and cyclic operation may be summarized as follows:

1. System voltage regulation control.
2. System load demand sense.
3. Abnormal load demand sense.
4. Generator power output sense.
5. Battery charge rate control.
6. Battery charge level sense and control.
7. Battery discharge voltage control.
8. DC-DC converters.
9. Auxiliary load bank.

The design of an efficient system will combine the functions of sensing and control mechanisms and integrate the logic network so far as possible to minimize controls weight, volume and power requirements.

In the operation of the conversion system, it will be essential that load power remain reasonably constant. In the region of the design point, most converters

operate as constant power devices and will adjust voltage or current output to maintain power output with minor variations in load impedance. If load is removed or greatly reduced, however, the converter is subjected to severe thermal transients. The emitter temperature will rise very rapidly and emitter work function will change greatly due to the removal of cesium atoms from the heated surface. In this case, even when the load is restored, it requires some time before normal operation can be resumed. This temperature excursion is conducive to thermal stressing of other components, cracking of the emitter structure, and rapid evaporation of the emitter material. This evaporation is, of course, undesirable because it deposits on vehicle structure and solar concentrators outside the converter and coats the collector with a higher emissivity surface within the converter. Both actions cause a reduction in system performance and efficiency. Also, the voltage regulation characteristics of the thermionic generator will necessitate the use of some voltage regulation device in order that a specified system voltage be maintained. Since fuel consumption at part load is no problem, but peak load capacity is limited with solar-powered systems, a shunt type parasitic load is the best voltage regulating device. This type of regulator draws a minimum of power at full system load and works well with generators having poor regulation. In this case, an auxiliary load will serve two purposes, voltage regulation and generator load stabilization.

Several design approaches are possible for the auxiliary load and control. The use of high-temperature, high-watt-density radiators is suggested in any event to minimize weight and bulk. The size and voltage regulation requirements of the vehicle system will dictate the controls circuitry design. For smaller power systems it appears possible to use a simple stepping motor and hermetically sealed commutator to step in or out the required load increments necessary to provide regulation. This stepping arrangement is felt suitable because the thermal response characteristics of the generators are sufficiently long to prevent any truly instantaneous voltage changes due to system load variations. A stepping motor and low frequency sampling network can easily keep pace with the anticipated rates of change.

For large power systems or close regulation requirements,heavier and higher speed mag-amp or controlled rectifier type gates may be used to regulate load bank power dissipation.

Where secondary batteries are used to supply power in the shade, voltage regulation of their output will be required during at least part of the shade time to protect the system from the high terminal voltage developed near full charge. A voltage-dropping resistor will fulfill this requirement with a minimum energy loss. It may be, however, that in many cases the battery discharge voltage regulation can also be insured by the auxiliary load recommended for voltage control and stabilization of the generator system. Since the period of high initial battery discharge voltage is short, it may be possible to reduce the voltage to the system by simply loading up the batteries with the auxiliary load bank. The power associated with the high initial voltage will have to be dissipated parasitically in any case, and if the batteries can be shown to withstand the higher initial current drain without excessive heating or deterioration of cycle life, the controls hardware requirement will be simplified.

The selection of batteries suitable for a one-year orbital application is limited and Sil-Cad seems most acceptable. General specification for Sil-Cad batteries include the capability of obtaining 77% charge efficiency, sufficient cycle life with moderate derating, and a good watt-hour per pound figure. Typical discharge and charge characteristic curves for Sil-Cad batteries are shown in Figures 3.6.8 and 3.6.9, respectively.

For charging secondary batteries, a voltage higher than system voltage is required. This voltage may be obtained by placing in series with the line an additional generator. This generator may consist of either a group of thermionic generating modules or a DC-DC converter which draws its power from the 28 volt line. The latter choice is preferred because:

1. The additional generating modules cannot, in general, be made the same size and power as the other system modules.

2. The gains in reliability achieved by the series-parallel connection of system modules would not apply to the additional generating modules.

3. The DC-DC converter can be conveniently combined with a battery charging regulator and the system voltage regulator.

DISCHARGE CURVE 54 AMPS
26 x YS 85 (S)SP BATTERY

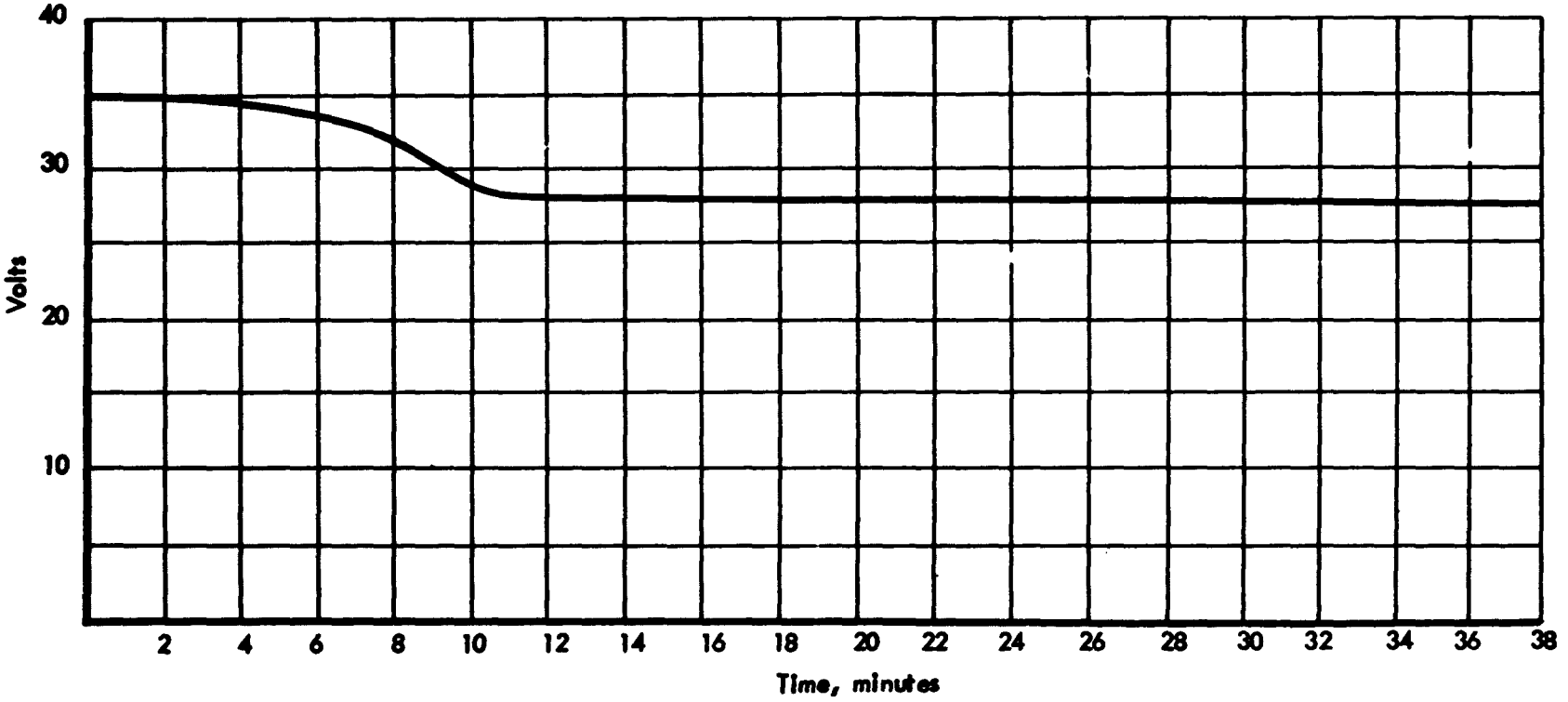

Fig. 3.6.8

CHARGE VOLTAGE AND CURRENT
26 x YS 85 (S) SP BATTERY

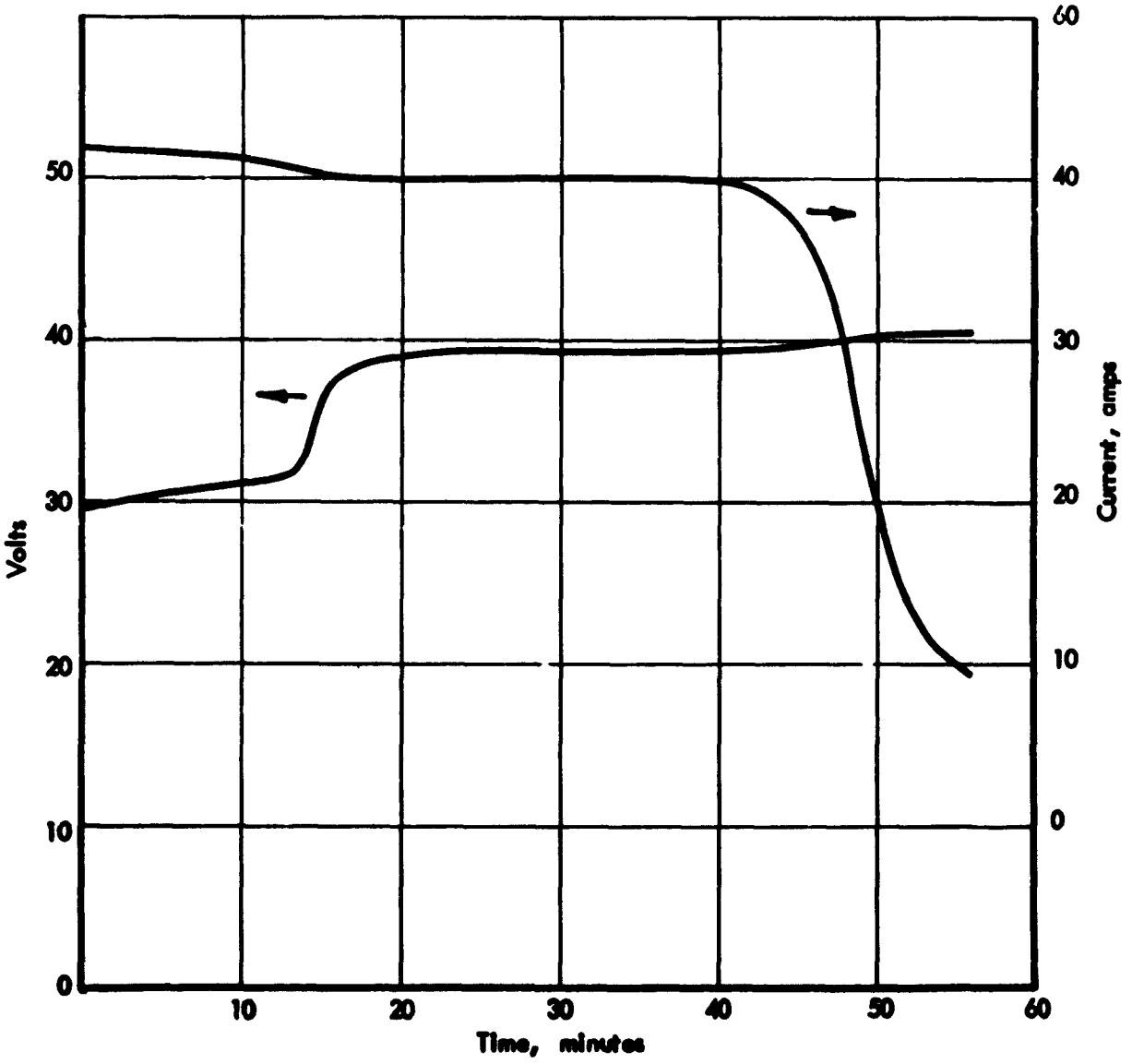

Fig. 3.6.9

The last item regarding the integration of a battery charging control is, of course, necessary because of the variation in terminal voltage which results from the changing charge state. One of the recommended charging methods is to control the current at a predetermined level. For the battery charge characteristics shown in Figure 3.6.9 a current-limited control that held 40 amps as the maximum level would be satisfactory. Such a charge current control may be built into the DC-DC converter used to obtain the topping voltage. Such a converter circuit is shown in the block diagram(Figure 3.6.10) and schematically in Figure 3.6.11. This converter-current limiter circuit has been used successfully by Thompson Ramo Wooldridge for several similar control applications.

Figure 3.6.12 presents a state-of-the-art summary of DC-DC converter efficiency weight and volume as a function of input voltage. With the incorporation of the current limiting feature discussed, these curves will require an upward adjustment.

Numerous system and control concepts are possible. The control scheme selected and integrated with the vehicle system and generating system is strongly dependent upon the specific mission requirements. While it is impossible to present all systems and controls combinations, several typical approaches can be presented for comparative evaluation. The two circuits shown in Figure 3.6.13 are suggested for application in a 1.5 KW system. The first circuit uses a DC-DC converter to provide a regulated 27.5 volt output with an input of approximately 21 volts. The battery charging voltage is 1.45 volts per cell and the discharge voltage 1.10 volts. These voltages have the same ratio as system voltage and thermionic generator voltage. In this instance the 27.5 volts is impressed on the system load and the battery bank during the sun portion of the cycle. During the shade portion, the output of the thermionic converter disappears and the loss of voltage drop across R1 causes the battery bank to be switched to supply the DC-DC converter. The auxiliary load is sensitive to line voltage so as to respond by applying load when the voltage rises towards the upper limit maintained by the regulator circuit in the DC-DC converter. This rise in line voltage would, of course, be related to the system load levels. Also, there is a provision in the battery charging control to place the battery on standby when full charge is reached. The power absorbed

CURRENT LIMITED DC-DC CONVERTER BLOCK DIAGRAM

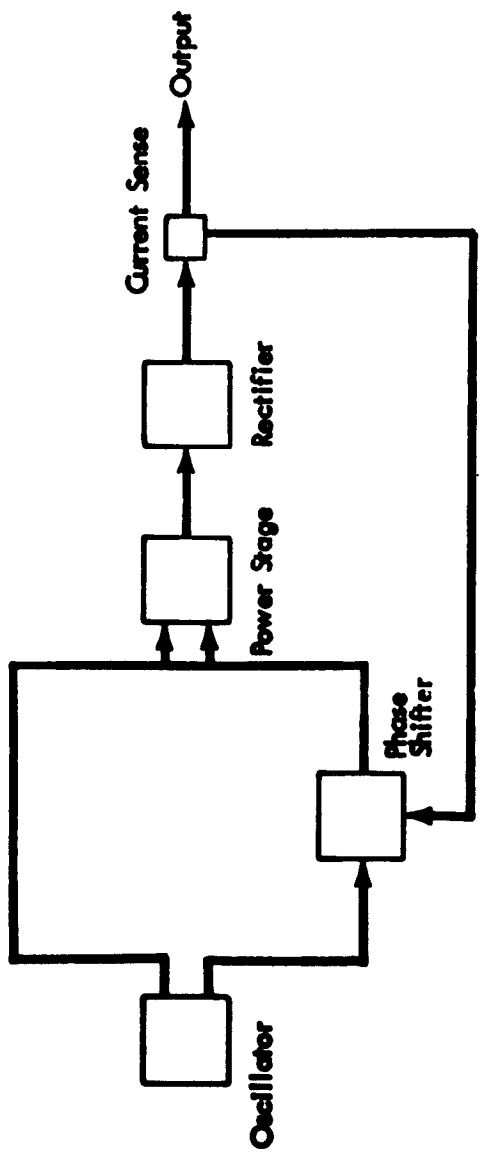

Fig. 3.6.10

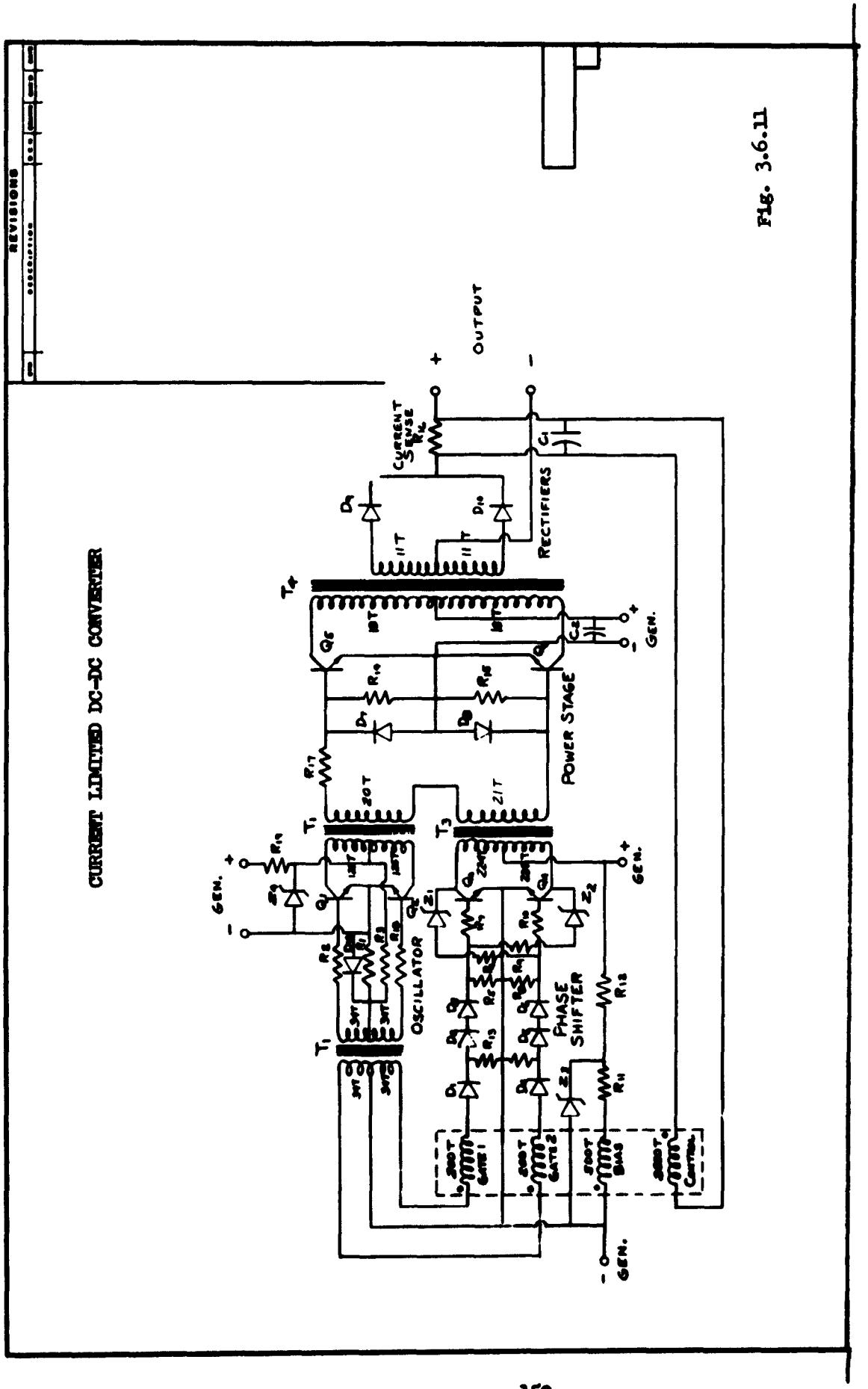
REVISIONS
CURRENT LIMITED DC-DC CONVERTER
OUTPUT
+
-
CURRENT SENSE
RECTIFIERS
POWER STAGE
OSCILLATOR
PHASE SHIFTER
GEN.
GEN.
GEN.
GEN.

Fig. 3.6.11

ESTIMATED PERFORMANCE CHARACTERISTICS FOR CURRENT STATE OF THE ART DC TO DC STATIC CONVERTERS
(POWER OUTPUTS IN 1 TO 10 KW RANGE)

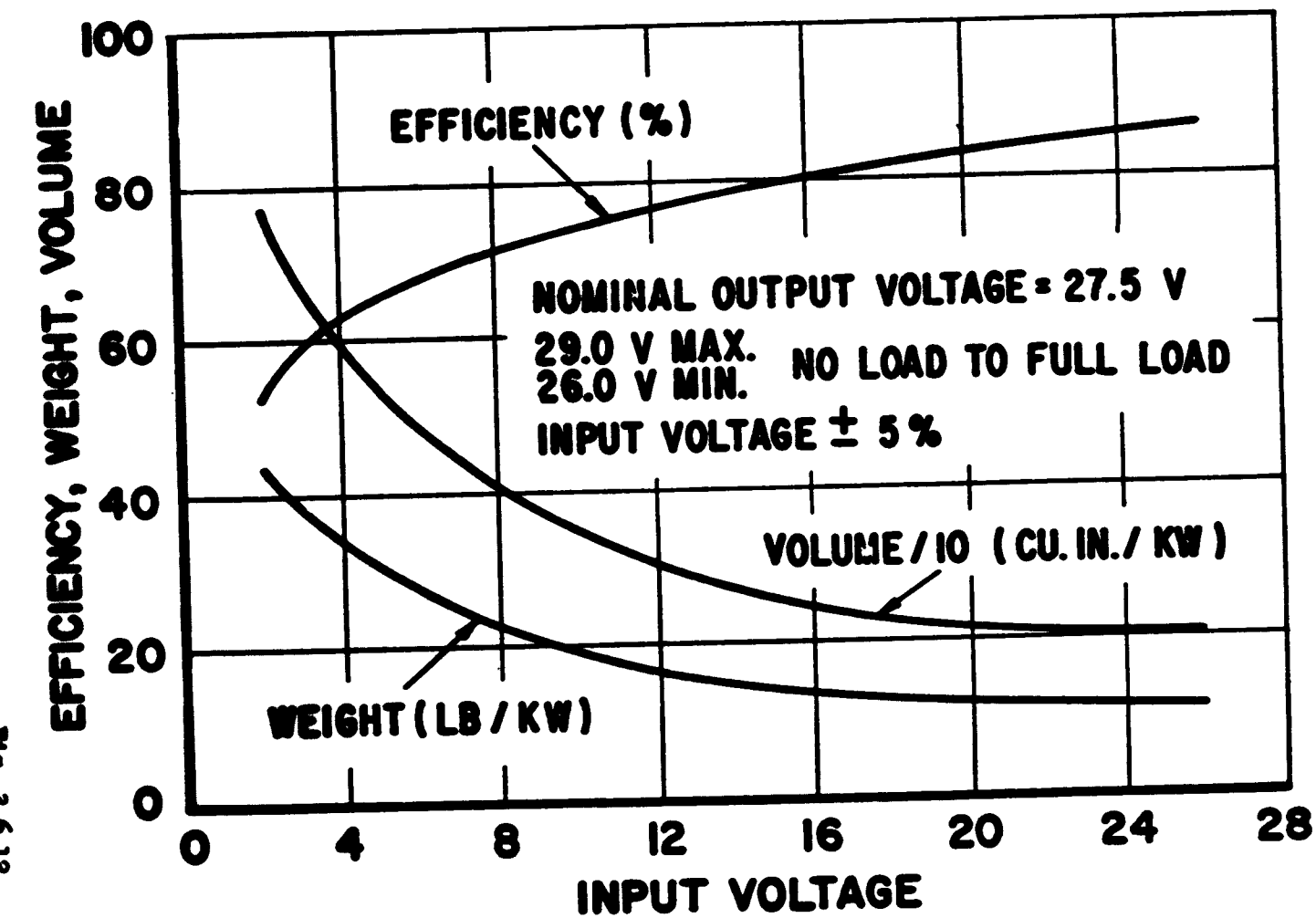

Fig. 3.6.12

DC-DC CONVERTER SYSTEM CIRCUIT NO.1

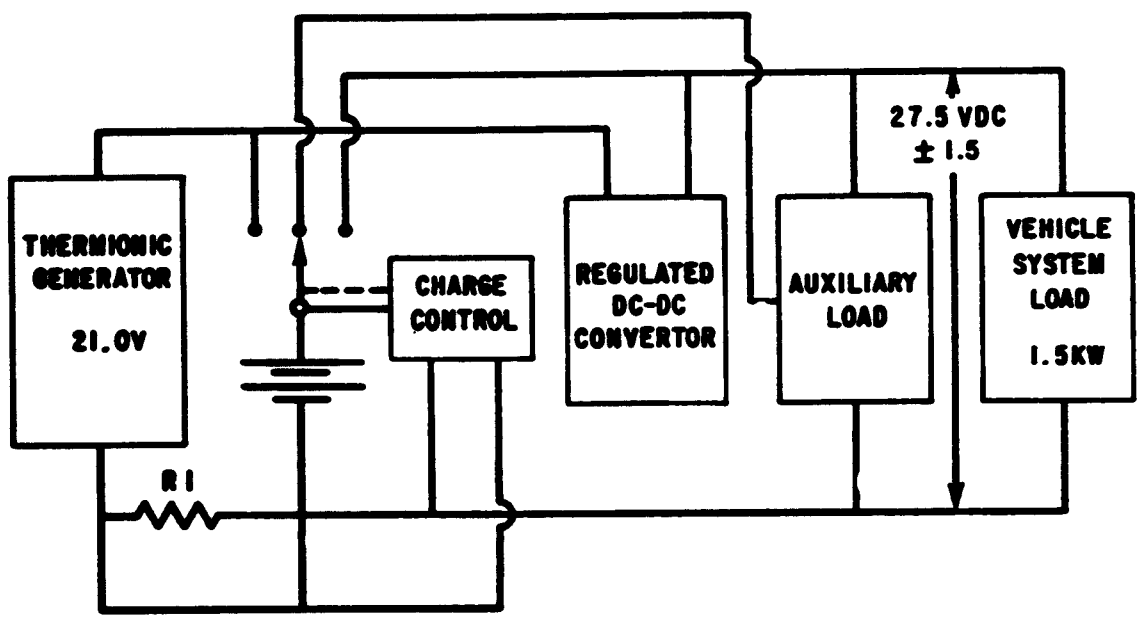

CIRCUIT NO.1

Fig. 3.6.13A

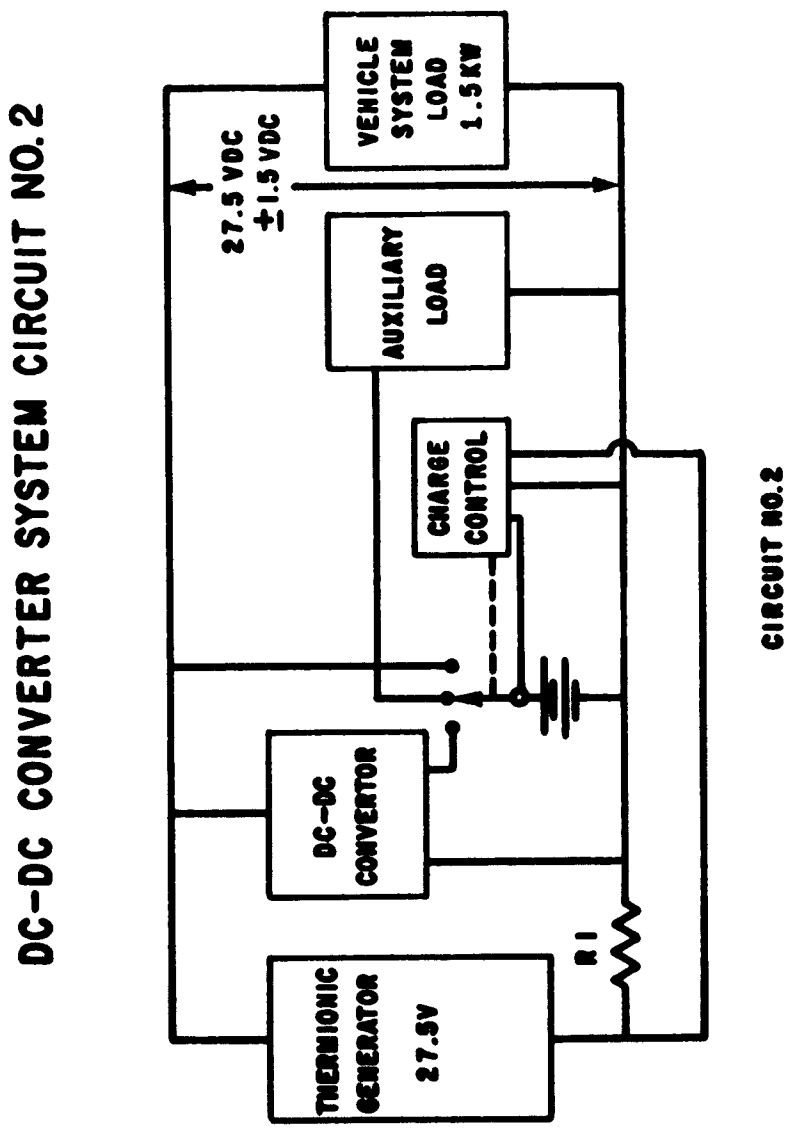
DC-DC CONVERTER SYSTEM CIRCUIT NO.2
VEHICLE SYSTEM LOAD 1.5 KW
27.5 VDC ±1.5 VDC
AUXILIARY LOAD
CHARGE CONTROL
DC-DC CONVERTOR
R1
THERMIONIC GENERATOR 27.5V
CIRCUIT NO.2

Fig. 3.6.13B

during battery charging is then absorbed by the auxiliary load. The total power output of the DC-DC converter is held nearly constant at 27.5 volts and the input to the converter, whether from the battery supply or the thermionic generator, is held nearly constant at 21 volts.

The second circuit utilizes an identical battery charge control and auxiliary load bank but only a small unregulated DC-DC converter to assist in obtaining the voltage required to charge the batteries during the sun portion of cycle. The supply voltage in this case is more dependent upon the gain of the auxiliary load and the batteries or the generator as a relatively stable voltage source.

Although other circuits similar to Circuit 1 can be devised, the second circuit is deemed superior for several reasons. The power requirement placed on the thermionic generator in Circuit #1 is larger, and the converter regulator circuitry is more complicated and less efficient as is shown by the following calculations.

Circuit 1

The generator is assumed to generate full power in one minute after entry into the sun. And from Figure 3.6.12, the DC-DC converter will be 84% efficient. The generator power output may be calculated

$$P_g = \frac{P_s T_s}{N_c T_s} + \frac{P_s T_{sh}}{N_c N_b T_s} + P_c = 3355 \text{ watts} \qquad (23)$$

where P_g = generator power watts

P_s = system power 1500 watts

T_s = sun period 54 minutes

T_{sh} = shade period 36 minutes

N_c = DC-DC converter efficiency 84%

N_b = battery charging efficiency 77%

P_c = charging and auxiliary load control power 15 watts

Circuit 2

$$P_g = \frac{P_s T_s}{T_s} + \frac{P_s T_{sh} E_s}{N_b E_c T_s} + \frac{P_s T_{sh} (E_c - E_s)}{N_b E_c N_d T_s} + P_c = 2878 \text{ watts}$$

where

E_s = system volts 27.5 volts

E_c = charging voltage 36.3 volts

N_d = Unregulated DC-DC converter efficiency 83% with current limiting

It can be seen that only the topping voltage ($E_c - E_s$) is produced by the DC-DC converter and that only this portion of the charging voltage is subject to the losses associated with converter efficiency. Also, since the topping voltage is used only in battery charging there is little concern over regulation except in the gross sense, and there is no need for a filter network to insure a quality DC output to the system. The system receives a nearly pure DC from either the generator or batteries and in both cases the regulation will be very good with total load power held relatively constant.

Heat Rejection

The proper operation and life requirements of the batteries and associated electronic control hardware is dependent upon the maintenance of a reasonable temperature environment in space. Based on the charging efficiency of Sil-Cad batteries of 77%, it can be shown that about 430 Btu/hr must be rejected to prevent a temperature buildup in the batteries for each kilowatt of system capacity. With a maximum operating temperature of 100°F specified for Sil-Cad batteries, the heat rejection area required for direct radiant power dissipation can be estimated.

$$Q = \sigma \varepsilon A_r (T^4)$$

$$A_r = \frac{430}{.9 \times .173 \left(\frac{560}{100}\right)^4}$$

$$= 2.79 \text{ ft}^2$$

where

σ = Boltzmann Constant

ε = .9 emissivity

The surface area of a single battery case sized for a 1 KW system load is calculated to be approximately 3.6 ft^2. It follows that the heat can be rejected satisfactorily by radiation alone. The above estimate neglects added heat inputs from the sun and earth or the rest of the power or vehicle system, but is still indicative of the ability of a storage system to operate without recourse to an auxiliary heat rejection system. The surface area to storage capacity ratio will also suffer as the size of the system increases towards the 10 KW level, but it is not anticipated that a serious problem will arise. Actually, the vehicle frame and helionic system structure to which the batteries are mounted can also be useful in rejecting excess heat.

The rejection of heat in the electronics packages is somewhat simplified because the permissible operating environment is considerably higher than the $100^{\circ}F$ specified for the batteries. The most critical electronic components are, of course, the semiconductors used in the control on logic circuitry. The specification of silicon components raises the operating temperatures to over $125^{\circ}C$, thereby allowing a power dissipation at the rate of 123 watts per ft^2 with an emissivity of .9. It is quite certain that the nominal power requirements of the controls hardware will not present a problem. Again it should be easily possible to maintain proper operating temperatures by controlling emissivity and radiation from the controls container or the vehicle frame. In both cases, however, a critical heat balance calculation will be required for any proposed system to insure proper heat flux and freedom from localized hot spots.

4.0 PARAMETRIC DESIGN STUDY FOR SOLAR THERMIONIC POWER SYSTEMS IN THE 1 TO 10 KW RANGE

System Design Philosophy

The basic objective of the solar thermionic system is to provide regulated DC power to a load at 28 volts. The amount of power to be provided depends on the load specified. This study investigates systems providing loads in the 1 to 10 KW range.

One of the design objectives has been specified as 10 per cent efficiency for the system. Because of the difficulty of attaining this objective compared with other objectives, it assumes the status of a guiding design criterion. However, the effort to obtain efficiency must be tempered with the practical consideration of system weight. Efficiency is not important from a fuel consumption standpoint since the system is powered by solar energy, but it is important from the standpoint of system size, both stowed and extended. Large size has its disadvantages relative to stowage volume and vehicle inertia in orbit. The optimum power system is somewhere between the maximum efficiency system and the minimum weight system, the exact location depending on poorly defined tradeoffs between weight and size. The problem of optimization is not as serious as it might first appear since there is some mutual consistency in reducing both weight and size. The best approach appears to be to design for maximum efficiency using lightweight materials and construction methods.

Since the thermionic converter is a low voltage device (about one volt), the methods of obtaining line voltage must be considered. The alternatives are (1) the use of a DC-DC converter to obtain the voltage, and (2) series operation of a sufficient number of thermionic converters to obtain line voltage. The power loss associated with static DC-DC conversion is quite high, especially with low input voltages. The series operation, therefore, is to be preferred from an efficiency standpoint and, for the reasons discussed above, will be used wherever possible. Systems in the 1 to 10 KW range operating at 10% efficiency in the specified orbit will require solar collection areas of 128 to 1280 square feet. Precision solar concentrators of this size are beyond the state-of-the-art.

Obtaining the required area with a folding concentrator is not feasible because of the loss of precision associated with the folding mechanism. The solar collection area may be obtained without loss of precision by dividing the area between smaller stowable one-piece concentrators. This approach is consistent with that of dividing the line voltage requirement between a multiplicity of thermionic converters. Thus, the system will consist of modular generating units, each module being composed of a precision solar concentrator and its associated thermionic generator.

With the modular concept, the system design problem is one of choosing a module size and an arrangement of modules which:

a) produce the required voltage
b) are readily stowed and deployed
c) are readily fabricated
d) can be adapted to various power levels in the 1 to 10 KW range with a minimum of change.

Figure 4.1 illustrates the functional block diagram which has been developed for the parametric analysis of helionic power systems. The significant input and output parameters of each of the system's functional parts are indicated alongside the appropriate flow lines, while the significant design parameters are indicated in each block. Figure 4.1 is followed by a list of the equations used in the program and a nomenclature of the terms and definitions used in the study.

Development of the system performance equations is straightforward. The definition of component characteristics is based on a variety of assumptions and data as summarized in Section 3.0 of this report. Thus, the thermionic converter characteristics were obtained by fitting laboratory test data to empirical equations while the solar concentrator parameters result from rigidity analyses, and the DC-to-DC static converter characteristics were defined by fitting analytic curves through the best estimate available on the state of the art for these devices. It is assumed that no DC-to-DC converter would be required if the system output voltage is in the range of 26 to 29 volts DC . The battery charger characteristics were assumed to be similar to the static

FUNCTIONAL BLOCK DIAGRAM HELIONIC POWER SYSTEM

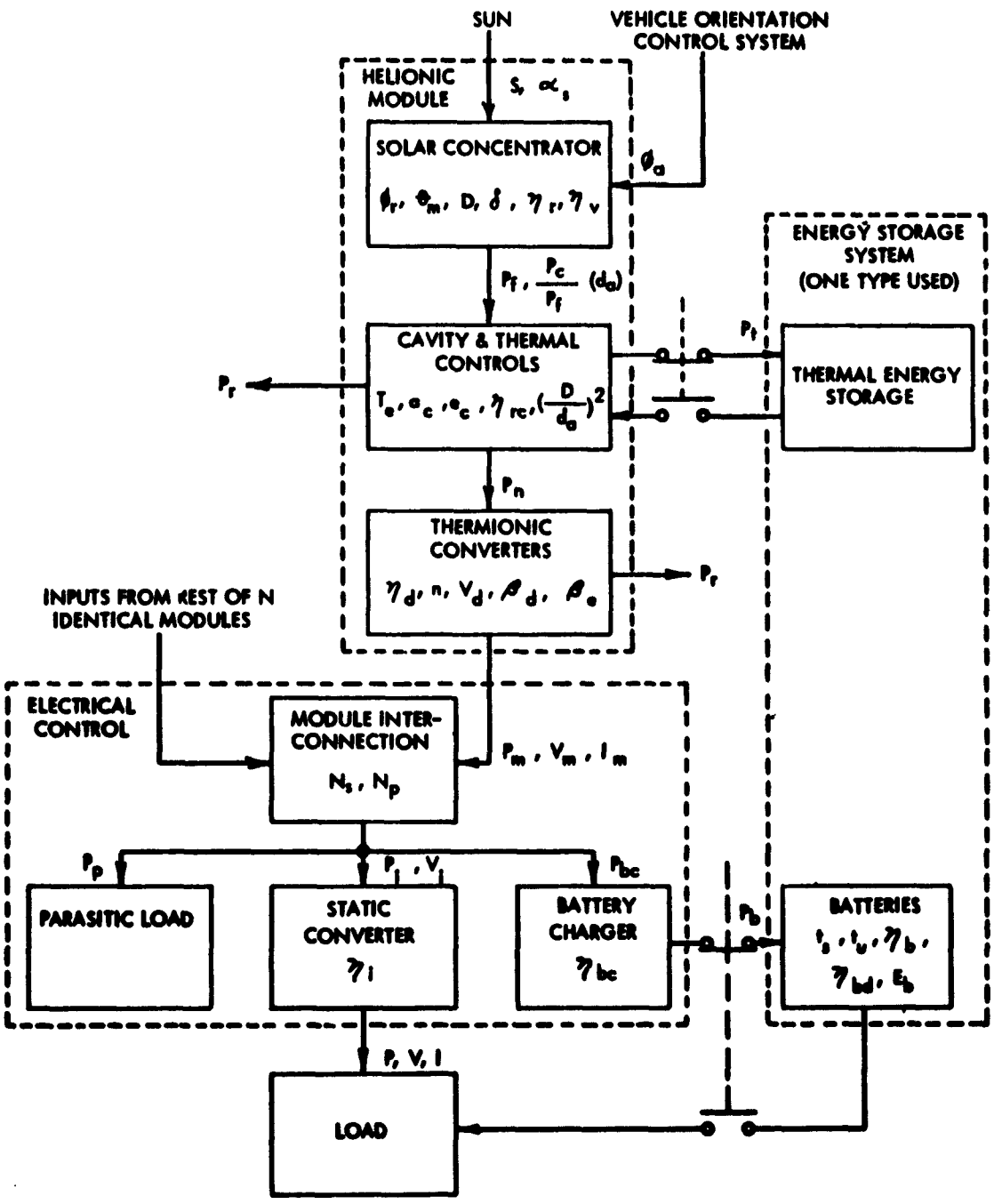

Fig. 4.1

converter characteristics, since the charger would probably consist mainly of a converter to attain the required voltage. The characteristics of silver-cadmium storage batteries were obtained from the data available from programs currently studying batteries for similar applications. Weight of the module deployment structure is based on an analysis treating this structure as buss bars.

One of the inputs to this program is tabular data of the solar power distribution in the solar concentrator focal plane. This data is obtained from a separate modified **pseudosun** computer program developed for analysis of solar concentrators. This program considers such effects as solar limb darkening, concentrator misorientation, concentrator surface inaccuracies, and apparent solar diameter, as was discussed in detail in Section 3.3.

The major input variables to the system parametric analysis program are the solar concentrator diameter and rim angle, the number of thermionic converters per module, and the system power output. Possible module interconnection schemes could be examined for each combination of input variables.

4.1 Main Program Equations

1. $\eta_v = K_{\eta 1} - \frac{K_{\eta 2}}{D}$

2. $\frac{P_n}{P_f} = a_c \left[\frac{P_c}{P_f} - \frac{e_c \sigma T_e^4 \alpha_s^2}{16\, a_c\, S\, \eta_v\, \eta_r \tan^2 \frac{\theta_m}{2}} \left(\frac{d_a}{f \alpha_s} \right)^2 \right]_{max}$

Obtain corresponding value of $\frac{d_a}{f\alpha_s}$ as well as $\left(\frac{P_n}{P_f} \right)$

3. $\eta_{rc} = \eta_v \eta_r \left(\frac{P_n}{P_f} \right)$

4. $\left(\frac{D}{d_a} \right)^2 = \left[\frac{4 \tan \frac{\theta_m}{2}}{\left(\frac{d_a}{f\alpha_s} \right) \alpha_s} \right]^2$

5. $P_m = \frac{\pi D^2 S \eta_d \eta_{rc}}{4}$

6. $U_m = \eta U_d$

7. $P_r = P_m \left(\frac{1}{\eta_d} - 1 \right)$

8. $\eta_m = \eta_d \eta_{rc}$

9. $\beta_m = \beta_d^{\,n} \beta_e$

10. $P_b = \dfrac{P\, t_u}{\eta_b\, t_s}$

11. $E_b = \dfrac{P\, t_u}{\eta_{bd}}$

12. $\eta_i = K_{i1} + K_{i2} \cdot \sqrt{U_i - 2} - K_{i3} (U_i - 2)$, $U_i \leq 26$

12 a. $\eta_i = 1$, $26 < U_i < 29$

13. $\eta_{bc} = K_{c1} + K_{c2} \sqrt{U_i - 2} - K_{c3} (U_i - 2)$

14. $N_s = \dfrac{1}{N_p} \; nl \left[\dfrac{\dfrac{P}{\eta_i} + \dfrac{P_b}{\eta_{bc}}}{\beta_m P_m} \right]$

15. $U_i = N_s U_m$

16. $N = N_s N_p$

* Solve equations (12) to (16) iteratively for all combinations of N_s and N_p satisfying the criteria:

$1 \leq N_p \leq N$, N_s integer, $2 \leq U_i \leq (U_i)_{max}$

Solve equations (17) and up for each combination of N_s and N_p obtained from equations (12) to (16).

17. $$N^1 = nl \frac{\frac{P}{\eta_i} + \frac{P_b}{\eta_{bc}}}{P_m}$$

18. $$P_p = N P_m - \frac{P}{\eta_i} - \frac{P_b}{\eta_{bc}}$$

19. $$\eta = \frac{4 P (t_s + t_u) + 4 P_p t_s}{\pi N D^2 S (t_s + t_u)}$$

20. $$\eta' = \frac{4 P}{\pi N D^2 S}$$

21. $$\delta = K_\delta \sqrt[3]{D}$$

22. $$b = \frac{\sqrt{\frac{\delta D}{\sin \frac{\theta_m}{2}}}}{2 \sqrt[4]{12 (1 - \mu^2)}}$$

23. $$z = D \left(\frac{1}{4 \tan \frac{\theta_m}{2}} - \frac{1}{2 \tan \theta_m} \right)$$

24. $$A = \frac{\pi K_A N (D + 2 b)^2}{4}$$

25. $$\xi_x = \frac{N_p!}{(N_p - x)!\ x!} (1 - \beta_m)^x \beta_m^{N_p - x}$$

26. $$\beta_k = 1 - \sum_{x=k+1}^{N_p} \xi_x \qquad (k = y \text{ or } y')$$

27. $$y = nl \left[\frac{N - N'}{N_s}\right]$$

28. $$y' = ns \left[\frac{N - N}{N_s}\right]$$

29. $$\beta_{mn} = \beta_{y'}^{y N_s - N + N'} \beta_y^{N - N' - (y-1) N_s}$$

30. $$\beta = \beta_{mn} \beta_i \beta_{bc} \beta_b \beta_p$$

31. $$W_r = \frac{\pi D^2 \delta w_r}{6} \left(\frac{1 - \cos^3 \frac{\theta_m}{2}}{\cos \frac{\theta_m}{2} - \cos^3 \frac{\theta_m}{2}} \right) + 5 \pi b \delta w_r (D + b)$$

32. $$W_{da} = w_{da} P_m$$

33. $$W_{ea} = w_{ea} P_m D$$

34. $$W_{tc} = w_{tc} D^2$$

35. $W_m = W_r + W_{da} + W_{ea} + W_{tc}$

36. $W_b = \frac{E_b}{w_b}$

37. $W_i = (K_{i4} - K_{i5}\sqrt{U_i} + K_{i6} U_i) P, \quad U_i \leq 26$

37a. $W_i = 0, \quad 26 < U_i < 29$

38. $W_{bc} = (K_{c4} - K_{c5}\sqrt{U_i} + K_{c6} U_i) P_b$

39. $W_p = K_{p1} + K_{p2} (P_p + \frac{P}{\eta_i})$

40. $W_w = \frac{K_w}{U_i} (N P_m + P_p)$

41. $W_{ec} = W_i + W_{bc} + W_p + W_w$

42. $K_{ms} = \frac{1.1 N_p D}{U_m} \sqrt{\frac{\mu_{ms} w_{ms} P_m}{W_m}}$

43. $W = N W_m (1 + K_{ms}) + W_b + W_{ec}$

44. $C_r = K_r D^2$

45. $C_{da} = \eta C_d$

46. $C_{sat} = K_{sat} D^{2/3}$

47. $C_m = C_r + C_{da} + C_{sat}$

48. $C_b = K_{b1} E_b$

49. $C_i = K_{i7} + K_{i8} P$

50. $C_{bc} = K_{c7} + K_{c8} P_b$

51. $C_p = K_{p3} + K_{p4} (P_p + \frac{P}{\eta_i})$

52. $C_{ec} = C_i + C_{bc} + C_p$

53. $C_{at} = K_{at} \sqrt{N}$

54. $C = N C_m + C_b + C_{ec} + C_{at}$

55. $V_m = \frac{\pi (D + 2b)^2 z}{4}$

56. $V_b = K_{b2} E_b$

57. $V_i = K_{i9} W_i$

58. $V_{bc} = K_{c9} W_{bc}$

59. $V_p = K_{p5} P_p$

60. $V_{ec} = V_i + V_{bc} + V_p$

61. $V = N K_v V_m + V_b + V_{ec}$

4.2 System Selection Auxiliary Program

Data Input Subroutine

F_W, F_β, F_A, F_V, F_C

System performance parameters of each system (W, β, A, V, C)

Main Programs

1. $R_W = F_W \frac{W_{max}}{W}$

2. $R_\beta = F_\beta \frac{\beta}{\beta_{min}}$

3. $R_A = F_A \frac{A_{max}}{A}$

4. $R_V = F_V \frac{V_{max}}{V}$

5. $R_C = F_C \frac{C_{max}}{C}$

6. $R = R_W + R_\beta + R_A + R_V + R_C$

Printout Subroutine

Performance rating for each system (R, R_W, R_β, R_A, R_V, R_C)

4.3 Nomenclature

a_c Effective absorptivity of converter cavity

A Area occupied by deployed system (ft^2)

b Width and depth of concentrator support ring (ft)

C Overall cost of helionic power system

C_{at} Cost of final assembly and test of power system

C_b Cost of energy storage batteries

C_{bc} Cost of battery charger

C_d Cost of fabricating one thermionic diode

C_{da} Cost of fabricating a diode converter subassembly

C_{ec} Cost of electrical controller

C_i Cost of dc - to - dc static converter

C_m Cost of helionic module

C_p Cost of parasitic load

C_r Cost of fabricating solar concentrator

C_{sat} Cost of structure, assembly, and testing for helionic module subassembly

d_a Diameter of converter cavity aperture (ft)

D Diameter of solar concentrator (ft)

e_c Effective emissivity of converter cavity

E_b Rated watt-hour output of storage batteries

f Focal length of solar concentrator (ft)

F_A Performance weighting factor for deployed area

F_c Performance weighting factor for system cost

F_v Performance weighting factor for stowed volume

F_w Performance weighting factor for system weight

F_ρ Performance weighting factor for system reliability

I System load current

I_m Helionic module current output

K_{at} Constant for cost of system assembly and testing

K_A Deployment area space factor

K_{b1} Constant for cost of energy storage batteries

K_{b2} Specific volume of storage batteries (ft^3/w-hr)

K_{c1}, K_{c2}, K_{c3} Constants for efficiency of battery charger

K_{c4}, K_{c5}, K_{c6} Constants for weight of battery charger

K_{c7}, K_{c8} } Constants for cost of battery charger

K_{c9} Specific volume of battery charger (ft^3/lb)

K_{i1}, K_{i2}, K_{i3} } Constants for efficiency of static converter

K_{i4}, K_{i5}, K_{i6} } Constants for weight of static converter

K_{i7}, K_{i8} } Constants for cost of static converter

K_{i9} Specific volume of static converter (ft^3/lb)

K_{ms} Ratio of weight of module deployment arms to total weight of helionic modules

K_{p1}, K_{p2} } Constants for weight of parasitic load

K_{p3}, K_{p4} } Constants for cost of parasitic load

K_{p5} Specific volume of parasitic load (ft^3/w)

K_r Specific cost of solar concentrator fabrication ($\$/ft^2$)

K_{sat} Constant for cost of helionic module structural elements, assembly, and testing

K_w Constant for weight of system interconnecting cables (lb volts/w)

K_V Stowage volume space factor

K_f Constant for thickness of solar concentrator

$K_{\eta 1}$, $K_{\eta 2}$ Constants for shading of solar concentrator

n Number of thermionic diodes per helionic module

N Number of helionic modules in system

N^1 Minimum number of operating modules required

N_p Number of modules connected in parallel

N_s Number of modules connected in series

P System output power (watts)

P_b Power supplied to storage batteries (watts)

P_{bc} Input power to battery charger (watts)

P_c Focal plane power within cavity aperture (watts)

P_f Power available in solar concentrator focal plane (watts)

P_i Power input to system static converter (watts)

P_m Power output from a helionic module (watts)

P_n Net thermal power available to helionic module thermionic converter assembly (watts)

P_p Power dissipated in system parasitic load (watts)

P_r Power radiated by radiator of helionic module thermionic converter assembly (watts)

P_R Power reradiated from cavity aperture (watts)

P_t Power input to the helionic module thermal energy storage (if used) (watts)

R Weighted system performance rating

R_A Weighted system deployment area rating

R_c Weighted system cost rating

R_V Weighted system stowage volume rating

R_W Weighted system weight rating

R_ρ Weighted system reliability rating

S Solar constant (watts/ft^2)

t_s Time in sun per orbital period (hours)

t_u Time in earth's umbra per orbital period (hours)

T Total mission duration (hours)

T_e Thermionic diode emitter temperature (^oK)

U System load voltage

U_d Output voltage per thermionic diode

U_i Input voltage to system static converter

U_m Voltage output of helionic module

V Volume occupied by stowed system (ft^3)

V_b Volume of energy storage batteries (ft^3)

V_i Volume of dc - to - dc static converter (ft^3)

V_{bc} Volume of battery charger (ft^3)

V_{ec} Volume of electrical control (ft^3)

V_m Stowage volume of helionic module (ft^3)

V_p Volume of parasitic load (ft^3)

w_b Reciprocal of specific weight of batteries ($^{w-hr}/_{lb}$)

w_{da} Specific weight of diode converter subassembly ($^{lb}/_{w}$)

w_{ea} Specific weight of diode erection arm ($^{lb}/_{w-ft}$)

w_{ms} Specific weight of module deployment arm ($^{lb}/_{ft^3}$)

w_r Specific weight of solar concentrator ($^{lb}/_{ft^3}$)

w_{tc} Specific weight of diode converter thermal control ($^{lb}/_{ft^2}$)

W Weight of system (lb)

W_b Weight of energy storage batteries (lb)

W_{bc} Weight of battery charger (lb)

W_{da} Weight of diode converter assembly (lb)

W_{ea} Weight of diode erection arm (lb)

W_{ec} Weight of electrical controller (lb)

W_i Weight of system static converter (lb)

W_m Weight of helionic module (lb)

W_p Weight of system parasitic load (lb)

W_r Weight of solar concentrator (lb)

W_{tc} Weight of diode converter thermal control (lb)

W_w Weight of system interconnecting cables (lb)

y, y^1 Maximum number of failures which can be tolerated out of a parallel combination of N_p modules

z Maximum depth of solar concentrator (ft)

α_s Apparent solar diameter (radians)

β Overall system reliability

β_b Reliability of storage batteries

β_{bc} Reliability of battery charger

β_d Reliability of a thermionic diode

β_e Reliability of module erection

β_i Reliability of system static converter

β_k Probability of having (N_p-K) modules out of a parallel combination of N_p modules working at end of mission

β_m Reliability of a helionic module

β_{mn} Reliability of subsystem of interconnected helionic modules

β_p Reliability of system parasitic load

δ Thickness of module solar concentrator (ft)

η Ratio of the sum of the energy outputs to system load and parasitic load to the total solar energy intercepted

η' Ratio of energy output to the system load to the total solar energy intercepted

η_b Charge-discharge efficiency of storage batteries

η_{bc} Efficiency of battery charger

η_{bd} Storage battery discharge depth

η_d Efficiency of thermionic diode

η_i Efficiency of system static converter

η_m Efficiency of helionic module

η_r Reflectivity of solar concentrator

η_{rc} Collector-cavity efficiency

η_v Fraction of solar concentrator not shaded

θ_m Rim angle of solar concentrator

μ Poisson's ratio

μ_{ma} Resistivity of module deployment arms (ohm ft)

ξ_x Probability of having x failures out of a parallel combination of N_p modules

π The constant 3.14159. . .

σ The Stefan - Boltzmann constant

$$(5.2698 \times 10^{-9} \quad \frac{W}{ft^2-(^\circ K)^4})$$

ϕ_a Maximum solar concentrator orientation error

ϕ_r Maximum angular surface deviation on solar concentrator

NOTATION

nl $[x]$ The next integer value greater than x if x is non-integer; x if x is integer

ns $[x]$ The next integer value smaller than x if x is non-integer; x if x is integer

x_{max} The maximum value for x

x_{min} The minimum value for x

4.4 Discussion of Results

Subsequent runs made with the program quickly indicated several limitations on state-of-the-art helionic systems, and also suggested a reduction in the scope of the study. In many areas such as reliability or system cost, the results could be considered meaningless if not misleading. It was immediately apparent that no satisfactory information regarding these areas was available and the consequence of assumptions made could be completely unrealistic. Also, the great number of conditions and combinations possible with the program described made the costs of pursuing the program prohibitive in terms of computer time required. The preliminary runs did indicate that most of the extensive programming anticipated would not contribute meaningfully to the understanding of the state-of-the-art in solar thermionic systems.

Practical considerations such as the maximum attainable diameter in state-of-the-art concentrators, minimum sizes for thermionic converter or generator assemblies, and the structural complications of trying to utilize or deploy large numbers of smaller modular assemblies help to define the limits for helionic systems. The practical range for systems for orbital applications would seem to be for power ranges of from 200 watts to 3000 watts. It is also shown in Figures 4.2 and 4.3 that for a power requirement (in this case 1.5 KW) the cost is almost directly proportional to the number of modules used, regardless of concentrator diameter. Also, the spread of points shown in Figure 4.2 indicates the limited variation which results from different series-parallel combinations on weight. In general, the effect on weight is sufficiently small to disregard this factor and specify systems designs based on the most efficient structural arrangement. The weight of the system is also shown to be directly proportional to the number of modules. The diameter of the module does in this case make a significant difference, however. The best results for most systems are obtained with concentrators of 3 to 6 feet in diameter which fortunately lies within the state-of-the-art in concentrator fabrication capabilities.

With the size limitation of 200 to 3000 watts dictated by practical structural consideration and the relative insensitivity of the systems to various stack-up arrangements, a 1.0 or 1.5 KW system design can be considered typical of all practical helionic systems. The support and deployment arrangements may vary with the power level, but the weights, costs and overall efficiencies will retain nearly the same relation to the specified power level. Figure 4.4

SYSTEM WEIGHT AND COST FOR
3.5 FT CONCENTRATORS

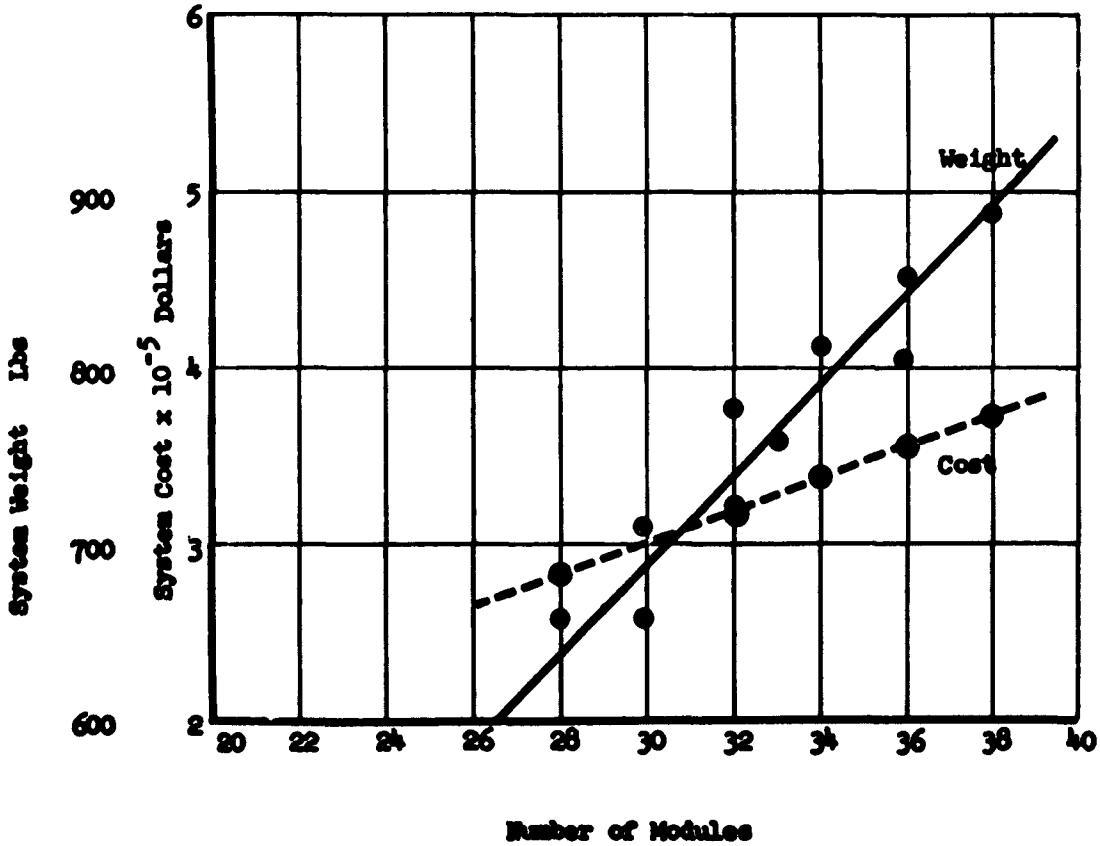

Fig. 4.2

SYSTEM WEIGHT AND COST FOR
5 FT. CONCENTRATORS
(1.5 KW SYSTEM)

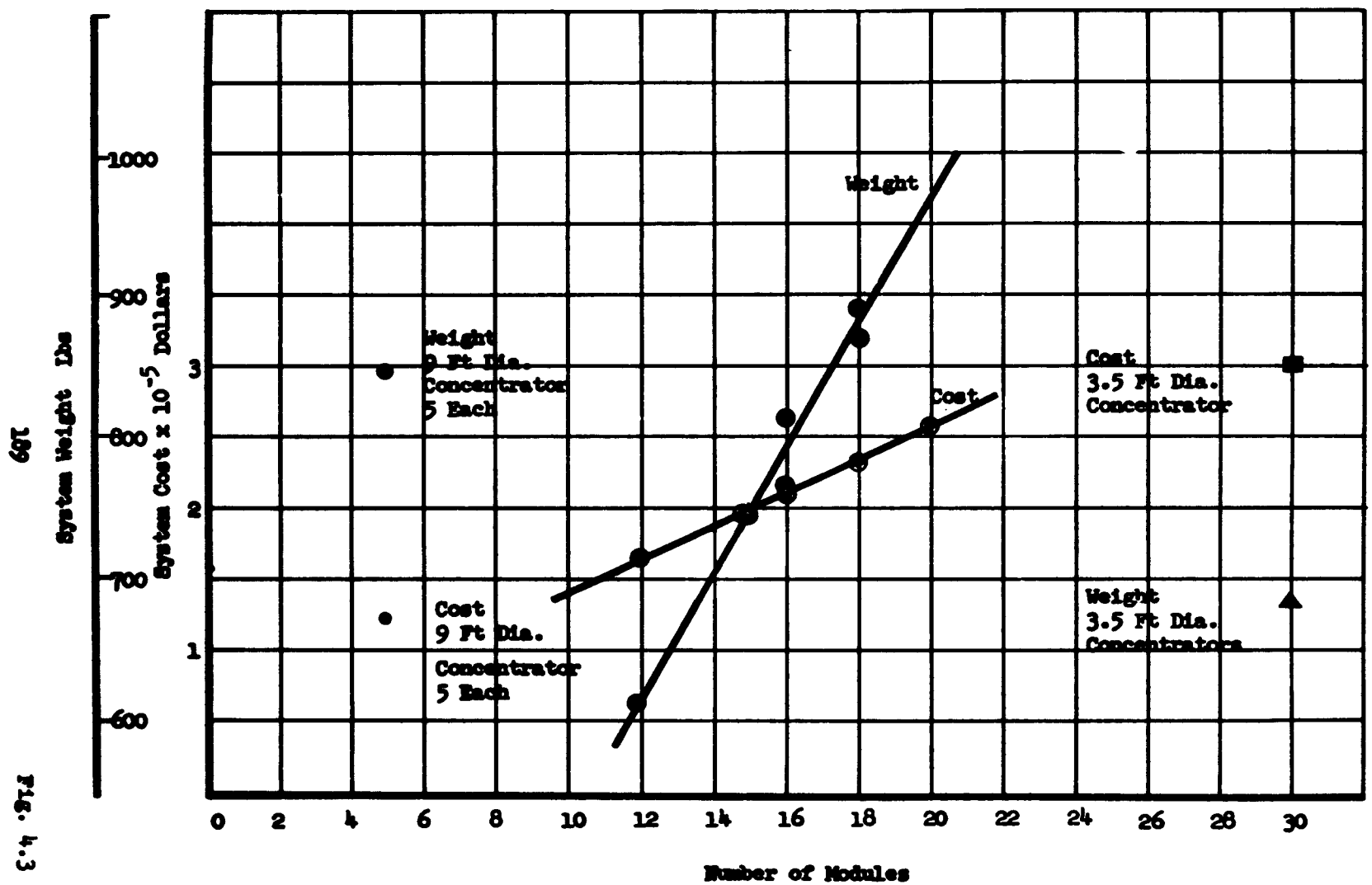

Fig. 4.3

OVERALL EFFICIENCY AS A FUNCTION OF
THE NUMBER OF MODULES (1.5 KW SYSTEM)

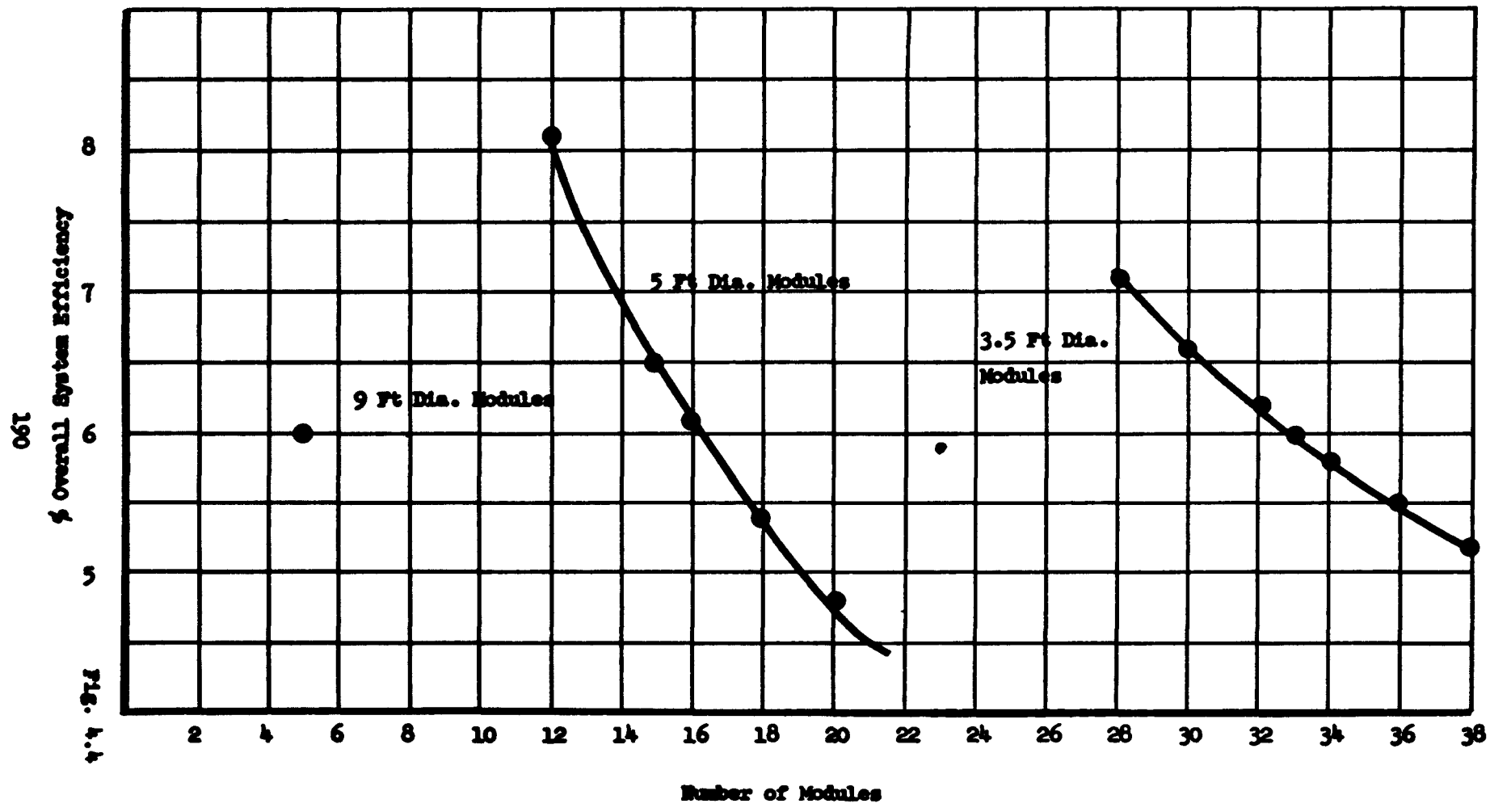

190

Fig. 4.4

also shows the typical relation between overall efficiency and the number of modules. Again, the best performance is observed with the minimum number of modules possible. The optimum size for the concentrators is close to 5 feet.

Utilizing a structure similar to those shown in Figures 3.6.4 and 3.6.5, or variation of these with approximately the same structural weight to power ratios, a summary of the parametric evaluation as applies to a 1.5 KW prototype system can be carried out. The complete orbital power system will include: (1) orientation systems to keep the generators aligned with the sun, (2) batteries to store energy for use during the shaded portion of the orbit, (3) power regulators for both the battery and the system load, and (4) a system for deploying the generators from their vehicle.

These figures show two methods by which the generators might be extended from a vehicle. Each concentrator is held by a ring which is supported by a yoke. The yoke is attached to the extension arm through a gimbal arrangement which allows the concentrator to pivot about its focal point. The concentrator is then aligned with the sun by bimetallic elements which become heated when the concentrator is misaimed. A developmental model of such an orienting device called a heliotropic mount was shown in Figure 3.4.4. The absorber containing the thermionic converters is fixed to the extension arm at the focal point of the concentrator.

Solar Concentrator Optical Performance

When a solar concentrator is aimed at the sun, the solar energy intercepted will be focused near the focal point of the concentrator. Stated in optical terms, an image of the sun will be formed in the focal plane. The distribution of the solar energy about the focal point is dependent on the following:

1. Intensity distribution of the solar disc.
2. Surface finish of the concentrator.
3. Reflectivity of the concentrator.
4. Aperture ratio (diameter: focal length).
5. Geometric accuracy of the concentrator.
6. Aiming accuracy of the concentrator.

7. Size of the concentrator.

The intensity distribution of the solar disc is shown in Figure 4.5. When the sun is reflected from a polished surface, the intensity distribution is modified by the imperfections in the surface and is decreased by absorption by the reflecting surface. The modified intensity distribution we call the "psuedosun intensity distribution." (Refer to Section 3.3, Figure 3.3.4) Figure 4.5 shows this distribution for a polished aluminum surface. The intensity shown has been scaled up to exclude reflectivity effects.

The effect of aiming errors is to displace and distort the flux profile. The displacement is the product of the angular aiming error and the focal distance and the distortion is negligible for errors up to about one solar diameter (0^{o} -32'). (See Section 3.3, Figures 3.3.5 through 3.3.8).

Geometric inaccuracies may be expected to be present in any lightweight solar concentrator. These inaccuracies will be manifested as surface ripples or as a gross distortion of the concentrator, and they will cause the image to be spread and less intense.

Solar Concentrator Weight

The weight of the solar concentrator and its support structure was treated in detail in Section 3.3 where it was shown that the concentrator shell weight is proportional to the surface slope error ϕ to the minus 2/3 power ($\phi^{-2/3}$) and the support ring weight is proportioned to ϕ^{-1}.

Test of a five foot diameter electroformed nickel concentrator with a thickness of 0.020 inch and a rim angle of sixty degrees, shows an image spread corresponding to an effective surface slope error of 2.7 minutes. Using this information, the proportionality constant, $K = \phi ER/\lambda^{3}$ (see Section 3.3) was determined to be 10,000 min-lb/in. The optimum concentrator weights were then calculated and the P/W curve shown in Figure 4.6 was obtained. The thicknesses for a five foot, sixty-degree concentrator are also shown.

Solar Absorber

For a cavity-type absorber, the absorptivity is dependent on the surface absorptivity and the number of reflections of the incoming rays before they

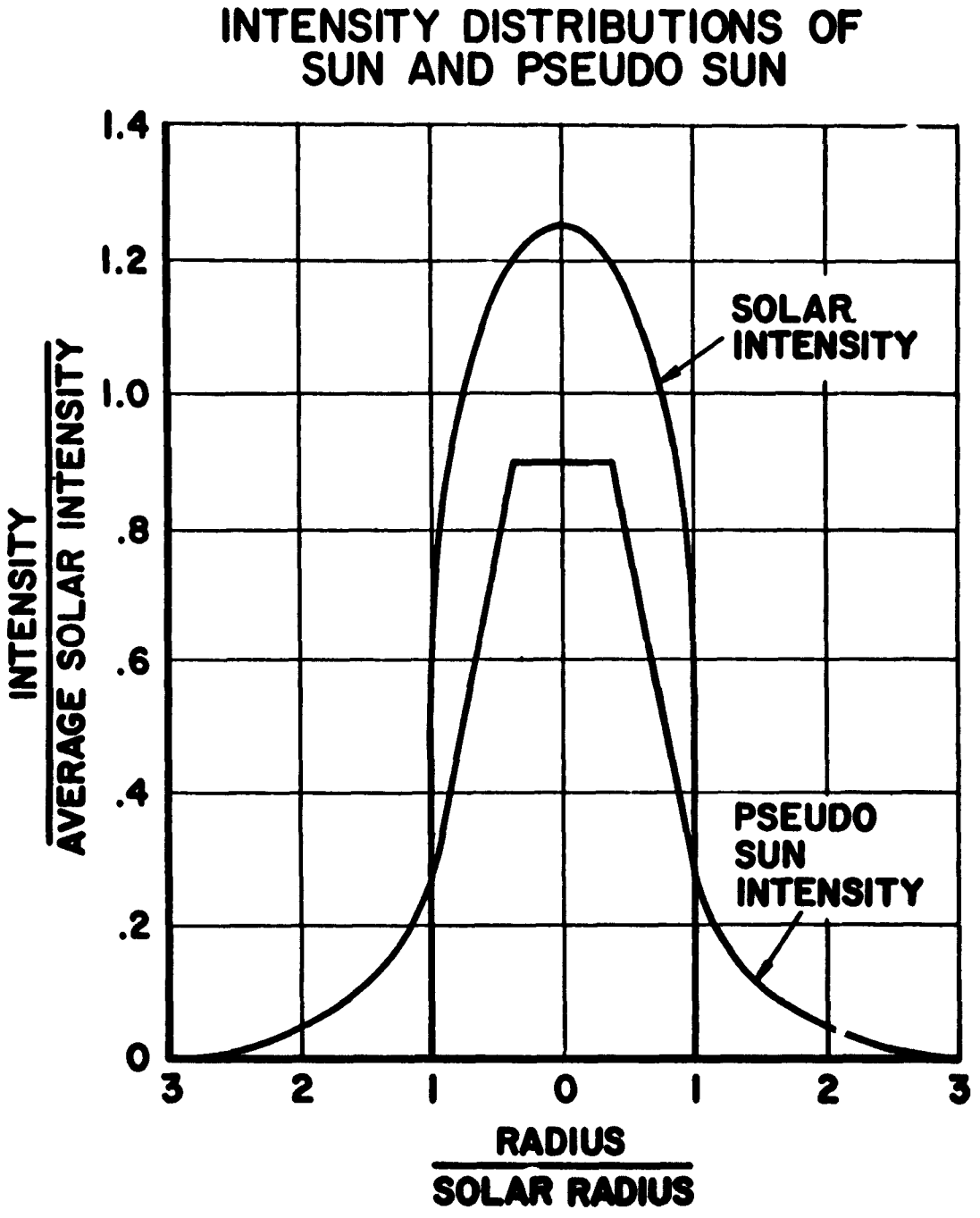
INTENSITY DISTRIBUTIONS OF
SUN AND PSEUDO SUN
1.4
1.2
1.0
.8
.6
.4
.2
0
INTENSITY
AVERAGE SOLAR INTENSITY
SOLAR
INTENSITY
PSEUDO
SUN
INTENSITY
3
2
1
0
1
2
3
RADIUS
SOLAR RADIUS

FIGURE 4.5

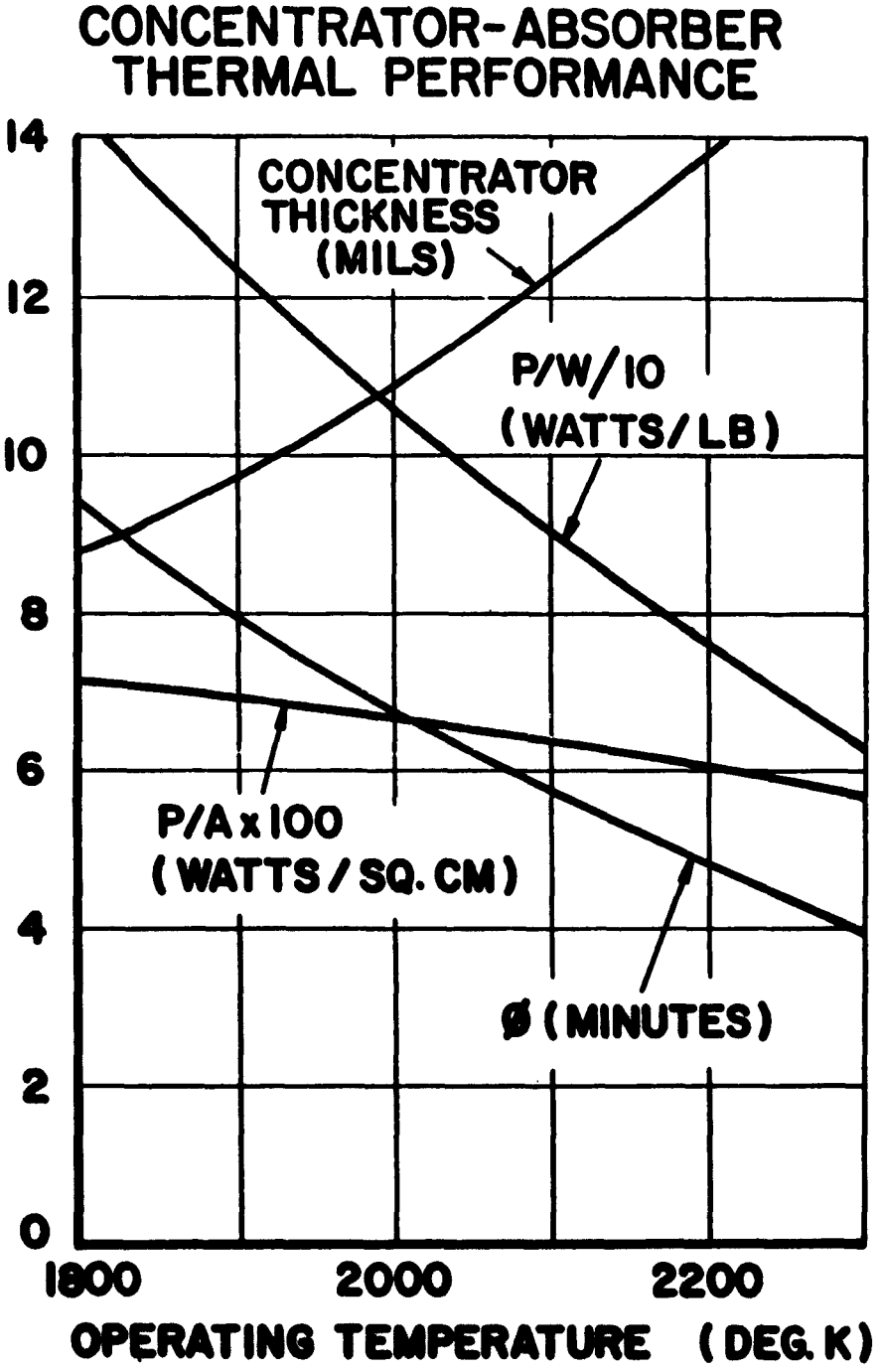
CONCENTRATOR-ABSORBER
THERMAL PERFORMANCE
14
12
10
8
6
4
2
0
CONCENTRATOR
THICKNESS
(MILS)
P/W/10
(WATTS/LB)
P/A x 100
(WATTS / SQ. CM)
Ø (MINUTES)
1800
2000
2200
OPERATING TEMPERATURE (DEG. K)

FIGURE 4.6

leave through the aperture. The number of reflections is dependent on the obliqueness of the incoming rays and the shape of the cavity. Calculations have shown that a cavity absorptivity of 93% can be achieved with a cavity having a diameter or width equal to the depth and a surface absorptivity of 45%, when used with a 60° rim angle concentrator.

The emissivity of a cavity is a function of the surface emissivity and the cavity shape. The shape parameters generally used are the depth, aperture ratio and the surface area, aperture area ratio. For a typical square cavity having a surface emissivity of 23%, the cavity emissivity is 75% (see Section 3.2).

Solar Concentrator - Absorber Combination

The object of the design of the solar concentrator-absorber combination is to make available to the thermionic converters a maximum amount of power at a minimum penalty. The associated penalty is a combination of several factors: weight, extended area, stowage volume, cost, and reliability. Since the concentrators constitute a large share of the mass of the power system and since area and volume are closely linked to weight, a weight optimization will produce a system with near minimum penalty. Reliability will not be compromised in minimizing weight.

Maximum power will be delivered to the absorber when the radius of the absorber aperture is that radius at which the reradiated flux equals the absorbed flux. However, the power delivered is not very sensitive to changes in aperture radius or concentrator rim angle when the optimum radius is near three solar image radii or greater,as is usually the case. Therefore, in order to simplify the analysis, it has been assumed that the optimum radius is three times the product of the solar half-angle (.00465 rad.) and the concentrator radius, and 96% of the focused power passes through this radius.

The above power considerations apply to a rigid concentrator perfectly aimed. When there is an aiming error, the aperture radius must be increased to accommodate the displaced image. As the concentrator is made thinner, surface slope errors increase,causing a spread of the solar image and requiring a larger cavity aperture. This spread may be assumed to be equivalent to increasing the angular radius of the pseudosun by an amount 2 ϕ where ϕ is the surface

slope error. The aperture radius is then:

$$r_A = 3 r_c \left(\frac{\alpha}{2} + 2\phi\right) + f\gamma \qquad (24)$$

where γ = misorientation angle
f = focal length
r_c = concentrator radius
$\frac{\alpha}{2}$ = solar half-angle

since $f \gg r_c$

The area ratio is then

$$\frac{A_a}{A_c} = \left(\frac{r_a}{r_c}\right)^2 = \left(\frac{3}{2}\alpha + 6\phi + \gamma\right)^2 \qquad (25)$$

Power delivered to the absorber is then

$$P = q \rho a A_c - \varepsilon \sigma T^4 A_a \qquad (26)$$

where q = solar flux constant
ρ = concentrator reflectivity
a = absorber absorptivity
ε = absorber emissivity

$$\frac{P}{A_c} = q \rho a - \varepsilon \sigma T^4 \left(\frac{3}{2}\alpha + 6\phi + \gamma\right)^2 \qquad (27)$$

Assuming

$$\frac{W}{A_c} = K \phi^{-\frac{2}{3}} \qquad (28)$$

Then

$$\frac{P}{W} = \left[q \rho a - \varepsilon \sigma T^4 \left(\frac{3}{2}\alpha + 6\phi + \gamma\right)^2\right] \frac{\phi}{K}^{\frac{2}{3}} \qquad (29)$$

Maximizing $\frac{P}{W}$ yields

$$\phi = \frac{\frac{3}{2}\alpha + \gamma}{48}\left[\sqrt{9 + \frac{16\, q\, \rho\, a}{\varepsilon \sigma T^4 \left(\frac{3}{2}\alpha + \gamma\right)^2}} - 5\right] \qquad (30)$$

Thus, the concentrator thickness which gives maximum thermal power per pound is that which limits the surface slope error to the optimum.

Figure 4.6 shows optimum ϕ as a function of T for the case where:

$q = 0.14$ watts/sq. cm.

$\rho = 0.90$

$a = .935$

$\varepsilon = .753$

$\alpha = 32' = .0093$ rad.

$\gamma = 6' = .00175$ rad.

Thermionic Converter

The thermionic converter characteristics must be determined so that they may be examined in combination with the concentrator and the absorber to determine the optimum operating conditions. The characteristics have been obtained by fitting laboratory test data to empirical equations.

Since power output follows closely the emission capabilities of the thermionic cathode, an equation of the form $P_o = K_3 T^2 \left(e^{-\frac{K_2 \times 11{,}600}{T}}\right)$ was fitted to the test data. This is the form of the Richardson emission equation. For the converter tested, with all parameters optimized except temperature, $K_2 = 1$, $K_3 = .009$, and K_3, of course, depends on converter size.

For the input power, an equation of the form $P_i = K_4 P_o + K_5 T^{5/2}$ was fitted to the test data. The $T^{5/2}$ term is the form of the solution to the combined radiation-conduction problem. It also closely represents the case of parallel radiation and conduction when the two are nearly equal. Analyses

of conditions in the converter have shown that this is usually the case. The results of the curve fit yielded $K_4 = 3$ and $K_5 = 3.45 \times 10^{-6}$

Then efficiency may be expressed as

$$N_t = \frac{P_o}{P_i} = \frac{P_o}{3\,P_o + 3.45 \times 10^{-6}\ T^{5/2}} \qquad (31)$$

$$= \frac{1}{3 + \dfrac{3.45 \times 10^{-6}\ T^{5/2}}{.009\ T^2\ \exp\ (-11{,}600/T)}}$$

$$N_c = \frac{1}{3 + 3.73 \times 10^{-4}\ \sqrt{T}\ \exp\ (11{,}600/T)} \qquad (32)$$

This relation is shown in Figure 4.7.

Generator Module

By multiplying the thermal power plotted in Figure 4.5 by the thermionic conversion efficiency, a plot of power output as a function of temperature may be obtained as shown in Figure 4.7. Note the maximum power per solar concentrator pound occurs at a temperature of about 2100°K. Efficiency can be increased at higher temperatures but system weight will go up. Also, the maximum power obtainable at 2000°K, which is considered realistic in terms of life requirements, is only slightly below the optimum. This lower operating temperature is therefore selected for the design.

Conclusion

Results obtained from the parametric design study, various solar concentrator development programs, as well as the extensive thermionic generator performance tests carried out under this program, have been evaluated. Where minimum system weight is the design criteria, system weights of the order of 440 pounds per kilowatt of continuous power for a 90 minute orbital application can be achieved with current state-of-the-art components.

GENERATOR ELECTRICAL PERFORMANCE

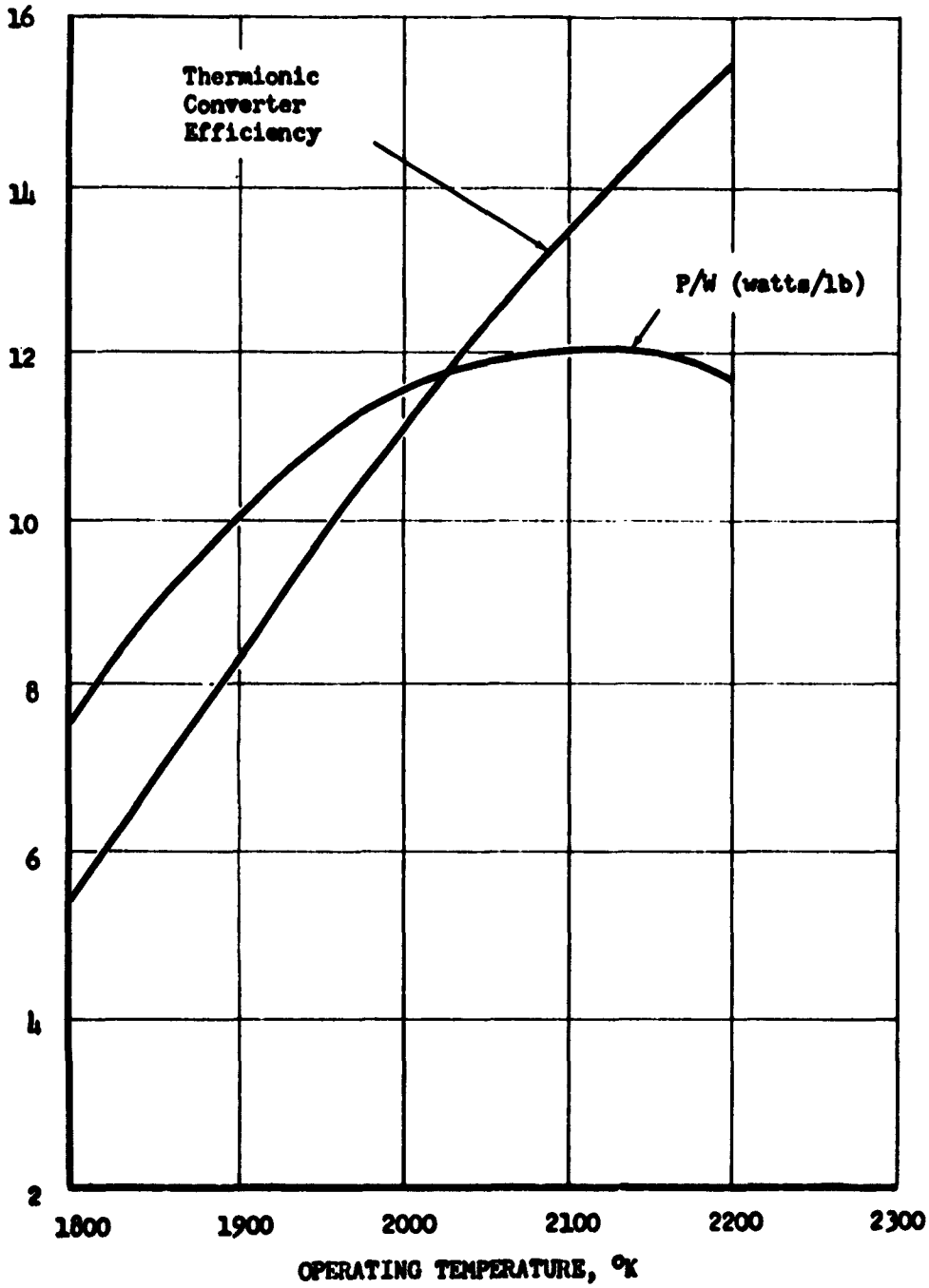

Fig. 4.7

Solar concentrator weight reductions, which could result from current efforts to develop high precision aluminum concentrators, as well as the attainment of higher cavity absorber and thermionic converter efficiencies which should result from many current development efforts will permit a reduction in the specific weight.

The Appendix of this report presents a detailed design of a 1.5 KW continuous power solar thermionic system based on the evaluation of all study and test results acquired during the conduct of this program.

APPENDIX

DESIGN AND TEST SPECIFICATION FOR

1.5 KW SOLAR THERMIONIC POWER SYSTEM

Introduction

The 1.5 kw thermionic power system specified for a one year orbital application represents a careful integration of many concepts and state-of-the-art components. The system is somewhat larger than estimates made early in this program would have indicated but it is still very competitive with all other auxiliary power systems suitable for the prescribed application. Also the design presented is quite flexible in that it can easily be modified to provide many other power or voltage requirements with only minor changes within the system. The system as specified actually has the capability of supplying from zero to 4.5 kw of power under certain circumstances as well as the continuous 1.5 kw used as the nominal design level. All of the components and structures presented in the system are felt to be realistic in all respects. The weights and efficiencies attributed to components such as the solar concentrators or thermionic generators may not be as optimistic as other studies would indicate, but all such components have been tested and proven beyond a reasonable doubt to be capable of fulfilling the needs of this system.

The reliability of such a system is still subject to question. None of the major components has actually been tested under the conditions or for the time specified for this application. All components do represent a considerable improvement over hardware available at the time this program was initiated. Life test programs and environmental test programs of many sorts are currently being conducted to determine component capabilities and reliability. With the progress made to date in the state-of-the-art in various component areas as a guide it seems quite reasonable that all components specified for this system can be fully qualified in a reasonable time span.

System Description

The overall system is shown in block diagram form in Figure 1, and in the systems layout Figure 2. The basic system is made up by a structural support and deployment system, a modular assembly constituted by a generator and solar concentrator assembly, and controls and power distribution system. The entire array can be stowed within a vehicle volume 9 feet in diameter and 16 feet high. The system is shown in the stowed and deployed positions in Figure 2.

COMPLETE SYSTEM BLOCK DIAGRAM

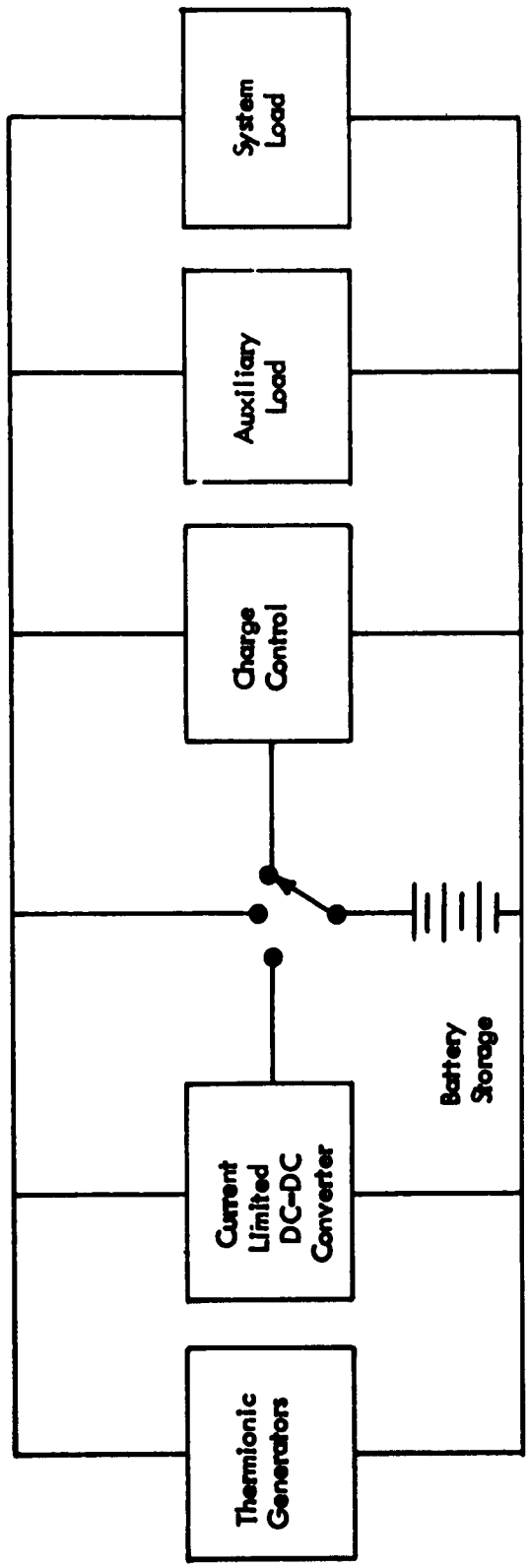

Fig. 1

1.5 KW SOLAR THERMIONIC SYSTEM LAYOUT

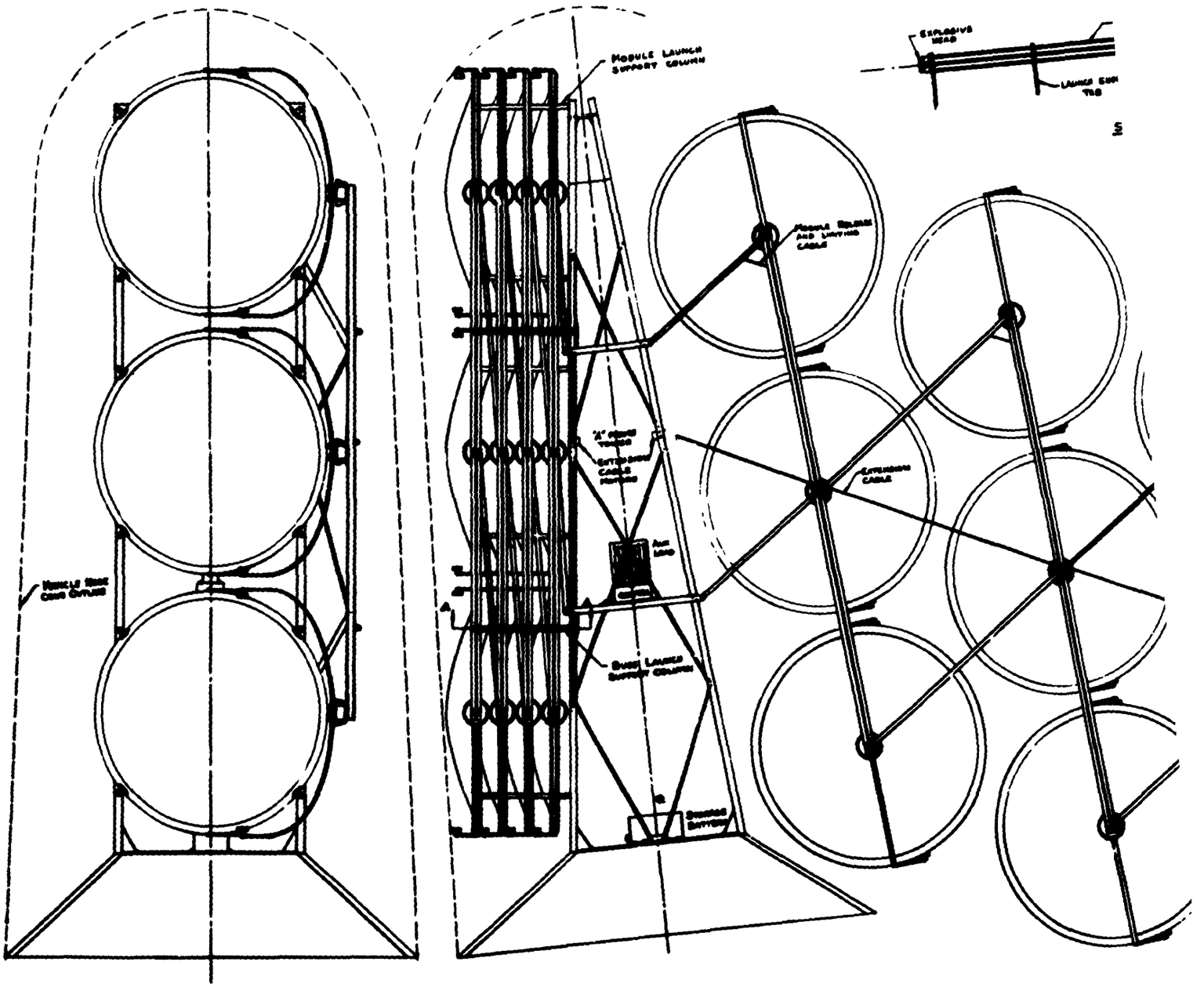

KW SOLAR THERMIONIC SYSTEM LAYOUT

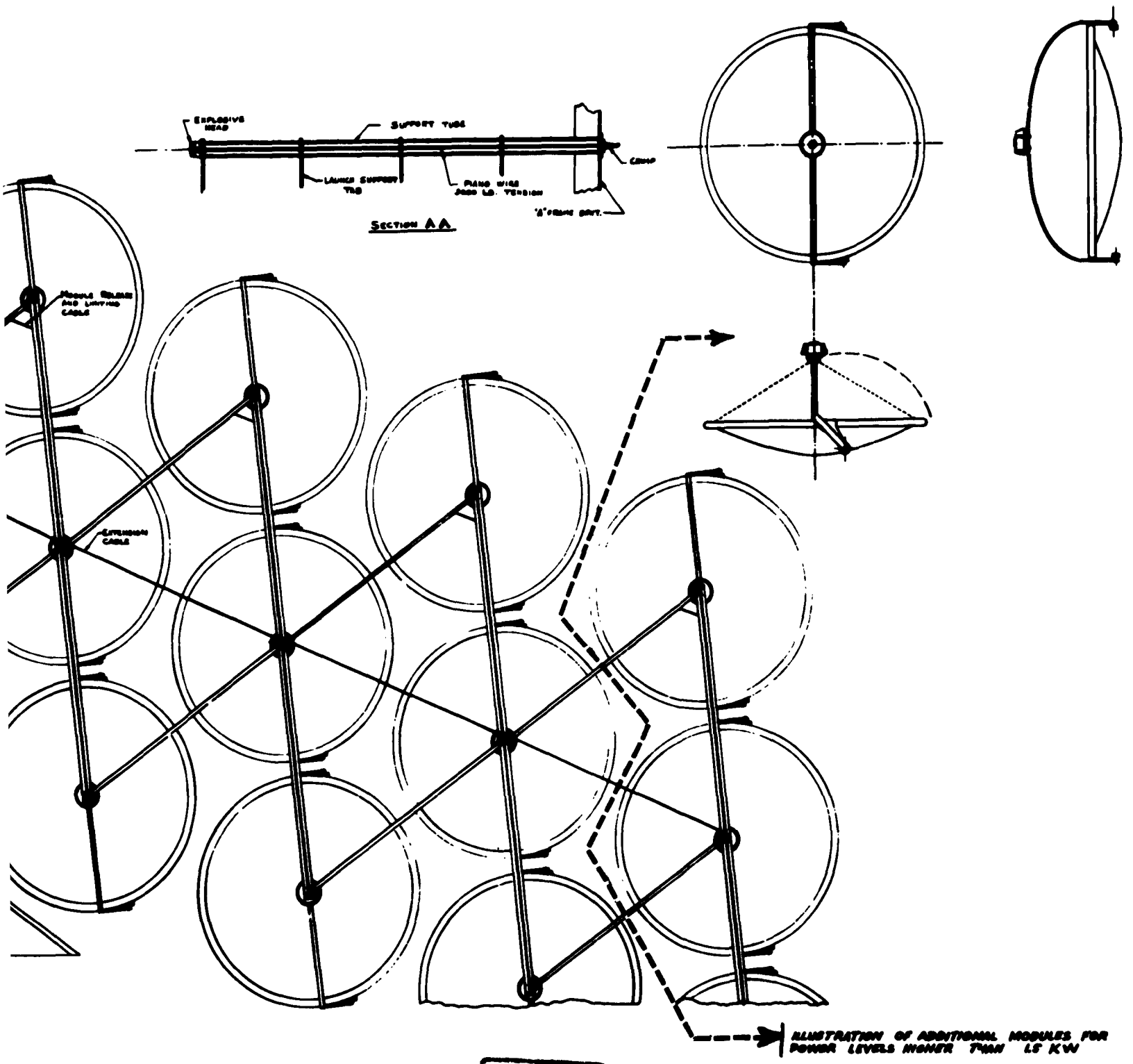

2

Fig. 2

The operational sequence of the system is described as follows.

1. With the vehicle in orbit and sun oriented within 5 degrees the nose cone is jettisoned.
2. Upon radio or timer command the explosive head of the support tube assemblies are fired and the extension drive motors activated.
3. The extension drive motors pay out cable at a controlled rate. The extension springs located at each hinge point between the conductor struts and buss channel are graduated in stiffness to insure the outer most buss section is completely deployed before the following section begins to move.
4. As each buss section reaches the fully extended position a second cable, fastened to the conductor struts and fed through the buss structure, is placed in tension and extracts the clips holding the bucket handle and generator assembly secured to the support pin and bracket assembly on each concentrator rim.
5. The actuator spring located at the hinge point between the bucket handle and the hinge bracket causes the concentrator assembly to slowly rotate until it arrives at a point 90° removed from the stowed position. The disc-type viscous dampers mounted on the shaft assembly provide a control of the rate at which the concentrator rotates into position. This damper assembly is charged with a heavy high-vacuum grease capable of withstanding hard vacuum and extremes in temperature for long periods if necessary. Also the eventual loss of part or all of this grease will not subsequently affect the system.
6. Upon reaching the erect position, 90° removed from the supported position, the bucket handle is locked into place on the concentrator rim by a simple spring latch and stop assembly. This places the focal point of the concentrator within the area controlled by the heliotropic mounts on the generator assembly, assuming the initial 5° orientation is held by the vehicle.
7. The extension motors release cable until all modules and structures are in their proper position. The cables that release the module concentrators also serve as a stop to limit the extension of each buss section. (It is also possible with some modifications to

restow the entire structure in space by rewinding the cables, should such a feature be necessary).

8. The support tube assembly is jettisoned, section by section, as the buss section is extended. The wire tension member will whip each tubular section away from the vehicle as it is retracted in the extension process.
9. In the deployed position the modules will generate power during the sun portion of the orbital cycle to supply the vehicle system load, the battery load, and the control power requirements.
10. During full system load requirements the system will receive 1.5 kw. The batteries will be charged at a rate of 40 to 41 amps as determined by the current limiting character of the DC-DC converter charge control. The charge control will also disconnect the battery bank when the charge level, as indicated by the terminal voltage, reaches full charge. The auxiliary load bank will automatically cut in sufficient load to utilize the output of the thermionic generators and to maintain the voltage supplied to the vehicle system near the 28 volt level. If the vehicle should demand more than 1.5 kw the line voltage would drop. This would completely cut off the auxiliary load and if this were not sufficient and the voltage level drops to below the minimum 26 volt specification the battery load bank will be cut in to supplement the system generators. A total of nearly 4.5 kw can be delivered for a short period in this manner.
11. During the shade portion of the orbital cycle the generators will cool. As the generator output drops off the auxiliary load, if activated, will be automatically reduced to help maintain system voltage. The charge control will also sense the decline in generator output and switch the batteries to the vehicle load. Initially the auxiliary load may be activated and absorb large amounts of power. This is due to the high initial discharge voltage characteristics of the battery. As this excess in battery potential declines the auxiliary load will be cut off and the batteries will provide a constant 27.5 volts throughout the balance of the discharge cycle. The battery bank will also provide a small amount of control power and cesium reservoir heater power throughout the shade portion of the cycle.

The basic building block for the system is the modular assembly shown in Figure 3. By altering the size and number of modules used, a wide variety of power outputs can be obtained over a range of from 100 to 3000 watts at voltages from 0.6 volts to 144 volts or more. Figure 2 illustrates the ease with which additional modules can be added to the system. Two sections or six additional modules are shown attached to the 1.5 kw system (18 modules).

The module consists of a generator assembly, a concentrator assembly, and the associated support or erection structure.

The concentrator assembly consists of a precise parabolic electroformed nickel shell mounted to a nickel torus and fitted with support brackets and hinge brackets. This assembly is formed by the use of blind rivets and epoxy adhesives. Other techniques for producing such an assembly have been used successfully but the complications and cost involved with techniques such as the integral electroforming of support ring and concentrator shell are not justified.

The generator assembly is shown in detail in Figure 4. The basic converter structure shown in Section G-G is identical to the configuration used in the cubical cavity assembly discussed in this report. The emitter structure has been modified to provide a more efficient cavity geometry. The radiator also has been changed to obtain a geometry which is felt to be a considerable simplification over the cubical cavity geometry. The block into which the converters are inserted and the methods of mounting are also an improvement over the cubical cavity arrangement. The heliotropic mount assembly is made to fasten directly to the generator block.

The advantages of this generator configuration are summarized as follows:

1. Larger cavity-to-aperture area.
2. All converters are identical.
3. Cavity aperture actually formed by emitters.
4. Radiator geometry simplified.
5. Converter mounting and interconnection simplified.
6. Effective emitter area to cavity area ratio is large.
7. Internal flux distribution is more uniform with no bottom converter.
8. Shielding against radiant heat loss is improved.
9. Cavity block configuration more suitable for mounting.

MODULE ASSEMBLY LAYOUT

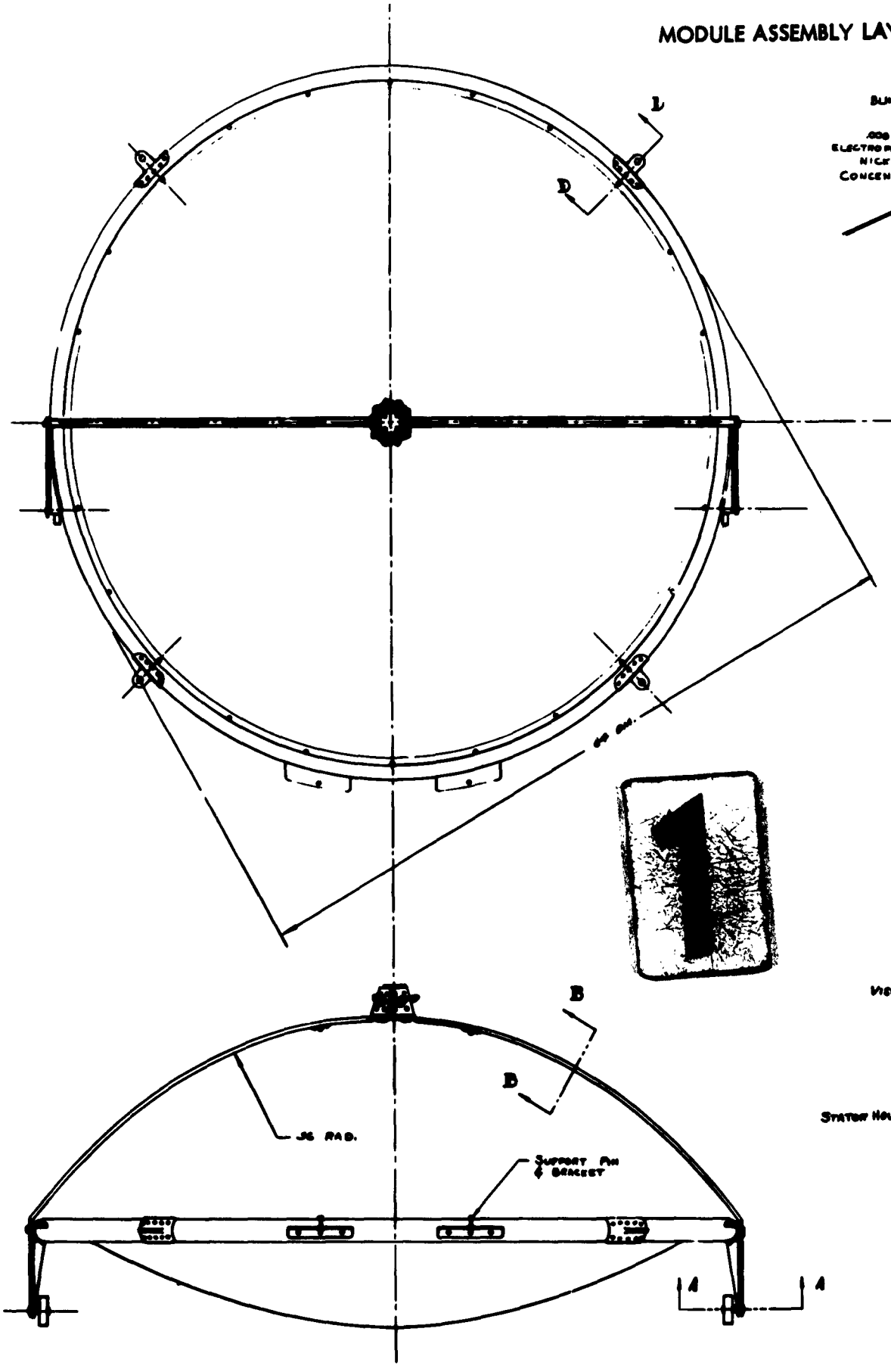

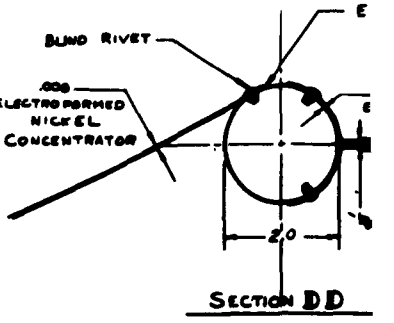

SECTION DD

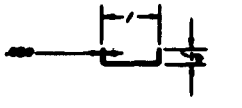

SECTION CC

SECTION BB

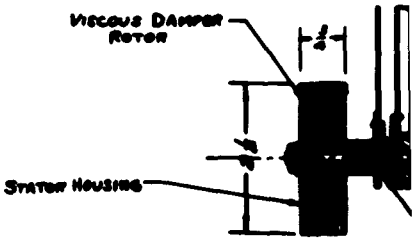

SECTION AA

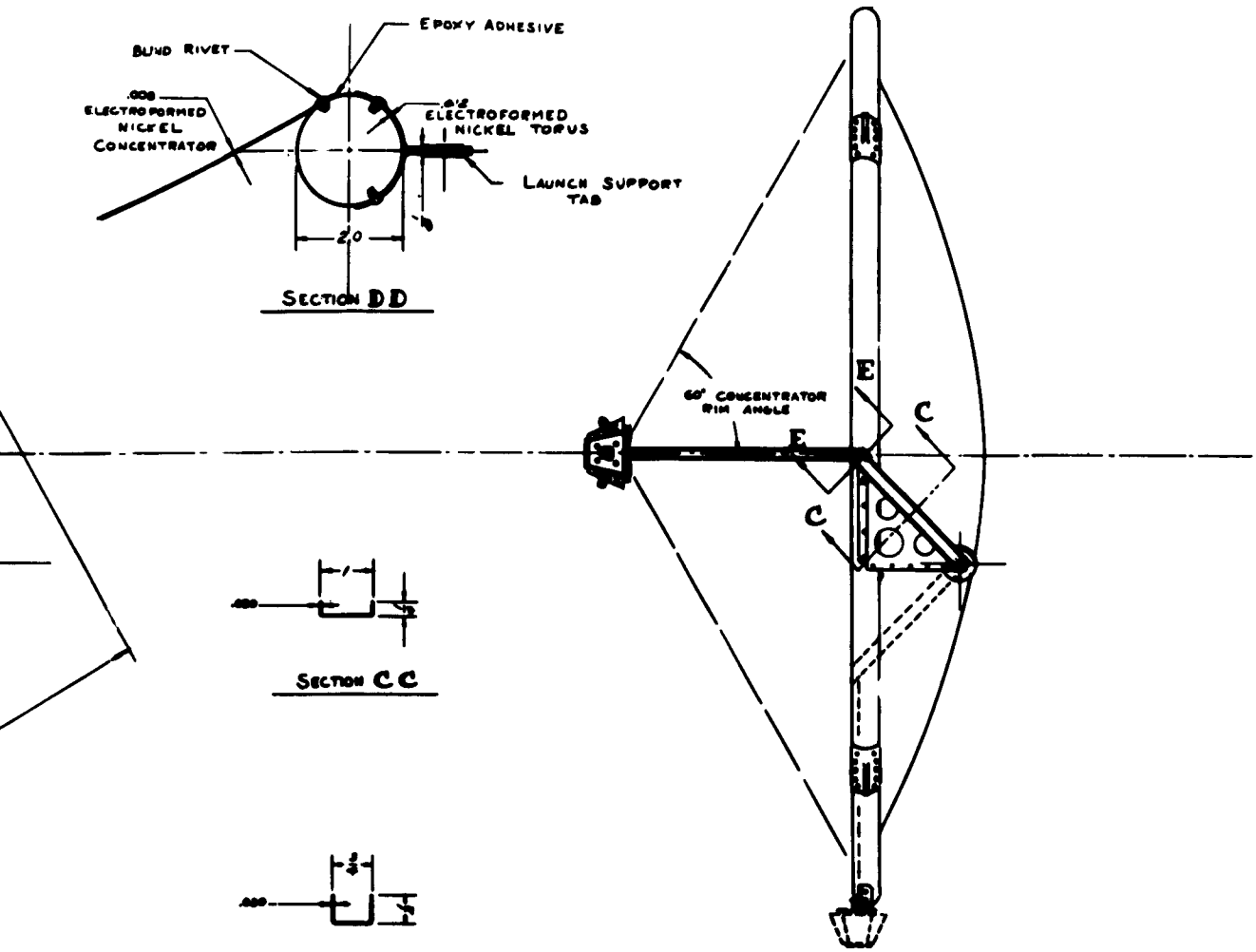
BLIND RIVET
EPOXY ADHESIVE
.008 ELECTROFORMED NICKEL CONCENTRATOR
.012 ELECTROFORMED NICKEL TORUS
LAUNCH SUPPORT TAB
2.0
SECTION DD
60° CONCENTRATOR RIM ANGLE
E
C
SECTION CC
SECTION BB

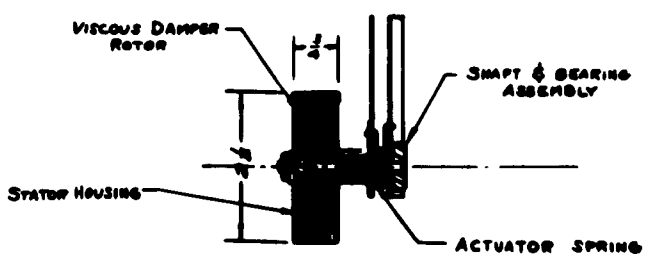
VISCOUS DAMPER ROTOR
SHAFT & BEARING ASSEMBLY
STATOR HOUSING
ACTUATOR SPRING
SECTION AA

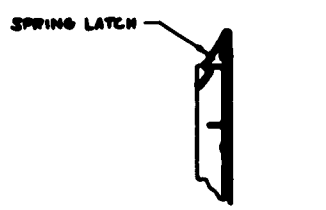
SPRING LATCH
SECTION EE

Fig. 3

2

ASSEMBLY-PROTOTYPE THERMIONIC GE

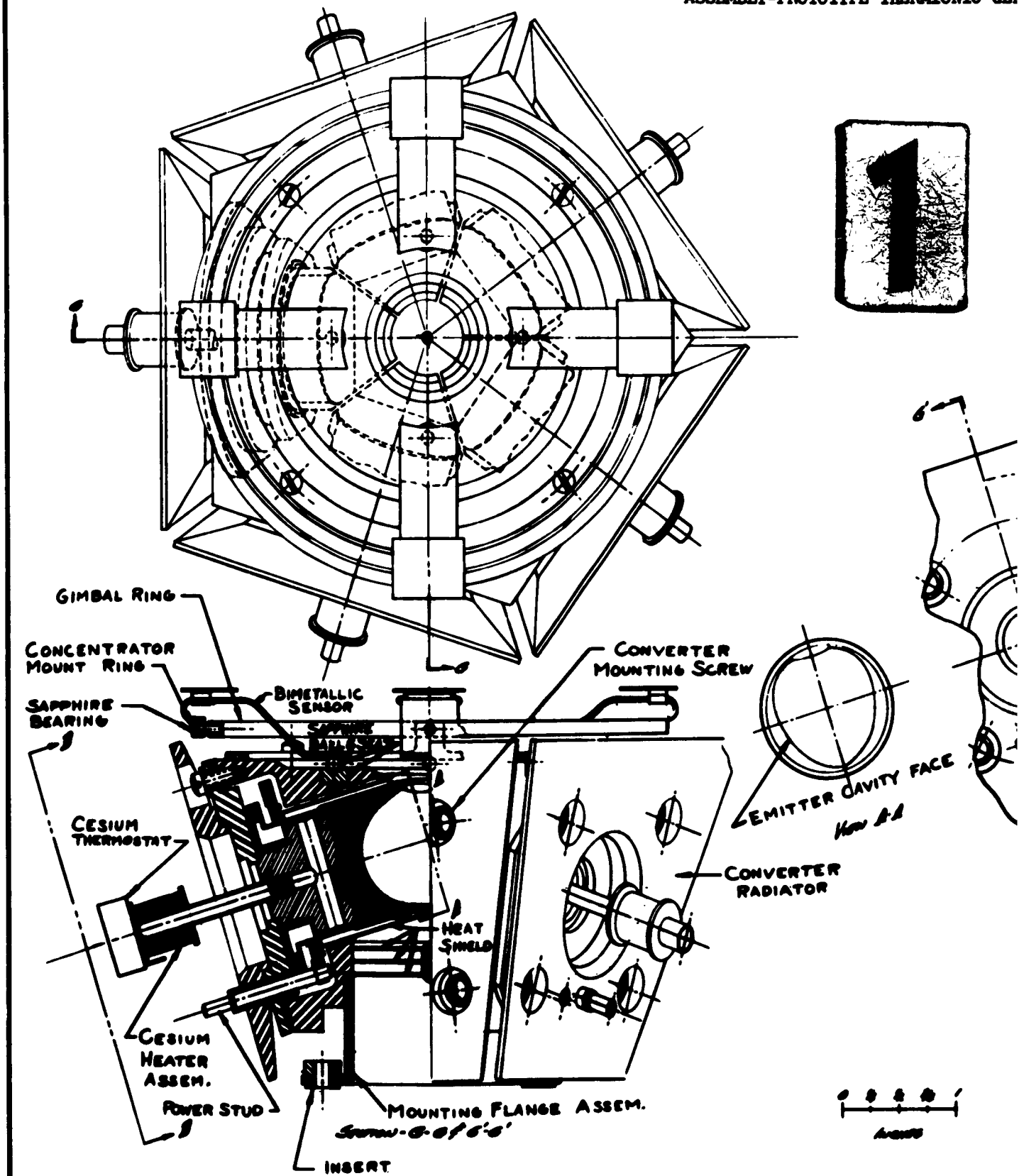

SEMBLY-PROTOTYPE THERMIONIC GENERATOR

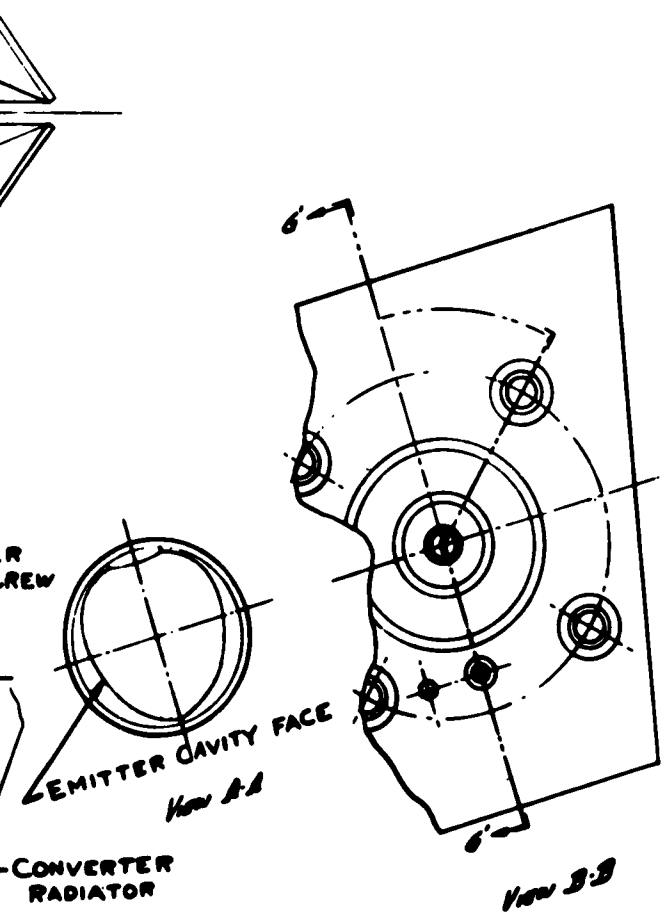

-CONVERTER
RADIATOR

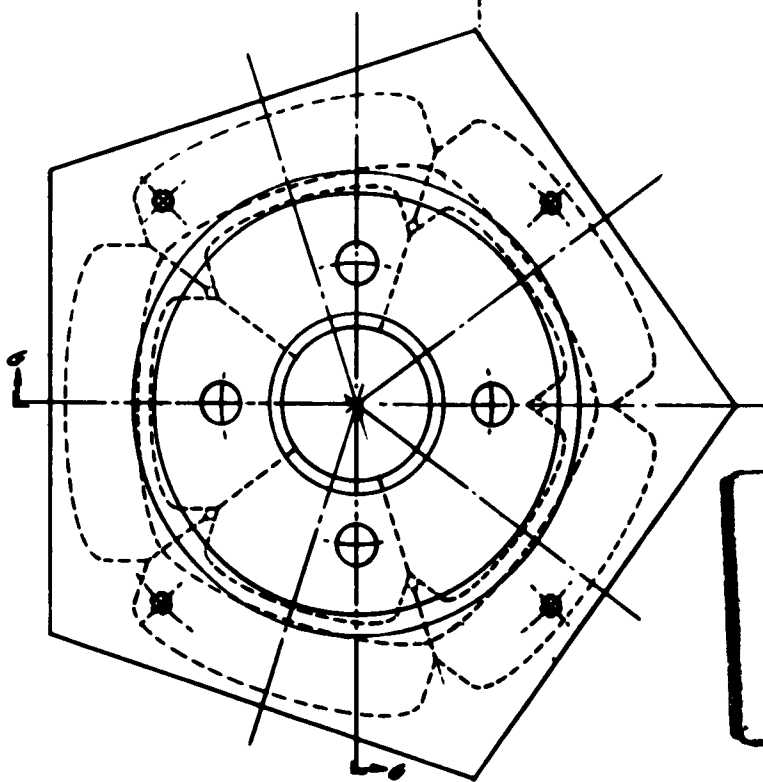

2

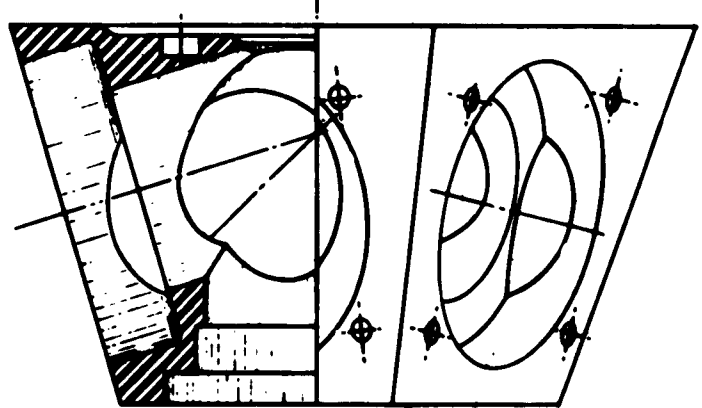

Fig. 4

NICKLE GENERATOR BLOCK

Section C-C

10. Cavity block easily integrated with heliotropic mount.
11. Assembly is lighter in weight.
12. The converter configuration has been proven most reliable under test and has demonstrated satifactory performance capabilities.

The other structures associated with the module may be altered as required by the vehicle system for any specified power level. For the 1.5 kw system the scissors or folding gate type structure seems particularly suitable. The structure is simple, keeps the number of parts required to a minimum, permits easy electrical interconnection and is strong and stable. The size of the system modules and other members is such as to permit easy handling and assembly. The nature of the assembly would also make the interchanging or substitution of components or modules an easy matter.

The frame structure which permits the helionic array to be assembled to the vehicle is shown in Figure 5. A simple rigid "A" frame structure formed of aluminum angle and tubular sections is used. The corner angle pieces serve as the support members for all the modular assemblies during launch. The supporting action is accomplished by the tubular columns formed by rigidizing the short sections of support tube with an internal tensile member.

The deployment structure which also serves as the electrical conductors for the generator outputs is shown in Figure 6. The "C" channels are fastened back to back with suitable insulator fastener assemblies. The generator output from each three-module section is fed to these channel busses, one of which is positive and the other negative. The entire section assembly is fastened to adjacent sections by the conductor struts which are used to carry the generator outputs by proper use of jumper cables and insulator inserts. The struts are hinged to the section channels to permit extension of the sections due to the force applied at the hinge points by the extension springs.

The control circuitry provided for the system is shown in Figures 7, 8 and 9. The current limited DC-DC converter schematic is shown in Figure 7. This control provides a variable topping voltage necessary to give a charge current of approximately 41 amperes.

Using all silicon components as shown in the parts list, dissipations and efficiency for the current limited converter are as follows:

"A" FRAME TOWER ASSEMBLY

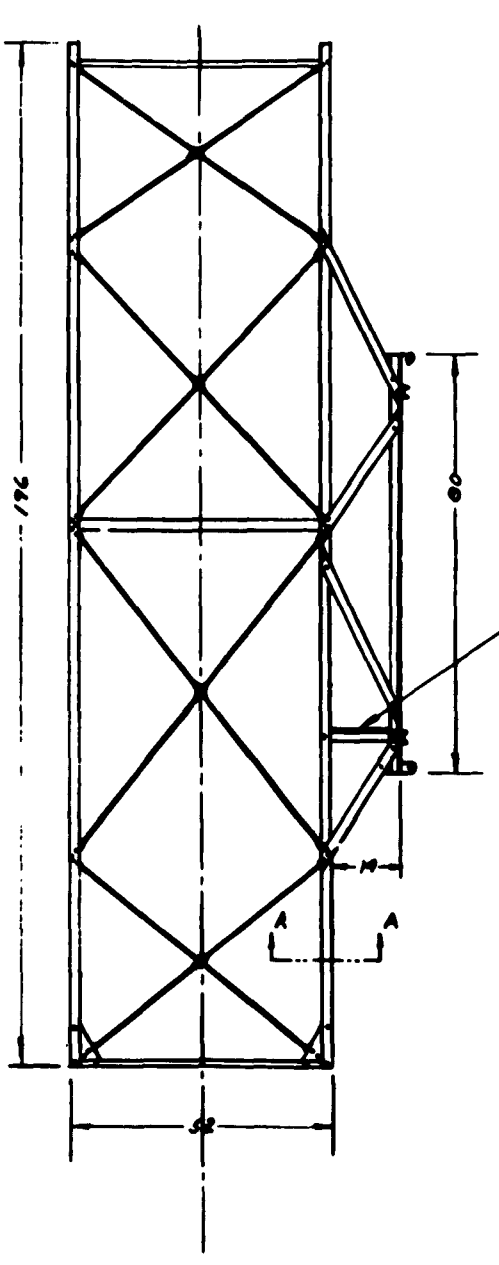

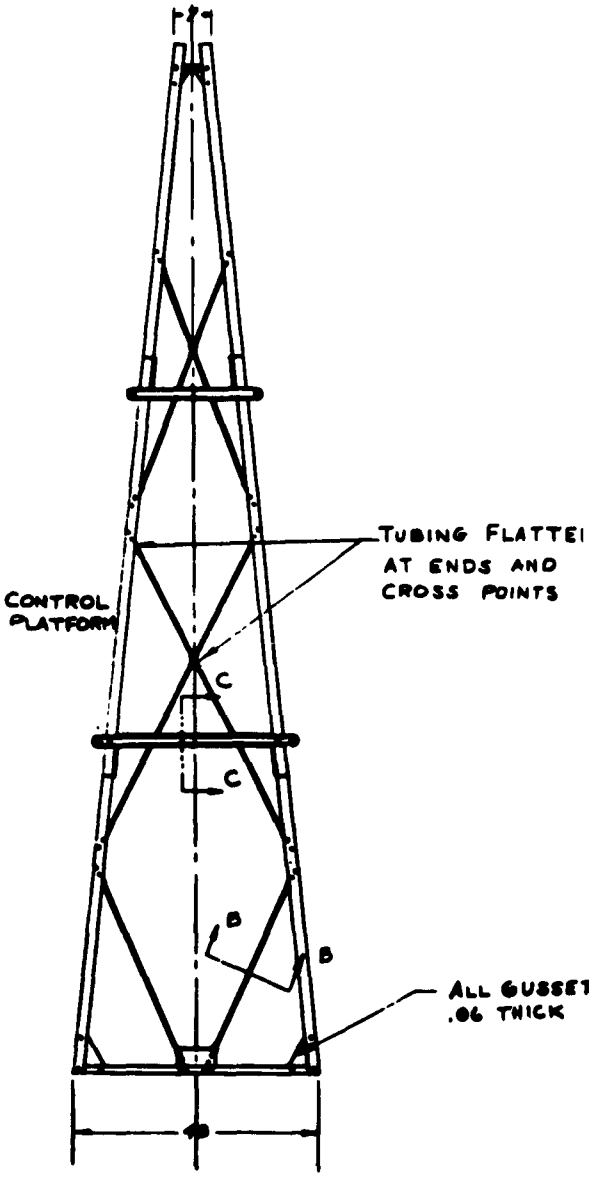

"A" FRAME TOWER ASSEMBLY

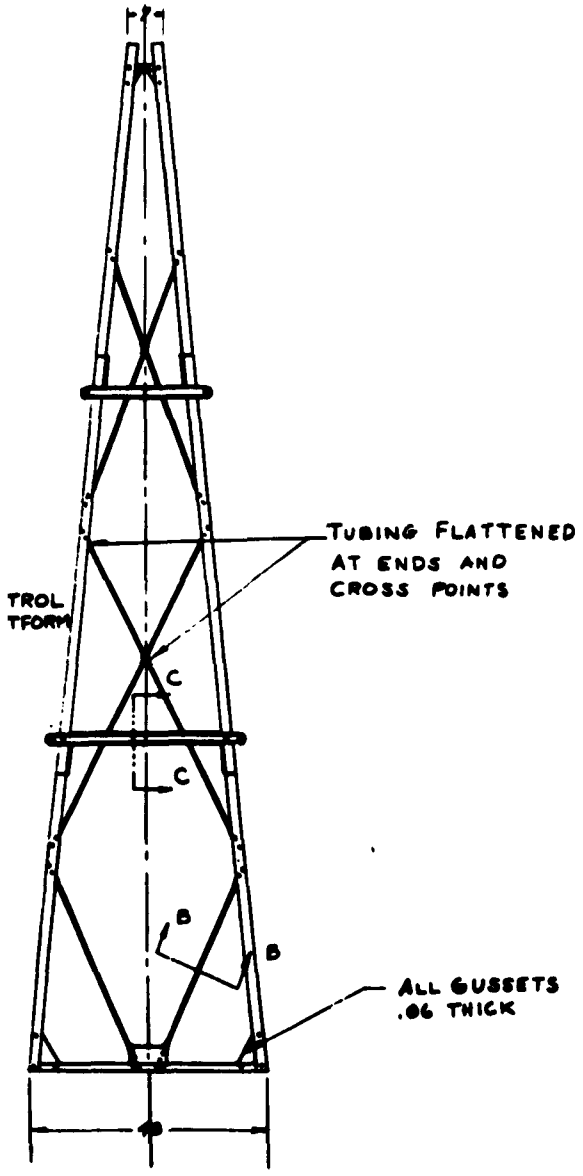

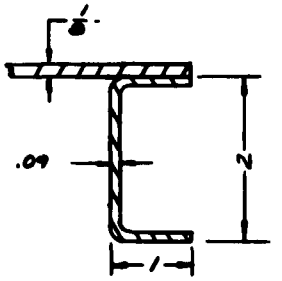

SECTION CC

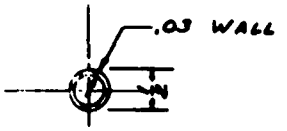

SECTION BB

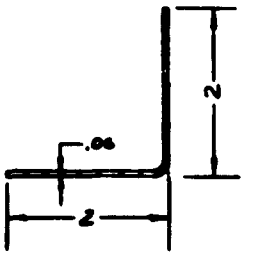

SECTION AA

2

Fig. 5

"A" FRAME TOWER

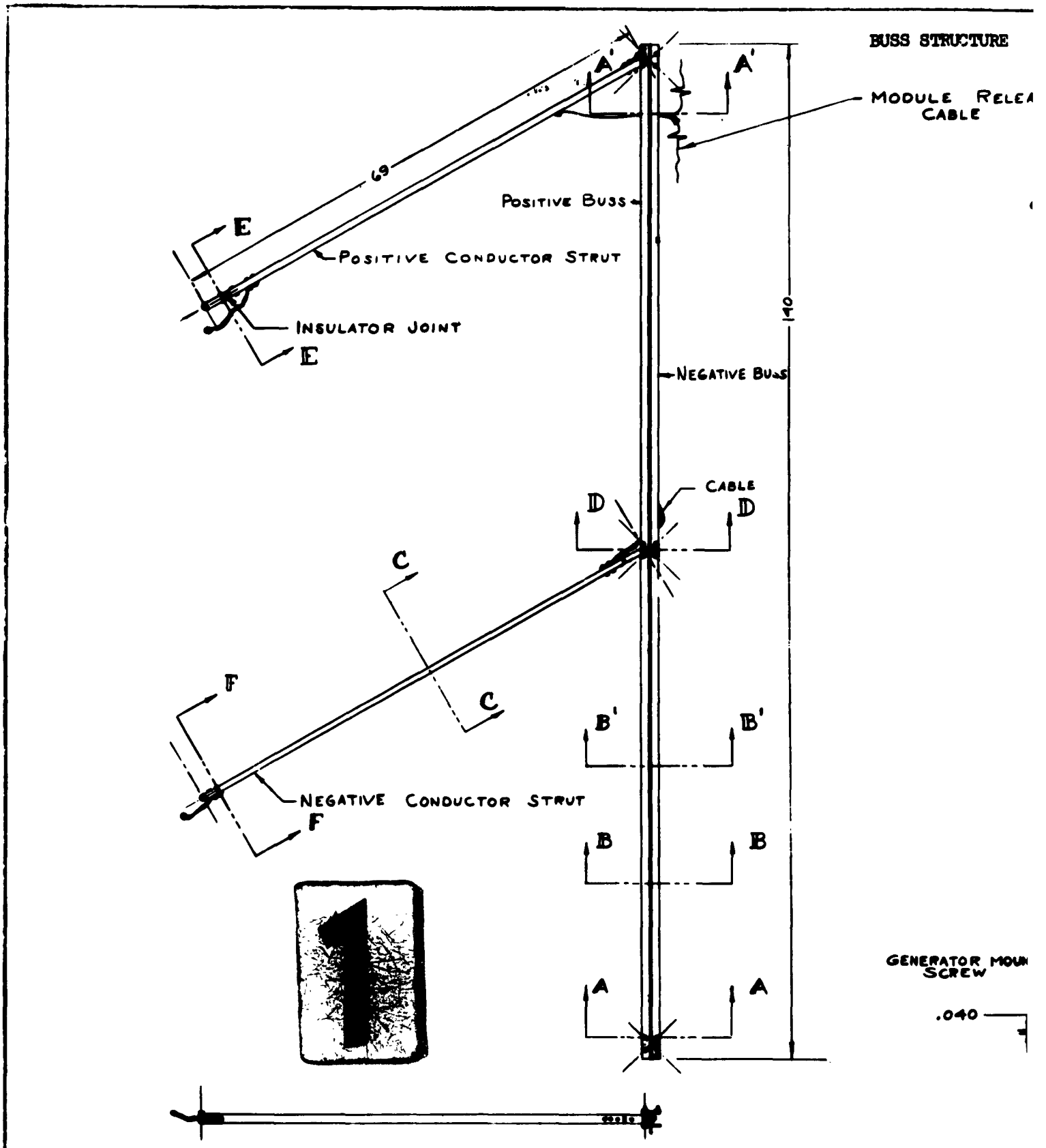
BUSS STRUCTURE
A'
A'
MODULE RELEA
CABLE
69
POSITIVE BUSS
E
POSITIVE CONDUCTOR STRUT
INSULATOR JOINT
E
90
NEGATIVE BUS
CABLE
D
D
C
C
F
F
B'
B'
NEGATIVE CONDUCTOR STRUT
B
B
A
A
GENERATOR MOUN
SCREW
.040

MODULE RELEASE CABLE

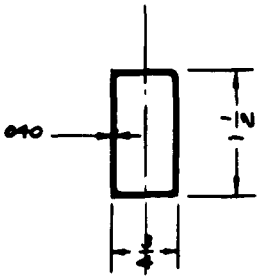

SECTION C C

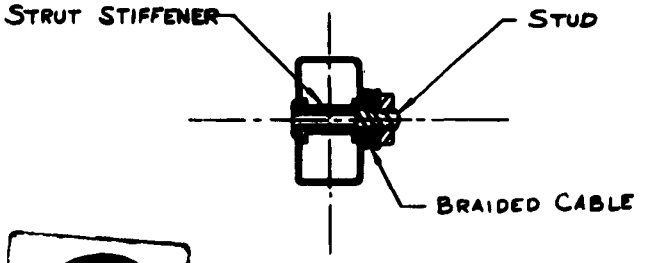

SECTION F F

2

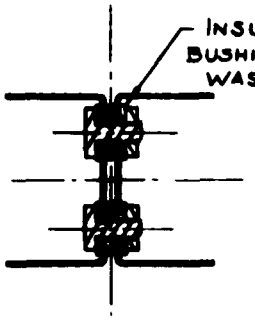

SECTION B B

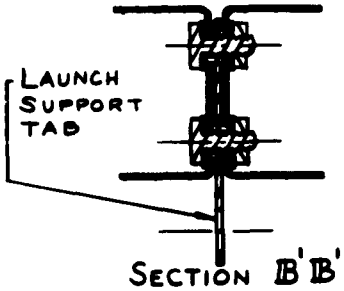

SECTION B'B'

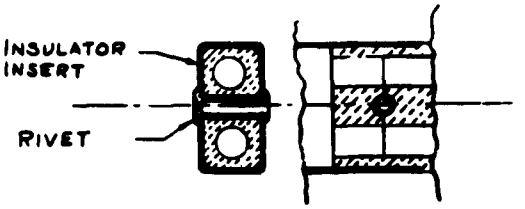

SECTION E E

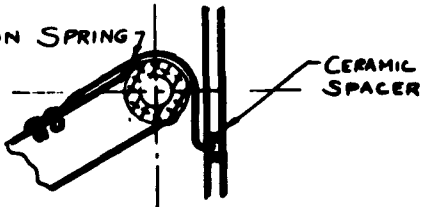

SECTION A A

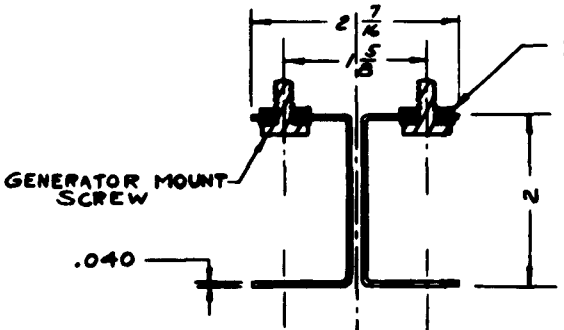

SECTION A A

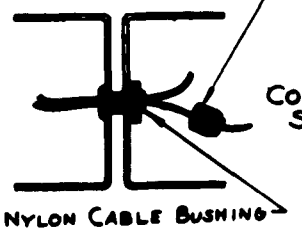

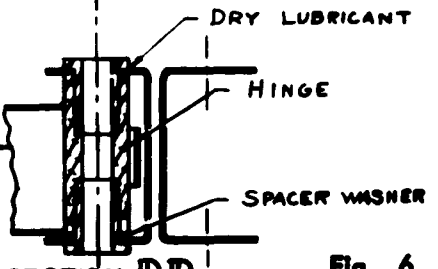

SECTION D D

Fig. 6

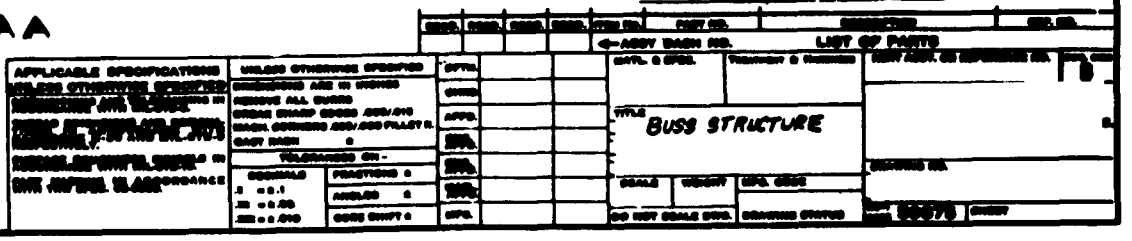

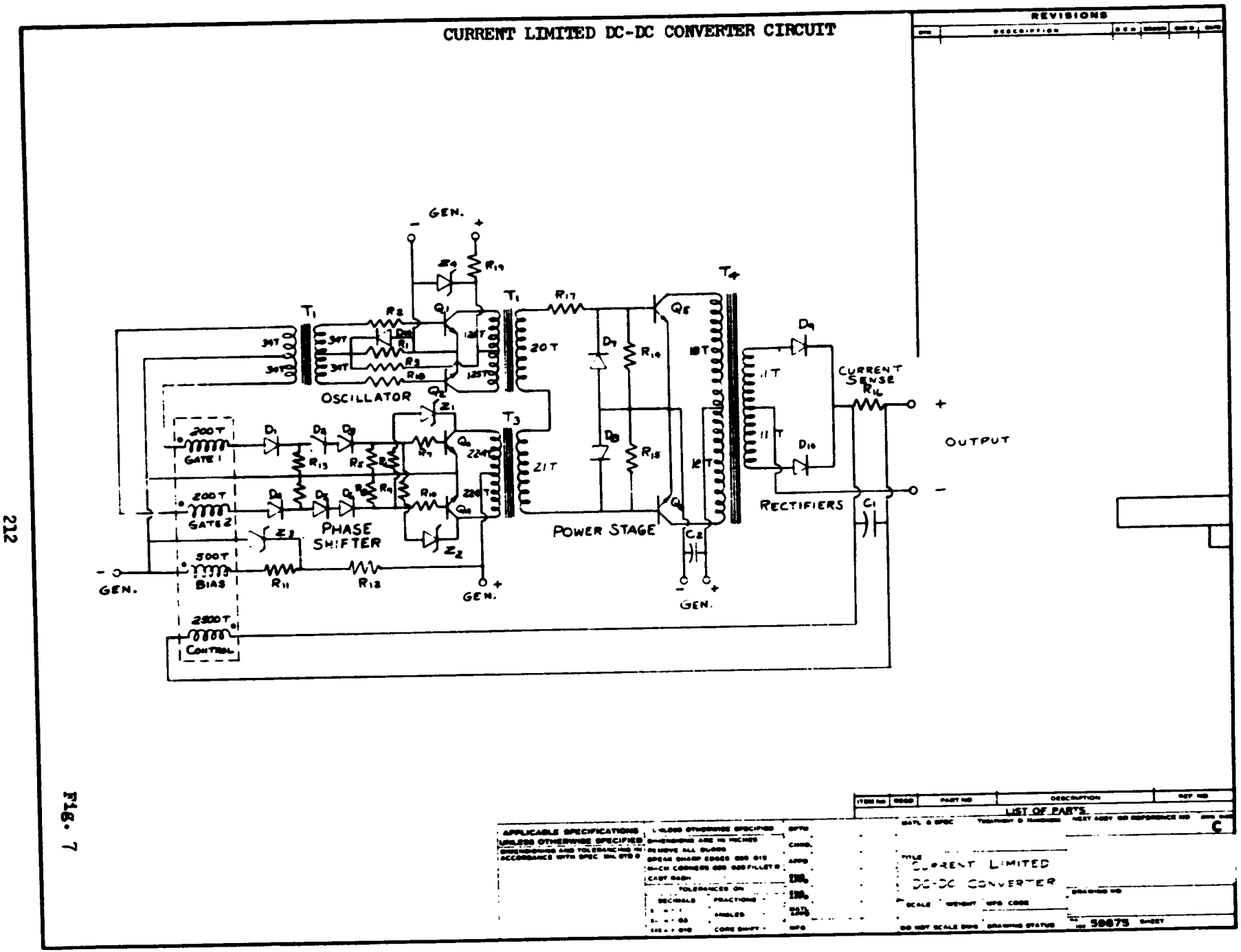
CURRENT LIMITED DC-DC CONVERTER CIRCUIT
REVISIONS
GEN.
OSCILLATOR
PHASE SHIFTER
POWER STAGE
RECTIFIERS
CURRENT SENSE
OUTPUT
GATE 1
GATE 2
BIAS
CONTROL
LIST OF PARTS
CURRENT LIMITED DC-DC CONVERTER

FIG. 7

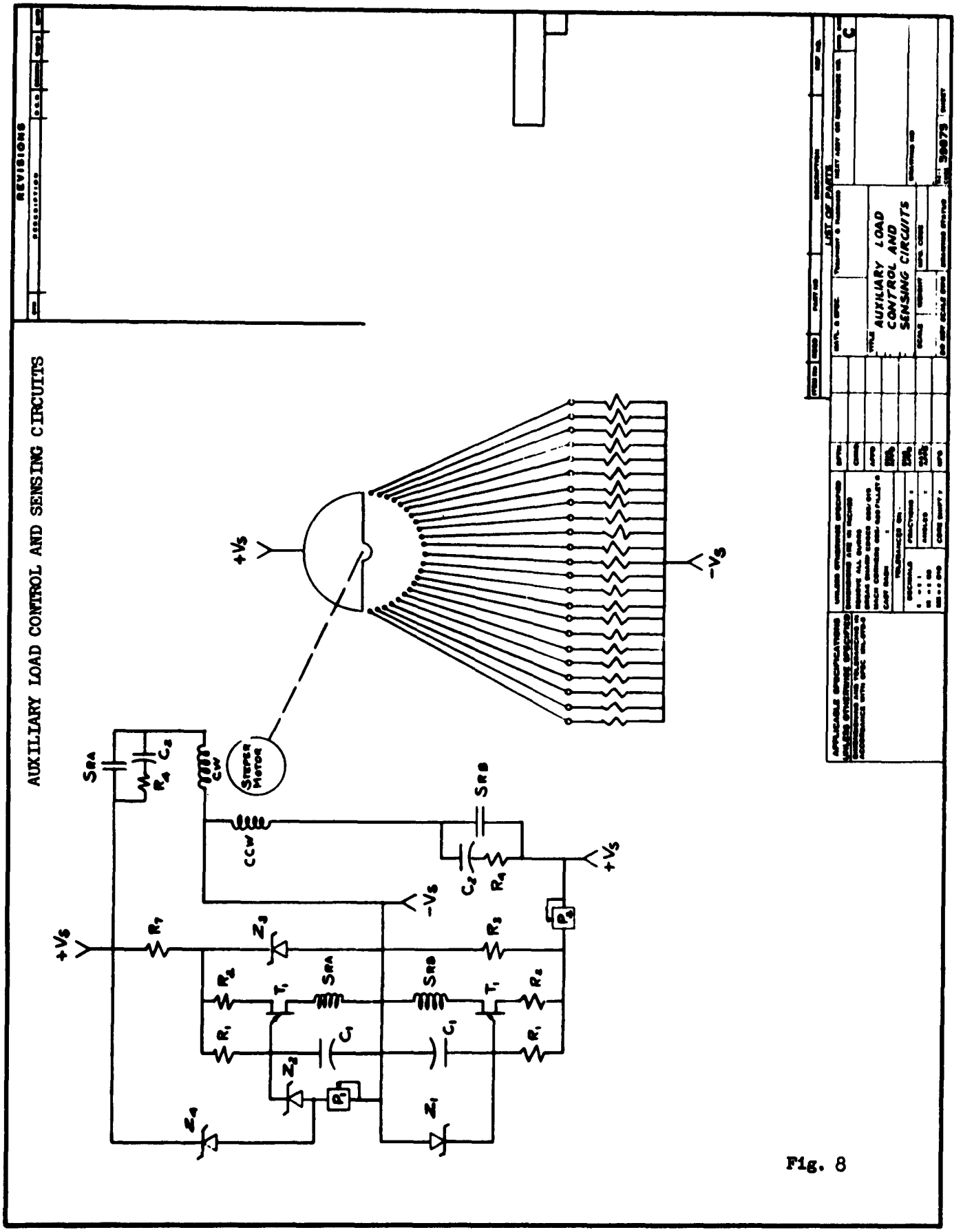
AUXILIARY LOAD CONTROL AND SENSING CIRCUITS
REVISIONS
AUXILIARY LOAD CONTROL AND SENSING CIRCUITS
+Vs
-Vs
Stepper Motor
CW
CCW
SRA
SRB
Ra
Ca
Cb
Rb
R1
R2
R3
R4
R5
Z1
Z2
Z3
Z4
T1
C1

Fig. 8

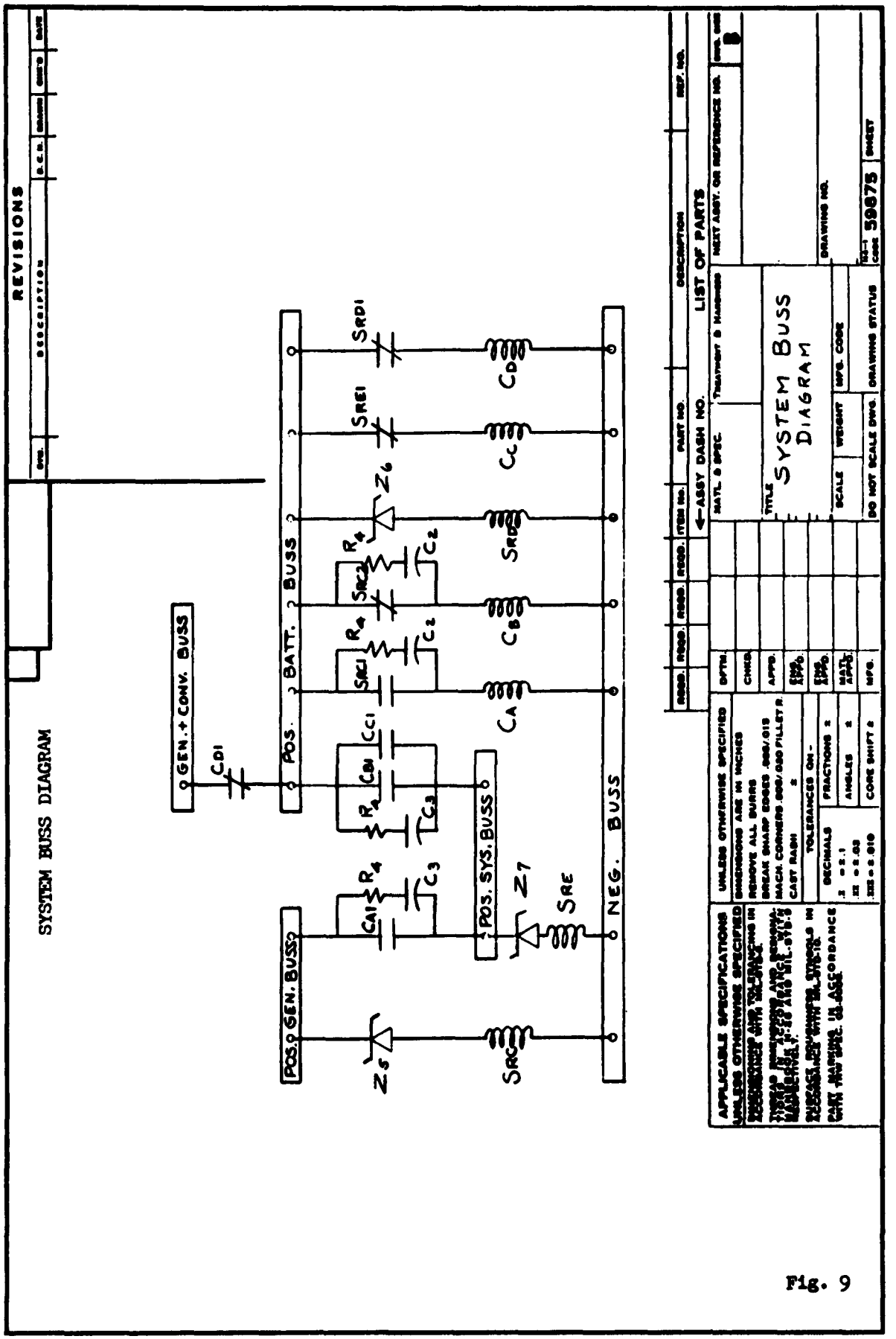
SYSTEM BUSS DIAGRAM
REVISIONS
GEN.+ CONV. BUSS
POS. BATT. BUSS
POS. GEN. BUSS
POS. SYS. BUSS
NEG. BUSS
SYSTEM BUSS DIAGRAM
LIST OF PARTS
SCALE
WEIGHT
DRAWING NO.
SIZE CODE 59875
SHEET

Fig. 9

Output power (12 v at 41A)	492 watts
Output rectifier loss (from data sheet)	30 watts
Current sense loss	10 watts
Output transformer loss	20 watts
Power transistor loss	50 watts
Logic power	25 watts
Total input power	627 watts

$$\eta = \frac{P_{OUT}}{P_{IN}} = \frac{492}{627} = 78.5\%$$

Replacing the silicon 2N2124 with germanium 2N2159 power transistors increases the efficiency as follows:

Output power	492 watts
Output rectifier loss	30 watts
Current sense loss	10 watts
Output transformer loss	20 watts
Power transistor loss	10 watts
Logic power	25 watts
Total input power	587 watts

$$\eta = \frac{P_{OUT}}{P_{IN}} = \frac{492}{587} = 83.8\%$$

Using germanium power transistors means the transistor studs must be kept to about 90°C which means a heat sink temperature of about 70°C maximum. With the silicon power transistors the transistor studs must be kept to about 145°C or a heat sink temperature of about 125°C.

Preliminary calculations indicate the use of germanium components is reasonable because the necessary heat dissipation can be managed by direct radiation from the controls housing.

The auxiliary load control and sensing circuitry is shown in Figure 8. The sensing circuitry is simple and yet very reliable and stable. The circuit can be adjusted to sample load voltage over a frequency range of from one cycle per several seconds to 30 cycles per second. The upper limit on the sampling rate is determined by the response of the switching or stepping motor. A

relatively low cycle rate can be tolerated because of the large thermal capacity of the generators which will prevent any step-type transients due to system load variations. This lower cyclic rate should help insure the ability of the stepper switch to meet the one-year operational life requirements of the system. The gain of this control can easily be varied but will be adjusted to apply or remove load in the range of from zero to 3 kw with a voltage variation between 27 and 28 volts d.c.

The logic and buss circuitry which controls system operation and power distribution is shown in Figure 9. The logic circuits employ simple contactor controls and zener diode referenced relays to affect proper operation of the system. The flow of current in S_{RC} due to generator output causes contactor C_A to apply the generator output to the system load. Contactor C_B is also de-energized disconnecting the battery buss from the system load. In the event the system load voltage is too low, as it may be during generator warmup, relay S_{RE} is de-energized, thereby energizing contactor C_C which again applies the battery buss to the system through contacts C_{C1}. As the batteries reach a full charge condition relay S_{RD} cuts out contactor C_D which removes the battery from the charging circuit. The battery would then remain on standby until either the generator output or the system buss voltage drops sufficiently to contacts C_{B1} or C_{C1} and again apply the battery bank to the system buss. The auxiliary load bank functions continuously to maintain system load voltage between the operating point of relay S_{RE} and an upper system voltage of 29 volts.

A preliminary parts list for all control components is shown in Table I. A complete control housing is shown in Figure 10. This housing is hermetically sealed and the package charged with dry nitrogen. An estimate of total controller weight is 22 pounds.

SYSTEM CONTROLLER LAYOUT

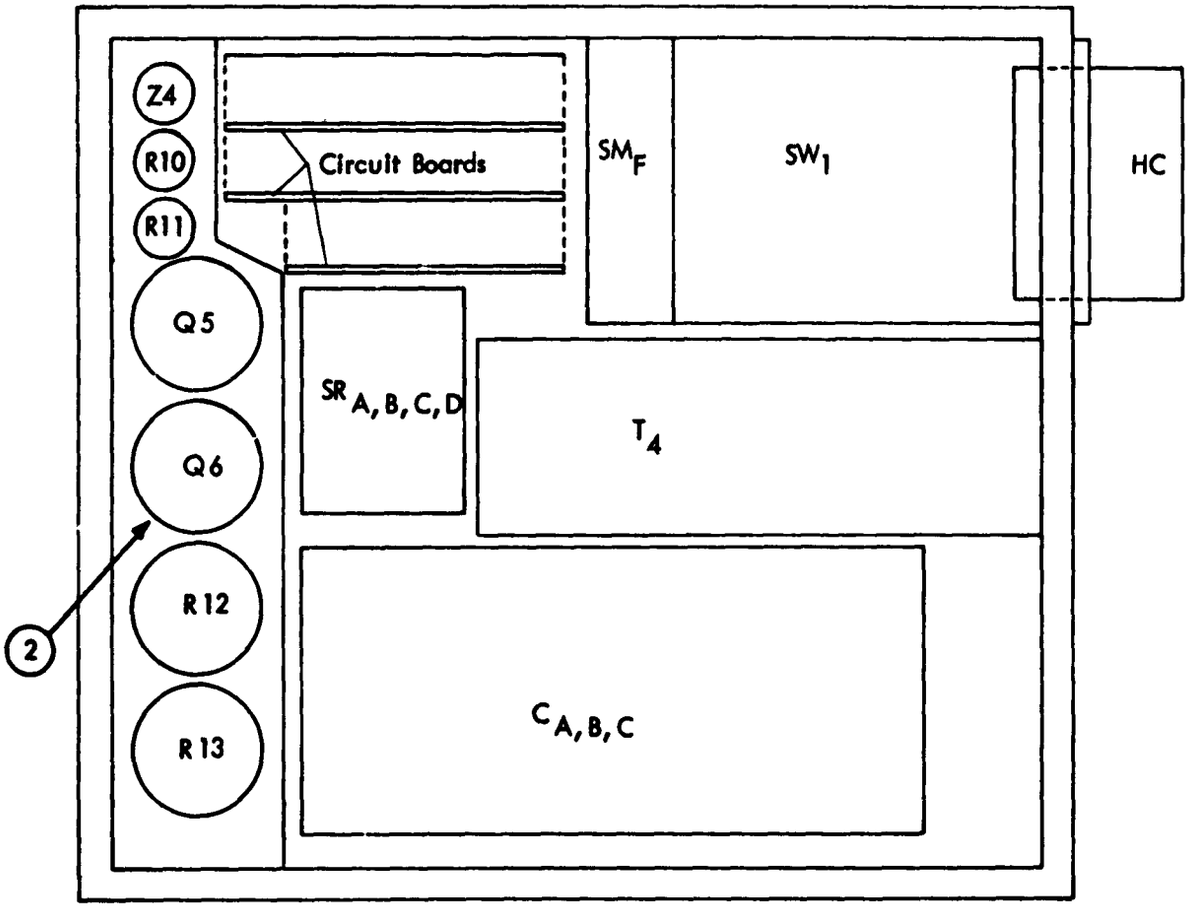

Fig. 10

TABLE I

Preliminary Parts List

Symbol	Vendor	Part No.	Specification
System Source Control			
$Z_{5,7}$	Motorola	4 - 1N751 Selected	MIL-S-19500/127
Z_6	Motorola	7 - 1N751 Selected	MIL-S-19500/127
$SR_{C,D,E}$	Couch	3 - 2R25A370-B	MIL-R-5757
$C_{A,B,C,D}$	Hartman	3 - A770FA	MIL-R-6106
R_4	Corning	4 - 10Ω RD60	MIL-R-11804, Char P
C_2	Electron	2 - WE4-564	MIL-C-18312
C_3	Electron	2 - WE4-105	MIL-C-18312
System Voltage Control			
SW_1	Ledex	1 - 215052 Special	MIL-E-5272
R_1	Corning	2 - 22KΩ RD60	MIL-R-11804, Char P
R_2	Corning	2 - 220Ω RD60	MIL-R-11804, Char P
R_3	Corning	1 - 10KΩ RD60	MIL-R-11804, Char P
R_4	Corning	2 - 10Ω RD60	MIL-R-11804, Char P
C_1	Sprague	2 - 143PM4	MIL-C-25
C_2	Electron	2 - WE4-564	MIL-C-18312
$SR_{A,B}$	Couch	2 - 2R25A390-B	MIL-R-5757
T_1	General Electric	2 - 2N489	MIL-T-19500/75
P_1	Bourns	1 - 2245-1-103 2KΩ	MIL-E-5272, Std-202A
P_2	Bourns	1 - 2245-1-103 2KΩ	MIL-E-5272, Std-202A
Z_1	Motorola	2 - 1N751	MIL-S-19500/127
Z_2	Motorola	2 - 1N753, IN746	MIL-S-19500/127
Z_3	Motorola	4 - 1N751 Selected	MIL-S-19500/127
Z_4	Motorola	5 - 1N751	MIL-S-19500/127
R_7	Corning	1 - 2KΩ RD60	MIL-R-11804, Char P

TABLE I (Cont'd)

Preliminary Parts List

Symbol	Vendor	Part No.	Specification
Current Limited Converter			
R_1	Corning	1 - 560Ω RD60	MIL-R-11804, Char P
$R_{2,18}$	Corning	2 - 22Ω RD60	MIL-R-11804, Char P
R_3	Corning	1 - 10KΩ RD60	MIL-R-11804, Char P
$R_{4,13}$	Corning	2 - 330Ω RD60	MIL-R-11804, Char P
$R_{5,8}$	Corning	2 - 1.8KΩ RD60	MIL-R-11804, Char P
$R_{6,9}$	Corning	2 - 4.7KΩ RD60	MIL-R-11804, Char P
$R_{7,10}$	Corning	2 - 68Ω RD60	MIL-R-11804, Char P
R_{11}	Corning	1 - 2.7KΩ RD60	MIL-R-11804, Char P
R_{12}	Corning	1 - 1.5KΩ RD60	MIL-R-11804, Char P
$R_{14,15}$	Corning	1 - 39Ω RD60	MIL-R-11804, Char P
R_{16}	Dale	1 - .006Ω RH25 Special	MIL-R-18546
R_{17}	Dale	1 - 1.0Ω RH10	MIL-R-18546
R_{19}	Dale	1 - 5.0Ω RH5	MIL-R-18546
C_1	General Electric	1 - 29F1623	MIL-C-3965
C_2	General Electric	1 - 29F1091	MIL-C-3965
$Q_{1,2,3,4}$	RCA	4 - 2N1486	SCL-7002/74A
$Q_{5,6}$	Westinghouse	2 - 2N2124	New
	Motorola	2 - 2N2159 Alt	New
$D_{1,2,3,4,5,6,14}$	Transitron	7 - 1N458A	MIL-E-1/1027
$Z_{1,2}$	Motorola	2 - 1N3034B	MIL-S-19500/115A
Z_3	Motorola	1 - 1N938B	MIL-S-19500/156
Z_4	Motorola	1 - 1N2980	MIL-S-19500/124
$D_{7,8}$	International	2 - 1N253	MIL-E-1/1024A
$D_{9,10}$	General Electric	2 - 1N3289	New

System Design Calculations

1.	Vehicle System Requirements	1,500 watts
2.	Battery Storage Requirements	
	a. System power (1500 watts x 36 minutes)	54,000 watt-min
	b. Cesium heater power (2 watts x 90 x 35 minutes)	6,300 watt-min
	c. Control power (15 watts x 36 minutes)	540 watt-min
	d. Battery discharge loss 6 volts x 54 amps x 8 minutes	2,590 watt-min
	Total	63,430 watt-min
	Battery Charge Efficiency = 77%	
	∴ Total Battery Storage Power	82,400 watt-min
3.	DC-DC Converter - Limiter Loss	
	12 volts x 40 amps x 54 minutes $\left(\frac{1}{N_c} - 1\right)$	4,100 watt-min
	where N_c = converter efficiency = 83.7%	
4.	Generator Power Requirements	
	a. System power	1,500 watts
	b. Storage power = $\frac{82,400 \text{ watt-min}}{54 \text{ min}}$	1,525 watts
	c. Converter limiter loss = $\frac{4100 \text{ watt-min}}{54 \text{ min}}$	76 watts
	d. Control power	15 watts
	Total	3,116 watts

System Array Specifications

Number of modules	18
Number of converters	90
System voltage (6 generators in series)	27.5 volts
System current (3 generators in parallel)	113 amps
Generator current	37.7 amps
Generator volts (5 converters in series)	4.58 volts
Converter volts	.918 volts
Emitter area at 8 watts/cm^2	4.33 cm^2

Ideal generator efficiency is 11% at 2000°K for 3.5 volts output. Operation at 4.58 volts will reduce efficiency to 10.5%.

Total system thermal power requirement $\frac{3116}{10.5\%}$ = 29,600 watts

For a 2000°K cavity temperature, cavity absorber efficiency will be 75%.

Total cavity input power requirement $\frac{29,600}{75\%}$ = 39,500 watts

Concentrator reflectivity is 89%.

Concentrator area is $\frac{39,500}{89\% \times 130 \times 18}$ = 18.9 ft^2

Shadow area is .6 ft^2.

∴ Total concentrator area = 19.5 ft^2.

Concentrator diameter = 4.98 ft.

System Weight (1.5 KW System)

A complete breakdown of the components, assemblies and subassemblies is given in Table II. The combined weight for the system, subassemblies, and components is summarized in this table. Also shown is the number of components of a type required and where applicable the materials used, and the volume and unit weights of these components.

TABLE II

1.5 KW SYSTEM COMPONENT AND SUBASSEMBLY WEIGHT BREAKDOWN

Item	Part Name or Description	Material	No. Rq'd	Volume (Cu In)	Unit Wt(Lbs)	Total Wt(Lbs)
	1.5 KW System					
1.	Thermionic Module Subassembly		18		22.106	398
2.	"A" Frame Tower Subassembly		1		48.40	48.40
3.	Deployment Structure Subassembly		1		61.96	61.96
4.	Battery Storage System		1		110.00	110.00
5.	Controls and Auxiliary Load Bank		1		26.00	26.00
6.	Launch Support Structures					7.10
7.	Miscellaneous (Leads, Operators, Timers)					10.00
	Total Weight					661.46
	Module Subassembly					
1.	Generator Subassembly		1		6.06	6.06
2.	Concentrator Shell (60.5" dia x .009"thick)	Nickel	1	25.8	9.52	9.52
3.	Concentrator Torus 62" dia x π x 2"dia x π x .011"thick	Nickle	1	12.6	4.64	4.64
4.	Viscous Damper and Shaft Assembly		2		.25	.5
5.	Spring Latch	Steel	2		.015	.03
6.	Bucket Handle Assembly	Aluminum	1	4.21	.408	.408
7.	Support Pin Brackets	Aluminum	2	.24	.023	.046
8.	Launch Support Tab	Aluminum	4	1.14	.11	.44
9.	Hinge Bracket	Aluminum	2	1.92	.186	.372
10.	Rivets and Adhesive					.09

TABLE II (Cont'd)

1.5 KW SYSTEM COMPONENT AND SUBASSEMBLY WEIGHT BREAKDOWN

Item	Part Name or Description	Material	No. Rq'd	Volume (Cu In)	Unit Wt (Lbs)	Total Wt (Lbs)
	Generator Subassembly					
1.	Pentagonal Block	Nickel	1	3.52	1.30	1.30
2.	Converter Assembly	Refractories	5		.75	3.75
3.	Heliotropic Mount Assembly	Nickel	1	1.18	.43	.43
4.	Insulators Mount Ring	Al_2O_3	5			.08
5.	Insulator Bushing & Washers Assembly	Al_2O_3	20			.06
6.	Mounting Screws	Steel	24			.18
7.	Thermostats & Reservoir Heater Assembly		5		.04	.20
8.	Miscellaneous Sapphire Ball & Seats, Heater Leads, etc.					.06
	"A" Frame Tower Subassembly					
1.	Corner Columns (200" x .06" x 4")	Aluminum	4	50	4.85	19.40
2.	Tubular Struts 1756 Lineal Inches (1/2" O.D 7/16" I.D.)	Aluminum		76		7.30
3.	Angle Braces 208 Lineal Inches (1" x 1" x .06" Angle)	Aluminum		26		2.50
4.	Angle Braces 392 Lineal Inches (2" x 2" x .06" Angle)	Aluminum		98		9.50
5.	Hinge Braces 66 Lineal Inches (2" x .09" Strip)	Aluminum	2	23.7	1.15	2.30
6.	Control Platform (14" x 32" x 1/8")	Aluminum	1	56	5.4	5.40

TABLE II (Cont'd)

1.5 KW SYSTEM COMPONENT AND SUBASSEMBLY WEIGHT BREAKDOWN

Item	Part Name or Description	Material	No. Rq'd	Volume (Cu In)	Unit Wt(Lbs)	Total Wt(Lbs)
	Deployment Structure Subassembly					
1.	Buss Channel(140"x 4.25"x .04")	Aluminum	12	23.8	2.31	27.8
2.	Section Conductor Struts (69"x 4.5"x .04")	Aluminum	12	12.4	1.20	14.4
3.	Hinge Bearing Assembly	Aluminum-Steel	24	.85	.083	2.00
4.	Strut Insulator Insert	Micarta	12	2.5	.13	1.56
5.	Jumper Cable Conductor Sets (11"x .75"x .12" Braid)	Aluminum	12	1.0	.097	11.62
6.	Jumper Cable Fastener Assembly	Steel	48		.015	.72
7.	Extension Springs	Steel	12		.06	.72
8.	Mounting Screws	Steel	168			1.26
9.	Insulator Bushing-Washer Assembly	Al_2O_3	264			.76
10.	Release Cable Assembly	Steel	2		.31	.62
11.	Cable Bushing Assembly	Nylon	18			.022
12.	Nuts	Steel	96			.48

1.5 KW DESIGN AND TEST SPECIFICATION

1.0 SYSTEM AND COMPONENT SPECIFICATIONS

1.1 System Performance

1.1.1 Power Output

The system shall be capable of producing a useful electrical power output which may be varied continuously or in discrete steps in the range from 0 watts to 1500 watts, when used in earth satellite vehicles. A continuous power output capability of 1.5 KW shall be required. Battery storage will be utilized to provide power during shade periods.

1.1.2 Regulation

The voltage shall be regulated at 27.5 volts and shall be maintained within $\pm$ 1-1/2 volts from 0 to full load. An automatically adjustable impedance load will be used in parallel with the useful load to insure constancy of total load on the power system.

1.1.3 Operating Life

The system shall be developed ultimately to attain a reliability of at least 95% for mission durations of one year.

1.1.4 Launch Power Requirements

No power will be required during launch. The system shall start within five minutes after reaching orbit, which shall occur from five minutes to six hours after launch, and course orientation of the vehicle toward the sun within $\pm$ 5 degrees.

1.2. Environmental Conditions

1.2.1 Launch Conditions

The power system when packaged within a vehicle shall be capable of withstanding the following environmental conditions before and during launch:

1.2.1.1 Temperatures ranging from $0^{\circ}F$ to $200^{\circ}F$.

1.2.1.2 Pressures ranging from 1 atmosphere to 0.

1.2.1.3 Relative humidity ranging from 0% to 100%.

1.2.1.4 Maximum acceleration of 10 g's along the longitudinal axis and 1 g along any lateral axis of the vehicle.

1.2.1.5 Vibration for a period of 10 minutes within the range of 20 to 2000 cps with 0.050 inch double amplitude of vibration.

1.2.2 Space Conditions

After injection into any earth satellite orbit above 300 nautical miles, the power system shall be capable of unfolding, and upon being properly orientated toward the sun, operating for one year under the following conditions:

Adequate energy storage shall be provided for any circular earth satellite orbit having orbital sun-shade periods of 55 and 35 minutes, respectively.

1.2.2.1 Zero-absolute pressure.

1.2.2.2 Linear accelerations up to 10^{-3} g continuously in any direction.

1.2.2.3 Angular accelerations of up to 1 degree/sec^2 and angular rotation rates up to 10 degrees/sec about any axis for periods of up to 5 minutes each. Angular orientation will be required to be performed without folding the solar concentrators. System operation during such maneuvers is not required.

1.2.2.4 Zero gravity during the operating life.

1.2.2.5 Meteor bombardment, Van Allen radiation, and cosmic radiation consistent with the latest scientific data.

1.2.2.6 Vehicle orientation toward the sun within $\pm$ 5 degrees.

1.3 Vehicle Compatibility

The following disturbing effects of the power system upon a representative space vehicle weighing from 2000 to 30,000 pounds shall be considered in the design of the system.

1.3.1 Vibration

The power system shall not impart to the vehicle support points any vibration disturbances with double amplitudes greater than 0.0001 inch when the vibration is unrestrained. In addition, instantaneous accelerations at the support points shall be less than 0.01 g at any frequency when the vibration is unrestrained.

1.3.2 Torque

Any torque resulting from moving parts within the power system shall be eliminated to the maximum extent practicable.

1.3.3 Electrical Interference

The electrical interference caused by the system shall be minimized.

1.3.4 Switching Transients

The power system shall be designed so that instantaneous values of surge current equal to twice the nominal maximum current can be tolerated without impairment of the system performance.

1.3.5 System Weight

The power system weight shall not exceed 700 pounds including battery storage system.

1.3.6 Volume

The power system in launch configuration shall fit within a volume which is a cylinder 9 feet 6 inches in diameter, 16 feet high, topped by a right circular cone of 15° half angle. No reliance shall be placed on an external nose fairing for mechanical support of the power system.

2.0 COMPONENT SPECIFICATIONS

The components of the power system shall meet the following specifications during and after exposure to the environmental reliability and endurance tests specified in paragraph 3.0.

2.1 Thermionic Generator Assembly

2.1.1 Power Output

Power output shall be 173 watts $\pm$ 5 % at a nominal voltage of 4.58 volts and current of 37.7 amps.

Power output shall reach 85% of the design value within one minute of application of full solar input power. Full power shall be attained within four minutes of startup.

2.1.2 Operating Life

Operating life of the generator shall be one year with a minimum of 5840 operational sun-shade cycles. Performance deterioration over the one year period shall not exceed 5%.

2.1.3 Cavity Absorber Efficiency

The cavity geometry of the generator shall be such as to accept at least 95% of all available flux with the concentrator misaligned up to six minutes. The cavity absorber efficiency including misalignment effects shall be at least 75% at the design operating temperature of 2000^{o}K.

2.1.4 Generator Weight

Generator weight shall be kept to a minimum consistent with good design practice and shall not exceed 6.1 pounds.

2.1.5 Generator Components

The generator assembly shall contain five identical thermionic converters mounted in nickel block. The converters shall be shielded against heat loss along the emitter support section and through the bottom of the block assembly with polished moly shields. The spacing between adjacent converters shall

be such as to limit direct flux leakage from the cavity to 3% assuming the openings function as black body absorbers.

2.1.6 Generator Efficiency

The overall generator conversion efficiency exclusive of the cavity absorber efficiency shall be not less than 10.5% at 2000°K.

2.2 Heliotropic Mount

The generator shall be fitted with a heliotropic mount mechanism to assist in controlling concentrator alignment to within $\pm$ 6 minutes in the face of $\pm$ 5 degree vehicle attitude variations relative to the sun.

2.2.1 Heliotropic Sensor Design

The mount sensors shall be designed with a minimum gain of 50 degrees per degree. The sensors shall at the same time be sufficiently stiff as to insure proper direction of the concentrator mass in the face of the perturbation noted in Section 1.2.2.

2.2.2 Mount Structure

The mount structure shall be designed to operate satisfactorily in the thermal and space environment for one year. The mount sensor and other structures shall be designed or shielded against possible burnout even under conditions of persistent misorientation with the concentrated energy of the collector striking the mount.

2.2.3 Mount Response

The response of the mount must be designed to insure maintaining the concentrator orientation without introducing overshoots or other system instabilities due to phase shifts in the modular system.

2.2.4 Mount Weight

The mount assembly shall be of minimum weight and not exceed .4 pounds.

2.2.5 Mount Power Requirements

The power intercepted by the mount shall not exceed 1% of the total intercepted flux for a full 5 degree vehicle misorientation under steady state conditions.

2.3 Thermionic Converters

2.3.1 Thermionic Converter Power Output

The converters shall produce a power output of 34.6 watts $\pm$ 5% at a nominal voltage of .918 volts and current of 37.7 amps.

2.3.2 Converter Power Density

The power density at 2000°K shall be not less than 8 watts/cm^2. Emitter area shall be 4.32 cm^2 $\pm$ .05 cm^2. Emitter to collector spacing .002 inches $\pm$ .0005.

2.3.3 Converter Operating Temperatures

Emitter operating temperature	1975°K $\pm$ 25°K
Collector operating temperature	950°K $\pm$ 25°K
Cesium reservoir temperature	624°K $\pm$ 5°K
Radiator temperature	850°K $\pm$ 25°K

2.3.4 Principal Converter Surface Emissivities

Emitter cavity surface emissivity	.6
Radiator surface emissivity	.78
Interior emitter emissivity	.24
Collector emissivity	.15

2.3.5 Principal Converter Materials

Converter materials shall be of the highest possible quality.

Emitter material - tantalum
Collector material - moly
Radiator material - copper
Reservoir material - copper

2.3.6 Cesium Reservoir Design

Reservoir assembly shall be designed to require a maximum 2 watts of thermal input to maintain the assembly temperature at $614^{\circ}K \pm 5^{\circ}K$.

This thermal input shall be supplied to the reservoir by means of a thermal conduction path from the converter collector during steady state sun operation. Electrical heating will be utilized during the shade periods. The electrical heater shall be designed to control temperature at $614^{\circ}K$.

2.4 Cesium Heater Assembly

2.4.1 Assembly Design

The assembly shall be demountable from the converter assembly for easy replacement. The surface area and emissivity shall be selected to insure a nominal operating temperature of $614^{\circ}K$ with a total continuous thermal input of 2 watts.

2.4.2 Assembly Components

The assembly shall include a heater element, thermostatic switch, adjustable shields for optimizing equilibrium temperature, and a shell structure capable of being easily affixed to the converter reservoir tube.

2.4.3 Power and Voltage Design Requirements

The electrical heater power requirement shall not exceed 2 watts to maintain the nominal $614^{\circ}K$ temperature. Heater design voltage shall be .918 volts. Heaters shall be designed to take a 300% overvoltage for one hour without burnout.

2.4.4 Assembly Life

The heater shall demonstrate the ability to operate for one year on a continuous or 10 minute on-off cyclic basis.

The thermoswitch shall demonstrate the ability to maintain operation on a cyclic basis for 500,000 cycles with a 2 watt resistive load at one volt DC. The heater insulating materials

shall demonstrate the ability to survive one year of 10 minute on-off cyclic life without decomposing, evaporating, loss of dielectric properties, or contributing to the failure of the heater element.

2.4.5 Thermo Switch Control

The thermoswitch shall be capable of 500,000 cycles maintaining operation about a 614°K setpoint.

The maximum initial switch differential shall not exceed $\pm$ 4°K with an increase not to exceed $\pm$ 8°K over the one year period.

2.5 Solar Concentrator Assembly

2.5.1 Optical Specifications

2.5.1.1 Specular Reflectance - Operational

The specular reflectance of the concentrator surface shall not be less than 89% and shall not degrade more than 3 percent during one year's operation in the space environment.

2.5.1.2 Specular Reflectance - Storage and Testing

The specular reflectance of the concentrator surface shall not degrade more than 2 percent for periods of storage up to 18 months.

2.5.1.3 Concentrator Thermal Stresses

The concentrator shall withstand the thermal stresses encountered during storage, transportation, launch and space flight without any decrease in the measured efficiency.

2.5.2 Structural Specifications

2.5.2.1 Concentrator Frontal Diameter

The concentrator frontal diameter shall be five feet, exclusive of support rings structure. The total frontal area shall be 19.5 ft^2.

2.5.2.2 Concentrator Rim Angle

The rim angle of the concentrator shall be selected to optimize concentrator-absorber efficiency.

2.5.2.3 Concentrator Materials

The concentrator shell and support ring shall be nickel. These structures shall be fabricated using the most advanced electroforming techniques. Supporting structures and appendages shall be made of materials compatible with the concentrator structural materials and the operational environment.

2.5.2.4 Concentrator Shell Geometry

Nominal shell thickness shall be .009 inches $\pm$ .002 inches with a maximum surface slope error of 5.5 minutes. Overall geometry shall be sufficient to insure 95% of all concentrated flux can pass through a 5/8 inch diameter aperture under conditions of zero misorientation.

2.6 Modular Assembly

2.6.1 General

The design of the module shall incorporate concentrator, thermionic generator assembly, support attachments for the generator, structural support members, actuator and mechanism for attachment of the thermionic generator to the spacecraft, to satisfy the optical, structural, and thermal requirements specified herein.

2.6.2 Support Member Thermal Stresses

The converter support members shall be required to withstand thermal stresses associated with operation in space.

2.6.3 Absorber Aperture Erection

The converter support members shall incorporate provisions for accurate erection of the absorber aperture into the focal plane at the focal point of the concentrator within 6 minutes of the concentrator axis.

2.6.4 Erection Control

The erection structure shall be actuated by springs of sufficient stiffness to permit operation in a 1 g environment. The structure shall be fitted with controls suitable for preventing excessive or destructive forces or shock from being induced in the erection process. The structure shall incorporate locks where necessary to insure proper maintenance of concentrator-generator alignment subsequent to erection. The structure may be allowed to deflect in the 1 g environment to an extent that would prevent operation so long as the deflection is not permanent and full recovery could be expected upon removal of the gravity induced forces.

2.7 Support and Deployment Structure

2.7.1 Support Members

The modules shall be supported on members which provide low resistance electrical connection to the thermionic generators. The measured loss, when the load is receiving maximum electrical power, shall be less than 1 percent of the conducted power.

2.7.2 Hinge Joints

Dry lubricants shall be utilized in all hinge joints. Joints shall be designed with clearances sufficient to limit misalignment in supporting structures to within $\pm$ 6 minutes in any section. Hinge joints shall demonstrate a capability of not less than 100 complete cycles under vacuum conditions of 10^{-5} mm Hg without loss of operational efficiency.

2.7.3 Extension

The deployment structure shall be capable of complete extension while maintaining alignment of all section busses. The structure may be supported so as to offset the effects of gravity which would introduce intolerable deflection in the assembly. The proper alignment of structural numbers within $\pm$ 6 minutes will be verified after extension. A total of 20 complete extension cycles without loss of alignment accuracy must be demonstrated

in the 1 g environment. Such cyclic test will be conducted without the modules affixed to the deployment structure.

2.7.4 Activation Mechanisms

All mechanical actuators shall be tested for positive operation under vacuums of 10^{-5} mm Hg or better. The operation of such mechanisms shall also be verified as part of the module and deployment structure tests. This shall include the motor operated cable feed systems, cable release systems, and explosive bolt release assemblies.

2.8 Battery Storage System

2.8.1 Battery Type

The type of battery shall be a sealed silver-cadmium battery.

2.8.2 Operating Characteristics

1. Nominal voltage 28 volts
2. Nominal current 54 amps
3. Maximum depth of discharge 52%
4. Cycle life 5840 cycles, 54 minute charge, 36 minute discharge
5. Operational life 1 year
6. Shelf life 2 years
7. Charge rate 40-41 amperes
8. Charge efficiency 77%
9. Temperature range $-20^{\circ}F$ to $100^{\circ}F$
10. Zero gravity to 1g
11. Zero pressure to 1 atmosphere

2.8.3 Battery Weight

Total weight including case but exclusive of external connections - 110 pounds.

2.8.4 Battery Volume

Total volume exclusive of external connections - 1450 cubic inches.

3.0 ENVIRONMENTAL RELIABILITY AND VIBRATION TESTING

3.1 General

These tests shall be performed by the contractor and shall be in addition to any other tests that have to perform to demonstrate the ability of the Thermionic Conversion System to satisfy the requirements detailed in other sections of this specification. These tests shall be performed on all converters, concentrators and components thereof. System structures and modular structures will be subject to test in the stowed position only.

3.2 Environmental Test

3.2.1 Temperature Sterilization

The assembled units,and components thereof, shall be placed in a suitable chamber and the temperature raised to 125°C (257°F) for 24 hours, or 160°C (320°F) for two hours. The time period shall begin after temperature stabilization of the largest centrally located thermal mass. The time required for this stabilization shall be recorded. During actual sterilization the temperature of the interior cannot be measured. This method is designed to insure sterilization of the interior of the materials, including cracks, cavities and joints. After 24 hours at 125°C, the temperature shall be raised to 140°C (285°F) for 5 minutes. The time period shall begin after temperature stabilization of the largest centrally located thermal mass.

3.2.2 High Temperature Test

The assembled units, and components, thereof, shall be placed in a suitable chamber and the temperature raised to + 160°C for 4 hours. The time period shall begin after temperature stabilization of the largest centrally located thermal mass. The time required for stabilization shall be recorded. This requirement is in addition

to the high temperature requirement that shall be imposed on the converter and support members due to actual operation.

3.2.3 Low Temperature Test

The assembled units, and components thereof, shall be placed in a suitable chamber and the temperature lowered to -150°C for 4 hours. The time period shall begin after temperature stabilization of the largest centrally located thermal mass. The time required for stabilization shall be recorded. If this test is performed in air, the water vapor shall be removed to prevent the formation of frost on units under test.

3.3 Vibration Test

3.3.1 Mounting

The vibration test fixtures designed to hold the Thermionic Conversion System, or individual components thereof, shall be vibrated alone and resonant frequencies noted. The lowest resonant frequency shall be higher than 300 cps. The Thermionic Conversion System, or individual components thereof, shall then be mounted on the respective fixture and a low-level (approximately 0.5 g) sine wave shall be applied. A search for the resonances of the fixture-system (component) combination shall be conducted. The vibration tests are intended to simulate the deleterious effects which accompanies Atlas and Centaur motor burning during their complete operation. The assembly shall be attached firmly and securely to vibration exciter without attempt to simulate spacecraft installation. The vibration level shall be observed on the exciter as near to the supporting bracket as possible. The assembly shall be subjected to the vibration test in a direction parallel to the vehicle axis of thrust and in two other orthogonal directions which are also perpendicular to the axis of thrust. The assemblies shall be removed from the exciter and shall perform satisfactorily.

3.3.2 Low Frequency Vibration Test

The assembly, or components, thereof, shall be subject to sinusoidal vibration at frequencies between 1 cps and 40 cps for 24 minutes in

each of three orthogonal directions. The displacement of the vibration shall be 3 inches from 1 to 3 cps and 3g, peak, from 3 to 40 cps. The sweep shall be such that the time rate of change of frequency increases directly with frequency and 8 minutes is required to sweep from 1 to 40 cps. The sweep shall be repeated three times. Resonances of the item shall not be dwelt upon.

3.3.3 High Frequency Vibration Complex Wave Test

The test shall consist of a programmed sequence of band-limited Gaussian noise and combined noise and sinusoidal vibration. The total time in each orthogonal direction will be 9 minutes, 12 seconds The test is as follows:

1. White Gaussian noise 15 g rms band-limited between 15 and 1500 cps for 6 seconds.

2. White Gaussian noise 10 g rms band-limited between 15 and 1500 cps for 3 minutes.

3. White Gaussian noise 4.5 g rms band-limited between 15 and 1500 cps plus at 4.5 g rms sinusoid superimposed on the noise. The frequency of the sinusoid is swept from 40 to 1500 cps in 2 minutes at a rate increasing directly with frequency. The sweep will be repeated 3 times making the total time 6 minutes.

4. White Gaussian noise 15.0 g rms band-limited between 15 and 1500 cps for 6 seconds.

3.3.4 Static Acceleration

The assembly, or component, shall be subjected to a static acceleration of 10 g in 3 orthogonal directions for five minutes in each direction, one direction being parallel to the axis of thrust.

3.3.5 Gas Sterilization Ethylene Oxide

The assembly shall be placed in a chamber and the ethylene oxide gas circulated in and through the chamber until negligible air

is present in mixture. Sufficient water vapor must be added to increase the humidity to 25%. The ethylene oxide gas shall be sampled to determine that these conditions are satisfied. The temperature in the chamber shall be maintained at 72°C, ± 3°C. The test period shall be 24 hours. At the end of the test period, the assembly shall be removed from the chamber and allowed to stabilize at room conditions. The assembly shall then perform satisfactorily.

Aeronautical Systems Division, Dir/Aeromechanics, Flight Accessories Lab, Wright-Patterson AFB, Ohio.
Rpt Nr ASD-TDR-62-877, ADVANCED SOLAR THERMIONIC POWER SYSTEMS, Final report, Dec 62, 239p. incl illus., tables.

Unclassified Report

This report contains a state-of-the-art survey of all components required for solar thermionic power systems in the 1-10 KW range suitable for application in aerospace vehicles. The results of the survey and development program were used in a comprehensive parametric study to determine design criteria applicable to these systems. The

(over)

development program included evaluation of thermionic converters of the vacuum and vapor type. The details of the design, fabrication, performance tests, and evaluation of thermionic converters and generators built during the program are presented. The Appendix presents a detailed design, performance, and test specification for a 1.5 KW, 28 volt solar thermionic power system.

1. Solar thermionic power systems
2. Energy conversion
3. Thermionic emission
4. Solar energy
5. Space vehicles

I. AFSC Project 8173 Task 817305
II. Contract AF 33(616) 7411
III. Thompson Ramo Wooldridge, Inc. Cleveland, Ohio
IV. Secondary Rpt No. ER-5038
V. Aval fr OTS
VI. In ASTIA collection

Aeronautical Systems Division, Dir/Aeromechanics, Flight Accessories Lab, Wright-Patterson AFB, Ohio.
Rpt Nr ASD-TDR-62-877, ADVANCED SOLAR THERMIONIC POWER SYSTEMS, Final report, Dec 62, 239p. incl illus., tables.

Unclassified Report

This report contains a state-of-the-art survey of all components required for solar thermionic power systems in the 1-10 KW range suitable for application in aerospace vehicles. The results of the survey and development program were used in a comprehensive parametric study to determine design criteria applicable to these systems. The

(over)

development program included evaluation of thermionic converters of the vacuum and vapor type. The details of the design, fabrication, performance tests, and evaluation of thermionic converters and generators built during the program are presented. The Appendix presents a detailed design, performance, and test specification for a 1.5 KW, 28 volt solar thermionic power system.

1. Solar thermionic power systems
2. Energy conversion
3. Thermionic emission
4. Solar energy
5. Space vehicles

I. AFSC Project 8173 Task 817305
II. Contract AF 33(616) 7411
III. Thompson Ramo Wooldridge, Inc. Cleveland, Ohio
IV. Secondary Rpt No. ER-5038
V. Aval fr OTS
VI. In ASTIA collection

Aeronautical Systems Division, Dir/Aeromechanics, Flight Accessories Lab, Wright-Patterson AFB, Ohio.
Rpt Nr ASD-TDR-62-877, ADVANCED SOLAR THERMIONIC POWER SYSTEMS, Final report, Dec 62, 239p. incl illus., tables.

Unclassified Report

This report contains a state-of-the-art survey of all components required for solar thermionic power systems in the 1-10 KW range suitable for application in aerospace vehicles. The results of the survey and development program were used in a comprehensive parametric study to determine design criteria applicable to these systems. The

(over)

1. Solar thermionic power systems
2. Energy conversion
3. Thermionic emission
4. Solar energy
5. Space vehicles
I. AFSC Project 8173 Task 817305
II. Contract AF 33(616) 7411
III. Thompson Ramo Wooldridge, Inc. Cleveland, Ohio
IV. Secondary Rpt No. ER-5038
V. Aval fr OTS
VI. In ASTIA collection

development program included evaluation of thermionic converters of the vacuum and vapor type. The details of the design, fabrication, performance tests, and evaluation of thermionic converters and generators built during the program are presented. The Appendix presents a detailed design, performance, and test specification for a 1.5 KW, 28 volt solar thermionic power system.

Aeronautical Systems Division, Dir/Aeromechanics, Flight Accessories Lab, Wright-Patterson AFB, Ohio.
Rpt Nr ASD-TDR-62-877, ADVANCED SOLAR THERMIONIC POWER SYSTEMS, Final report, Dec 62, 239p. incl illus., tables.

Unclassified Report

This report contains a state-of-the-art survey of all components required for solar thermionic power systems in the 1-10 KW range suitable for application in aerospace vehicles. The results of the survey and development program were used in a comprehensive parametric study to determine design criteria applicable to these systems. The

(over)

1. Solar thermionic power systems
2. Energy conversion
3. Thermionic emission
4. Solar energy
5. Space vehicles
I. AFSC Project 8173 Task 817305
II. Contract AF 33(616) 7411
III. Thompson Ramo Wooldridge, Inc. Cleveland, Ohio
IV. Secondary Rpt No. ER-5038
V. Aval fr OTS
VI. In ASTIA collection

development program included evaluation of thermionic converters of the vacuum and vapor type. The details of the design, fabrication, performance tests, and evaluation of thermionic converters and generators built during the program are presented. The Appendix presents a detailed design, performance, and test specification for a 1.5 KW, 28 volt solar thermionic power system.